# The role of Rho GTPases in megakaryopoiesis and thrombopoiesis

• • •

# Die Rolle von Rho GTPasen in der Megakaryopoese und Thrombopoese

Doctoral thesis for a doctoral degree
at the Graduate School of Life Sciences,
Julius-Maximilians-Universität Würzburg,
Section Biomedicine

submitted by

**Tobias Heib**
from Püttlingen, Saarland

Würzburg, 2020

Submitted on:

**Members of the Promotionskomitee:**
Chairperson: Prof. Dr. Thomas Dandekar
Primary Supervisor: Dr. Irina Pleines-Meinhold
Supervisor (Second): PD. Dr. Heike Hermanns
Supervisor (Third): Prof. Dr. Katrin Heinze

Date of Public Defense: ____________________
Date of Receipt of Certificates: ____________________

*Nothing great in the world has ever been accomplished without passion.*

**Georg Wilhelm Friedrich Hegel**

# SUMMARY

Platelets, derived from *megakaryocytes* (MKs) in the *bone marrow* (BM), are small, anucleated cells that circulate in the bloodstream and are critical for thrombosis and hemostasis. Megakaryo- and subsequent thrombopoiesis are highly orchestrated processes involving the differentiation and maturation of MKs from *hematopoietic stem cells* (HSCs), after which MKs are able to release platelets into the bloodstream, a process termed *proplatelet formation* (PPF). Here, the MK penetrates the endothelial lining and releases cytoplasmic portions (proplatelets) into the blood stream, which finally mature into platelets within the ciruculation. PPF requires an extensive crosstalk as well as a tight regulation of the MK cytoskeleton, in which small GTPases of the Rho family, such as RhoA and Cdc42 are critically involved and play opposing roles. MK- and platelet-specific Cdc42 or RhoA-deficiency in mice results in macrothrombocytopenia. Moreover, RhoA-deficient mice displayed a frequent mislocalization of entire MKs into BM sinusoids, a finding that was reverted upon concomitant lack of Cdc42 but accompanied by an aggravated macrothrombocytopenia. Whether receptors are involved in the process of transendothelial MK migration, however, remained unclear.

In the first part of this thesis, a centrifugation-based method (‘spin isolation’) to harvest murine BM cells was established, which not only reduces experimental time, costs and animals but is also highly suitable for studies on primary and *in vitro* cultured BM-derived cells. The spin isolation was used particularly for MK studies during the course of the thesis.

In the second part of this thesis, a MK- and platelet-specific RhoA/Cdc42 double-deficiency was shown to result in reduced expression of a variety of MK-specific glycoproteins and cytoskeletal regulators of importance during MK maturation and PPF, a phenotype culminating in virtually abolished platelet biogenesis. We thus uncovered that RhoA/Cdc42-regulated gene expression is a prerequisite for cytoplasmic MK maturation, but dispensable for endomitosis.

In the third part of this thesis we analyzed mice double-deficient in RhoA and prominent MK receptors which are potentially involved in the regulation of PPF in the BM environment. We were able to show that integrins as well as the inhibitory receptor G6b-B are dispensable for transendothelial migration of RhoA-deficient MKs. Surprisingly however, the myelofibrosis and concomitant osteosclerosis observed in G6b-B single-deficient mice was attenuated in RhoA/G6b-B double-deficient mice, thus implying an important role of RhoA during myelofibrotic disease progression. BM transplantation experiments furthermore revealed that not only the macrothrombocytopenia but also the transmigration of RhoA-deficient MKs is due to cell-intrinsic defects and not related to possible *Pf4-Cre* off-target effects in non-hematopoietic cells.

In the last part of this study we demonstrated that the new approach for MK- and platelet-specific gene ablatation using *Gp1ba-Cre* deleter mice is associated with intrinsic MK defects and in addition results in insufficient depletion of RhoA compared to the *Pf4-Cre* model, positioning the latter still as the gold standard for studying MK biology.

# ZUSAMMENFASSUNG

Thrombozyten, die von Megakaryozyten (MKs) im Knochenmark abgeschnürt werden, sind kleine, kernlose Zellen, die im Blutkreislauf zirkulieren und in Thrombose und Hämostase eine wichtige Rolle spielen. Während der Megakaryopoese differenzieren und reifen MKs von hämatopoetischen Stammzellen heran, um anschließend Thrombozyten in die Sinusoide des Knochenmarks zu entlassen. Dabei durchdringt der MK das Endothel und setzt zytoplasmatische Fragmente in den Blutstrom frei, die schließlich im Blutkreislauf zu Thrombozyten reifen. Der Prozess der Thrombozytenbildung erfordert eine umfangreiche Organisation des MK-Zytoskeletts, an der kleine GTPasen der Rho-Familie wie RhoA und Cdc42 kritisch beteiligt sind, wobei sie dabei gegensätzliche Rollen spielen. Der MK- und Thrombozyten-spezifische Verlust von Cdc42 oder RhoA in Mäusen führte zu einer Makrothrombozytopenie. Darüber hinaus wurde bei RhoA-defizienten Mäusen eine Fehllokalisation ganzer MKs in den Knochenmarkssinusoiden beobachtet, die bei gleichzeitigem Mangel von Cdc42, jedoch auf Kosten einer verschlimmerten Makrothrombozytopenie, wieder rückgängig gemacht wurde. Ob Rezeptoren am Prozess der transendothelialen MK Migration beteiligt sind, blieb bisher jedoch unklar.

Im ersten Teil dieser Arbeit wurde eine zentrifugationsbasierte Methode namens “Spin-Isolation” zur Gewinnung muriner Knochenmarkszellen etabliert, die nicht nur die Versuchszeit, Kosten und Anzahl der benötigten Versuchstiere reduziert, sondern sich auch sehr gut für Studien an primären und *in vitro* kultivierten Knochenmarkszellen eignet. Die Spin-Isolation wurde insbesondere für MK Studien im Rahmen der Dissertation eingesetzt.

Im zweiten Teil dieser Arbeit zeigten wir, dass der gleichzeitige Verlust von RhoA und Cdc42 in MKs zu einer reduzierten Expression MK-spezifischer Glykoproteine und Zytoskelettregulatoren von Bedeutung für MK Reifung führte, wodurch die Thrombozytenbildung stark beinträchtigt war. Dadurch konnten wir aufzeigen, dass RhoA/Cdc42-regulierte Genexpression eine Voraussetzung für die zytoplasmatische MK-Reifung, nicht aber für die Endomitose, ist.

Im dritten Teil dieser Arbeit analysierten wir Mäuse mit einer Doppeldefizienz in RhoA und prominenten MK-Rezeptoren, die möglicherweise mit der Regulation der Thrombozytenbildung im Knochenmark assoziiert sein könnten. Wir zeigten, dass sowohl Integrine als auch der inhibitorische Rezeptor G6b-B für die transendotheliale Migration von RhoA-defizienten MKs entbehrlich sind. Die bei G6b-B-defizienten Mäusen beobachtete Myelofibrose und Osteosklerose wurde jedoch bei RhoA/G6b-B doppelt defizienten Mäusen abgeschwächt, was eine wichtige Rolle von RhoA in myelofibrotischen Krankheitszuständen impliziert. Knochenmarktransplantationen zeigten darüber hinaus, dass nicht nur die Makrothrombozytopenie, sondern auch die Transmigration von RhoA-defizienten MKs auf zellintrinsische Defekte zurückzuführen ist und nicht mit den berichteten unspezifischen Effekten des *Pf4-Cre* Systems in nicht-hämatopoetischen Zellen einhergeht.

Im letzten Teil dieser Studie zeigten wir, dass der neue Ansatz für die MK/Thrombozyten-spezifische Gendeletion mithilfe der *Gp1ba-Cre* Maus mit intrinsischen megakaryozytären Defekten assoziiert ist und darüber hinaus im Vergleich zum *Pf4-Cre* Modell zu einer unzureichenden Deletion von RhoA führte, wodurch *Pf4-Cre* immer noch der Goldstandard für Studien zu Megakaryozytenbiologie bleibt.

# TABLE OF CONTENTS

# 1 INTRODUCTION

## 1.1 Background

Platelets, derived from *megakaryocytes* (MKs) in the *bone marrow* (BM), are small, anucleated cells that circulate in the bloodstream and are critical for thrombosis and hemostasis. Normal platelet counts in the blood range from 150 to 400 x $10^3$ $\mu L^{-1}$ in humans and up to 1000 x $10^3$ $\mu L^{-1}$ in mice. Platelets have an average diameter of 3-4 µm in humans and 1-2 µm in mice. Upon vessel injury, platelets can adhere to the exposed *extracellular matrix* (ECM) and rapidly become activated, followed by a change in their shape and release of their granules, which contain a wide range of proinflammatory, prothrombotic and angiogenic molecules as well as coagulation factors. As a result, platelets aggregate and form a clot to stop the bleeding. Platelet activation is a well-organized process, since uncontrolled platelet activation and aggregation can lead to vessel occlusion and subsequent lack of oxygen supply resulting in tissue damage. The latter is the cause for myocardial infarction or ischemic stroke, which are still among the leading causes of death worldwide.[1,2]

Back in 1910, James H. Wright already proposed that:

'*The blood platelets are detached portions or fragments of the cytoplasm of the megakaryocytes, which are in such relation to the blood channels in the marrow that detached portions of their cytoplasm are quickly carried by the blood current into the circulation. The breaking up of the cytoplasm into the platelets occurs only in cells which have reached a certain stage of growth and development, and is probably rapidly completed when once begun. It takes place in various ways but usually by the pinching off of small rounded projections or pseudopods from the cell body or from larger pseudopods, or by the segmentation of slender pseudopods, or by the pinching off of longer or shorter pseudopods which may or may not undergo segmentation later'.*[3]

Today we know that, in a complex cellular journey, MKs derive from *hematopoietic stem cells* (HSCs) by undergoing a highly orchestrated differentiation process towards the MK lineage in the extravascular compartment of the BM, a process called megakaryopoiesis.[4] Interestingly, although MKs are giant cells in the BM (50-100 µm), they only make up about 0.05% of all BM cells.[3]

During their differentiation, MKs acquire a polyploid nucleus (up to 128N) in a complex maturation process including DNA replication without cell division (endomitosis).[5] The cytoplasmic maturation comprises the synthesis of MK- and platelet-specific granules and the formation of an internal *demarcation membrane system* (DMS), also known as the *invaginated membrane system* (IMS), essential for platelet formation and platelet function.[6,7] The process of megakaryopoiesis also involves the interplay of several *transcription factors* (TFs), which ensure the expression of a defined set of mRNAs and proteins in the developing MK.[8]

After differentiation and maturation, the MKs proceeds with thrombopoiesis, during which the MK cytoplasm undergoes a massive reorganization into cytoplasmic extensions, the so-called proplatelets, a process referred to as *proplatelet formation* (PPF). Thereby, the mature MK penetrates the endothelium and releases up to 5000 platelets into the circulation.[9] While the efficient release of proplatelets into the bloodstream requires a tight regulation of the cytoskeleton, the mechanisms orchestrating polarized PPF into vessel sinusoid are only partially understood.[10]

## 1.2 Megakaryopoiesis

### 1.2.1 Hematopoiesis

MKs, like all other differentiated cells, develop from stem cells. The process of megakaryopoiesis describes the incredible cellular journey from HSCs to MKs. During embryonic development, stem cells successively populate the embryonic yolk sac at around day 7.5 in mice and around the third week in humans. This process is followed by a subsequent population of the fetal liver and spleen and in adults, the HSCs are primarily found in the BM.[11] The classical model describes a hierarchical order, in which MKs derive from *long-term hematopoietic stem cells* (LT-HSC) through a series of committed progenitors, the *multipotent progenitor* (MPP), *common myeloid progenitor* (CMP), *megakaryocyte-erythroid progenitor* (MEP) and *megakaryocyte progenitor* (MKP) (Figure 1A).[12,13] However, this well-defined hierarchical model has been challenged in the past decade due to the identification of *hematopoietic stem and progenitor cells* (HSPCs) with a differentiation bias towards the MK lineage including a subset of MPPs, which are capable to directly give rise to unipotent MKPs (Figure 1B). Whether those MK lineage-biased subsets play a role in native hematopoiesis, under pathological conditions or in situations of acute platelet need is still not clearly understood. Besides, those MK-biased HSPCs have not been convincingly demonstrated in humans yet, thus questioning the translational aspect of the results found in mice.[14]

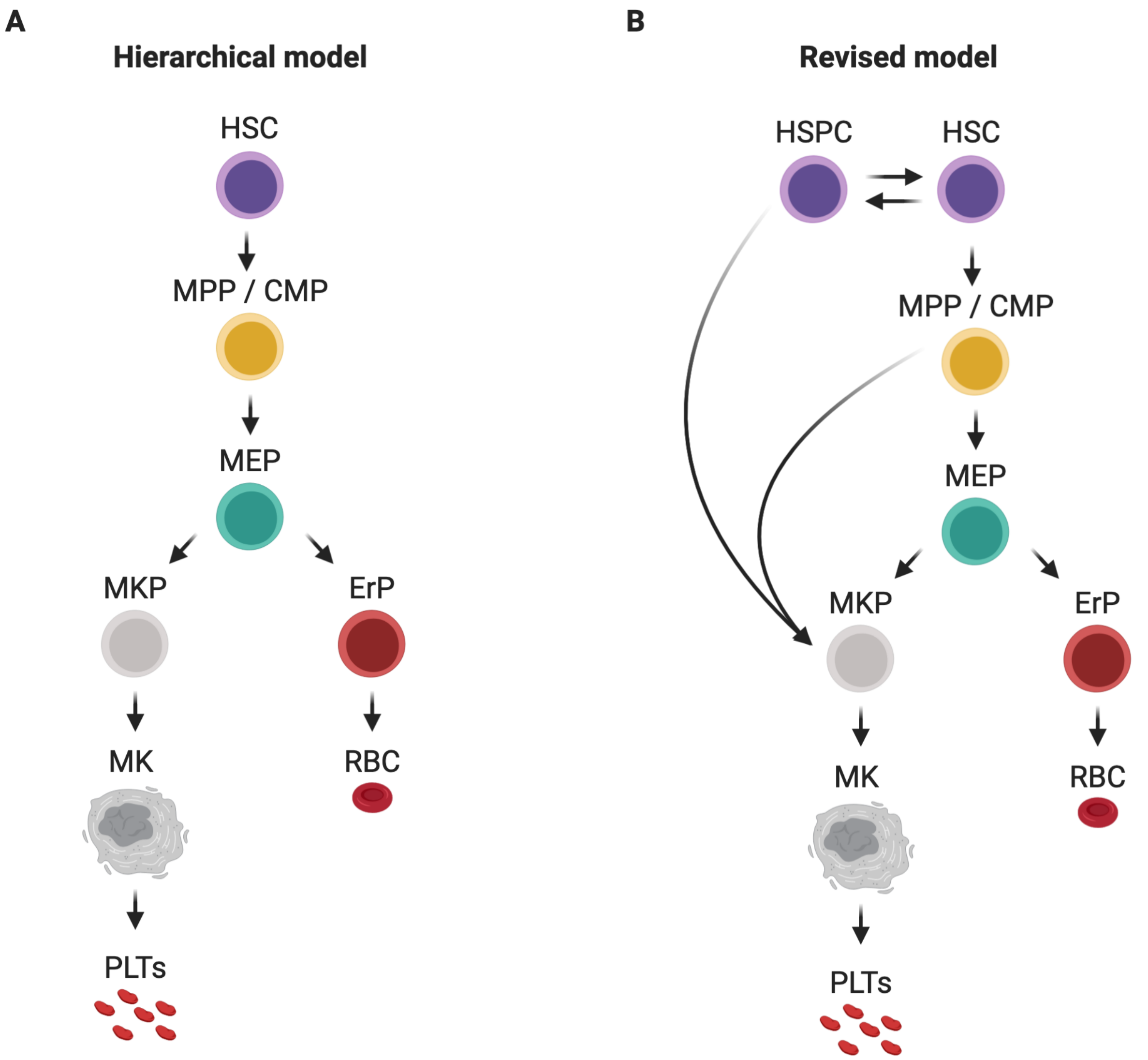

**Figure 1: Models of hematopoiesis. A** The classical hierarchical model of hematopoiesis, in which HSCs with self-renewal potential differentiate into unique, well-defined populations, the *multipotent progenitor* (MPP) and *common myeloid progenitor* (CMP), from which *megakaryocytic-erythroid progenitors* (MEPs) emerge, which then divide into *megakaryocyte progenitor* (MKPs) and *erythroid progenitors* (ErPs). The MKP develops into the MK to produce *platelets* (PLTs). **B** New studies hypothesize that *hematopoietic stem and progenitor cells* (HSPCs) with their differentiation bias towards the MK lineage as well as a subset of MPPs can directly commit to the MKP without undergoing the previous stages. Modified according to Xavier-Ferrucio & Krause, **Stem Cells**, 2018[15] and Noetzli *et al.*, **ATVB**, 2019.[14] Created with **Biorender.com**.

### 1.2.2 Megakaryocyte maturation

Once committed to the MK lineage, the immature MK progenitors undergo a complex maturation process, during which they acquire their future components essential for platelet production and platelet function.

As a hallmark of MK maturation, MKs undergo endomitosis through repeated cycles of DNA replication without cell division and thereby become polyploid.[16-19] However, evidence exists that polyploidization *per se* is not mandatory for PPF.[20,21] The same is true for terminal MK maturation, since so-called micro-MKs (2N – 4N) are frequently observed in *fetal liver cells* (FLCs), cord blood cell cultures or under disease conditions.[22-24] Endomitosis is a process that results from defective late cytokinesis and impaired abscission of the cells, leading to defective karyokinesis and polyploid MKs (up to 128N). The majority of MKs, however, display a modal ploidy of 16N.[20,25-28]

During endomitosis, MK cytoplasmic maturation is initiated, characterized by a substantial increase in cell volume and the synthesis of a high protein and lipid content[29]. During these steps, MKs initiate the expression and upregulation of MK- and platelet-specific receptors, e.g., αIIbβ3a (CD41/CD61), the *glycoprotein* (GP)Ib-V-IX complex and GPVI[30], which is accompanied by the biogenesis and maturation of granules.[31] There are multiple types of granules, most importantly α-granules, dense granules, and lysosomes. While α-granules contain a vast variety of (anti-)angiogenic proteins, growth factors, adhesion, and activatory proteins, which are essential for platelet activation, the dense granules mainly store calcium, adenine nucleotides, polyphosphates, and serotonin. Defective granule biogenesis is related to thrombocytopenia in humans and mice.[32-34]

An important hallmark of mature MKs is also the presence of a large and complex network of intracellular membranes, the so-called DMS/IMS. The DMS/IMS serves as a membrane reservoir for future platelets and originates from the plasma membrane, sourrounded by a *peripheral zone* (PZ), largely devoid of granules and clearly separating the MKs from surrounding cells (Figure 2).[7,35]

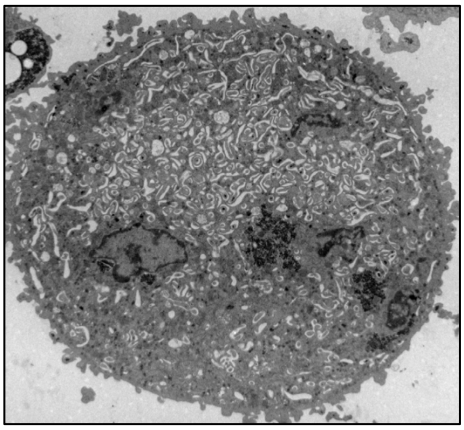

**Figure 2: Electron micrograph of a thin section through a mature MK h with well-defined DMS.** The DMS is a smooth membrane system organized into a network of narrow channels homogeneously distributed throughout the cytoplasm. It has been proposed to originate from the invagination of the plasma membrane and to function as a membrane reservoir for PPF. The MK shows a clearly defined peripheral zone and the presence of a polyploid nucleus, as well as the presence of α- and δ (dense)-granules. The figure was obtained from **Platelets, 4th edition**, 2019.[36]

DMS formation starts with GPIb-positive clusters at the cell membrane fueled continuously by fusion with Golgi vesicles and *endoplasmic reticulum* (ER).[35] A tight regulation of the actin cytoskeleton and its associated proteins is mandatory for proper DMS formation.[7,37-39] Mutations in patients or deletions in mouse genes affecting GPIb-V-IX, the cytoskeleton, or proteins regulating the cytoskeleton are associated with abnormal DMS formation and thrombocytopenia.[40,41] Besides, MKs also contain a dense tubular system, which is believed to be the site of prostaglandin and thromboxane synthesis in platelets and an internal calcium store that is key to platelet activation.[42,43]

## 1.3 Proplatelet formation

In the past, numerous ideas proposed how platelets are generated. The DMS was initially thought to demarcate preformed ‘platelet territories’ within the MK cytoplasm.[44] The release of individual platelets was postulated to take place along the DMS fracture lines by massive fragmentation of the MKs connected to an extensive internal membrane remodeling process[45]. This hypothesis was strengthened by the observations that mature MKs became packed with membranes and platelet-specific organelles.[46] This idea, however, has been challenged due to multiple observations: (i) platelet territories inside the MK cytoplasm do not contain *microtubule* (MT) rings, a key characteristic of resting platelets.[47] (ii) There was no evidence showing a rapid burst of the DMS into newly formed platelets in living MKs. In contrast, experiments revealed the importance of the MT network and proposed that the DMS is a membrane reservoir, delivering the plasma membrane for the nascent proplatelets. This also led to a proposal for an alternative name for the DMS, which clearly not only demarcates platelet territories, but is rather made up of tubular membrane invaginations.[48]

Today, multiple evidence supports the proplatelet hypothesis of platelet biogenesis. The term 'proplatelet' is typically used describing long cytoplasmic fragments extending from MKs, containing numerous platelet-sized swellings linked together by thin cytoplasmic bridges as observed *in vitro* using FLC-derived MKs.[49]

The development of MK cultivation methods, in combination with the discovery of *thrombopoietin* (TPO) and its receptor *myeloproliferative leukemia protein* (*MPL*) hasenabled studying the process of MK development and PPF *in vitro.*[50-57] *In vitro* studies using FLC-derived MKs showed that the MK extensively deploys its intracellular components into proplatelet processes, to develop the cytoplasmic extensions with platelet-sized swellings, also known as 'beads-on-a-string' appearance. These protrusions undergo dynamic bending and branching events, leading to several nascent proplatelet tips. The whole process takes 5-10 h and is initiated with the rupture at one single pole of the MK cytoplasm, followed by several points around the cell membrane. At the end, the MK is converted into a 'naked' nucleus, surrounded by an extensive network of proplatelet extensions (Figure 3).[10]

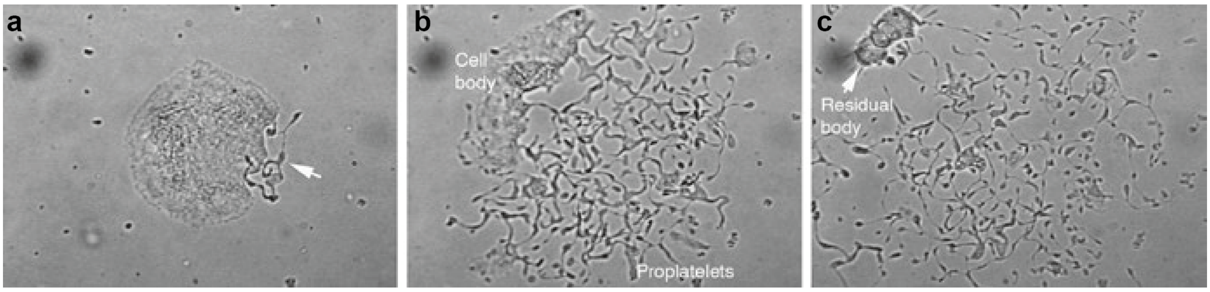

**Figure 3: Production of proplatelets by a cultured MK *in vitro*.** These images show a time-lapse sequence of a mouse fetal liver cell-derived MK demonstrating the events that lead to generation of proplatelets in culture. **a** Platelet generation begins when the MK cytoplasm starts to erode at one pole. **b** The majority of the cytoplasm has been transformed into multiple extensions that continue to elongate and develop platelet-sized swellings that decorate their length. These extensions are very dynamic and exhibit both bending and branching. **c** After the majority of the MK cytoplasm has been transformed into proplatelets, the process ends in a massive retraction that causes the proplatelets to separate from the residual cell body containing a naked nucleus. Figure was obtained from Schulze H., Italiano J. (eds) **Molecular and Cellular Biology of Platelet Formation**, 2016.[58]

In contrast, the process of PPF *in vivo* has been described as a directed and polarized process. Here, MKs penetrate selectively the endothelial barrier and extend long and thin protrusions into the vascular sinusoids[59], not comparable to the typical beads-on-a string appearance. Moreover, the view of long and thin proplatelet extensions has also been recently challenged, showing that MKs may predominantenly enter the circulation as large protrusions.[60,61] The molecular mechanisms regulating transendothelial PPF are still incompletely understood and remain under intensive investigation. In a final step, the proplatelet extensions or larger prortrusions are shed into smaller fragments in the circulation and ultimately sized to platelets by shear forces in the blood stream (Figure 4).[59,62-64]

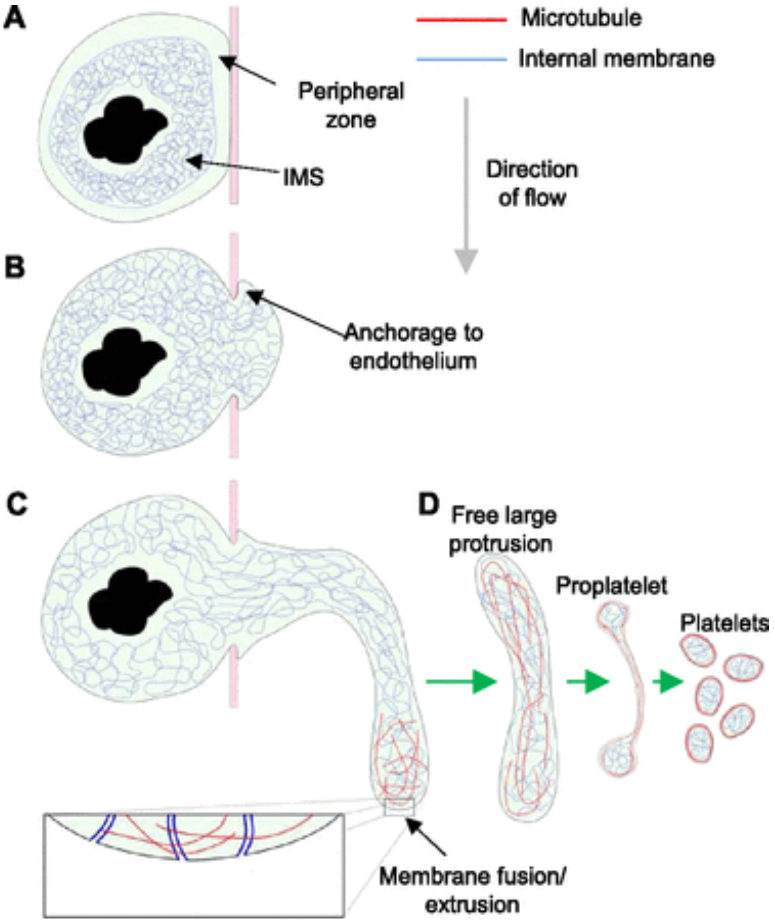

**Figure 4: Illustration showing PPF *in vivo*. A** Non-protruding MK with intact peripheral zone and densely packed IMS. **B** Loss of peripheral zone allows IMS to fuse with plasma membrane and a protrusion to form, which anchors to the luminal surface of the endothelium. **C** IMS trafficked along MTs continues to extrude into the protrusion plasma membrane resulting in extension into the sinusoid lumen in the direction of flow. **D** After release of the large protrusion, MT and membrane reorganization must occur to form proplatelets and ultimately platelets. Figure obtained from Brown *et al.*, **Life Science Alliance**, 2018.[61]

The downstream pulmonary microcirculation has been proposed as a potential site of proplatelet remodeling and further release. Moreover, a contribution of the lung not only for platelet remodeling, but also as a site of whole MK maturation and fragmentation is controversially discussed.[65-68] However, the current view is rather that the lung microcirculation serves as a vascular bed for final platelet maturation, while the BM is the major site for MK maturation and PPF.[69]

Currently, a lot of effort is put into the design and validation of platelet bioreactors, in order to recapitulate native platelet production *ex vivo*. The development of this field not only allows for the *ex vivo* production of platelets and development of targeted therapies for thrombocytopenia, but will also define the promise of regenerative medicine for the next century. Recent advances in the development have aimed to mimic the key physiological characteristics of the BM, including ECM composition/stiffness, blood vessel architecture comprising tissue-specific microvascular endothelium and shear stress. Nevertheless, how complex interactions within *3-dimensional* (3D) microenvironments regulate thrombopoiesis remains poorly understood and the technical challenges associated with designing and manufacturing biomimetic microfluidic devices are high.[70,71]

## 1.4 Regulation of megakaryopoiesis and thrombopoiesis

### 1.4.1 Extracellular signaling pathways

The MK development from primed HSCs is regulated on various levels by different cytokines, the most critical being TPO, released by the liver into the blood. Plasma TPO levels are regulated by a negative feedback loop, since it is sequestered by circulating platelets. In turn, a reduction in platelet counts, such as upon heavy bleeding or under conditions of thrombocytopenia, leads to increased levels of circulating TPO as well as to an enhanced stimulatory effect in the BM, thus increasing MK and, subsequently, platelet numbers.[72-74] During MK development, binding of TPO to its receptor MPL drives both lineage fate decision and differentiation, while being dispensable for terminal PPF.[75] TPO binding promotes the dimerization of MPL and activation of *Janus Kinase-2* (JAK2) and feedback phosphorylation of MPL itself, allowing the recruitment of multiple effectors, notably *signal transducers and activators of transcription* (STATs), *phosphatidylinositol 3-kinase* (PI3K) and *mitogen-activated protein kinase* (MAPKs).[76,77] MPL-induced JAK2/STAT signaling leads to the induction and repression of gene expression programs important for endomitosis, cytoplasmic maturation, PPF and ultimately platelet function.[8] Although sufficient to maintain hemostatic functions, mice deficient in TPO or its receptor MPL suffer from severely decreased platelet and MKs counts (~ 80-90%).[76] Of note, humans with a complete loss of functional MPL have a median platelet count of 21x10 $\mu L^{-3}$ or below, thus showing that they retain a form of platelet production to bypass the TPO-dependent signaling.[78] Indeed, TPO-independent pathways such as the role of *chemokine (C-C motif) ligand 5* (CCL5) / *regulated on activation, normal T cell expressed and secreted* (RANTES)[79] and *interleukin 1 alpha* (IL1α)[62] have been identified. However, the role of these extracellular factors on MKs in normal versus inflammatory conditions and acute platelet need remain to be clarified.[80]

Early studies proposed that progenitors in the BM migrate towards sinusoidal vessels along an *stromal cell-derived factor-1 alpha* (SDF1α) / *(C-X-C motif) ligand 12* (CXCL12) gradient, while the MK differentiation and maturation occurs close to endothelium, supported by a *fibroblast growth factor 4* (FGF4) gradient.[81] Furthermore, the process of proplatelet extensions into the vascular lumen was proposed to be guided by a *sphingosine-1-phosphate* (S1P) gradient from the blood.[82] However, this view has been challenged by recent studies, including one from our department, showing that HSCs and MKs are evenly distributed in close proximity to the vascular sinusoids.[14,69]

Thhe 3D environment of the BM and its underlying stiffness has been recognized to be important for MK development and PPF.[14,83] Within the BM, HSCs and MKs are in permanent contact with ECM proteins such as collagens, fibronectins and laminins or cross linking proteins like perlecan or nidogen.[84,85] Several collagen receptors are expressed during MK differentiation to mature MKs and platelets. The inhibitory collagen receptors *Leukocyte-associated immunoglobulin-like receptor-1* (LAIR-1) and *discoid domain receptor 1* (DDR-1) for example are expressed on early precursors, and in humans together with *cluster of differentiation 34* (CD34).[86,87] During MK maturation, those markers get downregulated and are not preset on circulating platelets. In turn, integrin α2 and GPVI become upregulated. Since collagen is a strong platelet agonist, it is plausible that these receptors are also capable of transducing distinct signaling cascades in MKs. The MK- and platelet-specific receptor GPVI is a type I transmembrane receptor containing a short cytoplasmic tail with a docking site for *Src family kinases* (SFK). GPVI is also associated with the *Fc receptor γ-chain* (FcRγ) chain containing a classical *immunoreceptor tyrosine-based activation motif* (ITAM), which upon phosphorylation on its tyrosine residues mediates *spleen tyrosine kinase* (Syk) binding and subsequent formation of the *linker of activated T cells* (LAT) signalosome and activation of *phospholipase C gamma 2* (PLCγ2).[88]

Integrins can bind both ECM and circulating ligands. The MK- and platelet-specific αIIbβ3 integrin for example binds *von Willebrand factor* (vWF), fibrinogen, and fibronectin. α2 belongs to the integrin family and forms heterodimers exclusively with β1, thus assembling the α2β1 receptor complex. Note that β1 can form a heterodimer with one of at least 12 different α subunits.[89] MKs and platelets express α2β1, α5β1, and α6β1, which bind to collagen, fibronectin, and laminin, respectively. Integrin α2β1 binds to collagen with high affinity by recognizing the proline-hydroxylated sequence G-F-O-G-E-R in collagen.[90,91] Integrins are usually present at a high density on the cell surface in a low affinity state for the binding of their respective ligand. This system allows the cells to dynamically move instead of being irreversibly glued to the matrix components. Upon extracellular stimuli of the cells, integrins switch to a high affinity state, also known as integrin inside-out signaling, which requires the direct interaction of Talin-1 and kindlins with the cytoplasmic domain of the β integrin subunit.[92,93]

The role of α2β1 integrin in platelets and its ability to bind collagen under certain conditions has been well studied both *in vivo* and *in vitro*.[94-97] Furthermore, its roles in cell adhesion, cell motility, angiogenesis, stem cell and immune/blood regulation as well its pivotal role in many diseases such as cancer have been described.[89] In addition, β1 integrins have been associated with the transendothelial migration of immune cells, such as the leucocytes[98], as well as cancer cells[99]. However, the highly controlled process of transendothelial platelet biogenesis from MKs stands in contrast to transendothelial migration of whole haematopoietic (progenitor) cells during mobilization and homing, thus suggesting differential regulation of both pathways.[100]

The regulatory impact of structural proteins present in the BM cavity on thrombopoiesis is well known.[101-105] Together, these studies suggested, that PPF is a cell-autonomous process, which is specifically, inhibited by collagen type I by preventing premature platelets release in the BM cavity, whereas collagen type IV and laminin support PPF at the sinusoids. The underlying mechanisms, however remained unclear until previous work from our department showed, that PPF is selectively inhibited by collagen type I through Syk-independent GPVI signaling. Adhesion assays using FLC-derived MKs indicated, that MK binding to collagen is mediated by α2β1, and that collagen IV at the vascular niche might displace collagen I from MKs and thus contribute to the prevention of premature platelet release into the BM cavity by simultaneously promoting directed transendothelial PPF at the vasculature.[106] Glycosylation to regulate GP and glycolipid expression and function is critical to MKs and thrombopoiesis. Mutations or loss of genes that affect sialylation and galactosylation in MKs are associated with enhanced β1 integrin signaling. The latter alterations result in dysplastic MKs with severely impaired DMS formation and PPF, thus supporting the hypothesis of the collagen type I inhibitory effect under certain conditions.[107,108] Interestingly, mice deficient for integrin α2 and / or GPVI showed normal platelet count and size and MK distribution in the BM, although the contact to collagen type I was decreased at sinusoids. Therefore, the decreased contact of MKs to collagen type I might at least partially explain the unaltered platelet count in these mice, thus arguing for other compensatory signaling pathways and receptors that play a role in the tight regulation of PPF at the sinusoids as well.[85]

Platelet reactivity is continuously controlled by activatory and inhibitory signaling pathways. Besides inhibitory extrinsic factors, *immunoreceptor tyrosine-based inhibiton motif* (ITIM)-containing receptors play an important role.[109,110] G6b-B is an ITIM-containing receptor uniquely expressed in mature MKs and platelets.[109,111] Activation of G6b-B leads to the phosphorylation by SFKs and subsequently the recruitment of *Src homology 2 domain-containing protein-tyrosine phosphatases 1* and *2* (Shp1 and 2), important to dephosphorylate key components of the ITAM signaling pathway in order to attenuate activation signals.[111,112] G6b-B *knockout* (KO) mice develop a severe macrothrombocytopenia, myelofibrosis, accompanied by aberrant MK and platelet function, establishing G6b-B not only as a critical regulator of platelet activation but also platelet production.[112,113] This phenotype, including the macrothrombocytopenia and myelofibrosis, was also observed in a mutant G6b-B loss-of-function mouse model (Mpig6bdiYF)[114] as well as humans with null mutations in the G6b-B gene.[115,116] Despite its important role in regulating platelet production and previous studies indicating that G6b-B binds to the *glycosaminoglycan* (GAG) heparin[117], its physiological ligand, the ECM protein perlecan, has just recently been discovered.[118] Perlecan is one of the best studied and most abundant *heparan sulfate* (HS) proteoglycans which is synthesized and secreted by endothelial and smooth muscle cells into the vessel wall. Interestingly, perlecan has also been reported to interact with other structural components of the ECM such as laminin, collagen type IV and fibronectin as well as FGF2, thus suggesting a potential interplay of G6b-B and other receptors in regulating transendothelial PPF.[119,120]

### 1.4.2 Transcriptional regulation

Disruption of the transcriptional regulation in differentiating hematopoietic cells, e.g. by mutations in the genes encoding the TFs GATA1, *Runt-related transcription factor 1* (RUNX1), or *Nuclear Factor, Erythroid 2* (NFE2), is associated with inherited platelet disorders, but also *acute myeloid leukemia* (AML).[8,14,121,122]

GATA1 is a zinc-finger transcription factor which together with its co-factor *friend of GATA1* (FOG1) plays essential roles during megakaryopoiesis.[123] Loss of GATA1 in mice is linked to decreased MK polyploidization and a lack of cytoplasmic maturation.[124-126] GATA1 mutations themselves are causative for a number of human disorders such as X-linked thrombocytopenia, *transient myeoloproliferative disorder* (TMD) and *acute megakaryoblastic leukemia* (AMKL).[127] Further illustrating its central role in megakaryopoiesis, a point mutation in the *GP1BB* promoter proximal region, important for GATA-binding, is associated with a specific form of *Bernard-Soulier syndrome* (BSS).

RUNX1 (also known as *acute myeloid leukemia 1*, AML1), together with its co-factor *core-binding factor, beta subunit* (CBFB) represents the most common mutational target in human acute leukemia. Conditional KO of RUNX1 in mice using the *platelet factor 4* (*Pf4)-Cre* system results in decreased polyploidization and cytoplasmic development of MKs.[128] Germline heterozygote mutations in the *RUNX1* gene lead to the autosomal dominant human syndrome *familial platelet disorder* (FPD) with propensity to develop AML (FPD/AML). These patients suffer from thrombocytopenia and impaired platelet function, which are marked by abnormal expression of the TPO receptor[129] and *myosin light chain 9* (MYL9).[130,131]

Another transcriptional regulator is the *serum response factor* (SRF), together with its co-activators *megakaryoblastic leukemia 1* (MAL, also referred to as MKL1 or MRTF-A) and *2* (MKL2, also referred to as MRTF-B). MKL-mediated activation of the transcription factor SRF predominantly modulates the expression of cytoskeletal genes and has mainly been studied in the context of cell motility, which is dependent on rapid cytoskeletal remodeling.[132,133] MKL shuttling to the nucleus requires its dissociation from monomeric (G)-actin and *Ras homolog family member (*Rho) *guanosine-5'-triphosphate* (GTP)ases, particularly RhoA, have been shown to regulate MKL1-dependent SRF activation via their ability to modulate actin polymerization.[133,134] Furthermore, an alternative, MAPK-dependent pathway of SRF activation exists, which may counteract Rho GTPase-mediated activation.[133-135] The importance of the MKL/SRF pathway in megakaryopoiesis and platelet production was revealed by knockdown studies in human MKs, as well as mice lacking *Srf* and *Mkl1/2* in MKs. Constitutive or conditional KOs of *Srf* or *Mkl1/2* resulted in thrombocytopenia, immature MKs, decreased PPF, and aberrant actin stress fiber formation in the case of *Srf* deficiency.[136-140]

*Friend leukaemia virus integration 1* (FLI1), acts in concert with GATA1, FOG1 and *GA binding protein TF alpha subunit* (GABPA), regulating the expression of MK-related genes such as *GPIBA, GP9, ITGA2B* and *MPL*. Loss of FLI1 results in the Paris-Trousseau syndrome, an inherited thrombocytopenia.

Final stages of MK maturation until the point of platelet shedding are regulated via NFE-2, potentially downstream of RUNX1. While its role is dispensable for polyploidization, NFE2-deficient MKs have a disorganized DMS with small and sparse granules, thus indicating a late maturation block.[141] Transcriptional targets of NFE2, such as TUBB1 (β1-tubulin) are associated with thrombocytopenia in human and mice.[142-144] Overexpression of NFE2 has also been reported in patients suffering from myelofibrosis, independent of the presence or absence of the most prominent driver, the JAK2V617F mutation.[145,146]

Other TFs involved in the regulation are *T-cell acute lymphocytic leukaemia 1* (TAL1), *ETS variant 6* (ETV6) and the *Growth Factor Independent* 1B (GFI1B).[122]

## 1.5 The MK cytoskeleton

The cytoskeleton consists of a highly interconnected structure of filamentous polymers and associated proteins that enables a eukaryotic cell to cope with deforming forces, allows active transport of intracellular cargos and facilitates the shape change of the cell, which is required for movement. This is achieved by the interaction of a plethora of cytoplasmic proteins and organelles. Although the term ‘cytoskeleton’ indicates a stable and rigid structure, it is a highly adaptive and dynamic network and the components are in a constant equilibrium of assembly and disassembly. Three major types of filaments can be distinguished: MTs, intermediate and actin filaments, which are interconnected by the cytoskeletal integrator spectrin. While the MT and actin filaments have been extensively studied in the process of PPF, the function of the spectrin membrane skeleton started to be appreciated.[147] MK development and subsequent PPF requires dynamic remodeling and profound changes in the actin and MT.

### 1.5.1 MT cytoskeleton

The MT protofilaments consist of different α- and β-tubulin isoforms, which in their GTP- bound state form heterodimers, which can be further assembled into long and polarized plus- (β-subunit is exposed) and minus-end (α-subunit is exposed) protofilaments. The temporal and spatial coordination of MT dynamics is essential as MT are responsible not only for cell structure maintenance, but are also of importance for cell migration, mitosis, meiosis, developmental processes and for the transport of intracellular cargos. Thirteen of these protofilaments can further associate laterally into a hollow cylinder appearance and build the MT filaments, with an average diameter of 24 nm and up to 50-100 µm in length.[148,149] The characteristic marginal band of resting platelets consists of a single MT filament approximately 100 µm in length which is coiled 8-12 times in the platelet periphery and important to maintain its discoid shape. Platelets lose their discoid shape upon treatment with MT depolymerizing drugs such as nocodazole, vincristine or colchicine.[150] The MK- and platelet-specific isoform β1-tubulin is important for PPF and the maintenance of the platelet discoid shape.[143,151] Besides, also other isoforms play important roles in MKs and platelets as well. α4A-tubulin for example is similar to β1-tubulin upregulated during late cytoplasmic maturation and important for PPF.

Dynamic instability is the term which describes the steady state of MTs. The assembly of MTs can occur at both the plus- and minus-end, the latter showing faster dynamics.[152] Removal through hydrolysis of GTP bound to the β-subunit of the polymerized heterodimer results in MT depolymerization. A rapid depolymerization, termed 'catastrophe' is initiated if the MT tip (plus-end) contains a critical amount of *guanosine diphosphate* (GDP)-tubulin, a process which can be rescued upon the addition of new GTP-tubulin heterodimers.[153] The protein family of *end-binding proteins* (EB) is able to stabilize heterodimers as well as protofilaments, thus preventing rapid depolymerization upon GTP hydrolysis by binding the growing plus-end[154], while MT depolymerization is further promoted by proteins of the stathmin family, which additionally prevent heterodimer polymerization.[155]

Posttranslational modifications of tubulin, such as acetylation, detyrosination and polyglutamylation are critical determinants of MT stability and turnover.[156] The thrombocytopenia due to the missense mutations in the α4A-tubulin gene have been linked to altered tubulin modifications in mice and humans.[157]

### 1.5.2 Actin cytoskeleton

The actin cytoskeleton participates in a large variety of cellular processes such as maintenance of cell polarity, cytokinesis and adhesion to the ECM, cell motility, gene transcription, as well as phago- and exocytosis. While the role of actin in the cytoskeleton is well recognized, the field of nuclear actin dynamics remains largely unexplored and is just recently emerging.[158,159] Several recent studies demonstrated the formation of transient, *filamentous actin* (F-actin) structures inside somatic cell nuclei (nuclear F-actin) during serum response[160], DNA damage repair[161] and recently upon cell adhesion and integrin activation[162], or the regulation of mitosis.[163] In addition, several proteins, which have been primarily associated with actin dynamics, have also been linked to MTs, thus showing that the cytoskeleton components are regulating each other rather than operating in isolation.

Due to their appearance in electron microscopy, the polar structure of F-actin was defined and is characterized by a fast growing barbed end and a slow growing pointed end.[164] The generation of F-actin is driven by the non-covalently assembly of *globular actin* (G-actin) proteins into double helical F-actin filaments which are about 7 nm in diameter.[165,166] Thereby, exisiting F-actin filaments can also be depolymerized to replenish the G-actin pool which is used for the modulation of various processes such as the regulation of TFs.[133,134] In mammals three isoforms of G-actin have been identified: the mainly muscle specific α-actin and the ubiquitously expressed β- and γ-actin isoforms.[167] Due to differences in G-actin affinity, F-actin assembly mainly occurs at the barbed (+)-end, while it is predominantly depolymerized at pointed (-)-ends. G-actin monomers are able to bind *adenosine di-* (ADP) or *tri-phosphate* (ATP) in the presence of divalent cations such as calcium, while only the ATP-bound G-actin is assembled into the growing barbed end. However, the association of new subunits hydrolyzes ATP into ADP and phosphate, favoring the dissociation from the newly forming complex.[165]

Actin is also among the most highly expressed proteins in murine MKs and platelets (~ 15% of total protein pool), ranging between 50 – 200 µM.[168] The rapid changes in the F-actin network e.g. upon platelet activation or during PPF are controlled by *actin-binding proteins* (ABP) governing the control of guided depolymerization at the pointed end and assembly at the barbed ends. The regulation of the actin-binding proteins in turn is ensured by Rho GTPases.[41]

The actin sequestering protein *Thymosin β4* (Tβ4) e.g. has its main function in the binding of free actin monomers, thus inhibiting actin *de novo* polymerization. In contrast, Profilin-1 is able to bind G-actin and catalyze the nucleotide exchange from ADP to ATP, thus allowing *de novo* polymerization at the barbed end.[169,170] Profilin-1 deficiency in MKs resulted in a *Wiskott-Aldrich-Syndrome*(WAS)-like platelet defect with a moderate microthrombocytopenia, represented by smaller platelets and a lower platelet count. The underlying alterations are highlighted by a partially disrupted actin cytoskeleton and increased tubulin stability.[171]

Since the *de novo* polymerization of actin filaments is kinetically unfavored, it requires the involvement of one of the three major classes of actin nucleators: (i) The *actin-related protein* (Arp) 2/3 complex, (ii) spire, or (iii) the formin homology proteins. All three classes are capable of nucleating G-actin and are involved in the *de novo* polymerization of actin filaments, whereas they employ different mechanism to fulfill their task.

(i) Arp2/3 nucleates the assembly of actin filaments at the pointed end. For this, Arp2/3 binds to already existing actin filaments and nucleates branched actin networks. (ii) Spire also binds to the pointed end, but in contrast generates linear unbranched actin filaments.[172] The Arp2/3 complex is only functional upon binding of the nucleation promoting factor *Wiskott-Aldrich syndrome family protein* (WASp)[165] and the subsequent activation by Rho family GTPases. WASp is also constitutively associated with *WASp-interacting protein* (WIP).[173-175] Loss of the Arp2/3 complex in mice[176,177], as well as mutations in the *ARPC1B* or *WAS* gene in humans[178-180] lead to the WAS phenotype, an X-linked inherited disorder, displayed by microthrombocytopenia, immunodeficiency, eczema and an increased risk of autoimmune disorders and cancer.[181] The severe phenotype found in these patients highlights the importance of the actin cytoskeleton during PPF. Interestingly, WASp-deficient mice exhibited a reduced platelet count but normal platelet size, marked by a pre-mature platelet release into the BM compartment[177], thus only partially resembling the WAS phenotype. WIP-deficient mice or patients carrying a mutation in the WIP gene suffer from thrombocytopenia, partially caused by increased platelet clearance, but unaltered platelet size.[175,182,183] Of note, also the deletion of Arp2/3 or Profilin-1 leads to the abnormal and unpolarized release of MK fragments into the BM compartment of mice.[171,176]

(iii) The formin homology proteins are capable of nucleating linear actin filaments by binding to the barbed end. Additionally, many formins, e.g. *mammalian diaphanous* (mDia) 1 (DIAPH1) or *adenomatous polyposis coli* (APC), remain associated with the barbed end during filament elongation and can thereby prevent the binding of the depolymerizing *capping proteins* (CP), thus further accelerating Profilin-1-dependent actin polymerization.[184-186] mDia1-mediated F-actin dynamics as well as its modulation of MT dynamics have been shown to be important for PPF since its loss results in macrothrombocytopenia.[187,188]

In contrast, the actin depolymerization at pointed ends is mainly dependent on the actin-severing proteins *cofilin 1* (Cof1) and *actin-depolymerizing factor* (ADF). Cof1 binds to actin-filaments, induces a twist in the filament, which weakens lateral and longitudinal binding, but does not directly induce dissociation of G-actin monomers.[189,190] While constitutive deficiency of the ubiquitously expressed Cof1 is embryonic lethal, MK- and platelet-specific Cof1 / ADF double-deficient mice generated using the *(Pf4)-Cre* system exhibited severe macrothrombocytopenia due to virtually abolished PPF.[191] The activity of Cof1 is regulated by

*LIM kinase* (LIMK), which upon phosphorylation inhibits actin severing in the resting state. Interestingly, *Limk1* deficient mice show normal platelet counts, indicating that LIMK2 may be the isoform involved in the process of PPF.[192]

*Twinfilins* (Twf) also contain two ADF-H domains, which are thought to restrict binding to monomeric G-actin. Three Twf isoforms have been identified in mammals, but only Twf1 and Twf2a are present in murine MKs and platelets, where they have been associated in areas with high platelet turnover.[193,194] The importance of Twf2a during PPF has been revealed by the analysis of *Twf2a*$^{-/-}$ mice resulting in a mild macrothrombocytopenia as well as aberrant Cof1 and Profilin-1 phosphorylation.[195] *Twf1*$^{-/-}$ mice did not show any alterations as compared to *wild type* (WT) mice. However, actin / MT crosstalk during platelet biogenesis in mice is critically regulated by both Twf1 and Cof1 together, as evidenced by impaired PPF both *in vitro* and *vivo*, marked by aberrant F-actin distribution and increased MT stability in Tfw1 / Cof1 double-deficient MKs.[196] Another member of the ADF-H family is *Coactosin-like 1* (Cotl1) which binds actin and was also shown to enhance biosynthesis of pro-inflammatory leukotrienes in granulocytes. MK- and platelet-specific deletion of Cotl1, however, resulted in normal platelet counts, while its presence is critical for shear-dependent thrombus formation in mouse platelets.[197]

Besides the *de novo* synthesis of actin filaments, also their contraction and organization into bundles, such as stress fibers, are a prerequisite for cell movement. MK express two isoforms of myosin II: *Non-muscle myosin IIB* (NMMIIB, gene: *MYH10*) and NMMIIA (*MYH9*), with only the latter one being present in mature MKs. Both NMMIIA and NMMIIB are members of the myosinmotor superfamily of actin-binding / cross-linking proteins that exert contractile forces on the actin cytoskeleton via sliding and movement of actin filaments. The so-called actomyosin contractility is an important regulator of cytoskeletal reorganization, intracellular trafficking and cell locomotion.[198] NMMIIA and other family members consist of two heavy chains (230 kDa), two *regulatory light chains* (RLCs; 20 kDa) important for the regulation of NMMIIA activity and two structure-stabilizing *essential light chains* (ELCs; 17 kDa).[199] Spatial-temporal regulation of NMMIIA and NMMIIB is e.g. essential during the process of endomitosis.[200] *MYH9-related disorder* (MYH9-RD) patients suffer from mutations in the *Non-muscle myosin heavy chain 9 (MYH9).* MYH9-RD is associated with macrothrombocytopenia, moderate bleeding complications and reduced PPF of *in vitro* cultured human MKs of these patients.[201,202] Key features of MYH9-RD patients are recapitulated in *knock-in* (KI) mice carrying point mutations in the *Myh9* gene.[201] Moreover, MYH9-deficient mice largely recapitulate these phenotypes as well, but show increased PPF of BM-derived MKs *in vitro.*[203]

Studies on the platelet cytoskeleton also indicated, that the actin filaments of the resting platelet are cross-linked at various points into a rigid cytoplasmic network, mainly via *filamin* (Fln) and α-actinin.[204,205] Fln is a scaffolding protein that draws binding partners and is able to arrange them closely to the plasma membrane.[206,207] Filamin is also known to bind the Rho GTPases *Ras-related protein A* (RalA), *Ras-related C3 botulinum toxin substrate 1* (Rac1), Rho, and *Cell division control protein 42* (Cdc42) or kinases such as *P21 (Rac1) Activated Kinase 1* (PAK1).[208,209] Three isoforms of Fln genes on chromsomes 3, 5, and X exist. *Filamin A* (FlnA, X-chromosomal) is among the highest expressed in MKs and platelets, with a tenfold excess compared to *Filamin B* (FlnB).[210] Critical to the structural organization of FlnA is the binding to the cytoplasmic tail of GPIbα, which together with GPIbβ, GPIX and GPV subunits forms the GPIb-IX-V complex. Additional parallel binding to actin is important for aligning the GPIb-V-IX complex into rows on the surface of the cell, allowing the simultaneous positioning of associated binding partner at the membrane.[209] In summary, the FlnA-GPIbα linkage not only regulates platelet size but also maintains the mechanical stability of the platelet plasma membrane. Loss of FlnA in mice leads to a severe macrothrombocytopenia, with large and fragile premature platelet release and increased bleeding times[211,212], similar to the BSS-like phenotype in GPIbα/β-null mice.[213,214] The other isoform present in MKs and platelets, FlnB, does not appear to compensate for the loss of FlnA.[215,216] *ACTN1* encodes α-actinin-1, a member of the actin-crosslinking protein superfamily that participates in the organization of the cytoskeleton. Transduction of mouse FLC-derived MKs with disease-associated *ACTN1* variants caused a disorganized actin-based cytoskeleton in MKs, resulting in the production of abnormally large proplatelet tips, which were reduced in number.[217] ACTN1 mutations in patients cause congenital macrothrombocytopenia.[217-219]

### 1.5.3 The role of the MK cytoskeleton during proplatelet formation

The cytoskeleton is important in preserving the discoid shape of the mature and resting platelet and also key for the activation-mediated shape change of platelets. The same cytoskeleton is essential for the morphological changes associated with the maturation of MKs, and subsequent, the production of platelets. The actin cytoskeleton is also key for unperturbed maturation of the DMS, by providing mechanical forces that drive DMS invaginations at the plasma membrane.[39]

*In vitro*, after protrusion formation started, the extension of proplatelets is depending on MT-based forces. Treatment of MKs with MT disassembling drugs, e.g. vincristine and nocodazole, prevents PPF and proplatelet extension.[220] Immature MKs that have not yet undergone PPF, show MT extensions from the cell center to the cortex. In the early stages of PPF *in vitro*, the membrane-associated and cortical MTs merge into thick bundles. Once the MK starts with the pseudopodia formation, MTs form thick linear arrays that run along the whole length of the proplatelet processes. The bundlers are thicker closest to the MK cell body while they are displaying fine thin structures of about seven bundles near proplatelet ends. The distal end always contains a platelet-sized bead (proplatelet tip), containing a looping MT bundle, that reenters the proplatelet shaft and shows typical characteristics of the MT coil observed in resting platelets, thus assuming that mature platelets are assembled principally at the ends of proplatelets, and not in the typical swellings of the proplatelet extensions ('beads-on-a-string').[221] Furthermore, the elongation of the proplatelet extensions *in vitro* does not occur continuously, but includes pausing and retraction of the growing protrusions. This process involves MT sliding controlled by dynein motors rather than *de novo* polymerization.[222] Besides, the elongation process is also necessary for the transport of granules and mitochondria into the emerging platelets, a process dependent on the motor protein kinesin.[223]

The mechanisms of PPF per se, however, seem to differ between *in vivo* and the above-mentioned *in vitro* conditions. *In vivo*, MKs differentiate in a complex environment, while being constantly in touch with extracellular factors. Furthermore, they need to penetrate the endothelial barrier to reach the circulation in order to release their proplatelet extensions.[59] The molecular mechanisms that ensure initial MK protrusion through the endothelial lining are not known. The formation of podosomes, actin rich structures, heavily relies on the Arp2/3 complex. *In vivo*, the lack of Arp2/3 has been associated with undirected proplatet release into the BM cavity, indicating that podosomes are involved in the degradation of ECM proteins in order to allow for directed proplatelet elongation / protrusion formation into vessel sinusoids.[224,225] Recent studies in our department have also shown pre-mature platelet release and impaired podosome formation from MKs in mice lacking the actin-regulatory *adapter protein* (ADAP), potentially downstream of Cdc42, thus suggesting podosomes to be of significant importance for PPF.[226] Once inside the sinusoid, these protrusions seem to form actin-rich anchor points at the luminal side of the endothelial cells, which could help the proplatelet to extend into the circulation.[60,64,227] Such actin-rich podosome-like protrusions were also recently visualized *in situ* in the BM of mice, able to deform the underlying endothelial cells while most MKs enter the sinusoidal space as large protrusions rather than extruding fine proplatelet extensions.[61,225] Thereby, the proplatelets elongate by several hundred micrometers, associated with constant fusion of the DMS with the plasma membrane.[61] Moreover, the MT organization of growing proplatelets seems to differ *in vivo*, while being rather heterogeneously distributed, than showing dense linear bundles of MTs.[60,61] Recent studies have also shown, that the equilibrium between the protrusive as well as pausing and retraction of the growing protrusion[222] is mediated by NMMIIA in mice, while MTs appeared to be less critical *in vivo* as initially thought, assuming that the blood Stokes' forces may be sufficient to promote proplatelet extension.[60] These findings were based on the fact, that Myh9-deficient mice still showed proplatelet extensions within the sinusoids, but being longer and thinner, without any signs of pause and retraction. In addition, treatment of *WT* mice with the tubulin depolymerizing drug vincristine led to rapid shrinkage of pre-existing proplatelet extensions, which was not true for Myh9-deficient mice.

Thus, this new theory might also explain why depletion or mutations of β1-tubulin or α4a-tubulin result in severely affected PPF *in vitro*, but only a moderate decrease in platelet count as well as impressively functional PPF *in vivo*. The loss of β1-tubulin, however, rather resulted in a decrease in the number of MKs showing *de novo* platelet extensions.[60,157] The process determining how many platelets can be released per MK, the proplatelet branching, is guided by NMMIIA and the actin cytoskeleton.[228] Whether the MT-based mechanisms decribed for *in* vitro PPF might still play a role during proplatelet remodeling in the microcirculation, remains to be clarified. A summary of the current findings is given in Figure 5.

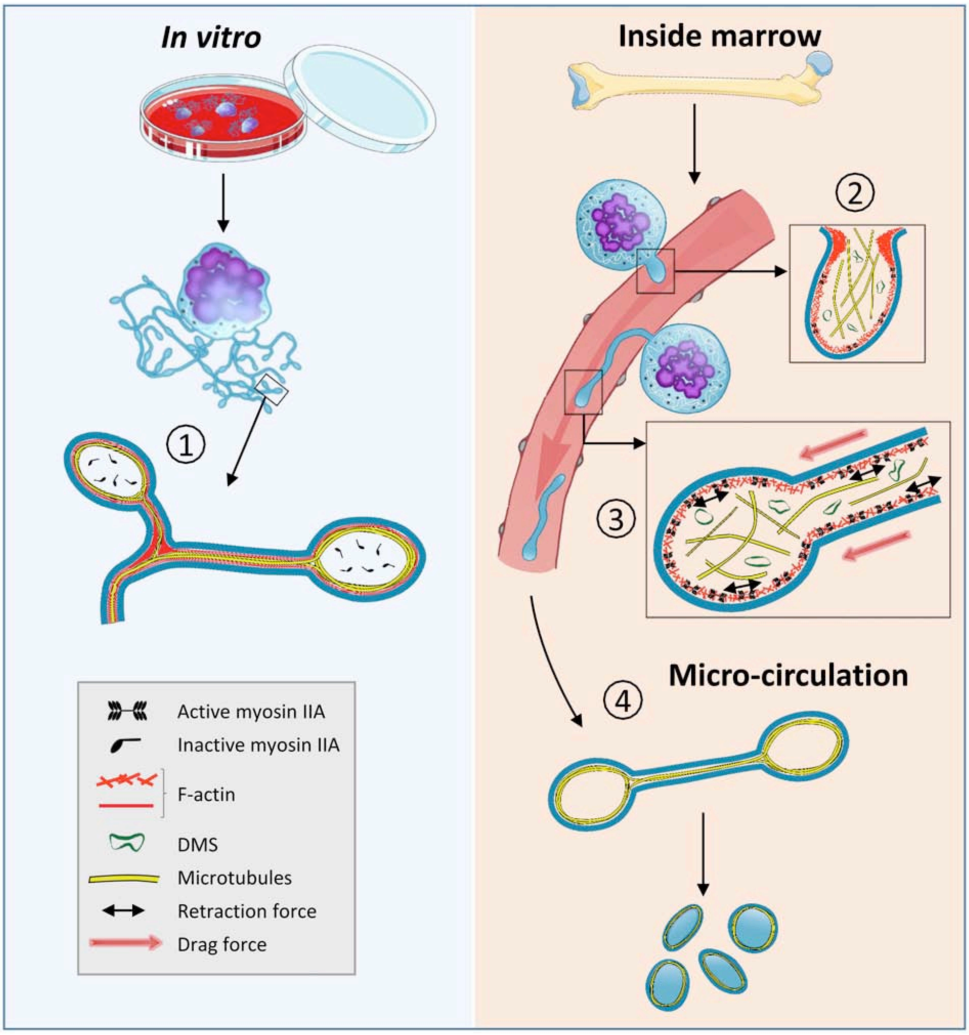

**Figure 5: The proposed model depicting the cytoskeletal-based differences between *in vivo* and in *vitro* PPF. (Left)** For proplatelets generated *in vitro*, initiation and elongation depend entirely on the MT cytoskeleton organized as linear bundles along the proplatelet shafts and ending as a coil (1), already prefiguring the marginal band of the future platelets, while F-actin would promote branching. **(Right)** *In vivo*, the initiation of PPF takes place in the marrow and depends on both the actin and the MT cytoskeleton (2). During proplatelet elongation / extension into the sinusoid circulation, MTs do not form a unique bundle but are mostly isolated and play a critical role to counteract myosin-based proplatelet retraction (3), while blood Stoke's forces contribute to the protrusive forces. The released elongated proplatelet fragments will further remodel in the downstream microcirculation to give the final circulating platelets, possibly through MT-based mechanisms similar to those *in vitro* (4). The figure was taken from Bornert *et al.*, **Haematologica,** 2020.[60]

## 1.6 Rho GTPases in megakaryopoiesis and thrombopoiesis

### 1.6.1 Small GTPases of the Rho family

Mammalian Rho GTPases comprise a family of 20 proteins which belong to the Ras superfamily of monomeric 20-25 kDa GTP-binding proteins. Rho GTPases govern several cellular processes, including cytoskeletal rearrangements, regulation of gene expression, vesicle trafficking, cell cycle progression, cell morphogenesis, polarity and migration, as well as pathological processes such as progression of inflammation and cancer.[229,230] Rho GTPases cycle between a GTP-bound (active) and a GDP-bound (inactive) state, a dynamic process which is regulated by three sets of proteins: (i) *Guanine nucleotide-exchange factors* (GEFs) promote the exchange of GDP to GTP, hence leading to activation. (ii) Accelerated hydrolysis of GTP to GDP by *GTPase-activating proteins* (GAPs) leads to inhibition of the Rho GTPases and (iii) *Guanine nucleotide-dissociation inhibitors* (GDIs) prevent spontaneous activation by sequestering GDP-bound Rho GTPases away from regulators and target proteins.[229,231] In the active conformation, Rho GTPases modulate a plethora of processes via downstream effector proteins, including vesicle transport, MT dynamics, actin dynamics, adhesion and migration.

The Rho GTPases can be divided into different members, including the most important members for thrombopoiesis in the following part: The Rac subfamily comprises Rac1, Rac2 and Rac3 and RhoG. Rac1 activates the *WASP-family verprolin-homologous protein* (WAVE) regulatory complex of the WASp family to drive Arp2/3 complex-mediated actin polymerization and has primarily been described to stimulate actin-based lamellipodia and membrane ruffle formation. The Cdc42 subfamily, namely Cdc42, RhoQ and RhoJ, have all been associated with filopodia formation. Active Cdc42 induces activation of WASp, thereby initiating the formation of parallel actin bundles. Cdc42 has been described to mediate filopodia formation in various cell types. PAKs are activated upon Rac and Cdc42 binding and induce formation of lamellipodia, filopodia, membrane ruffles and stress fibers via their effectors, the LIMKs. Note that Cdc42 deficiency was also associated with decreased platelet filopodia formation on vWF *in vitro*, suggesting a unique role of Cdc42 downstream of the vWF receptor complex GPIb-V-IX.[232] The Rho subfamily members RhoA, RhoB and RhoC are structurally highly homologous, but have different cellular functions. RhoA directly stimulates actin polymerization through diaphanous-related formins, while *Rho-associated coiled-coil containing protein kinase* (ROCK) proteins regulate myosin II activity. Of note, myosin II activity and LIMK-induced actin remodeling is also regulated via Cdc42 and *myotonic dystrophy kinase-related Cdc42-binding kinases* (MRCKs).[233] Further, Rho proteins play important roles in turnover of cell–ECM adhesions as well as in cell shape and polarity. An overview is given in Figure 6.

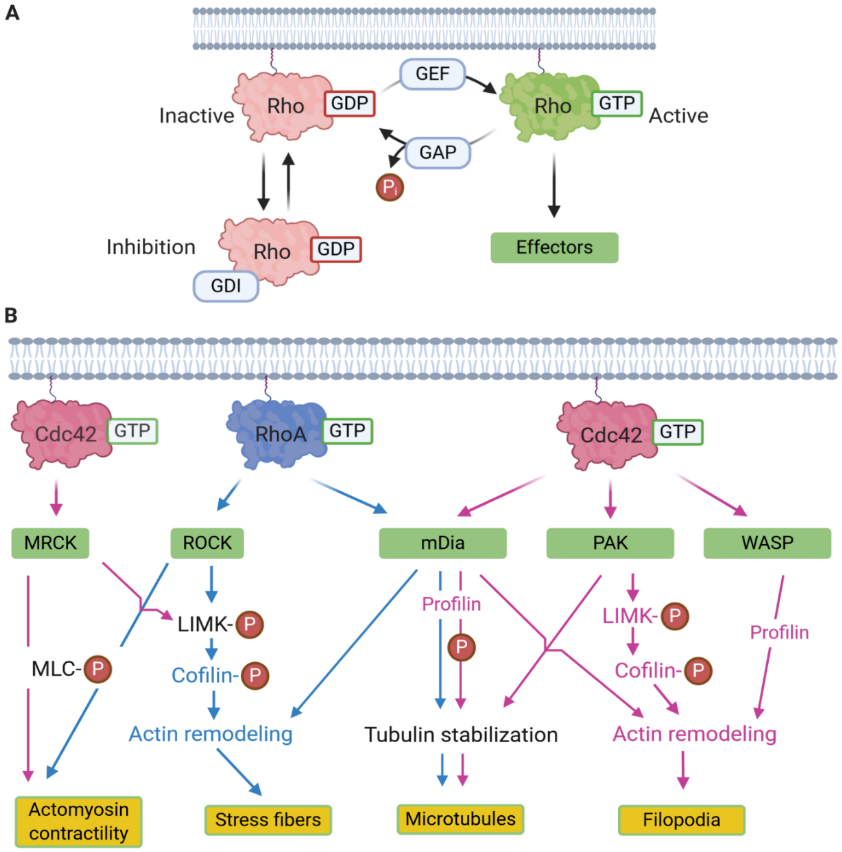

**Figure 6: The Rho GTPase cycle and signal transduction pathways. A** Activation and regulation of Rho GTPases. Rho GTPases cycle between an inactive, GDP-bound, and an active, GTP-bound, state in which they can interact with effector molecules. GEFs mediate the exchange of GDP to GTP. GAPs trigger the hydrolysis of Rho GTP to GDP and thus inhibit Rho GTPase activation. GDIs induce sequestering of Rho proteins away from regulators and target proteins and thus prevent interactions. **B** Overview of common and diverging signaling pathways of RhoA and Cdc42 in the regulation of cytoskeletal rearrangements. GEFs, guanine nucleotide-exchange factors; GAPs, *GTPase-activating proteins*; GDIs, *guanine nucleotide-dissociation inhibitors*; RhoA, *Ras homolog gene family member A*; Cdc42, *cell division control protein 42 homolog*; ROCK, *Rho-associated protein kinase*; MLC2, *myosin light chain 2*; MRCK, *myotonic dystrophy-related Cdc42-binding kinases*; LIMK, *LIM domain kinase*; PAK, *p21-activated kinase*; mDia, *mammalian diaphanous*; WASp, *Wiskott-Aldrich syndrome protein*. Figure created with **Biorender.com**.

### 1.6.2 Conditional knockout mouse models

The use of tissue-or lineage-specific deletion in mice to study the protein members of the Rho GTPases is unavoidable, since constitutive KOs of these highly conserved proteins result in embryonic lethality. The development of the *Pf4-Cre* transgenic mouse line time allowed the generation of conditional KOs restricted to the MK lineage for the first time[234] and greatly advanced the research of MK biology, enabling the investigation of the complex signaling mechanisms during the different stages from MK maturation to platelet release and function, both *in vitro* and *in vivo.*[235]

Recent studies, however, have also reported that the *Pf4-Cre* does not only recombine in MKs but also in a small subset of stem and progenitor cells and all their developing progenies, especially immune cells. Thus, certain conclusions drawn by using the *Pf4-Cre* system must also be interpreted with caution, especially when analyzing platelet-immune cell interactions.[236,237] To overcome these issues, a *Gp1ba-Cre* transgenic mouse model has been introduced. To allow for a more stringent MK lineage-specific expression of the *Gp1ba-Cre* transgene compared to the *Pf4-Cre* system, a constitutive KI of a T2A-improved-Cre has been inserted into the endogenous *Gp1ba* locus to drive Cre recombinase expression.[238] Whether the *Gp1ba-Cre* transgenic mouse model is suitable to study the role of the highly conserved Rho GTPases family in MK and platelet biology remains to be identified by comparing both the *Gp1ba-Cre* and *Pf4-Cre* transgenic mouse models. Furthermore, the implications of the reduced GPIbα expression (33%), due to the *Gp1ba-Cre* targeted insertion strategy[238] in MK and platelet biology *per se* remains to be clarified as well.

### 1.6.3 Elucidating the role of RhoA/Cdc42 during platelet biogenesis

Using *Pf4-Cre* conditional MK- and platelet-specific KO mouse models, we have previously shown that members of the Rho GTPase family play critical roles in platelet biogenesis and function. Cdc42, RhoA and Rac1 are among the best-characterized Rho GTPases in MKs and platelets.[41,239] Rac1 seems to have non-essential roles in MK function, but double-deficiency in the Rho GTPases Rac1 and Cdc42 affects MT stability and results in a severe macrothrombocytopenia.[240] This is to some part regulated by mDia1 and APC, both involved in the process of nucleating actin fibers, but also in stabilizing MTs by interacting with the plusend associated EB1.[188,241]

RhoA and Cdc42 have turned out as key regulators in platelet biogenesis. The underlying mechanisms, however, are only partially understood. MK-specific ablation of Cdc42 in mice was shown to result in macrothrombocytopenia and impaired platelet integrin activation, but increased platelet granule secretion.[232] This was associated with a decreased capacity of mutant fetal liver cell-derived MKs to form proplatelets *in vitro.*[240] Accordingly, *in vitro* inhibitor studies using CD34$^+$ cell-derived human MKs revealed that Cdc42 positively regulates DMS formation / polarization and PPF, by modulating actin dynamics.[242] The importance of Cdc42 driven F-actin dynamics during DMS biogenesis was also demonstrated by the inhibition of Cdc42 or Pak1/2/3 in murine MKs *in vitro.*[39] Interestingly, MK ploidy was not affected, indicating that Cdc42 is not essential for the endomitotic process and only partially during MK maturation.[240]

*In vitro* studies indicated that RhoA acts as a negative regulator of PPF. Overexpression of an active RhoA resulted in decreased PPF while Rho/ROCK inhibition increased PPF.[243,244] Contradictory, mice with MK-specific RhoA deficiency display a macrothrombocytopenia.[245,246] Accordingly, as mentioned before, mutations in the genes encoding the RhoA downstream effectors DIA1 (*DIAPH1*) and NMMIIA *(MYH9)* cause thrombocytopenia in humans as well as in corresponding mouse models in the case of NMMIIA.[187,188,201,247]

Furthermore, the Rho/ROCK signaling upstream of myosin II is important for inducing actomyosin contraction, necessary to complete cytokinesis.[248] Here, RhoA is the main regulator of cleavage furrow formation and ingression, permitting the formation of an actomyosin ring necessary to generate the contractile forces for cell separation. This is done via local induction of F-actin at the cleavage furrow, as well as accumulation and activation of myosin II, allowing progression of the furrow and to permit abscission. Differential regulation of NMMIIA and NMMIIB at the cleavage furrow is important for the process of endomitosis.Hence, downregulation of RhoA activity and accumulation of NMMIIB, but not NMMIIA at the cleavage furrow is required for the initiation of endomitosis.[200,249] Subsequent downregulation of NMIIB expression by RUNX1 facilitates progression of endomitosis and polyploidization.[200,250] In line with the required downregulation of RhoA and subsequently NMMIIA activity to initiate endomitosis, mice deficient for RhoA in the MK and plateletlineage using the *Pf4-Cre* system show unaltered endomotosis with even increased proportions of BM MKs with high ploidy.[245] MK morphology, ultrastructure and DMS formation was rather unaffected, thus assuming that RhoA deficiency is not required for MK maturation.[246,251]

A striking observation was made in RhoA-deficient mice, marked by the frequent transmigration of entire MKs into BM sinusoids *in vivo,* which was associated with increased Cdc42 activity. The transmigration phenotype in RhoA-deficient mice was reverted either upon concomitant ablation of Cdc42 or to some extend upon functional blockage of the MK-specific mechanoreceptor GPIb.[251] Interestingly, *intravital two-photon microscopy* (2P-IVM) of *RhoA*$^{-/-}$ mice revealed partly comparable *in vivo* defects as seen in the Myh9-deficient mice by forming longer and thinner protrusions. However, the rather increased PPF observed *in vivo*, the transmigration of whole MKs, as well as the release of large proplatelet-like fragments in *RhoA*$^{-/-}$ mice suggests additional alterations.[60,251] These findings in summary demonstrated that RhoA and Cdc42 are key players in a regulatory circuit that controls MK localization and polarization at BM sinusoids *in vivo* (Figure 7). We furthermore made the observation that RhoA/Cdc42 double-knockout (*DKO*) mice exhibit a severe macrothrombocytopenia and impaired PPF *in vivo*.[251] The mechanisms underlying these pronounced defects were investigated in this thesis.

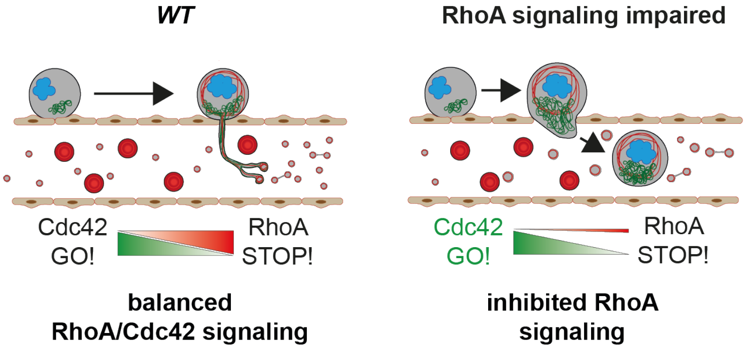

**Figure 7: Model of the RhoA/Cdc42 regulatory circuit controlling PPF.** MK polarization is a prerequisite for directed proplatelet release into sinusoidal vessels, a process driven by locally active Cdc42 (left panel). In the absence of RhoA (right panel), Cdc42 activity is locally increased resulting in hyperpolarized MKs entirely transmigrating through the endothelial barrier into sinusoidal vessels. Modified from Dütting *et al.*, **Nat. Commun.**, 2017.[251]

# 2 AIM OF THE STUDY

Megakaryopoiesis and thrombopoiesis require an extensive crosstalk and regulation of the MK cytoskeleton. The detailed molecular cues how the RhoA/Cdc42 regulatory circuit controls the cytoskeletal dynamics and transendothelial PPF remain elusive. To allow for further detailed investigations on the role of the Rho GTPases RhoA and Cdc42 in murine MK biology, the following studies required the extensive use of *in vitro* BM-derived MK cultures. The harvest of murine BM HSCs and their differentiation towards the MK lineage are not only time consuming and costly, but also come along with limitations in sample size and a high need of mice. Therefore, in the first part of this thesis, we compared the classical flush isolation with a previously described centrifugation-based spin isolation in terms of cell yield, harvest time and the suitability for the analysis of immune cells and HSCs, as well as MK-related *in vitro* assays.

The loss of RhoA in MKs leads to the transmigration of entire MKs into the BM sinusoids. Mice with a concomitant lack of Cdc42 showed a reversion of this MK localization defect, but at the same time displayed a severely increased macrothrombocytopenia compared to the single-deficient mice. The mechanisms underlying this severe defect upon loss of RhoA/Cdc42 signaling remained elusive and were in detail investigated in the second part of this thesis.

Besides the mechanoreceptor GPIbα, several other receptors regulating PPF have been proposed, such as their binding of soluble factors or their interaction with the ECM in the BM. Recent work at our department has especially highlighted the interaction of MKs with collagen type I and IV, mediated by an interplay of the collagen-binding receptor α2β1 and GPVI. Mice deficient in α2 and/or GPVI, however, did not show any alterations in platelet count, but the role of other β1 integrins (e.g. α5β1, and α6β1) in this process have not been fully elucidated yet. Further, light has been shed on the role of the ITIM-containing receptor G6b-B by unravelling its interaction with the highly abundant sinusoidal HS perlecan. Therefore, in the third part of this thesis, the role of these receptors and their potential interplay with the small GTPase RhoA were further investigated. Mice double-deficient in RhoA and integrin β1 (*RhoA/Itgb1*$^{-/-}$*)*, the intracellular β-integrin outside-in signaling activator Talin-1 (*RhoA/Talin-1*$^{-/-}$*)* - to decipher the role of integrin activation per se, as well as the ITIM-containing receptor G6b-B (*RhoA/G6b*$^{-/-}$*)* were generated and MK biology was analyzed, particularly in the context of transendothelial migration of RhoA-deficient MKs. BM transplantation studies were carried out to address whether the localization defects observed in RhoA-deficient mice using the *Pf4-Cre* system are potentially due to off-target effects.

The last part of the thesis deals with the comparison of *Pf4-Cre-* and *Gp1ba-Cre*-mediated deletion of RhoA, to further decipher its role during megakaryopoiesis and thrombopoiesis as well as platelet function.

# 3 MATERIALS AND METHODS

## 3.1 Materials

### 3.1.1 Chemicals and reagents

| Name | Company |
|---|---|
| *4',6-diamidino-2-phenylindole* (DAPI) | ThermoFisher Scientific (Waltham, USA) |
| ABT-737 (pan-Bcl-2 inhibitor) | MedChemExpress LLC (Monmouth Junction, USA) |
| *Adenosine diphosphate* (ADP) | Merck Millipore / Sigma-Aldrich (Steinheim, Germany) |
| *Adenosine triphosphate* (ATP) | Fermentas (St. Leon-Rot, Germany) |
| Agarose | Roth (Karlsruhe, Germany) |
| Amersham Hybond P 0.45 *Polyvinylidene fluoride* (PVDF) blotting membrane | Merck Millipore / Sigma-Aldrich (Steinheim, Germany) |
| Amersham Protran 0.45 nitrocellulose blotting membrane | Merck Millipore / Sigma-Aldrich (Steinheim, Germany) |
| *Ammonium peroxodisulfate* (APS) | Roth (Karlsruhe, Germany) |
| Aprotinin | Merck Millipore / Sigma-Aldrich (Steinheim, Germany) |
| Apyrase (grade III) | Merck Millipore / Sigma-Aldrich (Steinheim, Germany) |
| BlueBlock PF (10x) | SERVA Electrophoresis GmbH (Heidelberg, Germany) |
| *Bovine serum albumin* (BSA) fraction V | Merck Millipore / Sigma-Aldrich (Steinheim, Germany) |
| BSA low endotoxin | PAN-Biotech GmbH (Aidenbach, Germany) |
| Cacodylate | AppliChem (Darmstadt, Germany) |
| Calcium chloride | Roth (Karlsruhe, Germany) |
| Cell Clean | Sysmex Europe (Norderstedt, Germany) |
| Clodronate | Clodronate Liposomes (Haarlem, Netherlands) |
| Collagen Horm® suspension + SKF sol. | Takeda (Linz, Austria) |
| Complete protease inhibitors (+EDTA) | Roche Diagnostics (Mannheim, Germany) |
| *Convulxin* (CVX) | Enzo Life Sciences (New York, USA) |
| *Deoxynucleotide triphosphates* (dNTP) mix | Life Technologies (Darmstadt, Germany) |
| Dimethyl sulfoxide (DMSO) | Merck Millipore / Sigma-Aldrich (Steinheim, Germany) |
| DirectPCR Lysis Reagent (Mouse Tail) | Viagen Biotech (Los Angeles, USA) |
| DreamTaq DNA Polymerase (5 U L-1) | Life Technologies (Darmstadt, Germany) |
| DreamTaq Green PCR Master Mix, 2x | Life Technologies (Darmstadt, Germany) |
| Dulbecco's *phosphate-buffered saline* (DPBS) | Gibco (Karlsruhe, Germany) |
| Dulbecco´s *Modified Eagle´s Medium* (DMEM) GlutaMAX | Gibco (Karlsruhe, Germany) |
| DyLight-488 | Pierce (Rockford, USA) |
| EDTA | AppliChem (Darmstadt, Germany) |
| Eosin | Roth (Karlsruhe, Germany) |
| Ethanol | Roth (Karlsruhe, Germany) |
| *Ethylenediaminetetraacetic acid* (EDTA) | AppliChem (Darmstadt, Germany) |
| Eukitt® quick-hardening mounting medium | Merck Millipore / Sigma-Aldrich (Steinheim, Germany) |
| FeCl3·6 H2O | Roth (Karlsruhe, Germany) |
| Fentanyl | Janssen-Cilag GmbH (Neuss, Germany) |
| *Fetal calf serum* (FCS) | Perbio (Bonn, Germany) |
| Fibrinogen | Merck Millipore / Sigma-Aldrich (Steinheim, Germany) |
| Fibrinogen from human plasma (#F3879) | Merck Millipore / Sigma-Aldrich (Steinheim, Germany) |

| | |
|---|---|
| Fibronectin | Merck Millipore / Sigma-Aldrich (Steinheim, Germany) |
| *Fluorescein isothiocyanate* (FITC) | EUROPA (Cambridge, UK) |
| Fluoroshield™ | Merck Millipore / Sigma-Aldrich (Steinheim, Germany) |
| Fluorshield™ with DAPI | Merck Millipore / Sigma-Aldrich (Steinheim, Germany) |
| Forene® (Isoflurane) | Abott (Wiesbaden, Germany) |
| GeneRuler DNA Ladder Mix | Fermentas (St. Leon-Rot, Germany) |
| Glucose | Roth (Karlsruhe, Germany) |
| Glutaraldehyde solution (25%) | Science Services (Munich, Germany) |
| Glycine | AppliChem (Darmstadt, Germany) |
| Halt™ Protease and Phosphatase Inhibitor Cocktail (100x) | ThermoFisher Scientific (Waltham, USA) |
| *Hank's Balanced Salt Solution* (HBSS) solution (1x) (#H8264) | Merck Millipore / Sigma-Aldrich (Steinheim, Germany) |
| HEPES | Roth (Karlsruhe, Germany) |
| High molecular weight heparin | Ratiopharm (Ulm, Germany) |
| Igepal®CA-630 | Merck Millipore / Sigma-Aldrich (Steinheim, Germany) |
| Isofluran CP® | cp-pharma (Burgdorf, Germany) |
| Isopropanol | Roth (Karlsruhe, Germany) |
| iTaq Universal SYBR Green Supermix | Bio-Rad (Hercules, USA) |
| Leupeptin | Merck Millipore / Sigma-Aldrich (Steinheim, Germany) |
| Magnesium chloride | Roth (Karlsruhe, Germany) |
| Magnesium sulfate | Roth (Karlsruhe, Germany) |
| Manganese chloride | Roth (Karlsruhe, Germany) |
| Medetomidine (Dormitor) | Pfizer (Karlsruhe, Germany) |
| MEM Essential amino acids (50x) #11130 | Gibco (Karlsruhe, Germany) |
| MEM Non-essential amino acids (100x) #11140 | Gibco (Karlsruhe, Germany) |
| Membrane Amersham Hybond 0,45 µM PVDF | VWR (Darmstadt, Germany) |
| Methanol | Roth (Karlsruhe, Germany) |
| Midazolam (Dormicum) | Roche (Grenzach-Wyhlen, Germany) |
| Midori Green™ | Biozym Scientific (Oldenburg, Germany) |
| Neuraminidase (Sialidase) | Roche Diagnostics (Mannheim, Germany) |
| Nonidet P-40 (NP-40) | Roche Diagnostics (Mannheim, Germany) |
| Osmium tetroxide | Merck Millipore (Darmstadt, Germany) |
| PageRuler® Plus Prestained Protein Ladder | Fermentas (St. Leon-Rot, Germany) |
| PageRuler® Prestained Protein Ladder | Fermentas (St. Leon-Rot, Germany) |
| *Paraformaldehyde* (PFA) | Merck Millipore / Sigma-Aldrich (Steinheim, Germany) |
| *Penicillin/Streptomycin* (P/S) | Gibco (Karlsruhe, Germany) |
| Pepstatin | Roche Diagnostics (Mannheim, Germany) |
| Phalloidin-*Alexa Flour* (AF)647 (#A22287) | ThermoFisher Scientific (Waltham, USA) |
| Phalloidin-Atto647N | Merck Millipore / Sigma-Aldrich (Steinheim, Germany) |
| *Piperazine-N,N'-bis(2-ethanesulfonic acid)* (PIPES) | Roth (Karlsruhe, Germany) |
| *Phenylmethylsulfonyl fluoride* (PMSF) | Merck Millipore / Sigma-Aldrich (Steinheim, Germany) |
| *Poly-L-lysine* (PLL) 0.1% solution | Merck Millipore / Sigma-Aldrich (Steinheim, Germany) |
| Potassium chloride (KCl) | Roth (Karlsruhe, Germany) |
| *Propidium iodide* (PI) | ThermoFisher Scientific (Waltham, USA) |
| *Prostaglandine 2* ($PGI_2$) | Sigma (Deisenhofen, Germany) |
| Protease Inhibitor Cocktail | Merck Millipore / Sigma-Aldrich (Steinheim, Germany) |
| Proteinase K | Fermentas (St. Leon-Rot, Germany) |
| *R-phycoerythrin* (PE) | EUROPA (Cambridge, UK) |
| *Recombinant hirudin* (rHirudin) | Hyphen Biomed (Neuville-sur-Oise, France) |

| | |
|---|---|
| Recombinant mouse *stem cell factor* (SCF) | BioLegend (San Diego, USA) |
| RIPA Lysis Buffer, 10x | Cell Signaling (Denver, USA) |
| RNase A | ThermoFisher Scientific (Waltham, USA) |
| Rotiphorese Gel 30% (PAA) | Roth (Karlsruhe, Germany) |
| Sodium azide | Merck Millipore / Sigma-Aldrich (Steinheim, Germany) |
| Sodium cacodylate | Roth (Karlsruhe, Germany) |
| Sodium chloride | AppliChem (Darmstadt, Germany) |
| Sodium citrate | AppliChem (Darmstadt, Germany) |
| *Sodium dodecyl sulfate* (SDS) | Merck Millipore / Sigma-Aldrich (Steinheim, Germany) |
| Sodium hydrogencarbonate | Roth (Karlsruhe, Germany) |
| Sodium hydroxide | AppliChem (Darmstadt, Germany) |
| Sodium orthovanadate | Merck Millipore / Sigma-Aldrich (Steinheim, Germany) |
| Sodium-Di-HydrogenPhosphate Monohydrate ($NaH_2PO_4$) | Roth (Karlsruhe, Germany) |
| Sodium(meta)periodate | Sigma Aldrich (Steinheim, Germany) |
| StemPro®-34 | Gibco (Karlsruhe, Germany) |
| Sucrose | Merck Millipore / Sigma-Aldrich (Steinheim, Germany) |
| Sulfonic acid, 2N | AppliChem (Darmstadt, Germany) |
| *Super cryo embedding medium* (SCEM) | Section Lab Co Ltd. (Hiroshima, Japan) |
| SYTOX™ Orange Nucleic Acid Stain | ThermoFisher Scientific (Waltham, USA) |
| *Tetramethylethylenediamine* (TEMED) | Roth (Karlsruhe, Germany) |
| Thrombin from human plasma (#10602400001) | Roche Diagnostics (Mannheim, Germany) |
| Tissue-Tek® O.C.T.™ Compound | Sakura. (AJ Alphen aan denRijn, Netherlands) |
| TPO (recombinant) | Homemade; Villeval *et al.*, 1997[252] |
| TRIS ultra | Roth (Karlsruhe, Germany) |
| *Tris(hydroxymethyl)aminomethane* (TRIS) | Roth (Karlsruhe, Germany) |
| Tris/HCl | Roth (Karlsruhe, Germany) |
| Triton X-100 | Merck Millipore / Sigma-Aldrich (Steinheim, Germany) |
| TRIzol® | ThermoFisher Scientific (Waltham, USA) |
| Trypan Blue | Merck Millipore / Sigma-Aldrich (Steinheim, Germany) |
| Tween 20® | Roth (Karlsruhe, Germany) |
| U46619 | Alexis Biochemicals (San Diego, USA) |
| Uranyl acetate | EMS (Hatfield, USA) |
| Vectashield hardset mounting medium | Vector Labs, Inc. (Burlingame, USA) |
| Water, nuclease-free | Roth (Karlsruhe, Germany) |
| Western Lightning Chemiluminescence (*Enhanced chemiluminescence* (ECL)) | PerkinElmer LAS (Boston, USA) |
| β-mercaptoethanol | Roth (Karlsruhe, Germany) |

### 3.1.2 Consumables

| **Name** | **Manufacturer** |
|---|---|
| pluriStrainer Mini 70 µm | PluriSelect (Leipzig, Germany) |
| 6/12/24/48/96-well plates | Greiner (Frickenhausen, Germany) or Sarstedt |
| Falcon® 96-well Clear Flat Bottom TC-treated Culture Microplate | Corning (Corning, USA) |
| Cryofilm type 3C (16UF) | Section Lab Co Ltd. (Hiroshima, Japan) |
| Cryofilm type 2C (10) | Section Lab Co Ltd. (Hiroshima, Japan) |

| | |
|---|---|
| Tissue-Tek® Cryomold® | Sakura. (AJ Alphen aan denRijn, Netherlands) |
| 18 G, 20 G, 22 G, 25 G canula | BD Biosciences (Heidelberg, Germany) |
| Glass slide superfrost, | Roth (Karlsruhe, Germany) |
| Heparinized capillaries | Hartenstein (Würzburg, Germany) |
| Microcapillaries (100 µl) | Hartenstein (Würzburg, Germany) |
| Microcapillaries (50 µl) | Hartenstein (Würzburg, Germany) |

### 3.1.3 Commercial Kits

| **Name** | **Manufacturer** |
|---|---|
| Caspase-Glo® 3/7 Assay System | Promega (Madison, USA) |
| CellTiter-Glo® Luminescent Cell Viability Assay | Promega (Madison, USA) |
| DYNAL™ Dynabeads™ Untouched™ Mouse CD4 Cells | ThermoFisher Scientific (Waltham, USA) |
| High-Capacity cDNA Reverse Transcription Kit | ThermoFisher Scientific (Waltham, USA) |
| iScript Select cDNA Synthesis Kit | Bio-Rad (Hercules, USA) |
| Mouse TGF beta1 DuoSet | R&D Systems (Wiesbaden, Germany) |
| Mouse Thrombopoietin DuoSet | R&D Systems (Wiesbaden, Germany) |
| NE-PER Nuclear and Cytoplasmic Extraction Reagents | ThermoFisher Scientific (Waltham, USA) |
| PierceTM BCA Protein Assay Kit | ThermoFisher Scientific (Waltham, USA) |
| Reticulin Stain Kit | Polysciences, Inc. (Warrington, USA) |
| RNeasy Mini Extraction Kit | Qiagen (Hilden, Germany) |
| Simple Western Jess | ProteinSimple (San Jose, USA) |

## 3.1.4 Antibodies

### 3.1.4.1 Primary antibodies

| Antibody | Host organism | Manufacturer |
|---|---|---|
| monoclonal anti- alpha tubulin (total, clone B-5-1-2) #32-2500 | mouse | ThermoFisher Scientific (Waltham, USA) |
| monoclonal anti-alpha tubulin (acetylated) #sc23950 | mouse | Santa Cruz Biotechnology (Dallas, USA) |
| monoclonal anti-ARPC2 (clone EPR8533) #133315 | rabbit | Abcam (Cambridge, UK) |
| monoclonal anti-Cdc42 (clone M152) #41429 | mouse | Abcam (Cambridge, UK) |
| monoclonal anti-Cofilin (clone D3F9) #5175 | rabbit | Cell Signaling Technology (Danvers, USA) |
| monoclonal anti-GAPDH (clone GAPDH-71.1) #G8795 | rabbit | Merck Millipore / Sigma-Aldrich (Steinheim, Germany) |
| monoclonal anti-GATA-1 (clone D52H6) #3535 | rabbit | Cell Signaling Technology (Danvers, USA) |
| monoclonal anti-Integrin beta1 (clone D6S1W) #34971 | rabbit | Cell Signaling Technology (Danvers, USA) |
| monoclonal anti-IQGAP1 (clone D8K4X) #4762 | rabbit | Cell Signaling Technology (Danvers, USA) |
| monoclonal anti-Jak2 (clone D2E12) #3230 | rabbit | Cell Signaling Technology (Danvers, USA) |
| monoclonal anti-Lamin B1 (clone D9V6H) #13435 | rabbit | Cell Signaling Technology (Danvers, USA) |
| monoclonal anti-MKL1 (MRTF-A, clone G7) #sc-398675 | mouse | Santa Cruz Biotechnology (Dallas, USA) |
| monoclonal anti-mouse CD105 (clone MJ7/18) #120401 | rat | BioLegend (San Diego, USA) |
| monoclonal anti-mouse CD11b (clone M1/70) #101202 | rat | BioLegend (San Diego, USA) |
| monoclonal anti-mouse CD3 (clone 17A2) #100202 | rat | BioLegend (San Diego, USA) |
| monoclonal anti-mouse CD45R/B220 (clone RA3-6B2) #103202 | rat | BioLegend (San Diego, USA) |
| monoclonal anti-mouse Ly-6G/Ly-6C (clone RB6-8C5) #108402 | rat | BioLegend (San Diego, USA) |
| monoclonal anti-mouse TER-119 (clone Ter-119) #116202 | rat | BioLegend (San Diego, USA) |
| monoclonal anti-*Phospho* (p)-Stat3 (Tyr705, clone 3E2) #9138 | mouse | Cell Signaling Technology (Danvers, USA) |
| monoclonal anti-p-Stat5 (Tyr694, clone C71E5) #9314 | rabbit | Cell Signaling Technology (Danvers, USA) |
| monoclonal anti-RhoA (clone 54D6.1.16) #ARH05 | mouse | Cytoskeleton Inc. (Denver, USA) |
| monoclonal anti-ß-actin (clone 8H10D10) #3700 | mouse | Cell Signaling Technology (Danvers, USA) |
| monoclonal anti-Stat3 (clone124H6) #9139 | mouse | Cell Signaling Technology (Danvers, USA) |
| monoclonal anti-Stat5 (clone D2O6Y) #94205 | rabbit | Cell Signaling Technology (Danvers, USA) |
| monoclonal anti-Talin-1 (clone C-9) #sc-365875 | mouse | Santa Cruz Biotechnology (Dallas, USA) |
| monoclonal anti-tubulin (tyrosinated, clone YL1/2) #MAB1864 | rat | Merck Millipore (Darmstadt, Germany) |
| monoclonal anti-Vinculin (clone VLN01) #MA5-11690 | mouse | ThermoFisher Scientific (Waltham, USA) |
| polyclonal anti-beta tubulin (beta 1 isoform) #GTX107175 | rabbit | GeneTex (Irvine, USA) |
| polyclonal anti-DIAPH1 #ab11173 | rabbit | Abcam (Cambridge, UK) |

| | | |
|---|---|---|
| polyclonal anti-Filamin A #4762 | rabbit | Cell Signaling Technology (Danvers, USA) |
| polyclonal anti-LIMK1 #3842 | rabbit | Cell Signaling Technology (Danvers, USA) |
| polyclonal anti-MKL1 (MRTF-A) #14760 | rabbit | Cell Signaling Technology (Danvers, USA) |
| polyclonal anti-MKL2 (MRTF-B) #NBP1-46209 | rabbit | Novus Biologicals (Litleton, USA) |
| polyclonal anti-Myosin Light Chain 2 #3672 | rabbit | Cell Signaling Technology (Danvers, USA) |
| polyclonal anti-MYPT1 #2634 | rabbit | Cell Signaling Technology (Danvers, USA) |
| polyclonal anti-Phospho-Cofilin (Ser3) #3311 | rabbit | Cell Signaling Technology (Danvers, USA) |
| polyclonal anti-Phospho-Jak2 (Tyr1007/1008) #3771 | rabbit | Cell Signaling Technology (Danvers, USA) |
| polyclonal anti-p-MYPT1 (Thr696) #5163 | rabbit | Cell Signaling Technology (Danvers, USA) |
| polyclonal anti-RUNX1 #ab23980 | rabbit | Abcam (Cambridge, UK) |
| polyclonal anti-tubulin (detyrosinated) #AB3201 | rabbit | Merck Millipore (Darmstadt, Germany) |

### 3.1.4.2 Directly coupled or secondary antibodies

| **Antibody** | **Host organism** | **Manufacturer** |
|---|---|---|
| anti-mouse IgG *horseradish peroxidase* (HRP)-linked #P0260 | rabbit | Agilent (Santa Clara USA) |
| anti-mouse IgG-AF488 #A-11001 | goat | ThermoFisher Scientific (Waltham, USA) |
| anti-mouse IgG-AF #A-11032 | goat | ThermoFisher Scientific (Waltham, USA) |
| anti-mouse IgG-*Cyanine* (Cy)3 #115-165-003 | donkey | Jackson Immuno (Suffolk, UK) |
| anti-rabbit IgG HRP-linked #7074 | goat | Cell Signaling Technology (Danvers, USA) |
| anti-rabbit IgG-AF488 #A-21206 | donkey | ThermoFisher Scientific (Waltham, USA) |
| anti-rabbit IgG-AF647 #A-21245 | goat | ThermoFisher Scientific (Waltham, USA) |
| anti-rabbit IgG-Cy3 #111-165-003 | goat | Jackson Immuno (Suffolk, UK) |
| anti-rat IgG HRP-linked #112-035-003 | goat | Jackson Immuno (Suffolk, UK) |
| anti-rat IgG-AF488 #A-11006 | goat | ThermoFisher Scientific (Waltham, USA) |
| anti-rat IgG-Cy3 #712-165-153 | donkey | Jackson Immuno (Suffolk, UK) |
| monoclonal anti-alpha tubulin, AF488 (clone B-5-1-2) #322588 | mouse | ThermoFisher Scientific (Waltham, USA) |
| monoclonal anti-alpha tubulin, AF647 (clone B-5-1-2) #32-2500; In-house labeling | mouse | ThermoFisher Scientific (Waltham, USA) |

#### 3.1.4.3 In-house generated antibodies

| Antibody | Clone | Isotype | Antigen | Reference |
|---|---|---|---|---|
| p0p4 | 15E2 | IgG2b | GPIbα | [253] |
| p0p/B | 57E12 | IgG2b | GPIbα | [254] |
| DOM2 | 89H11 | IgG2a | GPV | [253] |
| p0p6 | 56F8 | IgG2b | GPIX | [253] |
| JAQ1 | 98A3 | IgG2a | GPVI | [255] |
| INU1 | 11E9 | IgG1 | CLEC-2 | [256] |
| ULF1 | 97H1 | IgG2a | CD9 | unpublished |
| LEN1 | 12C6 | IgG2b | α2 | [257] |
| EDL-1 | 57B10 | IgG2a | β3 | [258] |
| JON/A | 4H5 | IgG2b | αIIbβ3 | [259] |
| JON6 | 14A3 | IgG2b | αIIbβ3 | unpublished |
| WUG 1.9 | 5C8 | IgG1 | P-Selectin | [260] |
| HB.197 | 2.4G2 | IgG2b | FcγR | [261] |
| MWReg30 | 5D7 | IgG1 | αIIb | [262] |

If necessary, the in-house generated antibodies were conjugated to the desired fluorophore.

### 3.1.5 Buffers, Media and Solutions

All stock solutions and buffers were prepared in deionized water (MilliQ Water Purification System, Millipore, Schwalbach, Germany) and the pH was adjusted with HCl or NaOH.

**Lower buffer for separating gel for Western Blot, pH 8.8**

| | |
|---|---|
| TRIS | 1.5 M |
| EDTA | 60 mM |

**Upper buffer for stacking gel for Western Blot, pH 8.8**

| | |
|---|---|
| TRIS/HCl | 0.5 M |

**Cacodylate buffer, pH 7.2**

| | |
|---|---|
| Sodium cacodylate | 0.1 M |

**CATCH buffer**

| | |
|---|---|
| PBS | |
| HEPES | 25 mM |
| EDTA | 3 mM |
| BSA fraction V | 3.5% w/v |

**CO2 independent medium for live cell imaging**

| | |
|---|---|
| KCl | 5.33 mM |
| $KH_2PO_4$ | 0.441 mM |
| $Na_2HPO_4$ | 0.338 mM |
| Glucose | 5.56 mM |
| Sodium chloride | 138 mM |
| $CaCl_2$ (anhyd.) | 185 mg $L^{-1}$ |
| $NaHCO_3$ | 4.17 mM |
| $MgSO_4^-$ (anhyd.) | 97.6 mg $L^{-1}$ |
| L-Glutamine (100x) | 1% v/v |
| Penicillin/Streptomycin (100x) | 1% v/v |
| MEM Essential amino acids (50x) | 2% v/v |
| MEM Non-essential amino acid (100x) | 1% v/v |
| HEPES 1M (pH 7.0) | 2.50% v/v |
| FCS | 10% v/v |

*Note: The first eight ingredients are in the HBSS base which can be bought as 1x solution.*

**Cytoskeleton buffer I**

| | |
|---|---|
| MES pH 6.1 | 10 mM |
| NaCl | 150 mM |
| EGTA | 5 mM |
| Glucose | 5 mM |
| MgCl2 | 5 mM |
| Glutaraldehyde | 0.3% v/v (freshly added) |
| Triton X-100 | 0.25% v/v (freshly added) |

**Cytoskeleton buffer II**

| | |
|---|---|
| MES pH 6.1 | 10 mM |
| NaCl | 150 mM |
| EGTA | 5 mM |
| Glucose | 5 mM |
| MgCl2 | 5 mM |
| Glutaraldehyde | 2% v/v (freshly added) |

**Decalcification buffer, pH 7.4**

| | |
|---|---|
| PBS | |
| EDTA | 10% v/v |

**Fixation buffer with ions**

| | |
|---|---|
| Cacodylat | 50 mM |
| KCl | 50 mM |
| $MgCl_2$ | 2.5 mM |
| Glutaraldehyde | 2.5% v/v |

**IP buffer**

| | |
|---|---|
| TRIS/HCl (pH 8.0) | 15 mM |
| NaCl | 155 mM |
| EDTA | 1 mM |
| $NaN_3$ | 0.005% v/v |

**Karnovsky fixation buffer, pH 7.2**

| | |
|---|---|
| PFA | 2% w/v |
| Glutaraldehyde | 2.5% v/v |
| Cacodylate | 0.1 M |

**Laemmli buffer**

| | |
|---|---|
| TRIS | 40 nM |
| Glycine | 0.95 M |
| SDS | 0.5% w/v |

**MK medium (Normal culture)**

| | |
|---|---|
| DMEM GlutaMAX | |
| FCS | 10% v/v |
| P/S | 1% v/v |

**MK medium (Starvation)**

| | |
|---|---|
| DMEM GlutaMAX | |
| P/S | 1% v/v |
| FCS | none |

**StemPro MK medium**

| | |
|---|---|
| StemPro®-34 | |
| L-Glutamine | 2 mM |
| Nutrient | 2.6% v/v |
| P/S | 1% v/v |

**PBS⁄EDTA (for platelet lysates)**

| | |
|---|---|
| EDTA | 5 mM |
| PBS | |

**PHEM Buffer, pH 6.8**

| | |
|---|---|
| PIPES | 100 mM |
| HEPES | 5.25 mM |
| EGTA | 10 mM |
| $MgCl_2$ | 20 mM |

**PHEM fixation buffer (*immunofluorescence* (IF))**

| | |
|---|---|
| PHEM | |
| PFA | 4% w/v |
| Triton X-100 | 0.1% v/v |

**PBS, pH 7.14**

| | |
|---|---|
| NaCl | 137 mM |
| KCl | 2.7 mM |
| $KH_2PO_4$ | 1.5 mM |
| $Na_2HPO_4 \times 2H_2O$ | 8 mM |

**Platelet buffer, pH 7.4 (10x)**

| | |
|---|---|
| HEPES | 10 mM |
| NaCl | 140 mM |
| KCl | 3 mM |
| $MgCl_2$ | 0.5 mM |
| $NaHCO_3$ | 5 mM |
| Glucose | 10 mM |

**Protein lysis buffer, pH 7.4 (2x)**

| | |
|---|---|
| HEPES | 15 mM |
| NaCl | 150 mM |
| EGTA | 10 mM |
| Triton X-100 | 2% v/v |
| Leupeptin | 1 mM (freshly added) |
| Pepstatin | 1 mM (freshly added) |
| Aprotinin | 1 mM (freshly added) |
| PMSF | 1 mM (freshly added) |

**SDS sample buffer (4x)**

| | |
|---|---|
| β-mercaptoethanol (for red. conditions) | 2% v/v |
| TRIS buffer, pH 6.8 | 200 mM |
| Glycerol | 40% v/v |
| SDS | 8% w/v |
| Bromophenolblue | 0.04% w/v |

**Separating gel for Western Blot**

| | |
|---|---|
| $H_20$ | 2.5 mL |
| “Lower’ buffer | 1.5 mL |
| 30% Acrylamid | 2.0 mL |
| 10% SDS | 60 µL |
| APS | 60 µL |
| TEMED | 6 µL |

**Stacking gel for Western Blot**

| | |
|---|---|
| $H_20$ | 1.0 mL |
| “Upper’ buffer | 500 µL |
| 30% Acrylamid | 300 µL |
| 10% SDS | 20 µL |
| APS | 20 µL |
| TEMED | 2 µL |

**Stripping buffer for Western Blot, pH 2.0**

| | |
|---|---|
| PBS | |
| SDS | 1% w/v |
| Glycine | 25 mM |

**TAE, pH 8.0 (50x)**

| | |
|---|---|
| Tris base | 0.2 M |
| Acetic acid | 5.7% w/v |
| EDTA | 50 mM |

**Transfer buffer for Western Blot (Tank blot)**

| | |
|---|---|
| $NaHCO_3$ | 50 mM |
| $Na_2CO_3$ | 40 mM |
| Methanol | 20% v/v (freshly added) |

***Tris-buffered saline* (TBS), pH 7.3**

| | |
|---|---|
| TRIS/HCl | 20 mM |
| NaCl | 137 mM |

**HEPES-Tyrode’s-buffer without $Ca^{2+}$**

| | |
|---|---|
| NaCl | 137 mM |
| KCl | 2.7 mM |
| $NaHCO_3$ | 12 mM |
| $NaH_2PO_4$ | 0.43 mM |
| HEPES | 5 mM |
| $MgCl_2$ | 1 mM |
| BSA fraction V solution | 0.35% v/v (freshly added) |
| Glucose solution | 0.35% v/v (freshly added) |

**HEPES-Tyrode's-buffer with $Ca^{2+}$**

| | |
|---|---|
| NaCl | 137 mM |
| KCl | 2.7 mM |
| $NaHCO_3$ | 12 mM |
| $NaH_2PO_4$ | 0.43 mM |
| HEPES | 5 mM |
| $CaCl_2$ | 2 mM |
| $MgCl_2$ | 1 mM |
| BSA fraction V solution | 0.35% v/v (freshly added) |
| Glucose solution | 0.35% v/v (freshly added) |

**Washing buffer for Western Blot (TBS-T)**

| | |
|---|---|
| Tween 20 | 0.1% v/v in TBS |

**Washing buffer Kawamoto staining**

| | |
|---|---|
| PBS or PHEM | |
| FCS (optional) | 5% v/v |
| Tween 20 or Triton X-100 | 0.1% v/v |

## 3.2 Methods

### 3.2.1 Genetically modified mice

All animal studies were approved by the district government of Lower Franconia (Bezirksregierung Unterfranken).

**Table 3.1 Mouse models**

| **Mouse line** | **Background** | **Source** |
|---|---|---|
| *RhoA*$^{fl/fl}$*; Pf4-Cre*$^{tg/+}$ | SV129-BL/6J | Own breeding, Pleines *et al.*, 2012[246] |
| *Cdc42*$^{fl/fl}$*; Pf4-Cre*$^{tg/+}$ | C57BL/6J | Own breeding, Pleines *et al.*, 2010[232] |
| *RhoA*$^{fl/fl}$*; Cdc42*$^{fl/fl}$*; Pf4-Cre*$^{tg/+}$ *Pf4*$^{tg/+}$*Cre*$^{tg/+}$ | SV129-BL/6J | Own breeding, Dütting *et al.*, 2017[251] |
| *Itgb1*$^{fl/fl}$*; Pf4-Cre*$^{tg/+}$ | SV129-BL/6J | Raghavan *et al.*, 2000[263] |
| *RhoA*$^{fl/fl}$*; Itgb1*$^{fl/fl}$*; Pf4-Cre*$^{tg/+}$ *DKO* | SV129-BL/6J | Own breeding |
| *Tln-1*$^{fl/fl}$*; Pf4-Cre*$^{tg/+}$ | C57BL/6J | Petrich *et al.*, 2007[264] |
| *RhoA*$^{fl/fl}$*; Tln-1*$^{fl/fl}$*; Pf4-Cre*$^{tg/+}$ *DKO* | SV129-BL/6J | Own breeding |
| *G6b*$^{-/-}$ | C57BL/6J | Mazharian *et al.*, 2012[112] |
| *RhoA*$^{fl/fl}$*; G6b*$^{-/-}$*; Pf4-Cre*$^{tg/+}$ *DKO* | SV129-BL/6J | Own breeding |
| *RhoA*$^{fl/fl}$*; G6b*$^{-/-}$*; Pf4-Cre*$^{+/+}$ *(G6b*$^{-/-}$*)* | SV129-BL/6J | Own breeding |
| *Gp1ba-Cre*$^{KI/+}$ | C57BL/6J | Nagy *et al.*, 2019[238] |
| *RhoA*$^{fl/fl}$*; Gp1ba-Cre*$^{KI/+}$ | SV129-BL/6J | Own breeding |

First, mice carrying both the *RhoA*[246] and *Cdc42*[232] genes flanked by loxP sites (*RhoA*$^{fl/fl}$*; Cdc42f*$^{l/fl}$) were generated and crossed with transgenic mice carrying the Cre-recombinase under the control of the MK- and platelet-specific Pf4 promotor.[234] Double-deficient *RhoA*$^{fl/fl}$*; Cdc42*$^{fl/fl}$*; Pf4-Cre*$^{tg/+}$ (*RhoA/Cdc42*$^{-/-}$, further referred to as *DKO*) and littermate control mice *RhoA*$^{fl/fl}$*; Cdc42*$^{fl/fl}$*; Pf4-Cre*$^{+/+}$ (further referred to as *WT*) were used in all studies. To enable the discrimination between redundant and non-redundant functions of both GTPases, we additionally used the respective single-deficient mice *RhoA*$^{fl/fl}$*; Pf4-Cre*$^{tg/+}$ (further referred to as *RhoA*$^{-/-}$) and *Cdc42*$^{fl/fl}$*; Pf4-Cre*$^{tg/+}$ (further referred to as *Cdc42*$^{-/-}$) in some experiments.

Second, mice carrying both the *RhoA*[246] and *Itgb1*[263] genes flanked by loxP sites (*RhoA*$^{fl/fl}$*; Itgb1*$^{fl/fl}$) were generated and crossed with transgenic mice carrying the Cre-recombinase under the control of the MK- and platelet-specific Pf4 promotor.[234] Double-deficient *RhoA*$^{fl/fl}$*; Itgb1*$^{fl/fl}$*; Pf4-Cre*$^{tg/+}$ (*RhoA/Itgb1*$^{-/-}$) and littermate control mice *RhoA*$^{fl/fl}$*; Itgb1*$^{fl/fl}$*; Pf4-Cre*$^{+/+}$ (further referred to as *WT*) were used in all studies. To enable the discrimination between redundant and non-redundant functions of both proteins, we additionally used the respective single-deficient mice *RhoA*$^{fl/fl}$*; Pf4-Cre*$^{tg/+}$ (further referred to as *RhoA*$^{-/-}$) and *Itgb1*$^{fl/fl}$*; Pf4-Cre*$^{tg/+}$ (further referred to as *Itgb1*$^{-/-}$) in some experiments.

Third, mice carrying both the *RhoA*[246] and *Tln-1* (Talin-1)[264] genes flanked by loxP sites (*RhoA*$^{fl/fl}$*; Tln1*$^{fl/fl}$) were generated and crossed with transgenic mice carrying the Cre-recombinase under the control of the MK- and platelet-specific Pf4 promotor.[234] Double-deficient *RhoA*$^{fl/fl}$*; Tln-1*$^{fl/fl}$*; Pf4-Cre*$^{tg/+}$ (*RhoA/Talin-1*$^{-/-}$) and littermate control mice *RhoA*$^{fl/fl}$*; Tln-1*$^{fl/fl}$*; Pf4-Cre*$^{+/+}$ (further referred to as *WT*) were used in all studies. To enable the discrimination between redundant and non-redundant functions of both proteins, we additionally used the respective single-deficient mice *RhoA*$^{fl/fl}$*; Pf4-Cre*$^{tg/+}$ (further referred to as *RhoA*$^{-/-}$) and *Tln-1*$^{fl/fl}$*; Pf4-Cre*$^{tg/+}$ (further referred to as *Talin-1*$^{-/-}$) in some experiments.

Fourth, mice carrying the *RhoA*[246] genes flanked by loxP sites and constitutively lacking the *Mpig6b* (G6b-B) gene were generated (*RhoA*$^{fl/fl}$*; G6b*$^{-/-}$) and crossed with transgenic mice carrying the Cre-recombinase under the control of the MK- and platelet-specific Pf4 promotor.[234] Double-deficient *RhoA*$^{fl/fl}$*; G6b*$^{-/-}$*; Pf4-Cre*$^{tg/+}$ (*RhoA/G6b*$^{-/-}$) and littermate mice *RhoA*$^{fl/fl}$*; G6b*$^{-/-}$*; Pf4-Cre*$^{+/+}$ (further referred to as *G6b*$^{-/-}$), were used in all studies. We additionally used the respective single-deficient mice *RhoA*$^{fl/fl}$*; Pf4-Cre*$^{tg/+}$ (further referred to as *RhoA*$^{-/-}$) in some experiments as well as the littermate *RhoA*$^{fl/fl}$*; Pf4-Cre*$^{+/+}$ controls (further referred to as *WT*) in all studies.

Fifth, the new *Gp1ba-Cre* transgenic mouse model was used.[238] Mice carrying the *RhoA* gene flanked by loxP sites (*RhoA*$^{fl/fl}$) were crossed with transgenic *Gp1ba-Cre*$^{KI/+}$ mice, utilizing the MK- and platelet-specific endogenous *Gp1ba* locus to drive Cre expression, thus generating a constitutive *knock-in* (KI) of a T2A-improved-Cre in the endogenous *Gp1ba* gene. RhoA-deficient mice *RhoA*$^{fl/fl}$*; Gp1ba-Cre*$^{KI/+}$ (further referred to as *RhoA*$^{Gp1ba\text{-}Cre}$) and *RhoA*$^{+/+}$*; Gp1ba-Cre*$^{KI/+}$ mice (further referred to as *WT*$^{Gp1ba\text{-}Cre}$) were used as controls in all experiments. To exclude any side effects of the transgenic *Gp1ba-Cre*$^{KI/+}$ mice, which displayed a reduced (33%) GPIbα expression due to the *Gp1ba-Cre* targeted insertion strategy, *RhoA*$^{fl/fl}$*; Gp1ba-Cre*$^{+/+}$ or *RhoA*$^{+/+}$*; Gp1ba-Cre*$^{+/+}$ mice (further referred to as *WT*) were utilized as additional controls in all studies.

### 3.2.2 Mouse genotyping

#### 3.2.2.1 Isolation of murine DNA

A 5 $mm^2$ piece of the mouse ear was incubated in 100 µL tail lysis buffer containing 5 µL $mL^{-1}$ proteinase K [20 mg $mL^{-1}$] for 1 h 30 min at 56°C and under constant shaking at 1200 rpm. Optionally, the earpieces can also be lysed shaking at 900 rpm *over night* (O/N). The reaction was stopped by incubating lysed DNA at 86°C for 30 min.

#### 3.2.2.2 *Polymerase chain reaction* (PCR)

To verify the presence of the Cre recombinase cassette on chromosome 9 (*Pf4-Cre*$^{tg/+}$), the presence of the genes flanked by loxP sites (*GeneXY*$^{fl/fl}$), as well as the deletion of *G6b* gene (*Mpig6b*), different PCRs were conducted.

**Table 3.2: List of primers used for genotyping.** Note that all primers were dissolved to a final concentration of 1 µg $mL^{-1}$ in $H_2O$.

| **Primer** | **Sequence 5' → 3'** |
|---|---|
| Pf4_forward | CCC ATA CAG CAC ACC TTT TG |
| Pf4_reverse | TGC ACA GTC AGC AGG TT |
| RhoA_forward | AGC CAG CCT CTT GAC CGA TTTA |
| RhoA_reverse | TGT GGG ATA CCG TTT GAG CAT |
| Cdc42_forward | ATG TAG TGT CTG TCC ATT GG |
| Cdc42_reverse | TCT GCC ATC TAC ACA TAC AC |
| Itgb1_forward | GGA TTC TCC AGA AGG TGG TTT CG |
| Itgb1_reverse | TGC CAC CAA GTT TCC CAT CTC C |
| Talin-1_forward | AAG CAG GAA CAA AAG TAG GTC TCC |
| Talin-1_reverse | GCA TCG TCT TCA CCA CAT TCC |
| G6b_WT_forward | CAC ACA GCA TAA TTC CCT TTC C |
| G6b_WT_reverse | GTC TCT GTC TTC TGA GTG CTA GG |
| G6b_KO_forward | GCA ACT TTG GGT GCC TAG G |
| G6b_KO_reverse | CTT CCT GAC TAC CCC TAC C |
| G6b_ctrl_forward | GAG ACT CTG GCT ACT CAT CC |
| G6b_ctrl_reverse | CCT TCA GCA AGA GCT GGG GAC |
| Gp1ba-Cre_forward | GAA CAC AAC TCT CCT TGC TGG |
| Gp1ba-Cre_reverse | GAA GAG TTA ATG GCA GGA AAG AG |

## Genotyping of *Pf4-Cre* mice:

**Table 3.3: PCR program**

| Temperature [°C] | Time [s] | Repeats (cycles) |
|---|---|---|
| 96 | 300 | 1 |
| 94 | 30 | 35 |
| 54.1 | 30 | 35 |
| 72 | 45 | 35 |
| 72 | 30 | 1 |
| 22 (or 4) | ∞ | 1 |

**Table 3.4 Pipetting scheme (25 µL final volume)**

| Reagent | Volume in µL |
|---|---|
| DNA sample | 1 |
| DreamTaq$^{TM}$ green buffer (10x) | 2.5 |
| dNTPs [10 mM] | 1 |
| forward Primer (1:10 in $H_2O$) | 1 |
| reverse Primer (1:10 in $H_2O$) | 1 |
| $MgCl_2$ [10 mM] | 0.5 |
| DreamTaq DNA Polymerase | 0.25 |
| $H_2O$ | 17.75 |

Expected band sizes: 450 bp for positive samples

### Genotyping of RhoA floxed mice:

**Table 3.5: PCR program**

| Temperature [°C] | Time [s] | Repeats (cycles) |
|---|---|---|
| 94 | 120 | 1 |
| 94 | 30 | 35 |
| 55 | 30 | 35 |
| 72 | 30 | 35 |
| 72 | 600 | 1 |
| 22 (or 4) | ∞ | 1 |

**Table 3.6 Pipetting scheme (20 µL final volume)**

| Reagent | Volume in µL |
|---|---|
| DNA sample | 2 |
| DreamTaq$^{TM}$ green buffer (10x) | 2 |
| dNTPs [10 mM] | 0.4 |
| forward Primer | 0.2 |
| reverse Primer | 0.2 |
| DreamTaq DNA Polymerase | 0.125 |
| $H_2O$ | 15.075 |

Expected band sizes: WT locus: 297 bp; Floxed locus: 393 bp

**Genotyping of Cdc42 floxed mice:**

**Table 3.7: PCR program**

| Temperature [°C] | Time [s] | Repeats (cycles) |
|---|---|---|
| 95 | 120 | 1 |
| 95 | 30 | 10 |
| 63 (-1°C each cycle) | 30 | 10 |
| 72 | 45 | 10 |
| 95 | 30 | 35 |
| 53 | 30 | 35 |
| 72 | 45 | 35 |
| 72 | 240 | 35 |
| 22 (or 4) | ∞ | 1 |

**Table 3.8 Pipetting scheme (25 µL final volume)**

| Reagent | Volume in µL |
|---|---|
| DNA sample | 1 |
| DreamTaq$^{TM}$ green buffer (10x) | 2.5 |
| dNTPs [10 mM] | 1 |
| forward Primer (1:10 in $H_2O$) | 1 |
| reverse Primer (1:10 in $H_2O$) | 1 |
| $MgCl_2$ [10 mM] | 0.5 |
| DreamTaq DNA Polymerase | 0.125 |
| $H_2O$ | 17.875 |

Expected band sizes: WT locus: 200 bp; Floxed locus: 300 bp

**Genotyping of Itgb1 floxed mice:**

**Table 3.9: PCR program**

| Temperature [°C] | Time [s] | Repeats (cycles) |
|---|---|---|
| 96 | 300 | 1 |
| 94 | 30 | 35 |
| 54.1 | 30 | 35 |
| 72 | 45 | 35 |
| 72 | 240 | 1 |
| 22 (or 4) | ∞ | 1 |

**Table 3.10 Pipetting scheme (25 µL final volume)**

| Reagent | Volume in µL |
|---|---|
| DNA sample | 1 |
| DreamTaq$^{TM}$ green buffer (10x) | 2.5 |
| dNTPs [10 mM] | 1 |
| forward Primer (1:10 in $H_2O$) | 1 |
| reverse Primer (1:10 in $H_2O$) | 1 |
| $MgCl_2$ [10 mM] | 0.5 |
| DreamTaq DNA Polymerase | 0.125 |
| $H_2O$ | 17.875 |

Expected band sizes: WT locus: 160 bp; Floxed locus: 280 bp

**Genotyping of Talin-1 floxed mice:**

**Table 3.11: PCR program**

| Temperature [°C] | Time [s] | Repeats (cycles) |
|---|---|---|
| 95 | 240 | 1 |
| 95 | 30 | 35 |
| 58 | 30 | 35 |
| 72 | 30 | 35 |
| 72 | 480 | 1 |
| 22 (or 4) | ∞ | 1 |

**Table 3.12 Pipetting scheme (25 µL final volume)**

| Reagent | Volume in µL |
|---|---|
| DNA sample | 1 |
| DreamTaq™ green buffer (10x) | 2.5 |
| dNTPs [10 mM] | 1 |
| forward Primer (1:10 in $H_2O$) | 1 |
| reverse Primer (1:10 in $H_2O$) | 1 |
| $MgCl_2$ [10 mM] | 0.5 |
| DreamTaq DNA Polymerase | 0.125 |
| $H_2O$ | 17.875 |

Expected band sizes: WT locus: 700 bp; Floxed locus: 800 bp

**Genotyping of *Gp1ba-Cre* mice:**

**Table 3.13: PCR program**

| Temperature [°C] | Time [s] | Repeats (cycles) |
|---|---|---|
| 96 | 300 | 1 |
| 94 | 30 | 35 |
| 60 | 30 | 35 |
| 72 | 60 | 35 |
| 72 | 600 | 1 |
| 22 (or 4) | ∞ | 1 |

**Table 3.14 Pipetting scheme (25 µL final volume)**

| Reagent | Volume in µL |
|---|---|
| DNA sample | 1 |
| DreamTaq™ green buffer (10x) | 2.5 |
| dNTPs [10 mM] | 1 |
| forward Primer (1:10 in $H_2O$) | 1 |
| reverse Primer (1:10 in $H_2O$) | 1 |
| $MgCl_2$ [10 mM] | 0.5 |
| DreamTaq DNA Polymerase | 0.125 |
| $H_2O$ | 17.875 |

Expected band sizes: WT locus: 297 bp; KI locus: 372 bp

**Genotyping of *$G6b^{-/-}$* mice:**

**Table 3.15: PCR program for both G6b WT and G6b KO**

| Temperature [°C] | Time [s] | Repeats (cycles) |
|---|---|---|
| 96 | 300 | 1 |
| 94 | 30 | 35 |
| 60 | 30 | 35 |
| 72 | 60 | 35 |
| 72 | 600 | 1 |
| 22 (or 4) | ∞ | 1 |

**Table 3.16 Pipetting scheme G6b WT (25 µL final volume)**

| Reagent | Volume in µL |
|---|---|
| DNA sample | 1 |
| DreamTaq$^{TM}$ green buffer (10x) | 2.5 |
| dNTPs [10 mM] | 1 |
| WT forward Primer (1:10 in $H_2O$) | 1 |
| WT reverse Primer (1:10 in $H_2O$) | 1 |
| $MgCl_2$ [10 mM] | 0.5 |
| DreamTaq DNA Polymerase | 0.125 |
| $H_2O$ | 17.875 |

**Table 3.17 Pipetting scheme G6b KO (25 µL final volume)**

| Reagent | Volume in µL |
|---|---|
| DNA sample | 1 |
| DreamTaq$^{TM}$ green buffer (10x) | 2.5 |
| dNTPs [10 mM] | 1 |
| KO forward Primer (1:10 in $H_2O$) | 1 |
| KO reverse Primer (1:10 in $H_2O$) | 1 |
| Ctrl forward Primer (1:10 in $H_2O$) | 1 |
| Ctrl reverse Primer (1:10 in $H_2O$) | 1 |
| $MgCl_2$ [10 mM] | 0.5 |
| DreamTaq DNA Polymerase | 0.25 |
| $H_2O$ | 17.75 |

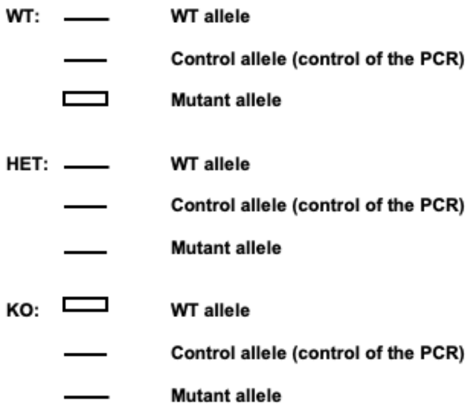

Expected band size G6b WT: WT: 195 bp; KO: no band

Expected band size G6b KO: Control: 585 bp; KO: 278 bp

#### 3.2.2.3 Agarose gel electrophoresis

PCR products were separated on agarose gels (1.5% or 2%). For a 1.5% agarose gel, 1.5 g of agarose per 100 mL TAE buffer was boiled. Midori Green™ [50 µl $L^{-1}$] was added to the cooled agarose (60°C) to allow visualization of DNA and poured into a sleigh containing a comb. The cast gel was then laid into a chamber filled with 1x TAE buffer. 20 µL of the PCR products were loaded onto the gel together with a molecular weight marker ranging from 100 to 10 000 bp. The samples were separated for 30-45 min at 140 V. DNA was visualized using *ultra violet* (UV) light and imaged with a camera (Herolab GmbH, Wiesloch, Germany).

### 3.2.3 Analysis of platelet function *in vitro*

#### 3.2.3.1 Preparation of washed platelets from whole blood

Washed platelets were prepared as previously described.[265] In detail, the mice were anaesthetized using isoflurane and retro-orbitally bled up to 1 mL into 300 µL heparin [20 U $mL^{-1}$ in TBS]. Additional 300 µL heparin were added followed by centrifugation at 800 rpm (300 xg) for 6 min. The upper phase together with the buffy coat and some *red blood cells* (RBCs) was transferred into a new tube containing 300 µL heparin and centrifuged again at 800 rpm (300 xg) for 6 min. Afterwards, the upper phase alone containing the *platelet-rich-plasma* (PRP) was transferred into a new tube, supplemented with 2 µL apyrase [0.02 U $mL^{-1}$, f.c.] and 5 µL $PGI_2$ [0.1 µg $mL^{-1}$, f.c.] to inhibit platelet activation. For washing, isolated PRP was centrifuged at 2800 rpm (800 xg) for 5 min and platelet pellet was diluted in 1 mL of Tyrode's buffer without $Ca^{2+}$, containing 2 µL of apyrase [0.02 U $mL^{-1}$, f.c.] and 5 µL $PGI_2$ [0.1 µg $mL^{-1}$, f.c.]. This washing step was repeated and 50 µL of the platelet suspension was diluted 1/1 in PBS to determine the platelet count using a Sysmex KX-21N™ Hematology Analyzer (Sysmex Europe, Norderstedt, Germany). Afterwards, platelets were centrifuged at 2800 rpm (800 xg) for 5 min at RT again, platelet counts were adjusted in Tyrode's buffer with or without $Ca^{2+}$, containing 2 µL of apyrase [0.02 U $mL^{-1}$, f.c.] where necessary and platelets were allowed to rest for 30 min at 37°C if necessary.

#### 3.2.3.2 Assessment of blood parameters

Analyses of blood parameters were performed as previously described.[265] Shortly, two drops of blood were taken from the retrobulbar plexus of isoflurane-anesthetized mice into EDTA-coated tubes, tubes were inverted 10 times and analyzed by a scilVetabcPlus$^+$ hemacytometer (scilVet, scil animal care company GmbH, Viernheim, Germany).

#### 3.2.3.3 Platelet count and size

In addition to analysis of blood parameters at the scilVet, platelet count and size were further determined by flow cytometry in some studies. Therefore, mice were bled 50 µL into 300 µL heparin using capillaries and the blood was diluted using 650 µL Tyrode's buffer without $Ca^{2+}$. Next, 50 µL of the diluted blood were incubated with 10 µL of fluorophore-conjugated antibodies against GPIbα (15E2-PE) as well as αIIbβ3 integrins (14A3-FITC) for 20 min at RT. The reaction was stopped using 500 µL PBS. Platelet size using the *forward scatter* (FSC) characteristics as well as platelet count (total amount of platelets measured within 30 s) was determined by flow cytometry at a FACSCalibur or Celesta (BD BioSciences, Heidelberg, Germany).

#### 3.2.3.4 Platelet GP expression

Surface expression of the major GPs on resting platelets were assessed by determination of *mean fluorescence intensity* (MFI) by flow cytometry using fluorophore-conjugated antibodies. Blood was prepared as described above.

#### 3.2.3.5 Analysis of platelet integrin activation and degranulation

In detail, the mice were anaesthetized using isoflurane and retro-orbitally bled up to 50 µL into 300 µL heparin [20 U $mL^{-1}$ in TBS]. Blood was washed twice in Tyrode's buffer without $Ca^{2+}$ at 2800 rpm (800 xg) for 5 min. After the last washing step, washed blood was resuspended in 1 mL Tyrode's buffer with $Ca^{2+}$, which is essential for the following activation of the platelets. 50 µL of washed blood was added to 10 µL of fluorophore-conjugated antibodies against activated αIIbβ3 integrins (JON/A-PE) as well as the α-granule specific protein P-selectin (WUG 1.9-FITC). Platelets were subsequently stimulated using agonists against *G protein-coupled receptors* (GPCRs) (thrombin, the thromboxane $A_2$ analogue U46619 and ADP) as well as against the (hem)ITAM receptors CLEC-2 (RC) and GPVI (CRP, CVX). Platelets were incubated for 6 min at 37°C, followed by 6 min at RT. The reaction was stopped by adding 500 µL PBS. MFIs were assessed by flow cytometry at a FACSCalibur or Celesta (BD Biosciences, Heidelberg, Germany).

### 3.2.3.6 Direct stochastical optical reconstruction microscopy (dSTORM) of spread platelets

8-well chamber slides (Cellvis, Mountain View, USA) were coated with 200 µL of human fibrinogen (10 µg mL$^{-1}$) for 2h at 37°C for spread platelets and 200 µL glycine (2M) for 10 min at RT for resting platelets. Platelets were washed as described in 3.2.3.1 and platelet counts were adjusted to 3x10$^{5}$ µL$^{-1}$ in Tyrode's buffer without $Ca^{2+}$. For spread platelets 60 µL of the platelet suspension was added to 200 µL Tyrode's buffer containing 2 mM $Ca^{2+}$ in each fibrinogen-coated well, stimulated with 0.01 U mL$^{-1}$ thrombin (Roche) and kept at 37°C for 30 min. For resting platelets 60 µL of the platelet suspension was added to 200 µL Tyrode's buffer without $Ca^{2+}$ in each glycine-coated well and kept at 37°C for 30 min as well. After 30 min, the supernatant was discarded and the platelets were fixed with 200 µL prewarmed cytoskeleton buffer I in each well for 2 min at 37°C, followed by 18 min at RT with 200 µL cytoskeleton buffer II. Subsequently the samples were quenched with 0.1% NaBH4 for 15 min and blocked with 5% BSA for 1h. Staining was done overnight at 4°C with either 5 µL AF647-conjugated Phalloidin (#A22287) or a total of 1 µg AF647-conjugated anti-α-tubulin antibody, diluted in 300 µL PBS for each well. For post-staining-fixation the samples were fixed with 4% PFA in PBS for 10 min at RT after washing. One color *d*STORM samples were imaged on a widefield setup based on an inverted microscope (Olympus IX-71) equipped with an oil immersion objective (Olympus APON 60xO TIRF, NA 1.49, Olympus, Hamburg, Germany). The dye was excited with a semiconductor laser at 639 nm at an irradiation intensity of ~ 7 kW/cm$^{2}$ (Genesis MX639-1000, Coherent). The excitation light was spectrally filtered from the emitted fluorescence using an emission filter Brightline HC 679/41 (Semrock, Rochester, USA). Imaging was performed with an EMCCD camera (iXon Ultra 897, Andor, Belfast, UK) with an exposure time of 10 ms for at least 30000 frames in photoswitching buffer containing 100 mM ß-mercaptoethylamin pH 7.4.[266] Spread platelets were imaged by *total internal reflection fluorescence* (TIRF) illumination, resting platelets were measured by epifluorescence (EPI). *d*STORM images were reconstructed using the open source software rapidSTORM 3.3.[267]

### 3.2.3.7 *Transmission electron microscopy* (TEM) of platelets

For analysis of platelet morphology by TEM, platelets were isolated as described in 3.2.3.1 and allowed to rest for 30 min at 37°C in the presence of apyrase [0.02 U mL$^{-1}$]. Afterwards, PRP was incubated in TEM fixation buffer with ions heated to 37°C for 1h at RT and stored at 4°C overnight. Samples were centrifuged at 1500 rpm for 5 min and washed in cacodylate buffer three times the following day and resuspended in 2% agarose solution, followed by a centrifugation at 18000 xg for 5min at 37°C. Hardened agarose pellets were cut into approximately 1 $mm^2$ pieces and incubated in 1% *osmium tetroxide* ($OsO_4$) in cacodylate buffer for 1h at RT, afterwards washed with cacodylate buffer again, followed by addition of $H_2O$ and 2% uranyl acetate (in $H_2O$) for 1h at 4°C. Samples were then dehydrated using an ethanol series (70%, 95% and 100%), incubated twice for 10 min in propylenoxide and then rotated in a 1:1 mixture of propylenoxide/epon for 1h at RT. Afterwards, propyleneoxide/epon was removed and samples were incubated overnight at RT in epon, or twice at RT for 2-3 h under rotation. Samples were embedded in gelatin capsules, left to harden for 48 h at 60 ºC and ultrathin sections were generated and stained using 2% uranyl acetate and lead citrate. Images were acquired at a JEM-2100 (JEOL, Freising, Germany) or Zeiss EM900 transmission electron microscope (Zeiss, Oberkochen, Germany).

#### 3.2.3.8 Immunoblotting of platelet lysates

For analysis of whole platelet lysates, platelets were isolated as described in 3.2.3.1. After the last washing step, PRP was resuspended in Tyrode's buffer without $Ca^{2+}$ and without BSA containing apyrase [0.02 U $mL^{-1}$] and 5 mM EDTA to adjust the platelet concentration [$1x10^6$ $\mu L^{-1}$]. Note, when using severely macrothrombocytopenic mice, e.g. RhoA/Cdc42 *DKO* mice, addition of 5 mM EDTA to the washing buffers already helps to keep the platelets in a resting state and prevent platelet loss. Furthermore, PRPs of two mice can be pooled before the washing procedure starts.

The platelets were allowed to rest for 30 minutes at 37°C prior to experiments and were lysed in an appropriate volume of 2x lysis buffer supplemented with Halt™ Protease and Phosphatase Inhibitor Cocktail (1:100) to prevent protease and phosphatase activity. For SDS-*Polyacrylamide Gel Electrophoresis* (PAGE), platelet lysates or MK lysates (3.2.5.8) were mixed with a reducing 4x loading dye and boiled for 5 min at 95°C under denaturing conditions. Denatured platelet or MK lysates were loaded on 10% or 12% gel for separation. Following SDS-PAGE, the separated proteins were transferred onto PVDF or nitrucellulose membrane via tank blot immunoblotting method. Membranes were blocked in Blue-Block for 1 h at RT and probed with antibodies against FlnA (Filamin A, 1:1000); IQGAP1 (1:1000); DIAPH1 (mDia1, 1:1000); Vinculin (1:500); detyrosinated tubulin (1:1000); acetylated tubulin (1:1000); Tyr-α-tubulin (Clone YL1/2, 1:1000); total α-tubulin (Clone B-5-1-2, 1:500); ß1-tubulin (1:500); ARPC2 (Arp2/3, 1:1000); total LIMK1 (1:1000); p-Cof-1 (Ser3) (1:1000); Cof-1 (1:1000); MLC2 (1:1000); GAPDH (1:5000); MKL1 (1:500, Santa Cruz Biotech; MKL1 (1:1000, CST); MKL2

(1:1000); Integrin ß1 (1:1000); Lamin B1 (1:1000); RhoA (1:500) and Cdc42 (1:300). Before incubation with the respective HRP-coupled secondary antibody (1:2500) for 1 hat RT, the membranes were washed three times with TBS-T. Lastly after another three washing steps, protein bands can be detected by ECL and images were acquired at an Amersham Image 680 (GE Healthcare).

#### 3.2.3.9 Immunoblotting with ProteinSimple Jess

Protein and/or phosphorylation levels for MLC2, MYPT1, GATA1, RUNX1 and ß-actin were analyzed using an automated capillary-based immunoassay platform; Jess (ProteinSimple). Preparation of lysates are explained in 3.2.3.8 (for platelets) and 3.2.5.8 (for MKs). Lysates were diluted to the required concentration with 0.1x Sample Buffer 2 (diluted from 10X Sample Buffer 2, #042-195). Lysates were prepared by the addition of 5x master mix containing 200 mM *dithiothreitol* (DTT), 5x sample buffer and fluorescent standards (Standard Pack 1, #PS-ST01-8) and boiled for 5 minutes at 95°C according to the manufacturer’s instructions.

The optimized antibody dilutions and respective lysate concentrations for each antibody are listed below (dilution; lysate concentration): p-MYPT1 (Thr696) (1:10; 0.8 mg mL$^{-1}$); MYPT1 (1:10; 0.8 mg mL$^{-1}$); MLC2 (1:10, 0.1 mg mL$^{-1}$); LIMK1 (1:10, 0.4 mg mL$^{-1}$); ß-actin (1:10, 0.1 mg mL$^{-1}$); JAK2 (1:20, 0.5 mg mL-1); p-JAK2 (Tyr1007/1008) (1:10, 0.5 mg mL$^{-1}$); STAT3 (1:40, 0.2 mg mL$^{-1}$); p-STAT3 (Tyr705) (1:10, 0.2 mg mL$^{-1}$); STAT5 (1:40, 0.1 mg mL$^{-1}$); p-STAT5 (Tyr694) (1:20, 0.5 mg mL$^{-1}$); GATA1 (1:80, 0.1 mg mL$^{-1}$); RUNX1 (1:10, 0.5 mg mL$^{-1}$). For all antibodies except MYPT1 and ß-actin, either Anti-Rabbit Secondary HRP antibody (#DM-001) or Anti-Mouse Secondary HRP Antibody (#DM-002) was utilized and the chemiluminescent signal was recorded by using the *high dynamic range* (HDR) profile. For detection of MYPT1 and ß-actin signals near-infrared Anti-Rabbit Secondary NIR Antibody (#DM-007) and infrared Anti-Mouse Secondary IR Antibody (#DM-010) was used, respectively, with the corresponding detection profiles. All antibodies were diluted in Antibody Diluent 2 (#042-203).

Samples, Antibody Diluent 2, primary and secondary antibodies, Luminol-S (#043-311) and Peroxide (#043-379) mix and Wash Buffer (#042-202) were displaced into 12-230 kDa prefilled microplates, (prefilled with Separation Matrix 2, Stacking Matrix 2, Split Running Buffer 2 and Matrix Removal Buffer, #SM-W004). The microplate was centrifuged for 5 minutes at 2500 rpm at room temperature. To start the assays, the capillary cartridge was inserted into the cartridge holder and the microplate placed on the plate holder. To operate Jess and analyze results Compass Software for Simple Western was used (version 4.1.0, ProteinSimple). Separation matrix loading time was set to 200 s, stacking matrix loading time to 15 s sample loading time to 9 s, separation time to 31 minutes, separation voltage to 375 *volts* (V), antibody diluent time to 5 minutes, primary antibody incubation time to 90 minutes and secondary antibody incubation time to 30 minutes.

## 3.2.4 Analysis of *in vivo* platelet function

### 3.2.4.1 Analysis of platelet lifespan

Mice were retro-orbitally injected with a DyLight 488-conjugated anti-GPIX antibody [0.2 µg $g^{-1}$ *bodyweight* (BW) for mice with normal peripheral platelet counts and 0.1-0.15 µg $g^{-1}$ BW for KO mouse strains with endogenous platelet counts of < 50% or <75% of *WT* control respectively]. The conjugated anti-GPIX antibody labels circulating platelets without interfering with platelet activation *in vitro* or *in vivo.*[253] The antibody concentration applied was sufficient to label only circulating, but not newly generated platelets. Platelet clearance from the circulation was determined by daily blood withdrawal and subsequent flow cytometric analysis of the percentage of fluorescently labeled platelet at the indicated time points using the FACSCalibur or Celesta (BD Biosciences, Heidelberg, Germany). In detail, mice were bled 50 µL into 300 µL heparin using capillaries and the blood was diluted using 650 µL PBS. Next, 50 µL of the diluted blood were further diluted with 500 µL PBS (1:10) and measured as described above.

### 3.2.4.2 Determination of platelet recovery upon depletion

Thrombocytopenia was induced by retro-orbital injection of a platelet depletion antibody [R300, 2 µg $g^{-1}$ BW; 1 µg $g^{-1}$ BW for KO mouse strains with endogenous platelet counts of < 50% of WT control] and blood samples were collected (as described in 0) at indicated time points until peripheral platelet counts recovered to values prior to platelet depletion and analyzed by flow cytometry.

## 3.2.5 *In vitro* analysis of MKs

### 3.2.5.1 Isolation of murine BM cells by centrifugation ('Spin isolation')

Mice were anaesthetized using isoflurane and killed by cervical dislocation. Femora and tibiae of mice were isolated and stored on ice in DMEM (only supplemented with 100 U $mL^{-1}$ penicillin and 50 mg $mL^{-1}$ streptomycin). To isolate BM cells, we used a modified version of the previously described centrifugation procedure.[268] In detail, a 18G needle was pushed through the bottom of a 0.5 mL microcentrifuge tube. If the hole was not big enough, another hole was made adjacent to the other. The knee side of the bone was cut open (different from the original publication to minimize shear forces on the cells during centrifugation). The long bones (maximum of 2 femora and 2 tibiae) were put in the tube with the knee-end facing down, and the lid of the reaction tube was closed. The 0.5 mL microcentrifuge tube was placed in a 1.5 mL microcentrifuge tube filled with 0.1 mL DMEM. Tubes were centrifuged at 2500 xg in a benchtop centrifuge for 60 s. Note that the centrifugation speed and time were modified from the initial protocol.[268] The 0.5 mL microcentrifuge tube with the empty bones was discarded. The BM plasma acquired in this process can immediately be frozen and stored at -80°C until further processing. The isolated cells in the 1.5 mL tube were resuspended in 1 mL DMEM or MK medium, filtered (70 µm, pluriStrainer Mini, Pluriselect) and filters were rinsed with additional DMEM or MK medium. Pre-wetting the filters with 1 mL DMEM or MK medium helps to allow better flow of the cells. Cells were centrifuged for 5 min at 300 xg and after removal of the supernatant, cells were used for further assays.

#### 3.2.5.2 Isolation of murine BM cells by flushing (‘Flush Isolation’)

Mice were anaesthetized using isoflurane and killed by cervical dislocation. Femora and tibiae of mice were dissected and stored on ice in DMEM [supplemented with 100 U mL$^{-1}$ penicillin and 50 mg mL$^{-1}$ streptomycin]. Bones were flushed as previously described.[83] In detail, bones were cut open on both sides and flushed into a 12-well using a 21G needle. Approximately 1 mL was used for one bone and the medium was reused until all cells were completely flushed out. Cells were resuspended three times using a 21G needle and a 23G needle and once using a 25G needle and stored on ice. Cells were filtered (70 µm, pluriStrainer Mini) and filters were rinsed with DMEM. Pre-wetting the filters with 1 mL DMEM helps to allow better flow of the cells. Cells were centrifuged for 5 min at 300xg and used for further assays.

#### 3.2.5.3 *In vitro* differentiation of BM-derived MKs (Boston protocol)

BM from both femora and tibiae was harvested using the spin isolation described in 3.2.5.1. Cells were resuspended and cultured for 2 days in StemPro MK medium supplemented with 50 ng mL$^{-1}$ recombinant SCF at 37°C and 5% $CO_2$. After, cells were collected and centrifuged at 300 xg, resuspended in StemPro MK medium and cultured for 2 days at 37°C and 5% $CO_2$ in the presence of 50 ng mL$^{-1}$ SCF and 0.5% of recombinant TPO. After, cells were collected and centrifuged at 300 xg, resuspended in StemPro MK medium and cultured for one more additional day in the presence of 0.5% recombinant TPO only. Afterwards, cells were collected and centrifuged at 300 xg, resuspended in 1 mL warm PBS and gently layered on top of a two-step BSA gradient (2 mL of 3% layered with 2 mL of 1.5% BSA/PBS), allowing them to sediment by gravity for 30 min at RT. All but 500-750 µL of the suspension was removed and the cells were washed once with 3 mL PBS (5 min at 300 xg). Enriched MKs were cultured for one more day in StemPro MK medium supplemented with 0.5% of recombinant TPO and used for further experiments.

#### 3.2.5.4 *In vitro* differentiation of BM-derived MKs (lineage depletion)

MK differentiation from murine BM cells in vitro can be induced either directly (3.2.5.3), or after lineage depletion (Lin$^-$). The lineage depletion results in a more homogenous cell population at the start of the culture by enriching for non-committed HSCs. In addition, the amount of required rHirudin and recombinant TPO needed is minimized. BM cells were obtained from both femora and tibiae by using the spin isolation described in 3.2.5.1. Subsequently, cells were resuspended in 1 mL of MK medium. Lineage depletion was performed by incubating cells with a cocktail of anti-mouse CD3, clone 17A2; anti-mouse Ly-6G/Ly-6C, clone RB6-8C5; anti-mouse CD11b, clone M1/70; anti-mouse CD45R/B220, clone RA3-6B2; anti-mouse TER-119/Erythroid cells, clone Ter-119 [1.5 µg = 3 µL of each antibody per mouse]. Antibody binding was achieved by rolling for 20 min at 4°C. After washing with MK medium (5 min at 300 xg), cells were incubated rolling for 15 min at RT with 1 mL MK medium containing 200 µL of washed magnetic beads per mouse (Dynabeads® Untouched™ Mouse CD4 Cells) The tubes were gently vortexed and placed in a magnetic holder for 3 min. The supernatant (Lin$^-$ cells) was recovered and washed once (5 min at 300 xg). Cells were cultured in one well of a 6-well plate, respectively, using 2.5 mL [~3-6x10$^6$ cells mL$^{-1}$] MK medium supplemented with 0.5% of recombinant TPO and rHirudin [100 U mL$^{-1}$]. Cells were incubated at 37°C and 5% $CO_2$ for 3 days. On day 4, cells were collected and centrifuged at 300 xg, resuspended in 1 mL warm PBS and gently layered on top of a two-step BSA gradient (2 mL of 3% layered with 2 mL of 1.5% BSA/PBS), allowing them to sediment by gravity for 30 min at RT. All but 500-750 µL were removed and the cells were washed once with 3 mL PBS (5 min at 300 x*g*). If necessary, cells were further cultured in a 12-well plate using 1 mL MK medium containing 0.5% of recombinant TPO and rHirudin [100 U mL$^{-1}$], or directly used for further assays.

#### 3.2.5.5 Analysis of PPF of *in vitro* BM-derived MKs under static conditions

For analysis of PPF under static conditions, MKs obtained after enrichment on a BSA gradient as described in 3.2.5.4 were resuspended in 1 mL MK medium containing 0.5% recombinant TPO and rHirudin [100 U mL$^{-1}$]. Cells were seeded into 96-well-plates in a dilution series in order to prevent differences in cell density. In detail, 200 µL of the cell suspension were added to the first well and 100 µL of the cell suspension was further diluted in 2-3 series with 100 µL of the above-mentioned MK medium in the other wells. Always use a 1 mL tip to avoid shear stress on the MKs and don't pipette down the walls, but directly into the center to avoid the MKs being pushed to the outer rims of the wells. Proplatelet-forming and round MKs in at least five visual fields per MK culture were counted manually at a Zeiss PrimoVert brightfield microscope (Zeiss, Oberkochen, Germany). Brightfield images were acquired at an Evos Microscope (ThermoFisher Scientific). If stated, cells were treated with 10 µM LIM Kinase Inhibitor I (LIMKi) or 0.01% DMSO as control.

#### 3.2.5.6 Time lapse video microscopy visualizing PPF of *in vitro* BM-derived MKs

PPF of cultured BM-derived MKs as described in 3.2.5.4 was analyzed using time lapse microscopy. In detail, a 96-well plate was coated with 100 µL of 0.01% Poly-L-Lysine for 15 min at 37°C and washed once using $H_2O$. MKs enriched by BSA gradient were resuspended in 1 mL $CO_2$ independent medium containing 0.5% recombinant TPO and rHirudin [100 U $mL^{-1}$] and a dilution series was performed in the 96-well plate as described above. Alternatively, if cells are also needed for other experiments, resuspend the cells in 200 µL MK medium containing 0.5% recombinant TPO and rHirudin [100 U $mL^{-1}$]. Transfer 50 µL into 600 µL of $CO_2$ independent medium containing 0.5% recombinant TPO and rHirudin [100 U $mL^{-1}$] (dilution has to be at least 1:8 if cells are resuspended in DMEM). Seed 300 µL, 200 µL and 100 µL into the 96-well plate. Imaging started two hours after enrichment and PPF was assessed for 24 h at 37°C using a Leica TCS SP8 (Leica Microsystems, Wetzlar, Germany). Pictures were taken every 30 min and the total number of PPF MKs in each well was counted over time.

#### 3.2.5.7 IF microscopy of proplatelet-forming MKs

After enrichment of MKs on a BSA gradient as described in 3.2.5.4, MKs were further cultured for 24 h in a 12-well plate in MK Medium and in the presence of 0.5% recombinant TPO and rHirudin [100 U $mL^{-1}$]. Thereafter, 250 µL of the supernatant (containing the proplatelets) was carefully removed using a 1 mL tip with a cut end and diluted in 500 µL in platelet buffer (1:2). The cells were spun down in a 24-well plate (4 min at 200 xg) containing 12 mm glass coverslips coated with 0.01% Poly-L-Lysine and were fixed in an equal volume of PHEM containing 4% PFA for 20 minutes [f.c. 2%]. Samples were washed with PBS and incubated for 10 min in PBS containing 0.1% Triton X-100. After washing, the samples were blocked in 3% fatty acid free BSA in PBS. Diluted in 300 µL PBS, F-actin was stained using Atto-647N-conjugated phalloidin (1:400), α-tubulin was stained using an AF-488 conjugated α-tubulin antibody [1 µg $mL^{-1}$] and the nucleus was stained using DAPI [300 nM]. Staining was performed for 1 h at RT or at 4°C O/N. After washing twice with PBS and once with $H_2O$, the coverslips were mounted with Fluoroshield and visualization was performed with a Leica TCS SP8 confocal microscope using a 40x or 63x oil immersion objective (Leica Microsystems, Wetzlar, Germany).

#### 3.2.5.8 BM-derived MK lysates for immunoblotting

After enrichment of MKs on a BSA gradient as described in 3.2.5.4, MKs were allowed to rest for at least four hours in MK medium containing 0.5% recombinant TPO and rHirudin [100 U $mL^{-1}$]. Cells can be immediately used or after another day of culture, if desired. Cells were collected using 1.5 mL protein low binding tubes (Eppendorf), centrifuged at 2800 rpm (~600 xg) for 1 min and washed once using PBS supplemented with 5 mM EDTA. For recombinant TPO signaling and detection of JAK2, STAT3 and STAT5 total protein and/or phosphorylation levels, $3.5 \times 10^4$ MKs were seeded into a 24-well plate and starved for 4 h in DMEM containing 0% FCS. Afterwards, they were stimulated using 0.5% recombinant TPO for 10 min, collected and centrifuged at 2800 rpm (~600 xg) for 1 min and washed once using PBS only.

Samples were immediately lysed with an appropriate volume (50-100 µL) of chilled 1x RIPA Buffer supplemented with Halt™ Protease and Phosphatase Inhibitor Cocktail in a 1:100 dilution. After 30min incubation on ice, the samples were clarified at 16000 xg for 10 min at 4°C and the supernatant was transferred into new tubes. Protein content was determined using a BCA protein assay according to the manufacturer's instructions by diluting 6 µL of the lysates in 54 µL 1x RIPA (1:10), followed by analysis of absorbance at 562 nm at a Tecan Spark microplate reader. Samples were aliquoted and frozen in liquid nitrogen and stored at -80°C for further use. For immunoblotting, 2-10 µg of the samples were used per lane.

#### 3.2.5.9 Spreading and IF stainings of BM MKs

To visualize the cytoskeleton, the cultured MKs from 3.2.5.3 or 3.2.5.4 were allowed to spread on different matrices. Glass coverslips (12mm) were coated with Horm collagen [50 µg $mL^{-1}$] for 2 h at 37°C (or O/N at 4°C) in a 24-well plate. After washing in PBS, coverslips were blocked using 1% BSA/PBS or MK medium for 30min at 37°C. After washing with PBS, 50-100 µL of the MK cell suspension were then seeded onto the coated coverslips in 500 µL Stempro MK medium containing 0.5% recombinant TPO or MK Medium containing 0.5% recombinant TPO and rHirudin [100 U $mL^{-1}$] and adhesion was allowed for 3 h at 37°C and 5% $CO_2$. Cells were washed with PBS, fixed and permeabilized for 20-30 min at RT in PHEM fixation buffer. MKs were stained for 1h at RT or 4°C O/N using 300 µL of an α-tubulin-AF488 labeled antibody [1 µg $mL^{-1}$]; 647N-conjugated phalloidin (1:400); anti-Arpc2 antibody (Arp2/3) [2 µg $mL^{-1}$]; anti-Vinculin antibody [0.5 µg $mL^{-1}$]; DAPI [300 nM]. If necessary, coverslips were washed three times with PBS and incubated with 300 µL of the respective AF-conjugated secondary antibody for 1h at RT (1:400). Afterwards, MKs were washed twice with PBS and once with $H_2O$ and CS were mounted using Fluoroshield. Visualization was performed with a Leica TCS SP8 confocal microscope and a 40x oil immersion objective (Leica Microsystems, Wetzlar, Germany).Analysis was performed as described in 3.2.9.

#### 3.2.5.10 Nuclear fractionation for immunoblotting

After enrichment of MKs on a BSA gradient as described in 3.2.5.4, $3.5x10^4$ MKs were seeded into a 24-well plate and starved for 4 h in DMEM containing 0% FCS. Afterwards, cells were stimulated using 0.5% recombinant TPO for 15 min, collected into protein low binding 1.5 mL tubes (Eppendorf) and washed once with PBS (3 min at 500 xg each step) and immediately lysed using the NE-PER Nuclear and Cytoplasmic Extraction Reagents. All the steps were carried out according to the manufacturer’s instructions for a packed cell volume of 10 µL. CERI and NER reagent contained Halt™ Protease and Phosphatase Inhibitor Cocktail in a 1:100 dilution. Note, that an additional washing step with 1 mL PBS was included to wash the nuclear fraction after extraction of the cytoplasmic fraction. Protein content was measured using the BCA protein assay as described in 3.2.5.8. For immunoblotting, 10 µg for the cytoplasmic fraction and 2 µg for the nuclear fraction were used per lane.

#### 3.2.5.11 Determination of Caspase 3/7 activity in cultured BM-derived MKs

Caspase 3/7 activity in BM-derived MKs was estimated by means of a commercially available Caspase-Glo® 3/7 Assay System according to the manufacturer’s instructions. Apoptosis was induced by treatment of MKs with 1 µM ABT-737 [1 µM] or DMSO [0.1%] as a control. Per well of a 96-well plate, 1000 MKs were seeded in a final volume of 50 µL after enrichment of MKs on a BSA gradient as described in 3.2.5.4. At the indicated timepoints, the cells were mixed with 50 µL of the reagents and absorbance was measured at a Tecan Spark microplate reader.

### 3.2.5.12 Cell Titer Glo Viability Assay of cultured BM-derived MKs

Cell viability of BM-derived MKs was estimated by means of a commercially available CellTiter-Glo® Luminescent Cell Viability Assay (Promega) according to the manufacturer's instructions. Apoptosis was induced by treatment of MKs with ABT-737 [1 µM] or DMSO [0.1%] as a control. Per well of a 96-well plate, 1000 MKs were seeded in a final volume of 50 µL after enrichment of MKs on a BSA gradient as described in 3.2.5.4. At the indicated timepoints, the cells were mixed with 50 µL of the reagents and absorbance was measured at a Tecan Spark microplate reader.

### 3.2.5.13 Quantitative RT-PCR on *in vitro* cultured BM-derived MKs

Total RNA was isolated from BM-derived MKs after enrichment on a BSA gradient as described in 3.2.5.8 using the TRIzol reagent (Invitrogen) according to the manufacturer's instructions. Briefly, cells were resuspended in 1 mL TriFast reagent after washing, vortexed for 15 sec and incubated for 15 min at RT. At this step, the samples can be stored at -80°C until further use or be suspended in 200 µL chloroform and mixed thoroughly for 15 sec. After 10 min incubation at room temperature samples were centrifuged at 12,000 xg for 5 min at room temperature. Total RNA was purified from the aqueous upper phase using the RNeasy Mini Kit (QIAGEN) according to the manufacturer's instructions. Reverse transcription of 400 ng of RNA was carried out with the High-Capacity cDNA Reverse Transcription Kit (Life Technologies). Quantitative PCR (qPCR) was performed with SYBR Select Master Mix on a ViiA7 (Life Technologies). Gene expression was calculated by the comparative ΔΔCt-method and normalized to the housekeeping gene Ppia and Hprt. All primers had melting temperatures of 58-60°C (Primer Express 3.0, Life Technologies).

**Table 3.18 Primers used for RT-PCR**

| Primer | Sequence 5' → 3' |
|---|---|
| Gata-1_Fw | CAC AAG ATG AAT GGT CAG AAC C |
| Gata-1_Rev | GTC GTT TGA CAG TTA GTG CAT T |
| Tuba4a_Fw | GCT TTC TGT TGA CTA TGG CAA A |
| Tuba4a_Rev | AGG TTG GAC GCT CAA TAT CTA G |
| Srf_Fw | TCC TTC CCC ATC ACC AAC TAC |
| Srf_Rev | CCT GTA CTC TTG AGC ACA GTC |
| Tpm4_Fw | GAG AAA GCT GAA GGA GAT GCA G |
| Tpm4_Rev | TCA TGG CTC GGT TCT CTA TTA C |
| Actn1_Fw | ACC CCT ATA CAA CCA TCA CG |
| Actn1_Rev | CTG CTG CCT TGC ATG TTC |

| | |
|---|---|
| Mpl_Fw | CTG CTA AAG TGG CAA TTT CCT G |
| Mpl_Rev | CTG AGG ACT TAG GGA GGA TTT C |
| Runx1_Fw | CCA TCA CCG TCT TTA CAA ATC C |
| Runx1_Rev | ATC ATC TAG TTT CTG CCG ATG T |
| Mkl1_Fw | GCC AAG GGA TCA TGC CG |
| Mkl1_Rev | CAT GAA ATG CAG CGG GG |
| Mkl2_Fw | ACC GCT CTG AGC TTG TCA GG |
| Mkl2_Rev | CAT GGG ACC AGG CCT TTG |
| Hprt_Fw | TCA GTC AAC GGG GGA CAT AAA |
| Hprt_Rev | GGG GCT GTA CTG CTT AAC CAG |
| Pp1a_Fw | GCG TCT CCT TCG AGC TGT TT |
| Pp1a_Rev | AAG TCA CCA CCC TGG CAC AT |
| Gp1ba_Fw | CTC TGT TCC TCC AAA GGA CTG TCT |
| Gp1ba_Rev | TCA CAG TTT ACT TCC AGC AGG C |
| Gp5_Fw | GGG TGC AGA ACT GCT TCA GAC |
| Gp5_Rev | AAA GGT TGG GCA CGC AAG |
| Gp6_Fw | CCA GGT ACC CAC GGA AGA ATC |
| Gp6_Rev | AAA ACC AAA TGG AGG GCT CAG |
| Gp9_Fw | TAC CAG CCC ACA AAA GGT GTG |
| Gp9_Rev | GGA GGC CCC AGG TAG TCA TC |
| FlnA_Fw | CAA CAG CCC CTT CCA AGT TAC |
| FlnA_Rev | ACA TCC AGC CCA TTA ACG C |

### 3.2.6 *In situ* and *ex vivo* analysis of BM MKs

#### 3.2.6.1 IF stainings on whole femora cryosections

IF stainings were largely performed as described previously.[106] In detail, mice were sacrificed, and femora was isolated. Bones were fixed in 4% PFA in PBS for 4 h at 4°C (or 1 h at RT) and subsequently transferred to a serial gradient of sucrose in PBS solutions of 10, 20 and 30% (w/v), each for 24 h at 4°C. Finally, the samples were embedded in SCEM medium into cryo mold dishes, deep-frozen and kept at -80°C until sectioning. For high-resolution imaging by using the Kawamoto method as previously described[269], all the previous and upcoming steps were performed with PHEM buffer instead of PBS. For IF-staining, organs were sliced into 10 µm sections on Kawamoto adhesive films[270] with a cryostat and fixed onto superfrost glass slides using adhesive stripes. For IF-staining, sections were thawed and rehydrated for 20 min in PBS. For high-resolution imaging sections, were instead immediately fixed for 10 min in 1% PFA in PHEM buffer containing 0.1% TX-100. After washing three times with PBS containing 5% FCS and 0.1% Tween20 or Triton X-100, unspecific binding was prevented using a blocking buffer (=washing buffer), which additionally contained 5% goat serum. After washing once, sections were incubated 45 min with 100 µL of AF488-conjugated anti-GPIX antibody [2 µg mL$^{-1}$,Xia.B4] to label platelets and MKs, unconjugated or AF647-conjugated anti-CD105 antibody [2.5 µg mL$^{-1}$ or 3.33 µg mL$^{-1}$ respectively] to stain the endothelium and DAPI [300 nM] to stain the nucleus. Antibodies were diluted in either washing buffer or PBS only. Optionally, slides were also stained with 100 µL of anti-Tubb1 antibody [5 µg mL$^{-1}$] and Atto-647N-conjugated phalloidin (1:400). After washing three times, slides were incubated with the respective secondary antibody anti-rabbit IgG Cy3 (1:400) for 45 min at RT. After washing three times slides were mounted with Fluoroshield. Tile scan images were acquired at a Leica TCS SP8 confocal microscope using a 25x water immersion objective while single MKs and *field of views* (FOV) were imaged using a 40x oil immersion objective (Leica Microsystems, Wetzlar, Germany). Sections were analyzed manually using Fiji (ImageJ) software. Using the FOV method in earlier images, at least 15 FOVs out of two sections were analyzed. FOV were distributed over the complete femur bone and were randomly selected.

#### 3.2.6.2 Assessment of MK Ploidy (FACSCalibur)

Both femora and tibia of mice were isolated and the BM was harvested by either flush or spin isolation. At least one tenth of the total cells were transferred to a new tube (volumes to be up-scaled when using the whole BM cells), centrifuged for 5 min at 300 xg and resuspended in 450 µL of a 1:1 dilution of CATCH buffer supplemented with 5% FCS. 50 µL of all samples were pooled for the isotype/unstained control and adjusted to 400 µL final volume. Unspecific binding sites were blocked by incubation with an anti-CD16/CD32 antibody [0.02 mg mL$^{-1}$; FcγRII/III, clone 2.4G2] for 15 min on ice. Subsequently, 100 µL in-house labeled FITC-conjugated anti-CD41 (GPIIb, MWReg30) antibody was added to reach saturating conditions (MWReg30). A FITC-labeled rat-IgG or no antibody staining was used as isotype control. Cells were incubated for further 20 min on ice. Cells were washed with PBS (5 min at 300 xg) and fixed in PBS containing 1% PFA/0.1% EDTA for 10-15 min on ice. Fixed cells were washed with PBS (10 min at 300 xg) and permeabilized in PBS containing 0.1% Triton X-100 for 10 min on ice. After an additional wash with PBS (10 min at 300 xg), the cells were stained with 0.5 - 1mL of a propidium iodide [50 µg mL$^{-1}$] staining solution containing RNase A [100 µg mL$^{-1}$] in PBS O/N at 4 °C in the dark. Data were collected on a FACS Calibur (BD Biosciences) by measuring at least 1x10$^{6}$ total cells and analyzed using FlowJo v10 software (FlowJo, LLC, Ashland OR, USA).

### 3.2.6.3 Assessment of MK Ploidy – Improved method (FACSCelesta)

Initial steps were carried out as described above Subsequently, MKs were labeled using a double staining. To this end, 100 µL of an antibody mix diluted in PBS were added, containing the MK-specific AF488-conjugated anti-CD41 [1 µg mL$^{-1}$; MWReg30] and AF647-conjugated anti-GPIX antibodies [1 µg mL$^{-1}$;Xia.B4]. An antibody only staining as well as SYTOX Orange only staining (see below) were used as isotype controls. After the fix and permeabilization of the cells described in the previous section, cells were stained with 0.5 - 1mL of a SYTOX orange staining solution (depending on the amount of cells used) O/N at 4 °C in the dark. The mix contains 1 µL per sample of SYTOX Orange [25 µM = 1:200 pre-diluted in PBS] and RNase A [100 µg mL$^{-1}$] diluted in PBS. Data were acquired using a FACSCelesta (BD Biosciences, Heidelberg, Germany) by measuring at least 3-5x10$^6$ total cells and analyzed using FlowJo v10 software (FlowJo, LLC, Ashland OR, USA).

### 3.2.6.4 Assessment of MK GP expression

Both femora (and tibia) of male mice were isolated using the spin isolation method described in 3.2.5.1. After centrifugation for 5 min at 300 xg, cells were resuspended in 2 mL of a 1:1 dilution of CATCH buffer containing 5% FCS. One tenth of the cells were used per condition. Unspecific binding sites were blocked by incubation with an anti-CD16/CD32 antibody [0.02 mg mL$^{-1}$; FcγRII/III, clone 2.4G2] for 15 min on ice. Subsequently, samples were stained with saturating conditions using 100 µL of the corresponding FITC conjugated antibodies targeting the different GPs, containing an AF647-conjugated anti-GPIIb antibody [1µg mL$^{-1}$; MWReg30] to additionally label MKs the same for all conditions. Cells were incubated for 20 min on ice and data was immediately acquired using a FACSCelesta (BD Biosciences, Heidelberg, Germany) and analyzed using FlowJo v10 software (FlowJo, LLC, Ashland OR, USA).

### 3.2.6.5 TEM of BM MKs

Mice were sacrificed, femora were isolated, cut into 4 mm pieces and immediately transferred into Karnovsky fixation buffer. Bones were fixed O/N at 4°C under rotation and afterwards decalcified in decalcification buffer over 4 days. Fatty components were fixed by incubation in 2% osmium tetroxide in 50 mM cacodylate buffer (pH 7.2). Afterwards, bones pieced were stained using 0.5% aqueous uranyl acetate, dehydrated in a graded ethanol series and embedded in epon. Ultra-thin sections were stained with 2% uranyl acetate (in 100% ethanol) followed by lead citrate. Images were taken on a Zeiss EM900 TEM (Zeiss or JEOL JEM-2100.

#### 3.2.6.6 BM explant PPF

Protocol was adapted from[203] and modified to match our technical prerequisites. Intact BM were obtained by flushing mouse femora with Tyrode-buffer without $Ca2^+$. Several 0.5 mm thick transversal sections from one femur from the same mouse were placed at 37°C in single wells of a 96-well plate containing 300 µL $CO_2$ independent medium supplemented with 5% mouse serum. MKs were observed at 37°C using a Leica TCS SP8 confocal microscope for 12 h by taking pictures every 10 min using a 10x air objective. To get a better overview, tile-scans of whole wells were acquired throughout the observation period using the Leica LasX Navigator.

#### 3.2.6.7 Generation of BM-chimeric mice

10-week old mice were irradiated for 14 min (160 V, 6.3 mA). BM cells of donor mice were harvested by spin isolation (3.2.5.1), resuspended in DMEM medium and counted. On the same day, $4\text{-}6\times10^6$ donor cells per mouse were retro-orbitally injected in a final volume of 150 µl. Neomycin [2g $L^{-1}$] was added to the drinking water for two weeks. Moreover, the mice only received high-energetic food. Mice were analyzed 8 weeks after irradiation and transplantation.

### 3.2.7 Cytokine levels in the BM

#### 3.2.7.1 Enzyme-linked immunosorbent assays on BM plasma

BM plasma was obtained as described in 3.2.5.1 and centrifuged at 14.000 rpm at 4°C for 10 min. BM plasma was prediluted (1:1). Assessment of TGFβ1 required activation of the samples using 1M HCl, followed by neutralization of the acidifed samples with 1.2M NaOH. TGFβ1 levels were analyzed using the mouse TGFβ1 DuoSet. Plates were analyzed at a Multiskan Ascent (96/384) plate reader (ThermoFisher Scientific, Waltham, USA) at 450 nm with wavelength correction (570 nm).

### 3.2.8 Statistical analysis

Results are displayed as mean ± *standard deviation* (SD) from at least three independent experiments per group, if not stated otherwise. Data distribution was analyzed using the Shapiro-Wilk-test and differences were statistically analyzed using unpaired, two-tailed Student's t-test, one-way ANOVA or Fisher's exact test. Tukey or Sidak's post-hoc test was used for multiple comparisons. P-values < 0.05 were considered as statistically significant *P≤0.05; **P<0.01; ***P<0.001. Results with a P-value > 0.05 were considered as *not significant* (ns).

### 3.2.9 Image processing and analysis

Adjustments of brightness and contrast, maximum intensities of z-projections as well as analysis of area, mean fluorescent intensity of spread MKs were performed using Fiji (ImageJ) and the use of self-written macros. Podosome number was quantified using the maximum intensity of a z-stack in Fiji (NIH, USA) using a modified macro recently described.[271] Adjustments were employed to the whole image and all images of the respective experiment were treated equally.

### 3.2.9.1 Macro: Maximum Intensity (Z-projections) of .lif files and save as .TIFF

```
macro 'convert LIF tiff' {

/*
 * - converts LIF files into TIFF.
 */

Z_PROJECT = "True"; // "True" to make a max projection; "False" to leave z stacks intact

run("Bio-Formats Macro Extensions");

dir1 = getDirectory("Choose folder with lif files");
list = getFileList(dir1);

setBatchMode(true);

// create folders for the tifs
dir1parent = File.getParent(dir1);
dir1name = File.getName(dir1);
dir2 = dir1parent+File.separator+dir1name+"_MIP";
if (File.exists(dir2)==false)
        {
        File.makeDirectory(dir2); // new directory for tiff
    }
 for (i=0; i<list.length; i++)
        {
    showProgress(i+1, list.length);
    print("processing ... "+i+1+"/"+list.length+"\n         "+list[i]);
    path=dir1+list[i];

    //how many series in this lif file?
    Ext.setId(path);//-- Initializes the given path (filename).
    Ext.getSeriesCount(seriesCount); //-- Gets the number of image series in the active dataset.

    for (j=1; j<=seriesCount; j++)
        {
        run("Bio-Formats", "open=path autoscale color_mode=Default view=Hyperstack stack_order=XYCZT 
series_"+j);
        name=File.nameWithoutExtension;
            //retrieve name of the series from metadata
        text=getMetadata("Info");

        n1=indexOf(text," Name = ")+8;  // the Line in the Metadata reads "Series 0 Name = ". Complete 
line cannot be taken, because
                                        // The number changes of course. But at least in the current 
version of Metadata this line is the
                                        // only occurence of " Name ="
        n2=indexOf(text,"SizeC = ");    // this is the next line in the Metadata
        seriesname=substring(text, n1, n2-2);
                seriesname=replace(seriesname,"/","-");
                rename(seriesname);

            // project and save
            getDimensions(width, height, channels, slices, frames); // check if is a stack of any kind

        if (slices>1) // it is a z stack
                {
        if (Z_PROJECT == "True")
                {
                run("Z Project...", "projection=[Max Intensity]");
                selectWindow("MAX_"+seriesname);
                run("8-bit");
                }
                saveAs("Tiff", dir2+File.separator+name+"_"+seriesname+"_MIP"+".tif");
                }
        else
        {
                saveAs("Tiff", dir2+File.separator+name+"_"+seriesname+"_MIP"+".tif");
        }
```

```
        run("Close All");
        run("Collect Garbage");
        }
        }
showMessage(" -- finished --");
run("Close All");
setBatchMode(false);

} // macro
```

### 3.2.9.2 Macro: Measurement of cellular shape descriptors, podosomes and MFI (e.g. F-actin or α-tubulin) in spread MKs

The maximum Z-projections created above can be further used for further analysis in the following macro:

```
// option set-up
run("Options...", "iterations=1 count=1 black do=Nothing");
run("Set Measurements...", "area mean standard modal min centroid center perimeter bounding fit shape
feret's integrated median skewness kurtosis area_fraction stack display redirect=None decimal=3");

dir = getDirectory("image");

outputDirName = dir + "Analysis"; //adds a new folder name to the image directory name from before
File.makeDirectory(outputDirName); //Creates the folder with the specified name

outputDirPath = outputDirName + File.separator; // important for later on when saving since the path
needs to end with an "/"

imageName = getTitle(); // get the title of the original image
run("Split Channels");

//define a variable for the channels to have it easier later on; Depending on how images are recored;
Assigne the right channels
dapi = "C1-" + imageName;
factin = "C2-" + imageName;
tubulin = "C3-" + imageName;
actubulin = "C4-" + imageName;

// Here it closes windows which are not needed; Can be adjustet for further measurments below
selectWindow(dapi);
close();
selectWindow(tubulin);
close();
selectWindow(actubulin);
close();

run("Duplicate...", "title=[copy_"+ factin +"]");
copyfactin = getTitle();
selectWindow(factin);
run("Duplicate...", "title=[podosome_"+ factin +"]");
podosome = getTitle();
selectWindow(copyfactin);

// User interference to draw black lines between neighbouring cells with pencil tool = black line
run("Line Width...", "line=5");
setTool("freeline");
setBackgroundColor(0, 0, 0);


waitForUser("Please seperate cells that touch each other and press OK afterwards (If not, draw a line
line in any black area, otherwise error)");
run("Clear", "slice");
run("Select None");
// End user interference
```

```
run("8-bit");
run("Gamma...", "value=0.5"); // Potential adjustment necessary 0.1-0.5 if cells are not detected right
run("Enhance Contrast...", "saturated=1 normalize");
run("Median...", "radius=5");
run("Auto Threshold", "method=Li white");
run("Analyze Particles...", "size=1000-Infinity exclude clear add"); // exclude can be removed if you
also want to consider cells that touch the edge of the image
run("Create Selection");
roiManager("Add");
close("Summary");

// Here starts the ROI Manager Part to include holes in the ROIs to save them later on
roiNumber = roiManager("count");
lastRoi = roiNumber-1

        for (roi = 0; roi < roiNumber; roi++) {
                                        selectWindow("ROI Manager");
                                        roiManager("Select", newArray(roi,lastRoi));
                                        roiManager("AND");
                                        roiManager("Update");
                                        selectWindow("ROI Manager");
                                        roiManager("deselect");

        }
                                        selectWindow("ROI Manager");
                                        roiManager("deselect");
                                        roiManager("Select", lastRoi);
                                        roiManager("delete");

// Here it ends

//Saving of overlay Image + ROIs
selectWindow("ROI Manager");
roiManager("deselect");
roiManager("Show All with labels");
run("Labels...", "color=white font=36 show draw bold");
run("Flatten");
saveAs("PNG", outputDirPath + imageName);
roiManager("Deselect");
roiManager("Save", outputDirPath + imageName + ".zip");
close();

run("Set Measurements...", "area mean perimeter shape integrated median display redirect=None
decimal=3");

roiNumber = roiManager("count");

//MFI F-Actin ; Also other MFIs could be beasured within the cell; See above and just choose another
window name
for (roi = 0; roi < roiNumber; roi++) {
        selectWindow(factin);
        roiManager("Select", roi);
        roiManager("Measure");
}
close(copyfactin);
close(factin);

// User interference before it continues with the podosomes
waitForUser("Please copy your Results first into an Excel sheet and press Okay to continue with
Podosome measurement");
selectWindow("Results");
run("Clear Results");

//Podosomes

for (roi = 0; roi < roiNumber; roi++) {
        selectWindow(podosome);
        roiManager("Select", roi);
        run("Duplicate...", "title=[measurepodosome_"+ podosome +"]");
        measurepodosome = getTitle();
```

```
        selectWindow(measurepodosome);
        run("8-bit");
        run("Smooth", "stack");
        run("Subtract Background...", "rolling=50");
        run("Convolve...", "text1=[-1 -1 -1 -1 -1\n-1 -1 -1 -1 -1\n-1 -1 30 -1 -1\n-1 -1 -1 -1 -1\n-1 -
1 -1 -1 -1\n] normalize");
        run("Median...", "radius=3");
        setOption("BlackBackground", false);
        run("Make Binary", "method=Default background=Default");
        run("Set Measurements...", "area redirect=None decimal=3");
        run("Analyze Particles...", "size=0.20-Infinity circularity=0.50-1.00 show=Masks display");
        close();
        close();
        close(measurepodosome);

        // The following prints the podosome number and average podosome size seperated by tabs; Just
copy+paste into Excel
        run("Summarize");
        N = nResults-4;
        N2 = nResults-4;
        mean_area = getResult("Area",N2);

        //Return values
        print(""+N+"\t"+""+mean_area);
        selectWindow("Results");
        run("Close");
        }
```

### 3.2.9.3 Macro: BM MK count in whole immunostained femora cryosections

The following macro allows to determine the MK count in whole immunostained femora cryosections after stitching of the tile scans. The macro works quite well with WT MKs, but also to some extend with KO MKs, depending on their cellular integrity. However, double-checking is necessary to exclude / include MKs which have been falsely or not detected, as well as to determine intrasinusoidal MK localization.

```
// option set-up
run("Options...", "iterations=1 count=1 black do=Nothing");
run("Set Measurements...", "area redirect=None decimal=3");
//roiManager("Delete");

//Change Stack colors; Adjust colors according to your channel order
// e.g. DAPI
Stack.setChannel(1);
run("Blue");
setMinAndMax(0, 210);
// e.g. vessels
Stack.setChannel(2);
run("Magenta");
setMinAndMax(10, 150);
// e.g. MKs
Stack.setChannel(3);
run("Green");
setMinAndMax(0, 150);

//Get directory Informations

dir = getDirectory("image");
outputDirName = dir + "Analysis"; //adds a new folder name to the image directory name from before
File.makeDirectory(outputDirName); //Creates the folder with the specified name
outputDirPath = outputDirName + File.separator; // important for later on when saving since the path
needs to end with an "/"
```

```
//Copy image + getFilenames
original = getTitle(); // get the title of the original image
run("Duplicate...", "title=[copy_"+ original +"] duplicate");

copy = getTitle(); // get the title of the original image
run("Split Channels");

//define a variable for the channels to have it easier later on
dapi = "C1-" + copy;
endoglin = "C2-" + copy;
mks = "C3-" + copy;

selectWindow(dapi);
close();
selectWindow(endoglin);
close();

//Segmentation
run("8-bit");
run("Gamma...", "value=2");
run("Enhance Contrast...", "saturated=1 normalize");
setAutoThreshold("Huang dark");
setOption("BlackBackground", true);
run("Convert to Mask");
run("Erode");
run("Median...", "radius=5");
run("Dilate");
//run("Dilate");
//run("Dilate");
run("Fill Holes");
//run("Median...", "radius=5");

//Measurements
run("Analyze Particles...", "size=250-Infinity circularity=0.2-1.00 display include add");


//Print
        run("Summarize");
        N = nResults-4;
        print(N);
        selectWindow("Results");
        run("Close");

selectWindow(original);
roiManager("Show All without labels");

//run("Channels Tool...");
Stack.setDisplayMode("composite");

run("Cell Counter");
```

# 4 RESULTS

## 4.1 Isolation of murine BM by centrifugation or flushing for the analysis of hematopoietic cells – a comparative study

Mice are commonly used to investigate the function of HSCs originating from the BM compartment.[272,273] The general limitation when studying HSCs in mice is that only a limited number of cells can be recovered. The isolation of BM cells from murine long bones is traditionally achieved by flushing with a liquid filled syringe (flush isolation).[83] However, this method is rather time consuming and prone to variability regarding cell yield and quality. This was a particular challenge for my projects when studying MKs, the giant, polyploid progenitors of platelets, which are anyhow very fragile and therefore highly susceptible to fragmentation during BM isolation. In order to study MK biology, one is in constant need of a high amount of BM HSCs. As an alternative to flushing, a centrifugation-based method for BM isolation has been described (spin isolation).[268,274] However, the suitability of the centrifugation-based protocol has so far not been compared to the traditional flushing method in terms of cell yield, quality and suitability for follow-up experiments and since all the former publications are based on the flushing method, a direct comparison of both methods was unavoidable. In this study, we adapted the centrifugation-based isolation protocol described by Amend *et al.*[268] for our research and compared cell viability and distribution of HSCs, immune cells and MKs to the flushing method.

The following study was carried out in collaboration with Carina Gross (Experimental Biomdecine, Stegner Group).[275]

### 4.1.1 Spin isolation shows superior cell yield with comparable distribution of native hematopoietic and immune cell populations

To address whether spin isolation of BM is suitable for the study of hematopoietic cells we directly compared the flushing[83] and the spin isolation[268] methods by using purchased male C57Bl/6J mice (10-14 weeks of age). Murine BM of femora and tibiae of C57Bl/6J mice was isolated as described in the methods section (3.2.5.1 and 3.2.5.2) (Figure 8). Strikingly, BM isolation of four mice was markedly faster with the spin isolation protocol (spin isolation: 10 min; flush isolation: 35 min). In addition, the bones appeared completely white and BM cell pellets were considerably bigger after centrifugation (Figure 8A,B), indicating that all BM was recovered.

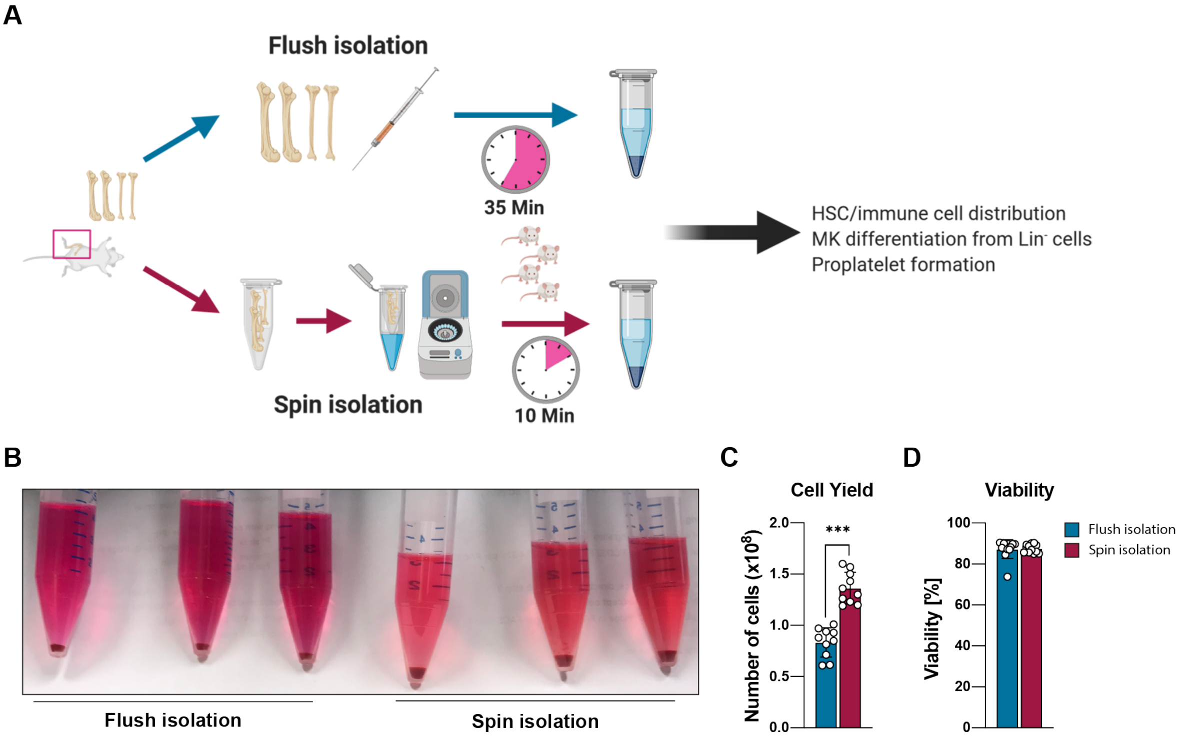

**Figure 8: Comparison of cell yield after flush and spin isolation. A** Workflow of both methods indicating the time used for the isolation of BM cells with each method. **B** Representative images of cell pellets obtained after flush and spin isolation (n = 3 mice per condition). **C** Determination of total cell numbers after BM isolation using a Countess® Cell Counting Chamber (cut-off set from 7-60 µm) (n = 10 mice per condition). **D** Cell viability was determined by flow cytometric analysis using a dead cell marker kit (Thermo scientific) (n = 10 mice per condition). One dot represents one animal. All data are indicated as mean ± SD. For **(C,D)** an unpaired Student's t-test was used. *p≤0.05, **p<0.01, ***p<0.001. **(D)** Experiment performed by Carina Gross (Experimental Biomedicine, Stegner Group). (**A)** was created with **BioRender.com**. Heib & Gross *et al.*, **Platelets**, 2020.[275]

Notably, the centrifugation step for BM extraction was modified from 10000 xg for 15-20 s described by Amend *et al.*[268] to 2500 xg for 1 min into a defined volume of medium (0.1 mL), allowing easier cell pellet reconstitution. This adaption furthermore allows recovery of the BM cell supernatant immediately after spin isolation, which can be used for cytokine analysis or comparable assays (see Figure 45). Quantification of total cell numbers after isolation with a Countess® Automated Cell Counter (counting range 7-60 µm) revealed significantly higher cell yield after spin isolation as compared to flush isolation (Figure 8C). The cell viability was equally high for both methods (Figure 8D), demonstrating that the centrifugation speed of the spin isolation method does not impair cell viability. Next, we addressed the question whether the two isolation methods had differential effects on HSC or immune cell distributions in the BM, whereas we obtained comparable results for both methods (Carina Gross, Thesis, 2020; Heib, Gross *et al.*, **Platelets**, 2020).[275]

In summary, the spin isolation method is superior with regard to cell yield but results in a similar distribution of the recovered HSC and immune cell populations.

### 4.1.2 Spin isolation shows comparable results in MK-related downstream assays

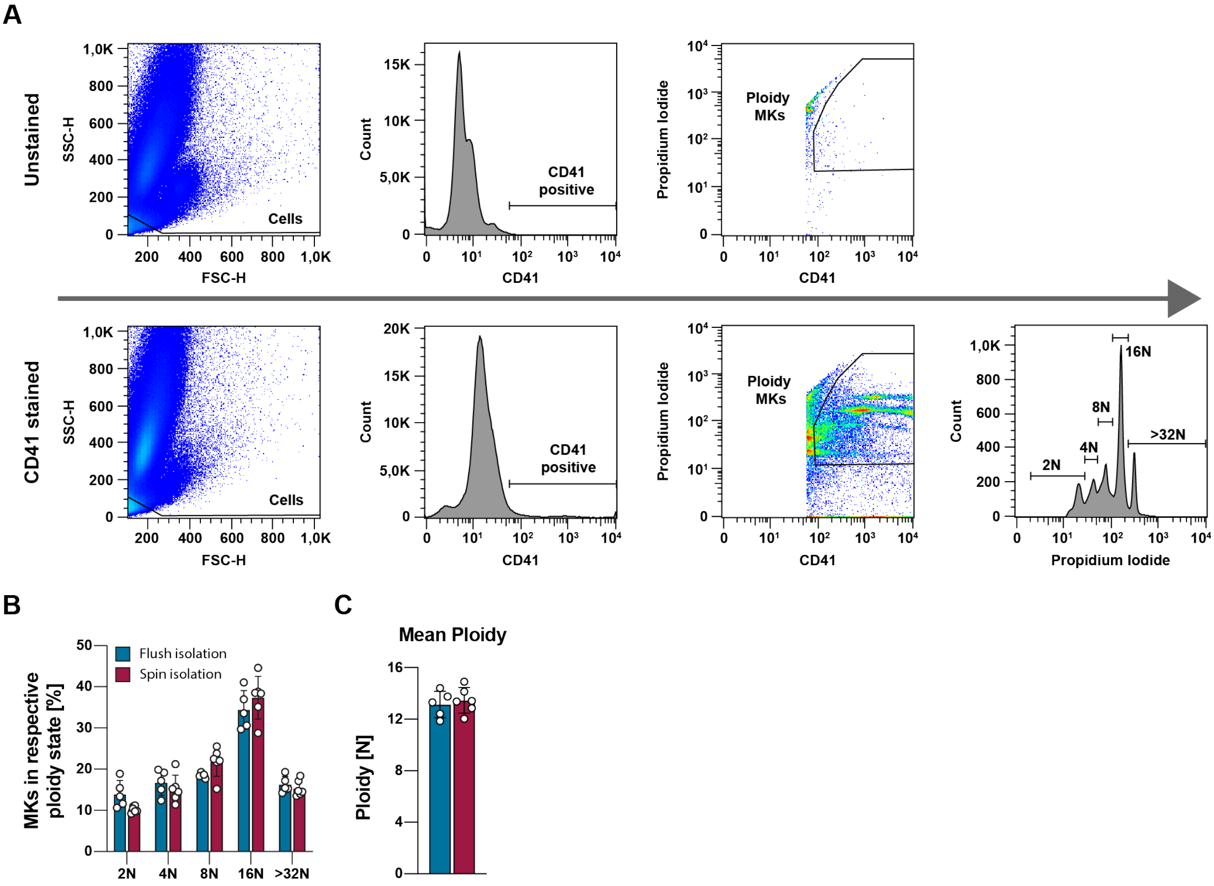

**Figure 9: Characterization of native BM MKs. A** Gating strategy for ploidy measurements of isolated native BM MKs by flow cytometry (FACSCalibur, BD Biosciences). Cells were identified by FSC and SSC properties. CD41 (MWReg30) positive cells were considered MKs and plotted against the PI signal to determine the ploidy distribution, which was quantified by histogram analysis. **B** Ploidy distribution of isolated primary BM MKs. **C** Mean MK ploidy (n = 5 vs 6 mice, representative of two independent experiments). One dot represents one animal. All data are indicated as mean ± SD. For **(B)** multiple t-tests (two-stage linear step-up procedure and **(C)** the Mann-Whitney-U-Test was used. *p≤0.05, **p<0.01, ***p<0.001. Heib & Gross *et al.*, **Platelets**, 2020.[275]

To compare both methods with respect to their suitability for MK studies, we first assessed ploidy levels of native BM MKs. MKs were identified by their *front scatter* (FSC) and *side scatter* (SSC) properties and expression of the integrin αIIb (CD41/GPIIb), a MK and platelet-specific GP. *Propidium iodide* (PI) staining was used to determine the ploidy status of CD41$^+$ cells

(Gating: Figure 9A). In line with the literature[5,276], we found comparable distributions of 2N to >32N MKs, the largest population being represented by the 16N peak (Figure 9B), resulting in a comparable mean ploidy (Figure 9C).

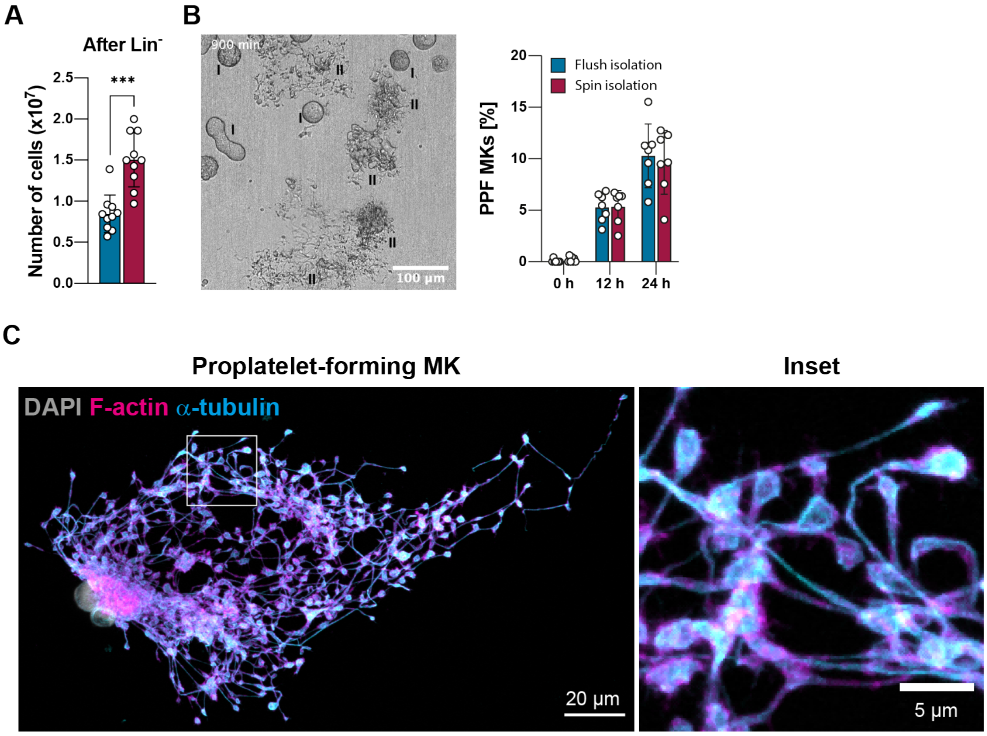

**Figure 10: Characterization of *in vitro* cultured MKs. A** Determination of Lin⁻ cell numbers using a Countess® Cell Counting Chamber (cut-off set from 7-60 µm after Lin⁻ depletion (n = 10 mice per condition). **B** Analysis of PPF of cultured BM-derived MKs over 24 h by time lapse microscopy in $CO_2$-independent culture medium (Leica TCS SP8). Left: Representative picture at 24 h. MKs were divided in Class I = Non-proplatelet-forming MKs (roundish or elongated) and Class II = PPF MKs. Right: quantitative analysis of PPF over time using Fiji software (n = 7 mice per genotype, two independent experiments were pooled). **C** Representative confocal images of an immunofluorescently labeled proplatelet-forming BM-derived MK at 24h after enrichment by BSA gradient. F-actin is stained by phalloidin (magenta), α-tubulin in cyan and the nucleus is counterstained with DAPI in grey. The inset panel shows a detailed view of proplatelet structures. One dot represents one animal. All data are indicated as mean ± SD. Unpaired Student's t-test was used. $^*p \leq 0.05$, $^{**}p < 0.01$, $^{***}p < 0.001$. Heib & Gross *et al.*, **Platelets**, 2020.[275]

To study potential differences between the isolation methods regarding the quality of the cells for further *in vitro* culture, a lineage depletion was performed and Lin⁻ cells were differentiated to MKs over several days in the presence of TPO and rHirudin.[277] Consistent with the higher total cell yield (Figure 8C) also significantly more Lin⁻ cells were recovered after spin isolation (Figure 10A). The disintegration of mature MKs into long cytoplasmic protrusions, so-called ‘proplatelets’, was analyzed by time-lapse microscopy over 24 h after enrichment of mature MKs. For analysis, MKs were grouped into class I (roundish or elongated MKs) and class II (proplatelet-forming MKs). PPF MKs were identified by the presence of multiple branched protrusions with characteristic swellings (‘beads-on-a-string’) and nascent proplatelet tips (Figure 10B,C).[278] Quantification showed that the number of PPF MKs was indistinguishable between both isolation methods at the indicated timepoints (0 h, 12 h and 24 h), revealing comparable cell quality (Figure 10B).

In summary, we demonstrate that the adapted centrifugation-based isolation protocol for murine BM cells pronouncedly reduces the experimental duration while minimizing variability through application of defined centrifugation forces. In addition, we were able to increase the cell yield by approximately 30%, while reducing experimental time, costs and animals needed, and showed at the same time that the spin isolation is highly suitable for studies on *in vitro* cultured BM-derived MKs. Therefore, the adapted spin isolation was used for all further studies.

## 4.2 RhoA/Cdc42 signaling drives cytoplasmic maturation but not endomitosis in MKs

We have previously shown that the Rho GTPases RhoA and Cdc42 are key players in a regulatory circuit that controls MK localization at BM sinusoids *in vivo*. We furthermore made the observation that RhoA/Cdc42 double-deficient mice exhibit a severe macrothrombocytopenia and impaired PPF *in vivo*[251], however, the mechanisms underlying these pronounced defects remained to be identified. To study RhoA/Cdc42 signaling in MK maturation and platelet biogenesis, we generated conditional KO (Pf4-Cre/loxP) mice lacking both RhoA and Cdc42 (*RhoA/Cdc42*$^{-/-}$*,* further referred to as *DKO*) in MKs and platelets and analyzed them alongside the respective single-deficient (*RhoA*$^{-/-}$ and *Cdc42*$^{-/-}$) mice (Figure 11A).

Note that some initial experiments were carried out by Dr. Deya Cherpokova (Experimental Biomedicine, Nieswandt Lab)[279] and were recapitulated for the better understanding of the story line.

### 4.2.1 Genetic ablation of RhoA and Cdc42 impairs platelet biogenesis and results in severe macrothrombocytopenia

In line with our previous study[251], we observed that the majority of MKs localized at BM sinusoids in *WT* mice, while a large proportion of intact MKs was situated in the sinusoidal lumen in *RhoA*$^{-/-}$ mice (Figure 11B,C). This unique mislocalization was fully reverted when Cdc42 was concomitantly ablated, but the number of BM MKs in the *DKO* mice was markedly increased, and the MKs displayed an abnormal, irregular morphology and clustered around the sinusoids (Figure 11B,D). Strikingly, *DKO* animals exhibited a severely aggravated macrothrombocytopenia compared to either of the single KOs with peripheral platelet counts lower than 30% of *WT* and a pronounced increase in platelet size (Figure 11E). Although plasma TPO levels are generally considered to be inversely related to platelet counts[73,280], we did not observe a significant elevation of TPO levels in *DKO* mice (Figure 12A) (Deya Cherpokova, Thesis, 2015).[279] These findings could, however, also be due to the increased numbers of MKs in *DKO* mice sequestering the TPO, thus compensating for the low platelet count. Of note, potential changes in HSCs populations have yet not been addressed.

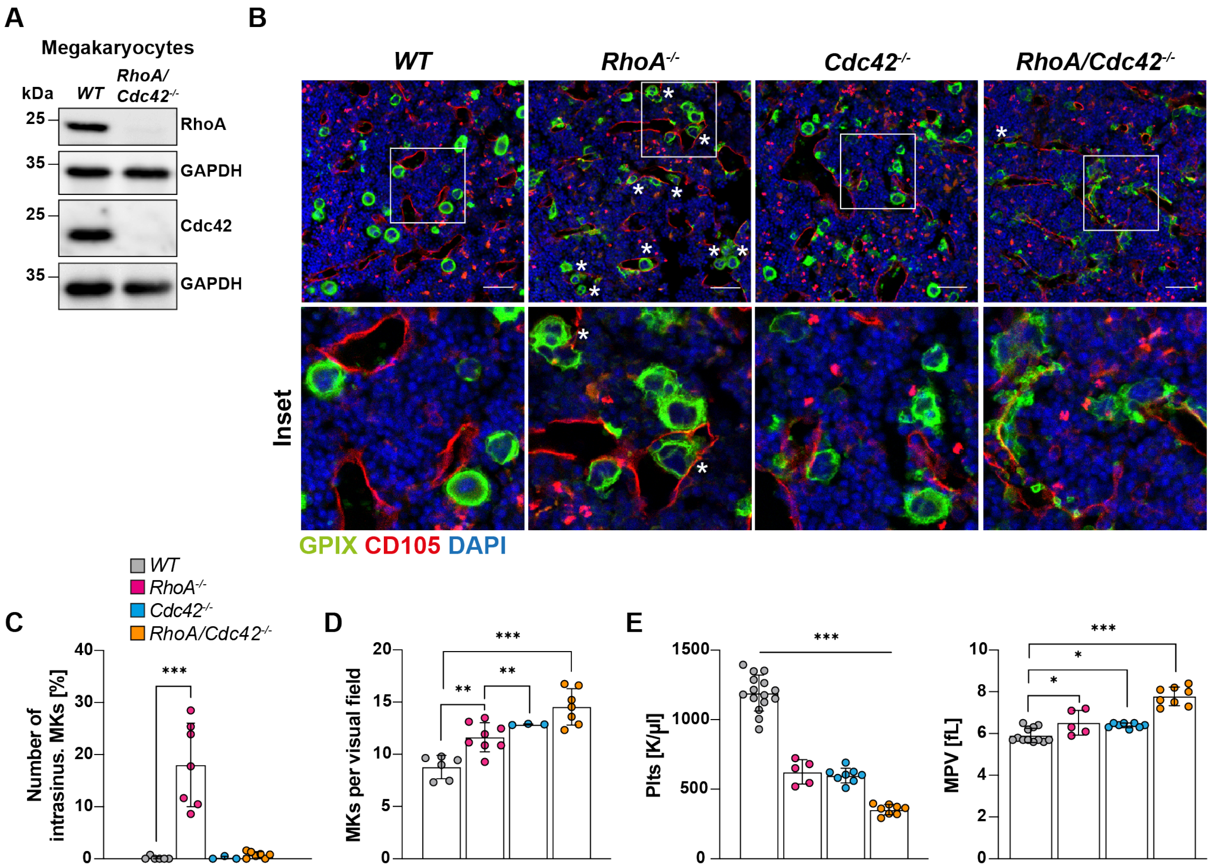

**Figure 11: Severe macrothrombocytopenia in *RhoA/Cdc42*$^{-/-}$ mice. A** Representative immunoblots showing the efficient deletion of RhoA and Cdc42 in MK lysates using the *Pf4-Cre* system. **B** Representative confocal images of immunostained BM cryosections of depicted mice (40x oil objective, Leica TCS SP8). MKs, proplatelets, and platelets are shown by GPIX staining in green. Endoglin staining (red) labels vessels. DAPI, blue. The asterisk indicates *intrasinusoidal* (intrasin.) MKs Scale bars, 50 µm. **C** Statistical analysis of intrasinusoidal MK localization using Fiji software (n = 6, 7, 3, 7). **D** Peripheral platelet count (n = 15, 5, 8, 8) and size (n = 12, 5, 8, 8) were measured using an automated hematology analyzer (scilVet). One dot represents one animal. All data are indicated as mean ± SD. One-way ANOVA test with Tukey's correction for multiple comparisons. *P≤0.05, **P<0.01, ***P<0.001. ns = *non-significant*. Heib *et al.,* **submitted.**

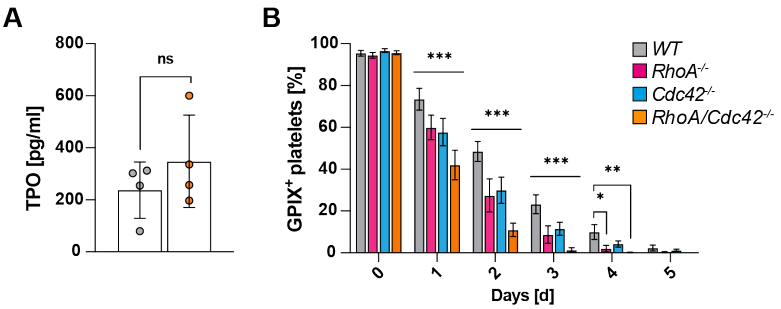

**Figure 12: Macrothrombocytopenia in *RhoA/Cdc42*$^{-/-}$ mice is not due to enhanced platelet clearance.** **A** Plasma TPO levels were determined by an ELISA system (n = 4 mice per genotype). **B** Platelet lifespan was determined by flow cytometry (FACSCalibur, BD Biosciences) by quantifying the percentage of fluorescently labeled GPIX$^+$ platelets at the indicated time points after injection of a DyLight 488-conjugated anti-GPIX antibody (n = 4 mice per genotype, representative of three independent experiments. For **(A)** Multiple unpaired two-tailed Student's t-test and **(B)** Two-way ANOVA test with Tukey's correction for multiple comparisons was used. *P≤0.05, **P<0.01, ***P<0.001. ns = *non-significant*. Experiments were performed by Deya Cherpokova, Thesis, 2015. Heib *et al.,* **submitted.**

Thrombocytopenia may be caused by enhanced platelet clearance by the reticuloendothelial systems in the liver and spleen. In *DKO* mice, the platelet life span was pronouncedly reduced to less than three days, compared to five days in *WT* and four days in the respective single-deficient mice (Figure 12B).[232,246] Accompanying the enhanced clearance, a significant increase in the proportion of circulating young, reticulated platelets (*thiazole orange* (TO)-positive) platelets was evident in *RhoA/Cdc42*$^{-/-}$ mice and to a lesser extent in *RhoA*$^{-/-}$ mice, while *Cdc42*$^{-/-}$ platelets were comparable to the *WT* (Figure 13).

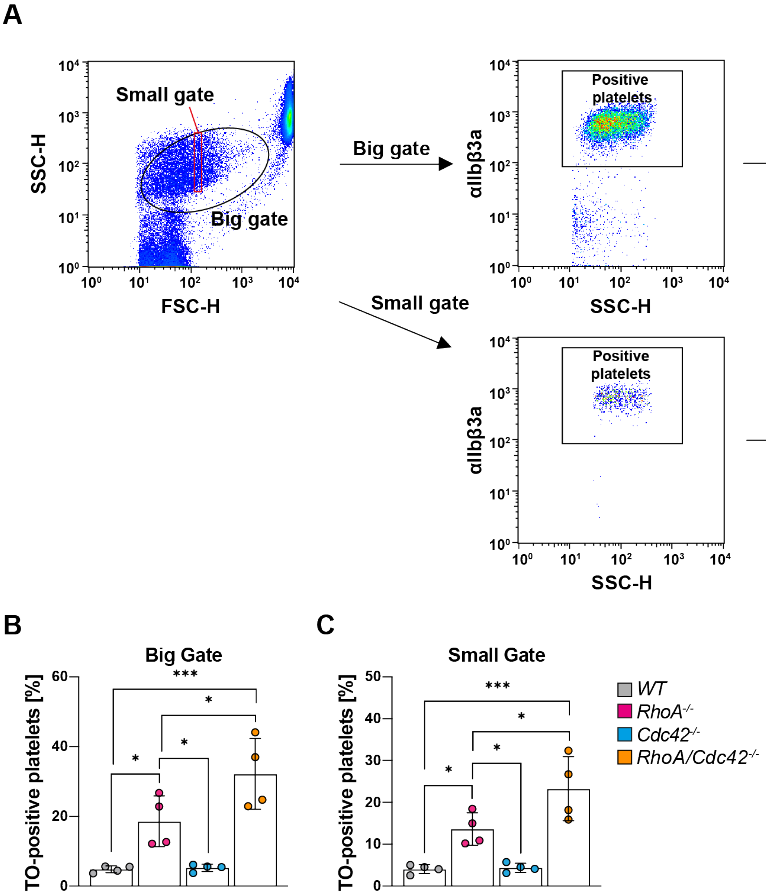

**Figure 13: Increased proportion of circulating reticulated platelets in *DKO* mice. A** Gating strategy used for the detection of young reticulated platelets, positive for *thiazole orange* (TO) by flow cytometry (FACSCalibur, BD Biosciences). **B,C** Quantification of TO-positive platelets using either (**B)** a big gate with all platelets or **(C)** small gate to exclude size differences of *DKO* platelets. One dot represents one animal. All data are indicated as mean ± SD. One-way ANOVA test with Tukey's correction for multiple comparisons was used. *P≤0.05, ***P<0.001. Heib *et al.,* **submitted.**

Notably, the platelet recovery rate after anti-GPIbα antibody-mediated platelet depletion *in vivo* was similar in *WT* and *DKO* mice. However, in contrast to the recovery process in the *WT*, no overshooting platelet counts above the initial levels were observed in *DKO* mice at six days after depletion (Figure 14). The spleen is known to contribute to platelet clearance, but extramedullary hematopoiesis in the organ may at the same time contribute to platelet production. We observed a mild splenomegaly (Figure 15A) (Deya Cherpokova, Thesis, 2015)[279] and markedly increased MK numbers in spleens of *DKO* mice (Figure 15B,C). However, splenectomy had virtually no impact on peripheral platelet counts in *DKO* animals (Figure 15D,E), and also macrophage depletion by clodronate treatment only slightly ameliorated the thrombocytopenia (Figure 15F). Together, these results confirm opposing roles of RhoA and Cdc42 in the regulation of MK localization in the BM, but additionally revealed severely defective platelet production in the BM upon combined ablation of RhoA/Cdc42 signaling.

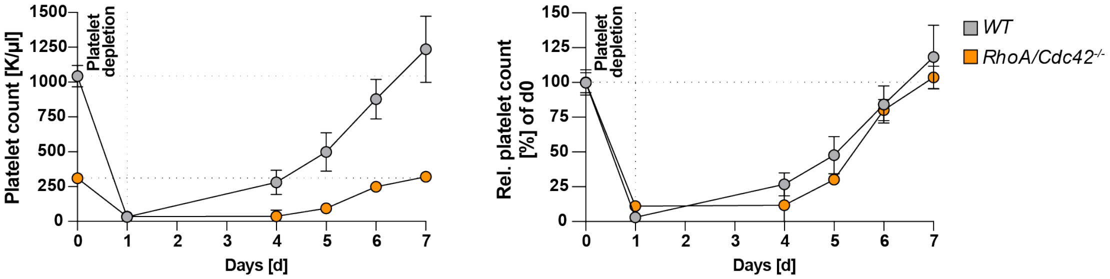

**Figure 14: Unaltered platelet recovery in *RhoA/Cdc42*$^{-/-}$ mice.** The recovery of peripheral platelet counts *in vivo* after experimentally-induced thrombocytopenia. Peripheral platelet counts were measured at the indicated time points until initial values were reached. Right panel shows normalized data compared to day 0 (n = 5 mice per genotype, representative of three independent experiments). All data are indicated as mean ± SD. Heib *et al.,* **submitted.**

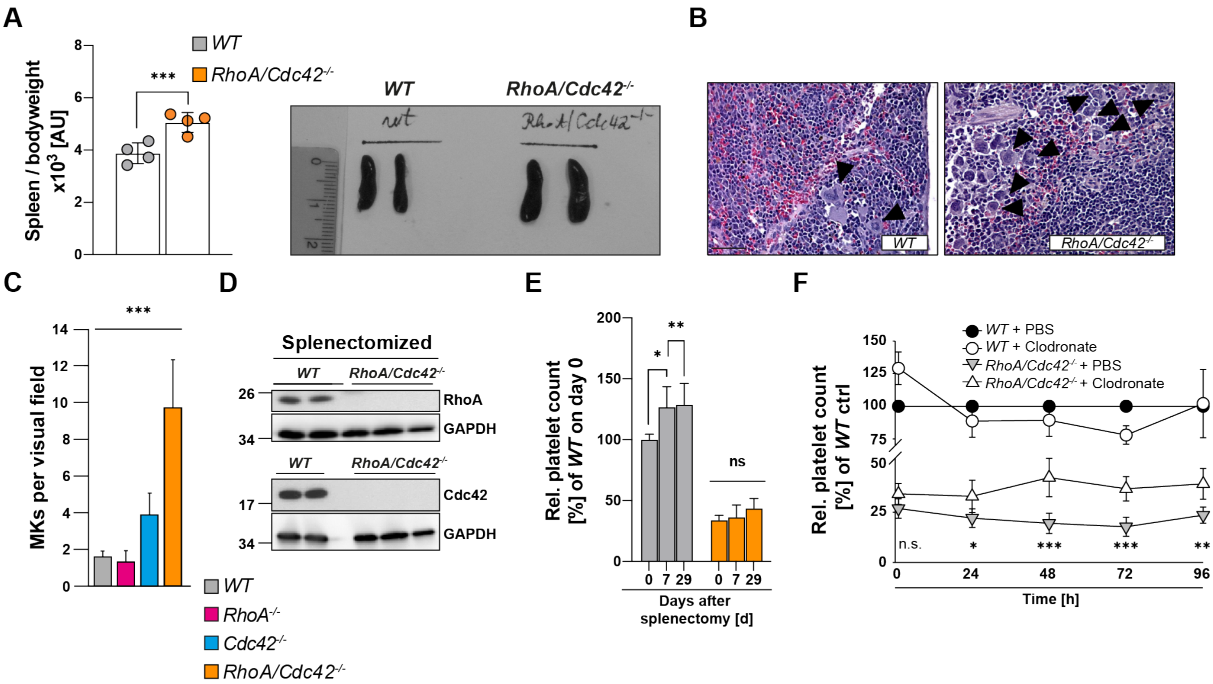

**Figure 15: Splenomegaly in *RhoA/Cdc42$^{-/-}$* mice is not causative for the observed macrothrombocytopenia**. **A** Mild splenomegaly in *DKO* mice (n = 4 mice per genotype). Spleen/body weight ratio (left) and representative images (right) are shown. **B** Increased MK numbers in spleens of *DKO* mice. Representative hematoxylin and eosin-stained sections of the spleen of *WT* and *DKO* mice. Arrowheads point at MKs. Scale bars, 50 µm (n = 7-8 mice per genotype). **C** Statistical analysis of MK numbers in spleens per visual field (328 x 246 µm) from depicted mice (n= 7-8 mice per genotype). **D** Immunoblotting shows efficient deletion of RhoA and Cdc42 on protein level in platelets from splenectomized *DKO* mice. **E** Macrothrombocytopenia of *DKO* mice is not rescued by splenectomy. Kinetics of peripheral platelet counts after splenectomy are shown at indicated timepoints. Values were normalized to *WT* levels which were set to 100% (n = 4 mice per group). **F** Macrophage depletion slightly ameliorates the macrothrombocytopenia in *DKO* mice. Peripheral platelet counts were monitored over time after clodronate-encapsulated liposome-mediated macrophage depletion in *WT* and *DKO* mice by flow cytometry (FACSCalibur, BD Biosciences). Values for platelet counts were normalized to *WT* control levels (*WT* mice treated with PBS liposomes) which were set to 100% (n = 4-6 mice per group, representative of two independent experiments). One dot represents one animal. All data are indicated as mean ± SD. (**A**,**C**,**E**,**F**) Multiple unpaired two-tailed Student's t-test, compared to *WT* or day 0. **(F)** Statistical significance solely indicates differences in clodronate-treated vs. vehicle-treated *DKO* mice. AU = *arbitrary unit*. **P<0.01, ***P<0.001. Experiments were performed by Deya Cherpokova, Thesis, 2015.[279] Heib *et al.*, **submitted.**

### 4.2.2 Defective cytoplasmic maturation, but normal endomitosis in RhoA/Cdc42 *DKO* MKs

To further investigate the platelet biogenesis defect in *DKO* mice, we examined MK morphology and ultrastructure *in situ* by TEM (Figure 16 A,B) (Deya Cherpokova, Thesis, 2015).[279] *WT* MKs displayed a defined DMS and a peripheral zone largely devoid of granules[7,35], clearly separating the MKs from surrounding cells. As previously shown, the ultrastructure of *RhoA*$^{-/-}$ MKs was similar to the *WT*, while membrane invaginations were slightly reduced in *Cdc42*$^{-/-}$ MKs (Figure 16A,B).[240] By contrast, *DKO* MKs exhibited a severely abnormal morphology and ultrastructure with strongly reduced membrane invaginations. The rarely formed DMS was highly disordered with increased numbers of large vacuoles and the presence of empty granules (Figure 16A,B), indicative of the absence of (pre) DMS structures.[35]

To follow up on this finding, we analyzed primary, flushed *WT* and *DKO* BM MKs by flow cytometry (Figure 17A). To estimate the degree of MK maturity, we divided the CD41 (GPIIb)-positive cell population based on their FSC characteristics into small (less mature, Type I), medium-sized (Type II) and big (more mature, Type III) subpopulations and assessed surface expression levels of the MK- and platelet-specific GPs GPIb$\alpha$, GPIX, GPV and GPVI. While levels of these GPs were similar between *WT* and *DKO* in the Type I population, they were significantly decreased in the more mature *DKO* Type II and III subpopulations (Figure 17A,B). Strikingly, we observed a subpopulation of highly granular, big MKs in *WT* mice (Type IV), likely representing mature MKs, which was absent in *DKO* mice.

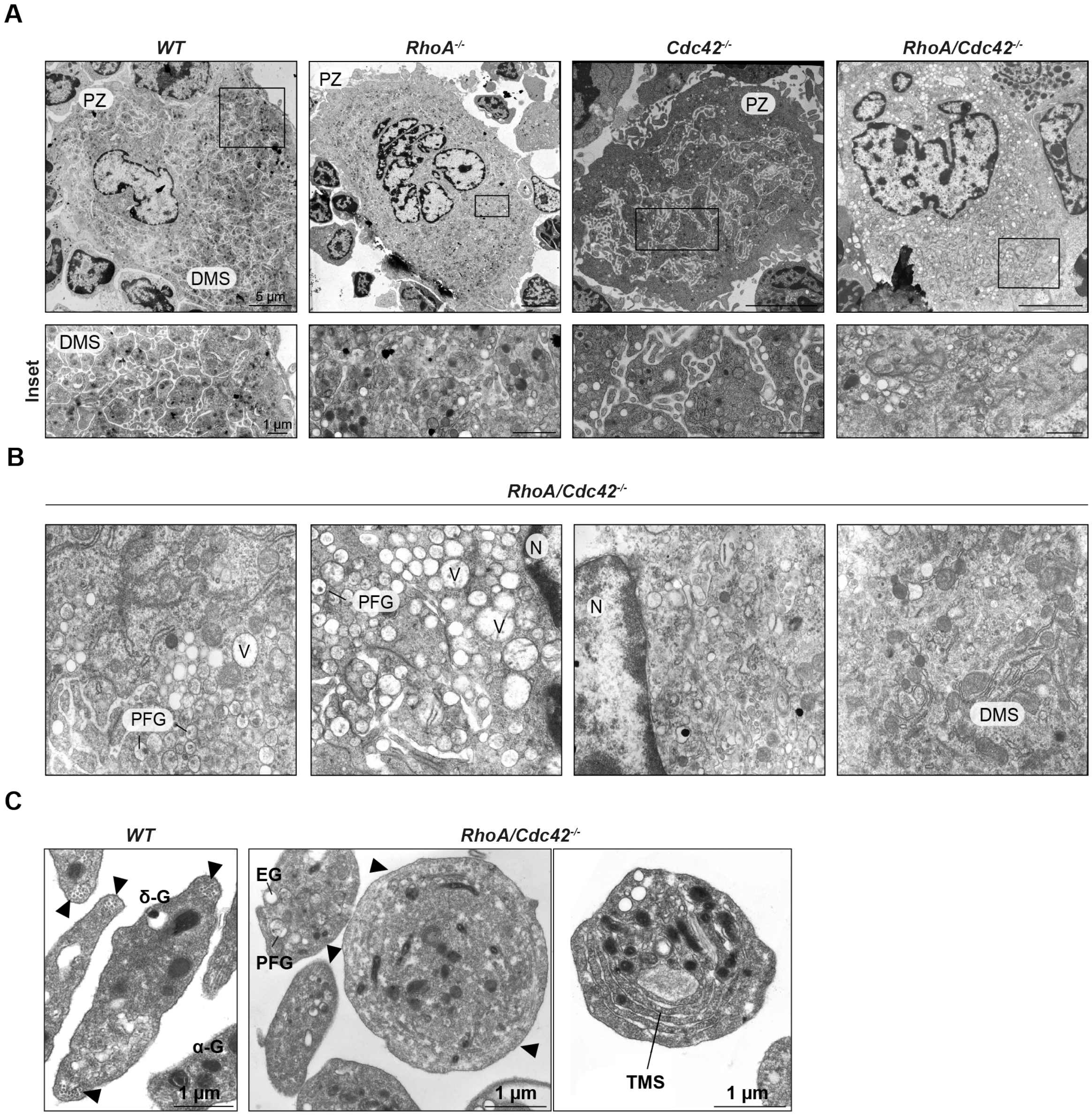

**Figure 16: *RhoA/Cdc42*$^{-/-}$ BM MKs display defective cytoplasmic maturation. A,B** TEM analysis of BM MKs (femur). **(A)** Overview (upper panel) and inset with a detailed view (lower panel) of representative images. Scale bars, 5 µm (upper), and 1 µm (lower). Note the loss of delineation to adjacent cells, aberrant DMS, and increased vacuole numbers in *DKO* BM MKs (n=5). **(B)** Detailed representative images of the MK ultrastructure in *DKO* mice reveal defective DMS formation. Scale bars, 1 µm. DMS = *demarcation membrane system*; N = *nucleus*; PFG = *partially filled granules*; PZ = *peripheral zone*; V = *vacuoles*. **C** Representative TEM images illustrating the aberrant ultrastructure of *DKO* platelets. Arrowheads indicate marginal MT coils clearly visible in *WT* but not *DKO* platelets. Scale bars, 1 µm; δ-G = *dense granule*; α-G = *α-granule*; EG = *empty granules*; PFG = *partially filled granules*; V = *vacuoles*; TMS = *tubular membrane sheets*. Experiments were performed by Deya Cherpokova, Thesis, 2015.[279] Heib *et al.,* **submitted.**

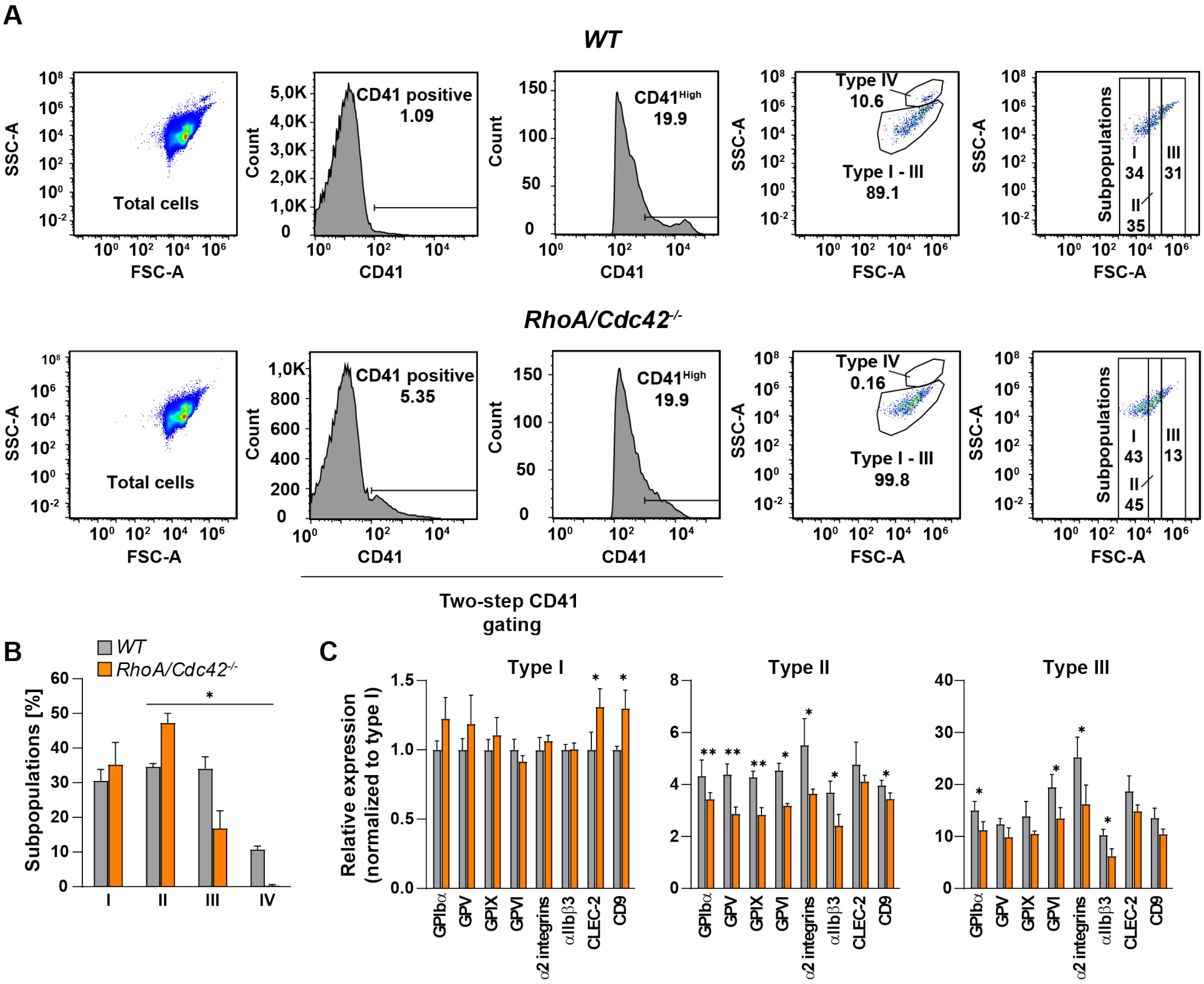

**Figure 17: Flow cytometry analysis of *RhoA/Cdc42*$^{-/-}$ MKs. A** Gating strategy used for the analysis of primary BM MKs by flow cytometry (FACSCelesta, BD Biosciences). MK- and platelet-specific AF647-conjugated anti-GPIIb antibody (CD41) was used to gate on high expressing CD41 cells (CD41$^{\text{High}}$). CD41$^{\text{High}}$ cells were further subdivided by size (FSC signal) into type I-III and a more granular type IV subpopulation and quantified. **B** *DKO* mice lack a highly granular MK subpopulation (n = 3). **C** Surface expression of important MK GPs was determined in the different subpopulations type 1 – type 3 of CD41$^{\text{High}}$ primary BM MKs. Expression levels within the highly granular type IV subpopulation was not assessed due to its absence in *DKO* mice. (**B,C**) Multiple unpaired two-tailed Student's t-tests compared to *WT*. *P≤0.05, **P<0.01, ***P<0.001. Georgi Manukjan (Experimental Biomedicine, Schulze Group) kindly helped to establish the settings for the flow cytometry data shown in this figure. Heib *et al.*, **submitted.**

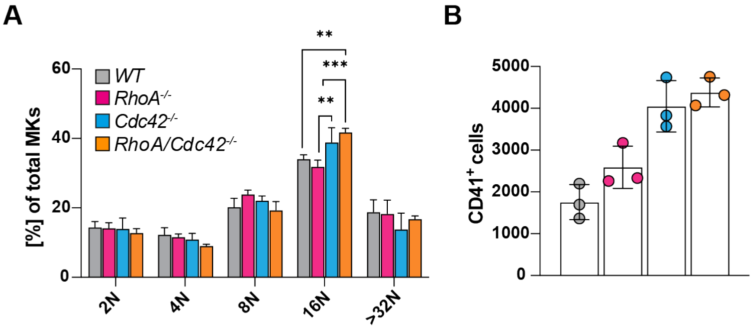

**Figure 18: Native *RhoA/Cdc42*$^{-/-}$ BM MKs display normal endomitosis**. **A** Functional endomitosis in *DKO, RhoA*$^{-/-}$*,* and *Cdc42*$^{-/-}$ MKs. The ploidy of primary, flushed BM MKs was assessed by flow cytometry (FACSCalibur, BD Biosciences) using a MK- and platelet-specific FITC-conjugated anti-GPIIb antibody (CD41) in combination with PI staining to determine DNA content. (n = 3 mice per genotype), representative of four independent experiments. **B** Amount of CD41$^{+}$ cells out of 1x10$^{6}$ total cells measured. One dot represents one animal. All data are indicated as mean ± SD. For **(A)** Two-way ANOVA and **(B)** one-way ANOVA test with Tukey's correction for multiple comparisons was used. *P≤0.05, **P<0.01, ***P<0.001. Heib *et al.,* **submitted.**

Alongside the induction of DMS formation and MK-specific GP expression, endomitosis is another hallmark of MK maturation.[5] Strikingly, the ploidy distribution of native flushed BM MKs was largely comparable between all groups, indicating that endomitosis during megakaryopoiesis does not require RhoA/Cdc42 signaling (Figure 18A). As an additional confirmation, the fraction of CD41$^{+}$ cells obtained for the ploidy assay by measuring 1x10$^{6}$ total cells matched the increase of MKs counted in BM cryosections of both single-deficient and *DKO* mice (Figure 18B).

In line with the defective cytoplasmic MK maturation, the few circulating platelets produced by *DKO* MKs displayed an abnormal shape and ultrastructure (Figure 16C). TEM analysis revealed a highly heterogeneous size and appearance of resting *DKO* platelets, associated with a partial or sometimes complete lack of the tubulin marginal coils, which is a characteristic feature of *WT* platelets. Furthermore, most *DKO* platelets lacked mature granules but contained multiple vacuoles and atypical *tubular membrane structures* (TMS), which were not present in the single KO platelets.[232,246]

Together, these results demonstrated that RhoA/Cdc42 signaling controls critical steps of cytoplasmic MK maturation, but is dispensable for endomitosis in the course of differentiation of these cells.

### 4.2.3 Defective hemostasis but largely intact thrombotic platelet activity in *RhoA/Cdc42 DKO* mice

Our results revealed that the few circulating platelets in *DKO* mice are immature and display aberrant morphology and granular composition. We thus asked whether these platelets were still able to perform their physiological role.

In accordance with the findings from MKs, levels of GPIb-IX-V and GPVI were reduced in *DKO* and to lesser extents in *Cdc42*$^{-/-}$ circulating platelets (Figure 20A). We next assessed platelet integrin αIIbβ3 activation, as well as degranulation (P-selectin surface expression) *in vitro* by flow cytometry. As previously shown[246], *RhoA*$^{-/-}$ platelets displayed selective integrin activation and degranulation defects towards G protein-coupled agonists (thrombin, ADP, Thromboxane A2 analog U46619) (Figure 20B,C). On the other hand, integrin activation was overall slightly reduced, but degranulation increased in *Cdc42*$^{-/-}$ platelets (Figure 20D,E).[232]

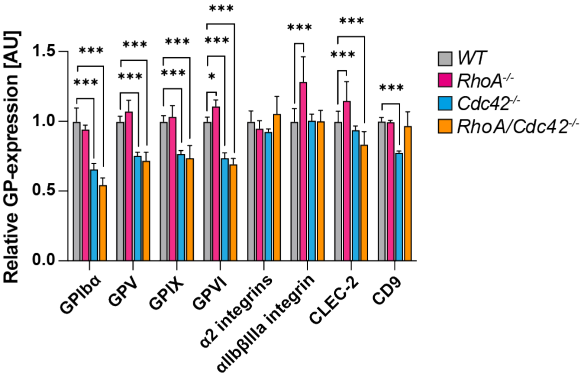

**Figure 19: Analysis of platelet GP expression.** Determination of levels of GPs in platelets of all indicated genotypes by flow cytometry (FACSCalibur, BD Biosciences). Experimental sets were normalized to their corresponding *WT* and pooled (n = 17, 5, 4, 7, data obtained from four independent experiments). For **(A)** Two-Way ANOVA test with Tukey's correction for multiple comparisons was used. *P≤0.05, **P<0.01, ***P<0.001. GP = *glycoprotein*; AU = *arbitrary unit*. Heib *et al.,* **submitted.**

Strikingly, *DKO* platelets displayed severely reduced integrin activation, which was nearly abolished in response to the GPVI/ITAM agonists CRP and CVX (Figure 20F). However, α granule secretion (P-selectin expression) was largely preserved in *DKO* platelets upon stimulation of GPCR signaling, but significantly decreased upon stimulation with CRP and CVX (Figure 20G), indicating overlapping functions of RhoA and Cdc42 in the GPVI signaling pathway. These results were also confirmed by analysis of secreted VWF and PF4, which are stored in platelet α–granules (Deya Cherpokova, Thesis, 2015).[279]

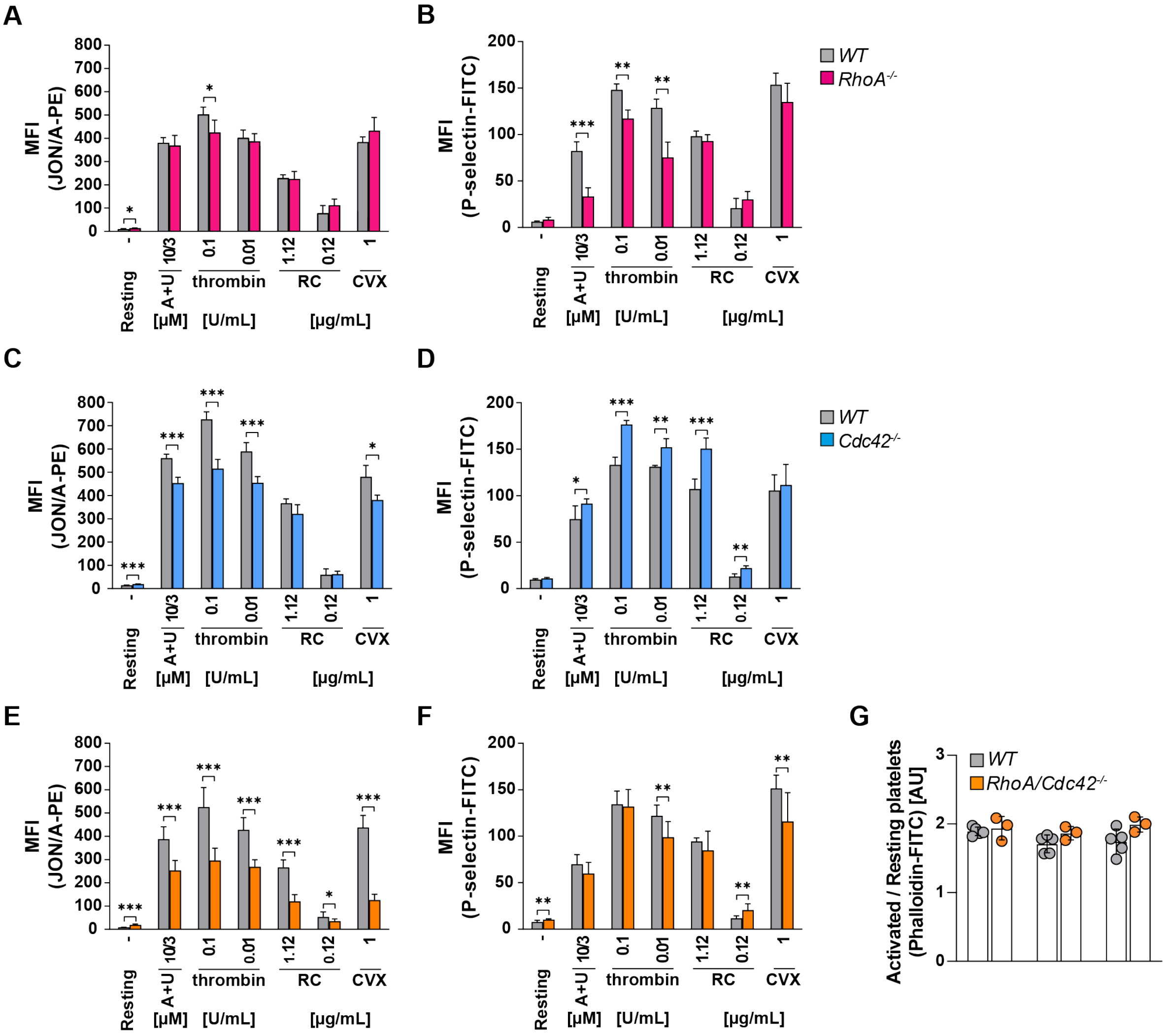

**Figure 20: Flow cytometric analysis of platelet activation. A-G** Flow cytometric (FACSCalibur, BD Biosciences) analysis of integrin αIIbβ3 activation (binding of JON/A-PE) and degranulation-dependent P-selectin exposure in response to the indicated agonists. ± SD. **(A,B)** Analysis of *RhoA*$^{-/-}$ mice (n = 4 per genotype). **(C,D)** Analysis of *Cdc42*$^{-/-}$ mice (n = 4, 5). **(E,F)** Analysis of *RhoA/Cdc42*$^{-/-}$ mice (n = 9, 7, two experiments were pooled). Data are mean fluorescence intensities (MFI) ± SD. **(G)** F-actin reassembly in platelets upon stimulation with indicated agonists measured by flow cytometry (FACSCalibur, BD Biosciences) (n = 5, 3, representative of two independent experiments). One dot represents one animal. All data are indicated as mean ± SD. For **(A-G)** multiple unpaired two-tailed Student's t-tests compared to *WT* was used. *P≤0.05, **P<0.01, ***P<0.001. AU = *arbitrary unit*; – indicates resting; CVX = *convulxin*; U46 = *U46619* and RC = *rhodocytin*. Heib *et al.,* **submitted.**

Finally, we investigated the role of RhoA/Cdc42 double-deficiency on platelet function *in vivo*. Strikingly, *DKO* mice displayed severely defective hemostasis, which was not observed to a similar extent in either of the single-deficient mice.[232,246] On the other hand, *DKO* mice formed stable occlusive thrombi with similar kinetics comparable to the *WT* in different experimentally induced intravital thrombosis models (Deya Cherpokova, Thesis, 2015). Notably, *DKO* platelets were also able to assemble F-Actin upon activation (Figure 20H) and spread on a fibrinogen matrix with kinetics similar to the *WT* (Deya Cherpokova, Thesis, 2015).[279] Thus, despite their importance for cytoskeletal rearrangements also in platelets, RhoA and Cdc42 are largely dispensable for platelet adhesion and spreading on fibrinogen.

Together, these results indicate that the partially preserved degranulation of *DKO* platelets may to some extent compensate for the other platelet defects under conditions of experimentally induced intravital thrombosis, but not hemostasis.

### 4.2.4 Loss of RhoA/Cdc42 signaling abolishes proplatelet formation

Our previous study revealed reduced PPF in the BM of *DKO* mice *in vivo*.[251] To dissect the underlying mechanisms, we assessed PPF of *in vitro* cultured, BM-derived MKs in the presence of TPO, and rHirudin (Figure 21A)[281] at 24h and 48h after enrichment by a BSA gradient. At 24h, 20-45% of *WT* MKs formed proplatelets, evident by multiple branched protrusions with characteristic swellings ('beads-on-a-string') and nascent proplatelet-tips containing peripheral MT coils[278] (Figure 21B,C + Figure 22). PPF of *RhoA*$^{-/-}$ MKs was not significantly altered (Figure 21B,C + Figure 22), which is in line with our previous observations using FLC-derived MKs.[251] By contrast, single-deficiency of Cdc42 led to an approximately 75% reduction in PPF after 24 h and 50% after 48 h. The reduced PPF was fiurthermore associated with an increased number of unbranched protrusions without swellings, and tips of variable size and morphology (Figure 21B,C + Figure 22). Strikingly, PPF was virtually abrogated in *DKO* MKs for up to 48 h after enrichment (Figure 21B). The few proplatelet-forming MKs displayed a few long, unbranched protrusions, which lacked swellings and contained tips of variable morphology and size. Furthermore, the MT organization was markedly altered, illustrated by the absence of MT coils in proplatelet tips, but thickened MT strands in formed protrusions (Figure 21C + Figure 22).

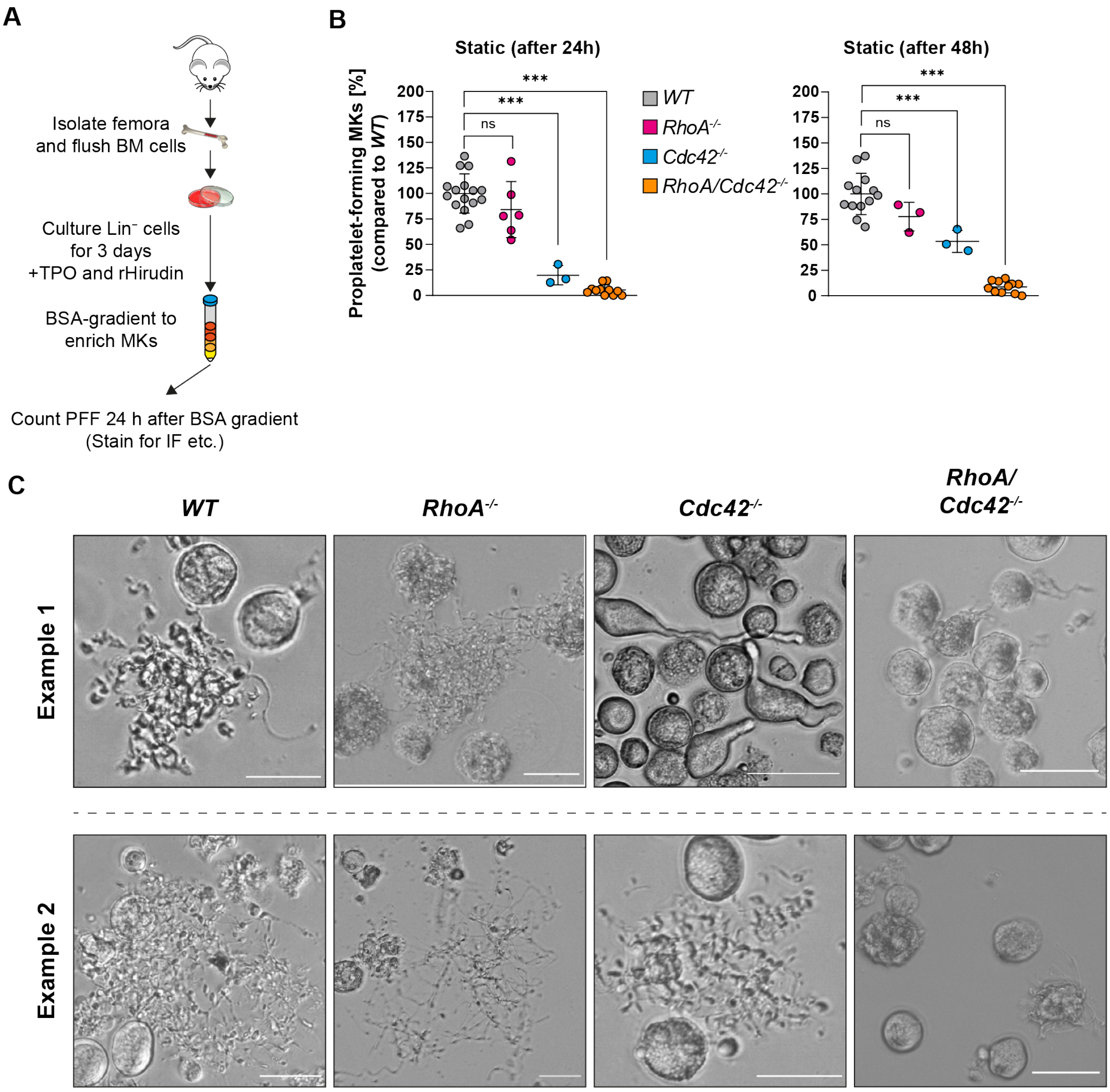

**Figure 21: Defective PPF of *RhoA/Cdc42*$^{-/-}$ MKs. A** Schematic overview describing the isolation and the culture method of BM-derived MKs. **B** Representative bright field images of MK and proplatelet morphology at 24 h after MK enrichment by BSA gradient. Scale bars, 50 µm. **C** Statistical analysis of PPF at 24 h (left) and 48 h (right) after MK enrichment by BSA gradient under static conditions. Different experimental sets were normalized to *WT* controls, which were set to 100% and pooled (24 h timepoint: n = 16, 6, 3, 11, four independent experiments; 48 h timepoint: n = 13, 3, 3, 11, four independent experiments were pooled. For **(A)** One-way ANOVA test with Tukey's correction for multiple comparisons. ***P<0.001. ns = *non-significant*. Heib *et al.,* **submitted.**

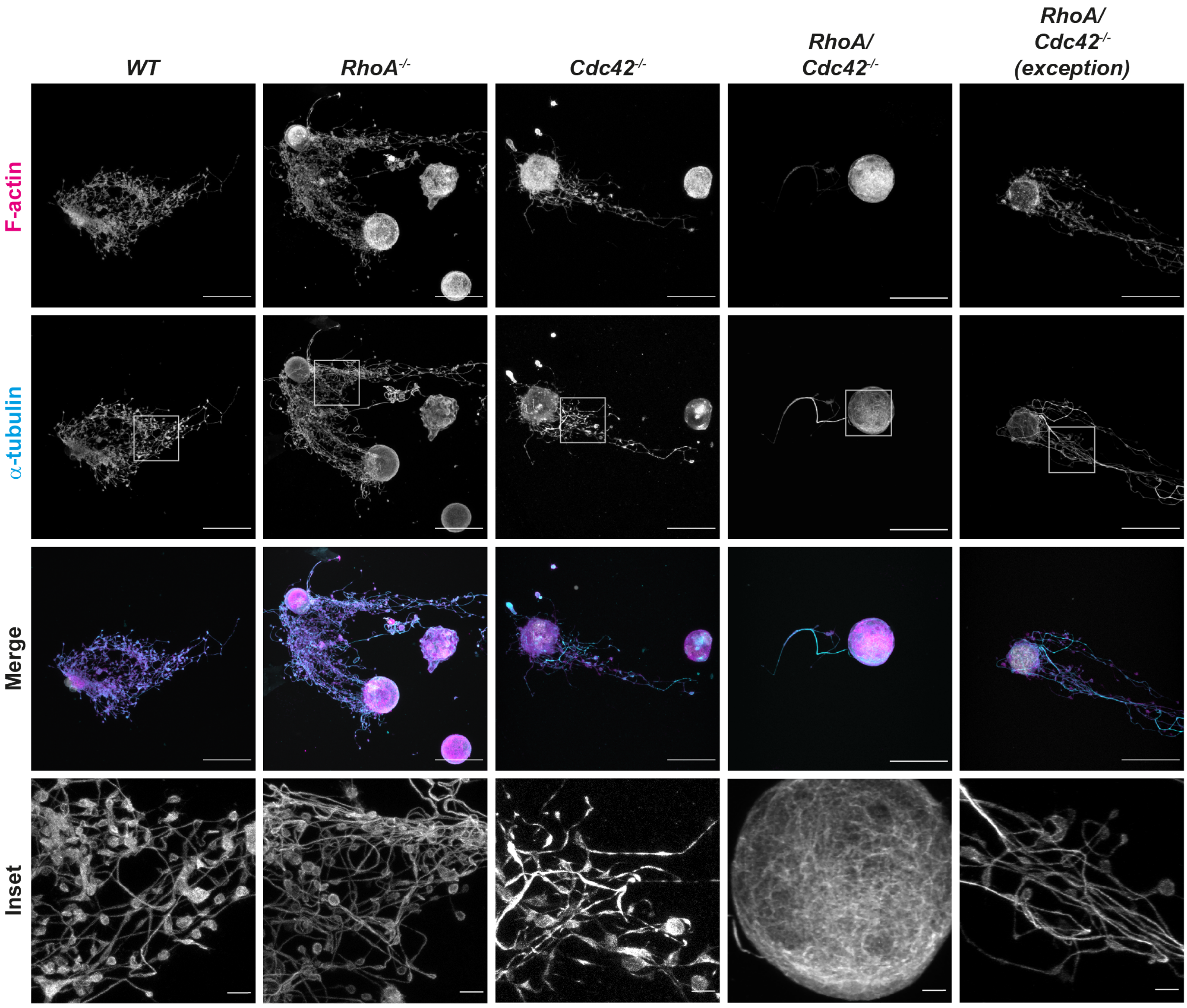

**Figure 22: Visualization of PPF by confocal immunofluorescence microscopy.** Representative confocal images of fluorescently stained proplatelet-forming BM-derived MKs 24h after enrichment under static conditions (40x oil objective, Leica TCS SP8). F-actin is stained by phalloidin (magenta), $\alpha$-tubulin is shown in cyan, and the nuclei were counterstained with DAPI in grey. The inset panel shows a detailed view of the proplatelet structures. Note the missing proplatelet tips in *Cdc42*$^{-/-}$ and *RhoA/Cdc42*$^{-/-}$ (*DKO*) mice (n = 3-4 mice per genotype). Scale bars = 50 µm (overview) and 5 µm (inset). Heib *et al.*, **submitted.**

To further investigate the kinetics of PPF in the absence of RhoA/Cdc42, we performed time-lapse video microscopy over 24h after MK enrichment. While PPF gradually increased in *WT* MKs up to 15-20% after 24 h under these conditions, *RhoA*$^{-/-}$ MKs displayed significant PPF already at the start of recording (~ 2 h after enrichment) (Figure 23A). At all later time points, however, PPF was similar to the *WT*. In *Cdc42*$^{-/-}$ MK cultures, PPF was comparable to the *WT* at 6 h, but did not increase further in the *Cdc42*$^{-/-}$ MKs (Figure 23B). By marked contrast, only very few *DKO* MKs showed any signs of PPF throughout the observation period (Figure 23C).

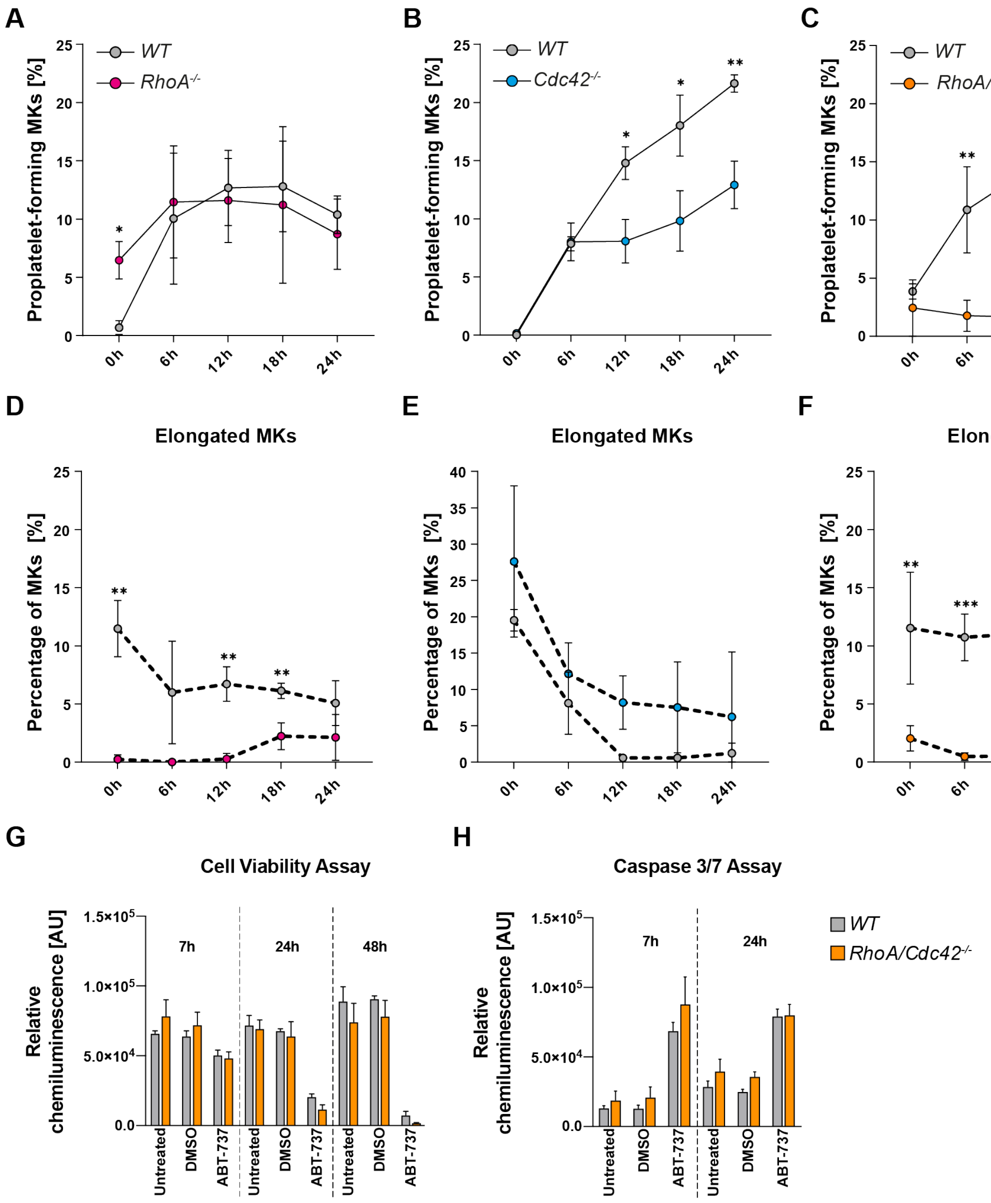

**Figure 23: Defective PPF of *RhoA/Cdc42$^{-/-}$* MKs is not due to increased MK death. A-F** Time-lapse microscopy of PPF of BM-derived MKs using CO$_2$-independent medium (20x water objective, Leica TCS SP8). Imaging started 2 hours after MK enrichment by BSA gradient. **(A-C)** Quantification of PPF MKs and **(D-F)** of MKs showing elongated forms, Visual fields with at least >150 MKs were counted (n = 3-4 mice per genotype). All results represent mean ±s.d. **G,H** Analysis of intrinsic apoptosis **(G)** and viability **(H)** of untreated, as well as vehicle (DMSO)- and ABT-737-treated cultured BM-derived MKs after enrichment by BSA gradient at the indicated time points (n = 3 mice per group, representative of two independent experiments). All results represent mean ±s.d. Multiple unpaired two-tailed Student's t-test with Holm-Sidak correction for multiple comparisons. AU = *arbitrary unit*. *P≤0.05, **P<0.01, ***P<0.001. Heib *et al.,* **submitted.**

We regularly observed *WT* MKs developing elongated shapes, reaching a peak after 12h, followed by a steady decline after which PPF commenced. Interestingly, *RhoA*$^{-/-}$ and *DKO* MKs showed a lack of elongated MKs, while this intermediate stage was prominently present in *Cdc42*$^{-/-}$ MK cultures throughout the observation period (Figure 21C + Figure 23D-F). In summary, these results revealed that the formation of the elongated MK intermediates was driven by RhoA and does not represent a distinct stage of PPF. Instead, it seems to be associated with the process of endomitosis, of which RhoA is known to be an important regulator.[27]

To further corroborate these observations, we employed the BM explant model, which allows native MKs to leave their natural BM environment and form proplatelets within several hours *in vitro.*[282] Both *WT* and *DKO* MKs migrated out of the BM explant, but only *WT* MKs formed proplatelets within the observation period of 12 h (Figure 24).

We thus asked, whether the defective PPF of cultured *DKO* BM MKs may be due to the induction of pathways leading to MK death. Therefore, we determined MK viability, as well as activation of the effector caspases 3 and 7 using ABT-737 as a control, which triggers rapid intrinsic apoptosis in MKs.[283] Notably, both viability and the response to ABT-737 were similar in *WT* and *DKO* MKs (Figure 23G,H).

In summary, these results revealed that RhoA/Cdc42 signaling is a fundamental prerequisite for PPF *in vitro* and *in vivo*.

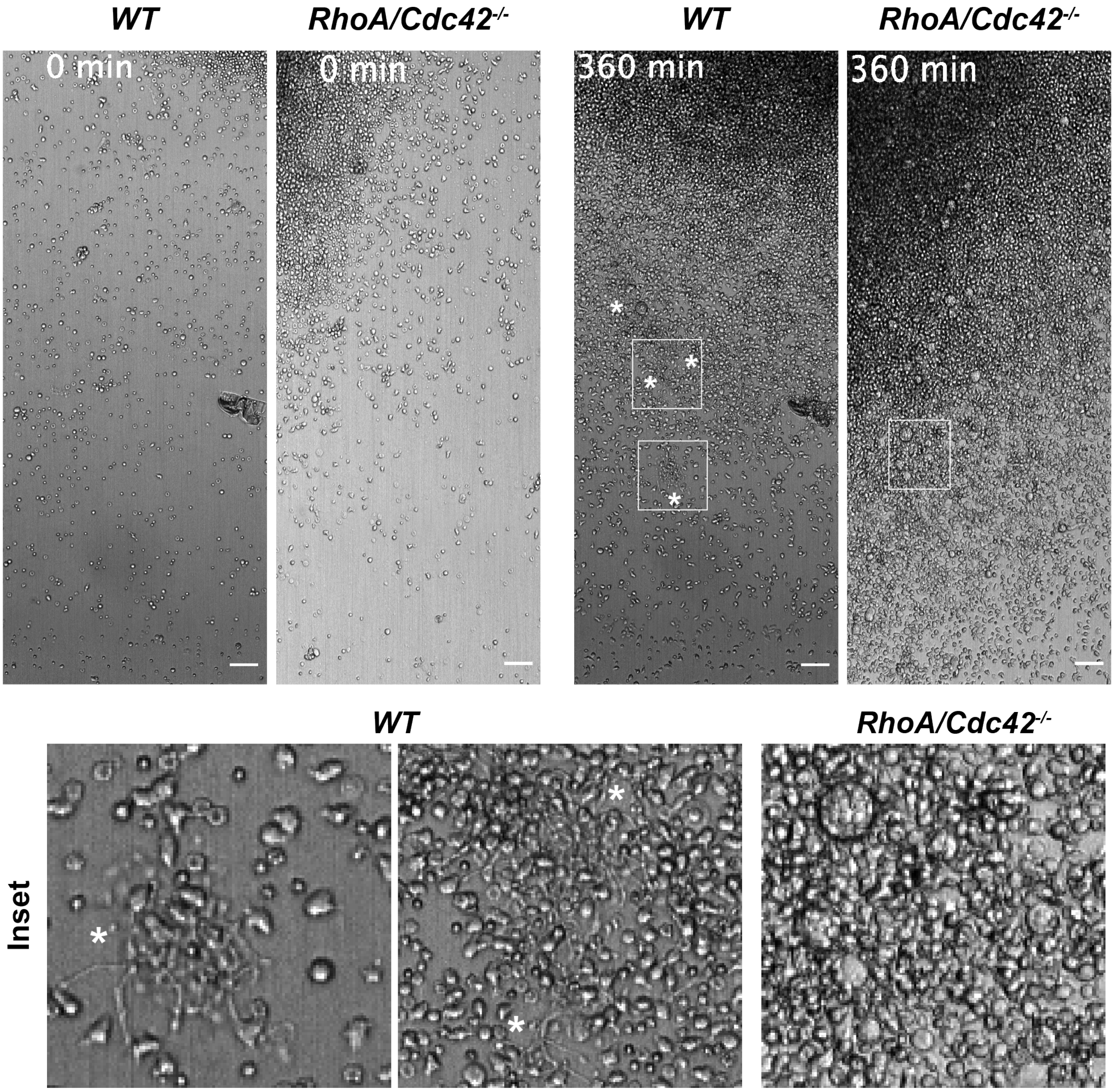

**Figure 24: *Ex vivo* BM explant model confirms the PPF defect in *RhoA/Cdc42*$^{-/-}$ mice.** Small pieces of the femora BM mass were imaged over time *ex vivo* using time-lapse microscopy and $CO_2$ independent media supplemented with additional 5% mouse serum. Representative pictures at the indicated time points are shown (10x air objective, Leica TCS SP8). White asterisks indicate PPF MKs. Scale bars = 50 µm. (n = 2 mice per genotype, one independent experiment). Heib *et al.,* **submitted.**

### 4.2.5 Lack of RhoA and Cdc42 results in abnormal F-actin and MT distribution upon MK adhesion to collagen and fibrinogen

To investigate the role of RhoA/Cdc42 in adhesion receptor-induced signaling, we analyzed adhesion and spreading of *in vitro* cultured BM-derived MKs on Horm collagen (consists mainly of collagen type I and to some extend of collagen type III) and fibrinogen coated cover slips by immunofluorescence confocal microscopy. On collagen, *WT* MKs spread extensively without exhibiting pronounced protrusion formation. The spread MKs displayed a well-developed MT and actin network, with moderate stress fiber formation as well as clearly visible podosomes at sites of contact with collagen fibers (Figure 25 + Figure 26). Podosomes are F-actin enriched structures, which are thought to contribute to the digestion of the extracellular matrix during the process of PPF *in vivo.*[224,284,285] On fibrinogen, *WT* MKs showed less pronounced spreading and less visible podosome formation as compared to Horm collagen (Figure 27).

Strikingly, *RhoA*$^{-/-}$ and *Cdc42*$^{-/-}$ single-deficient MKs showed largely opposing features upon adhesion to both matrices. *RhoA*$^{-/-}$ MKs could adhere and spread but exhibited abnormally long protrusions. As a result, albeit exhibiting an unaltered total spreading area, the cell perimeter was significantly increased and the circularity decreased in *RhoA*$^{-/-}$ MKs adherent to collagen compared to the control (Figure 25 and Figure 26). In contrast, spreading of *Cdc42*$^{-/-}$ MKs was significantly reduced, resulting in decreased spreading area and cellular perimeter (Figure 25 + Figure 26). These parameters were less pronouncedly also evident in MKs adherent to fibrinogen (Figure 28).

The organization of F-actin was only moderately different between *RhoA*$^{-/-}$ MKs and the *WT* but included the formation of enlarged podosomes on collagen (Figure 25 + Figure 26). By contrast, loss of Cdc42 was associated with dramatically increased stress fiber formation on both collagen and fibrinogen (Figure 25 + Figure 27), strongly impaired podosome formation on collagen, as well as the presence of thickened MTs in spread *Cdc42*$^{-/-}$ MKs (Figure 25 - Figure 27).

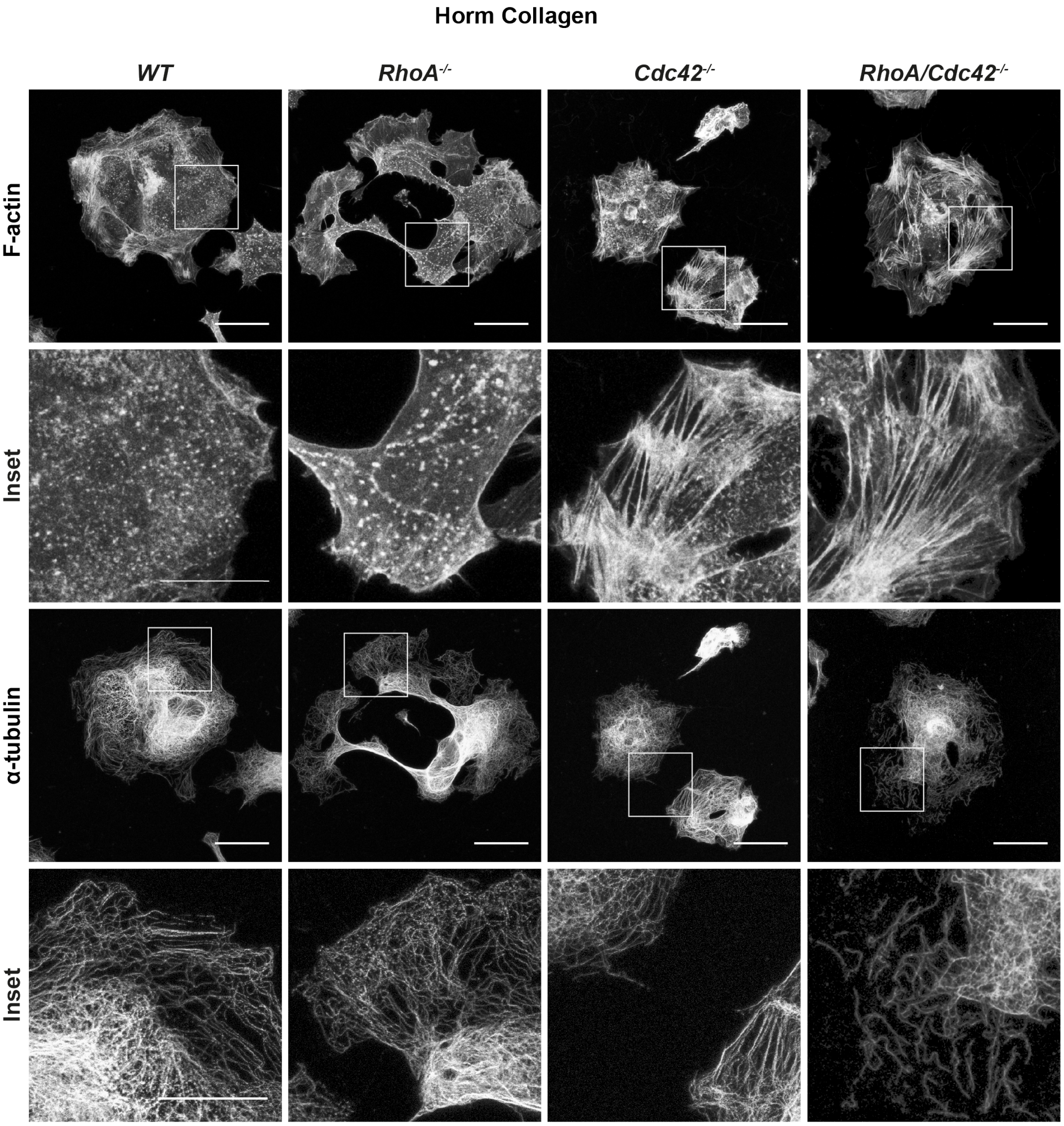

**Figure 25: Defective F-actin and MT organization in adherent cultured *RhoA/Cdc42*$^{-/-}$ BM-derived MKs.** Analysis of morphology, as well as F-actin and α-tubulin distribution of cultured BM-derived MKs upon adhesion to Horm collagen. Representative confocal images of fluorescently stained BM MKs (40x oil objective, Leica TCS SP8) are shown. MKs were stained for F-actin (phalloidin) and α-tubulin. The inset panel shows a detailed view of either F-actin or α-tubulin. Scale bars = 50 µm (overview) and 25 µm (insets). Heib *et al.,* **submitted.**

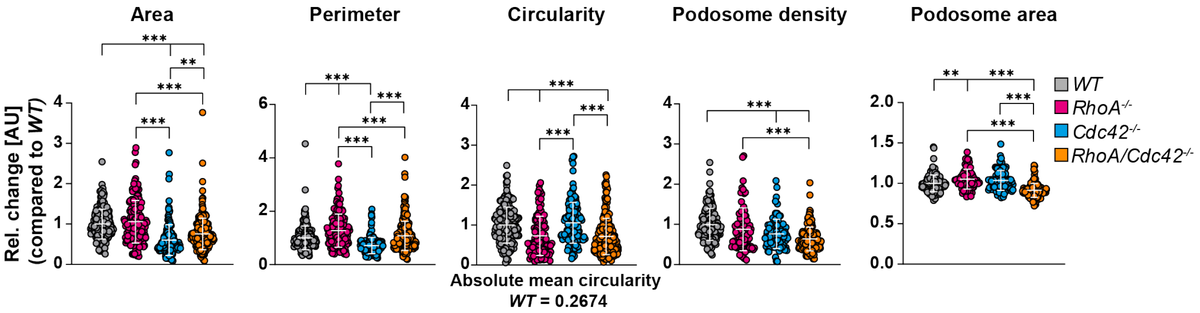

**Figure 26: Analysis of BM-derived MK spreading on Horm collagen.** Quantification of MK spreading area, perimeter, circularity, podosome density ($\frac{podosome\ number}{area}$), and podosome area. (n = 9, 6, 6, 10). Each dot represents one MK and at least over 100 MKs were counted per genotype combined in all mice. Different experimental sets were normalized to the *WT* control and pooled. All data are indicated as mean ± SD. One-way ANOVA test with Tukey's correction for multiple comparisons. AU = *arbitrary unit*. **P<0.01, ***P<0.001. Heib *et al.,* **submitted.**

Interestingly, adherent *DKO* MKs combined characteristics observed in the respective single-KOs. Cell perimeter and spreading area of *DKO* MKs were increased compared to *Cdc42*$^{-/-}$ MKs, but decreased compared to *RhoA*$^{-/-}$ MKs (Figure 25 - Figure 28). Similar to *Cdc42*$^{-/-}$ MKs, *DKO* MKs displayed markedly increased stress fiber formation, while podosome formation was even more affected (Figure 25 - Figure 27). Besides F-actin, also the MT organization was pronouncedly altered in *DKO* MKs, especially at the cell periphery, and characterized by the presence of fewer but thickened MTs as compared to the *WT* (Figure 25 + Figure 27). In addition, increased actin stress fiber formation and disrupted MT coils were confirmed by super-resolution microscopy (*d*STORM) of spread *DKO* platelets on a fibrinogen matrix (Figure 29). In summary, our results indicated that RhoA and Cdc42 may play critical, partially opposing / non-redundant roles in adhesion-mediated, outside-in signaling pathways induced by integrin αIIbβ3 (fibrinogen) and α2β1 (collagen) in MKs, resulting in a mixed adhesion phenotype upon double-deficiency.

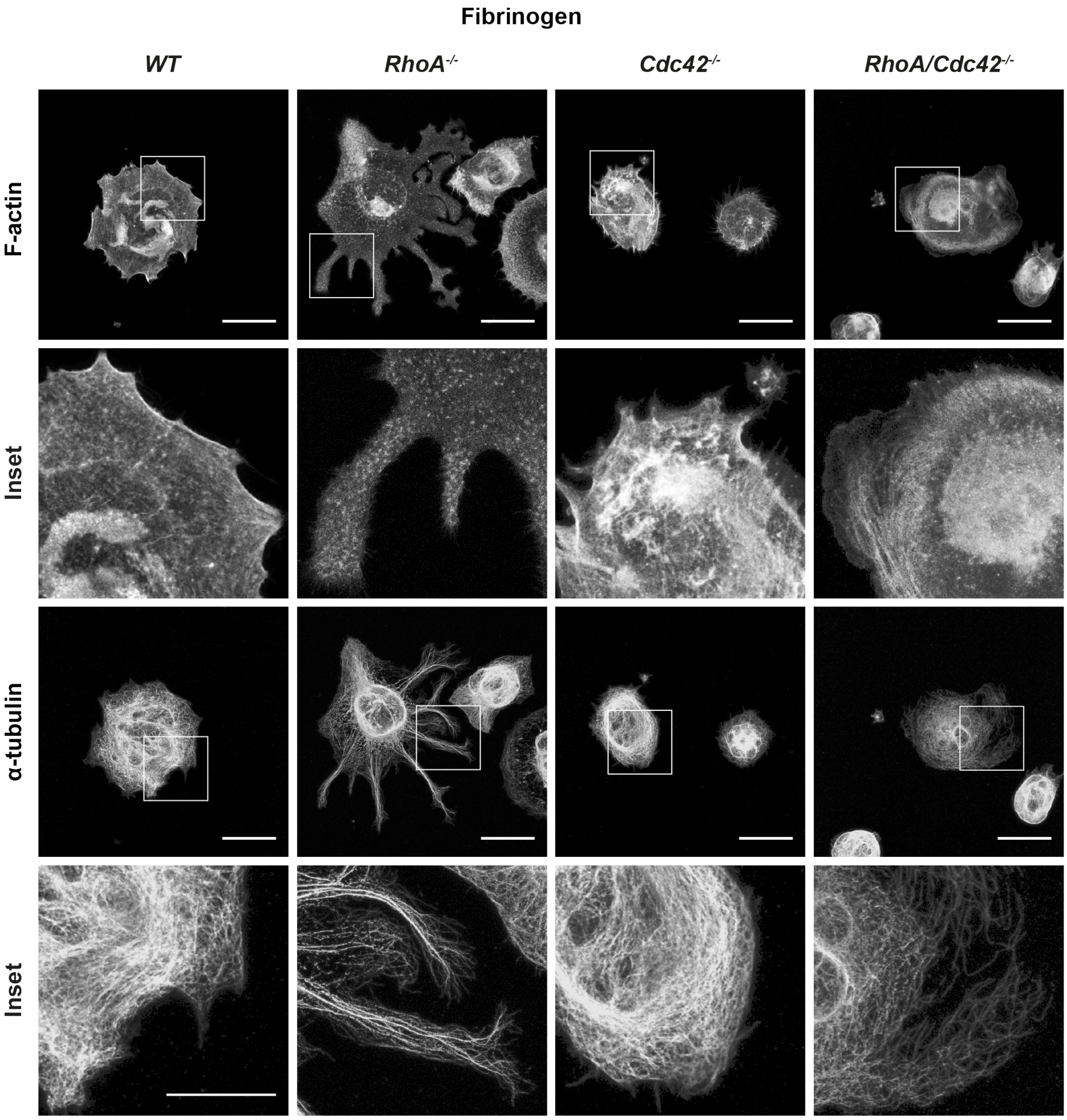

**Figure 27: Defective F-actin and MT organization in adherent cultured *RhoA/Cdc42*$^{-/-}$ BM-derived MKs*.*** Analysis of morphology, as well as F-actin and α-tubulin distribution of cultured BM-derived MKs upon adhesion to fibrinogen. Representative confocal images of fluorescently stained BM MKs (40x oil objective, Leica TCS SP8) are shown. MKs were stained for F-actin (phalloidin) and α-tubulin. The inset panel shows a detailed view of either F-actin or α-tubulin. Scale bars, 50 µm (overview) and 25 µm (insets). Heib *et al.,* **submitted.**

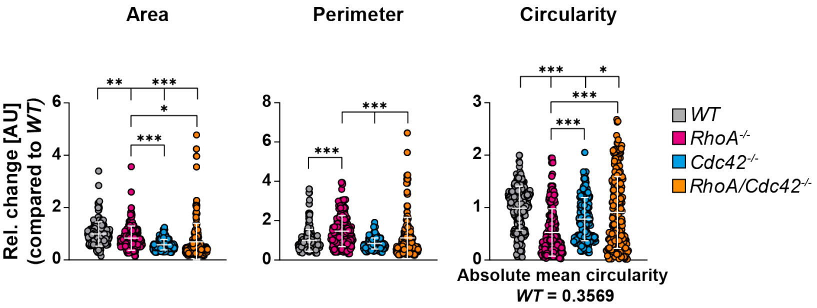

**Figure 28: Analysis of BM-derived MK spreading on fibrinogen.** Quantification of MK spreading area, perimeter and circularity. (n = 9, 6, 6, 10). Each dot represents one MK and at least over 100 MKs were counted per genotype combined in all mice. Different experimental sets were normalized to the *WT* control and pooled. All data are indicated as mean ± SD. One-way ANOVA test with Tukey's correction for multiple comparisons. AU = *arbitrary unit*. **P<0.01, ***P<0.001. Heib *et al.,* **submitted.**

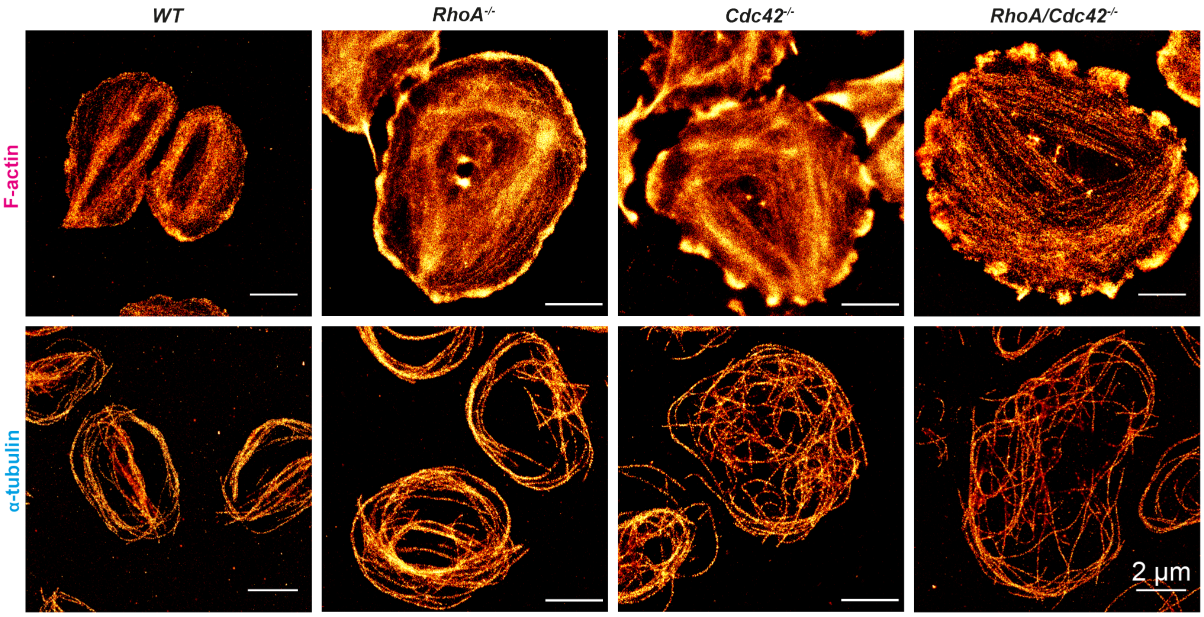

**Figure 29: Analysis of spread *RhoA/Cdc42*$^{-/-}$ platelets by superresolution microscopy.** Analysis of F-actin and α-tubulin distribution in spread platelets using *d*STORM. F-actin structures were visualized by phalloidin and MT structures by using an α-tubulin antibody. For each genotype two mice were pooled (n = 4, 2, 2, 4, representative of two independent experiments). Experiments were performed by Charly Kusch (Experimental Biomedicine, Nieswandt Group). Heib *et al.,* **submitted.**

### 4.2.6 Loss of RhoA/Cdc42 results in aberrant LIMK/cofilin-1 signaling, absence of myosin light chain 2 (MLC2) and a tubulin disequilibrium

RhoA and Cdc42 regulate cytoskeletal signaling pathways, which are fundamental for PPF and, ultimately, platelet release.[41] Both RhoA and Cdc42 are upstream regulators of the LIMK/Cof-1 pathway, which modulates actin turnover and stress fiber formation, and is involved in PPF.[191,229] Furthermore, Cdc42 regulates F-actin via WASP/Arp2/3, which in MKs has been associated with the formation of podosomes. In addition, RhoA is linked to MT dynamics in MKs via its effector mDia, and to cellular contractility via RhoA/ROCK-mediated regulation of myosin-IIA.[27,188,249,286]

To further investigate how these signaling pathways are affected, we stained native BM cryosections *in situ* for F-actin, DMS and - due to the MT alterations and defective maturation of *DKO* MKs - also for β1-tubulin, which is specifically expressed in mature MKs and important for PPF.[143,151] Mature *WT* MKs displayed a clearly defined DMS and F-actin network, as well as β1-tubulin expression (Figure 30). In marked contrast, β1-tubulin was virtually absent in *DKO* MKs and the cells displayed aberrant F-actin accumulations and a highly disorganized DMS (Figure 30).

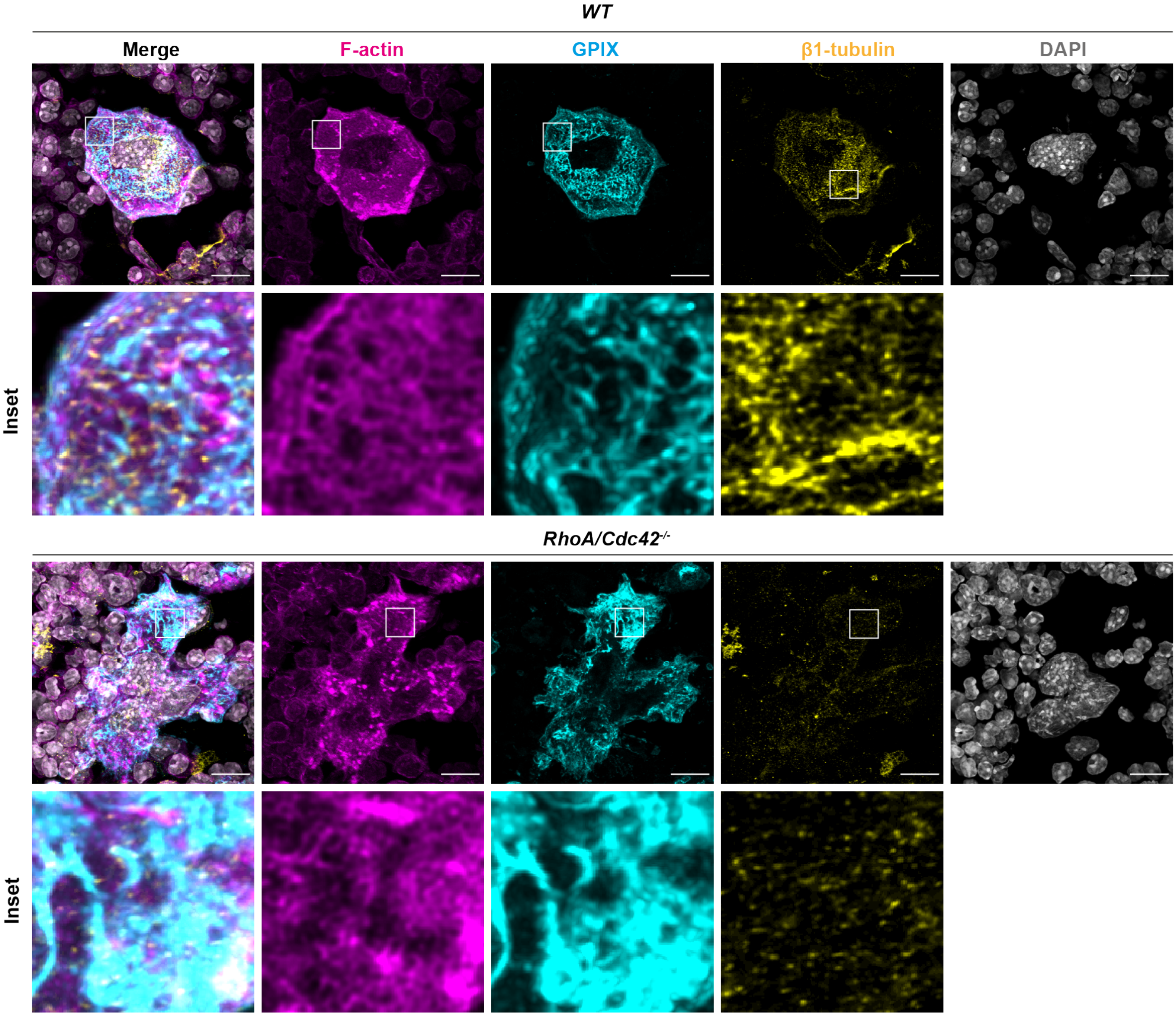

**Figure 30: Native *RhoA/Cdc42$^{-/-}$* BM MKs display defective DMS, aberrant F-actin accumulations, and reduced expression of β1-tubulin.** Representative high-resolution confocal images (63x oil objective, Leica TCS SP8) of native immunostained BM cryosections of *WT* and *DKO mice*. MKs and the DMS are shown by GPIX staining in cyan. F-actin was visualized by phalloidin (magenta), β1-tubulin (yellow), DAPI (grey). Scale bars, 20 µm. Heib *et al.,* **submitted.**

To mechanistically dissect these microscopical observations of both *in situ* and *in vitro* observations, we investigated protein expression in cultured MKs by immunoblotting. Platelets analyzed alongside served as a control that may best reflect protein expression profile of terminally maturated MKs *in vivo*. Defective podosome formation in *Cdc42$^{-/-}$* and *DKO* MKs indicated impaired WASP/Arp2/3 signaling. However, protein levels of the podosome markers Arp2 and vinculin[287] were largely unaltered (Figure 31A) and Arp2 still co-localized with F-Actin within the aberrant podosomes in *DKO* MKs (Figure 32).This indicated that the Arp2/3 pathway was affected in *Cdc42$^{-/-}$* and *DKO* MKs, but not directly linked to altered protein levels.

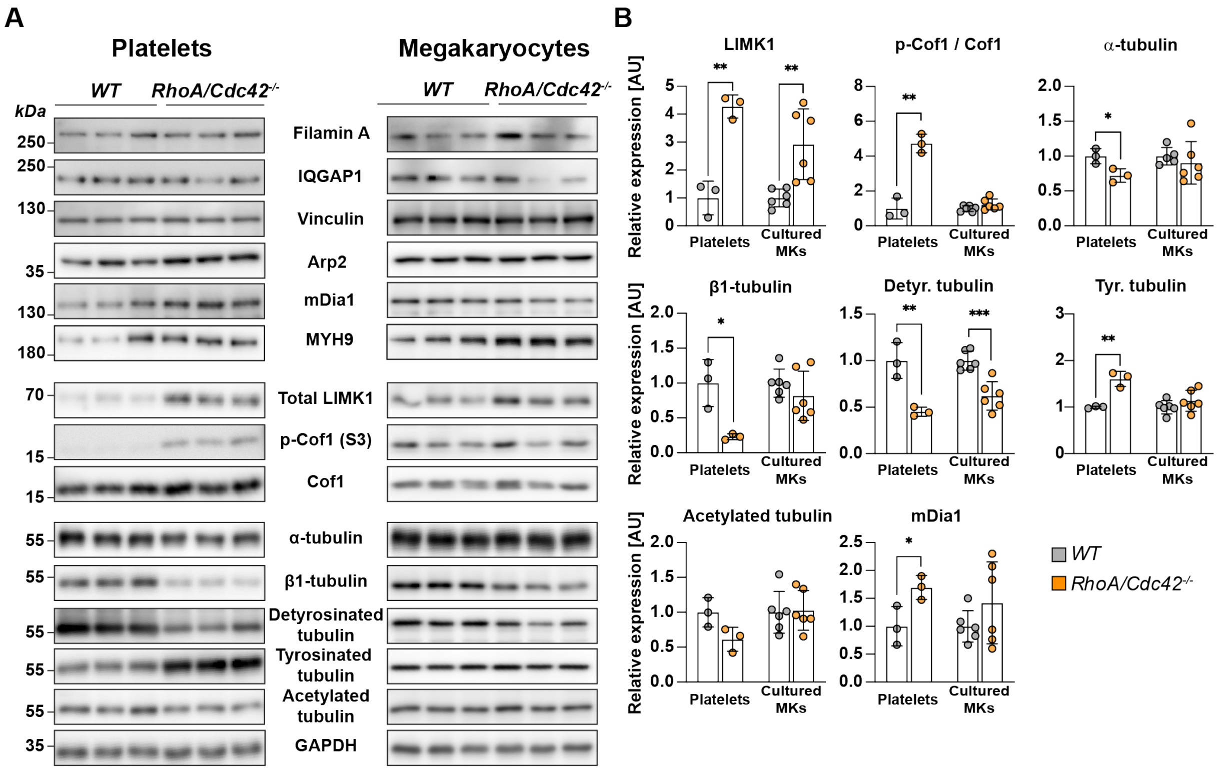

**Figure 31: Loss of RhoA/Cdc42 affects the expression of cytoskeletal regulators on protein level. A,B** Analysis of cytoskeletal proteins, as well as posttranslational modifications of tubulin by immunoblotting using GAPDH as a loading control. **(A)** Representative immunoblots of *WT* and *DKO* platelet (left) and MK lysates (right) are shown. (n = 3, for *DKO*, platelets of two mice were pooled). MK lysates were derived from cultured BM-derived MKs after enrichment on a BSA gradient (n = 6 mice per genotype). **(B)** Quantification of protein expression using densitometric analysis (Fiji software). Protein expression was first normalized to GAPDH and subsequently compared to the respective control. For **(B)** multiple unpaired two-tailed Student's t-tests were used. *P≤0.05, **P<0.01, ***P<0.001. AU = *arbitrary unit*. Heib *et al.,* **submitted.**

In contrast, levels of total LIMK, Cof1, and phosphorylated (inactive) Cof1 were markedly increased in *DKO* MKs as well as *DKO* and *Cdc42*$^{-/-}$ platelets, but largely unaltered in the absence of RhoA (Figure 31A,B + Figure 33A,B). This strongly suggested that the increased actin stress fiber formation in *DKO* MKs was predominantly caused by aberrant activation of the LIMK/Cof1 pathway downstream of Cdc42, with an additional contribution of RhoA. Notably, *LIMK inhibitor* (LIMKi) treatment could not restore PPF in cultured *DKO* MKs, unlike previously described in a mouse model[288], suggesting that aberrant LIMK/Cof1 signaling was not the sole reason for the defective PPF in the *DKO* mice (Figure 34).

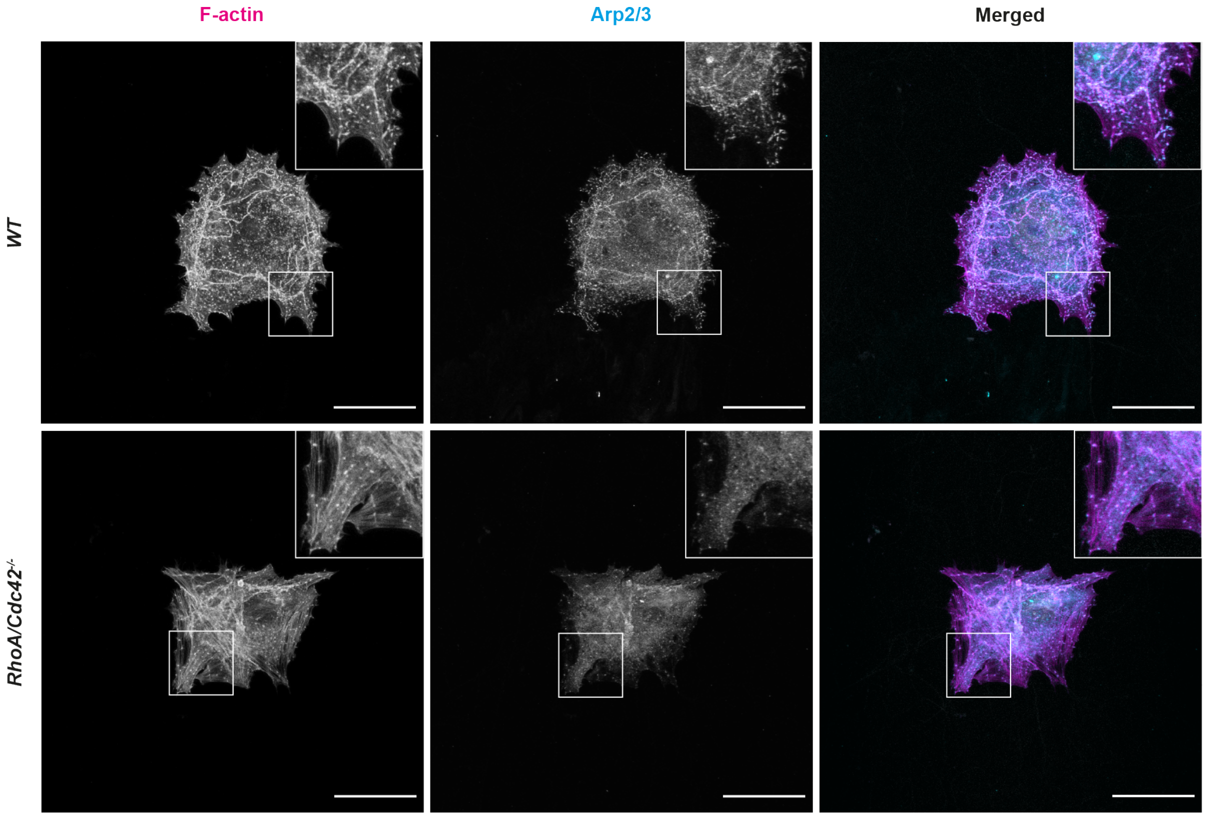

**Figure 32: Strongly impaired podosome formation in *RhoA/Cdc42*$^{-/-}$ MKs is not associated with impaired Arp2/3 localization.** Visualization of MK podosome formation of cultured BM-derived MKs upon adhesion to Horm collagen. Representative confocal images of fluorescently stained BM MKs are shown (40x oil objective, Leica TCS SP8). Podosomes are stained by phalloidin (F-actin) in magenta, the podosome marker Arp2/3 stained by Arpc2 in cyan and the nuclei are counterstained with DAPI in grey. The inset panel shows a detailed view of the podosomes and the overlap of both markers. Scale bars, 50 µm (n = 5 mice per genotype). Heib *et al.,* **submitted.**

Regarding RhoA signaling, the downstream effector mDia1 was not obviously deregulated in *DKO* MKs and also levels of NMM-IIa were unaltered (Figure 31A,B). Strikingly, however, a quantitative immunoassay platform (ProteinSimple Jess)[289], revealed that MLC2 (regulatory light chain) protein was virtually absent from *DKO* platelets, while expression of the upstream regulator *myosin phosphatase 1* (MYPT1) was not affected (Figure 33C). Furthermore, in line with our *in situ* observations (Figure 30) β1-tubulin was significantly reduced in cultured *DKO* MKs and virtually absent from *DKO* platelets (Figure 31A,B). Total α-tubulin was partially reduced in *DKO* platelets, but not MKs (Figure 31A,B). Posttranslational modifications of tubulin are critical determinants of MT stability and turnover[156]. We thus further investigated posttranslational modifications of α-tubulin, which include detyrosination (Detyr-tub) and acetylation (Ac-tub), associated with stable MTs and tyrosinated α-tubulin (Tyr-tub), which characterizes dynamic MTs.[290,291] Interestingly, *DKO* platelets and MKs exhibited strongly decreased levels of Detyr-tub, which were associated with highly upregulated Tyr-tub in *DKO* platelets, while Ac-tub was only slightly altered (Figure 31A,B). Together with the decreased β1-tubulin expression, this revealed a pronounced tubulin disequilibrium in the absence of RhoA/Cdc42.

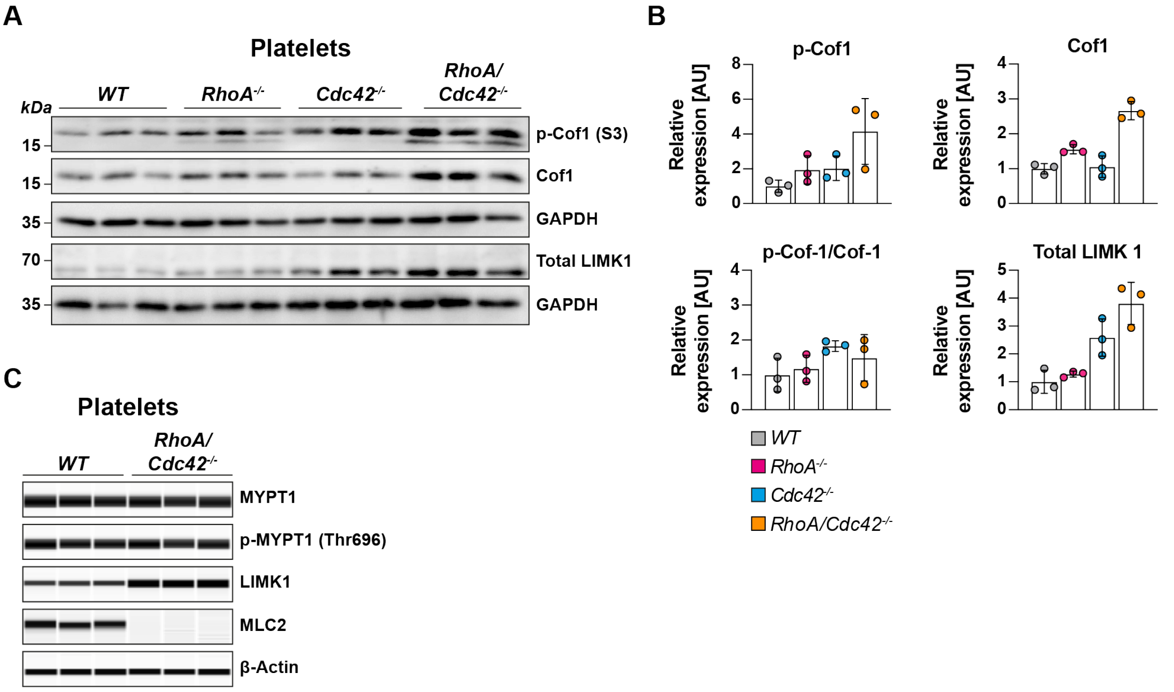

**Figure 33: Absence of MLC2 protein in *RhoA/Cdc42*$^{-/-}$ platelets. A,B** Analyses of the LIMK/Cof1 pathway also in single-deficient mice by immunoblotting using GAPDH as a loading control. **(A)** Representative immunoblots platelet lysates are shown. (n = 3, for *DKO*, platelets of two mice were pooled). **(B)** Quantification of protein expression using densitometric analysis (Fiji software). Protein expression was first normalized to GAPDH and subsequently compared to the respective control. **C** Analysis of MYPT1, p-MYPT1 (Thr696), LIMK1, MLC2, and β-actin protein expression in *WT* and *DKO* platelets using a JESS SimpleProtein analyzer (n = 3, for *DKO*, platelets of two mice were pooled). One dot represents one animal. All data are indicated as mean ± SD. For **(B)** multiple unpaired two-tailed Student's t-tests was used. *P≤0.05, **P<0.01, ***P<0.001. AU = *arbitrary unit*. Data depicted in **(C)** were partly generated by Zoltan Nagy (Experimental Biomedicine, Nieswandt Group). Heib *et al.,* **submitted.**

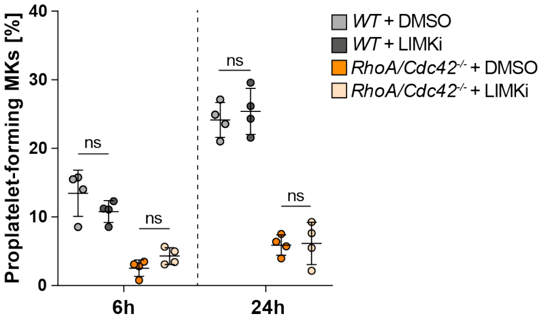

**Figure 34: Treatment of *RhoA/Cdc42$^{-/-}$* MKs with a LIMK inhibitor does not rescue the PPF defect.** Statistical analysis of proplatelet formation at 6h and 24 h after MK enrichment on a BSA gradient under static conditions. After enrichment, *WT* and *DKO* MKs were treated with either 10 µM of LIM Kinase inhibitor (LIMKi) or vehicle (DMSO, 0.1% final) (n = 4 mice per genotype). One dot represents one animal. All data are indicated as mean ± SD. Multiple unpaired two-tailed Student's t-test; *P≤0.05, **P<0.01, ***P<0.001. ns = *non-significant*. Heib *et al.,* **submitted.**

Summarizing, these results revealed that lack of RhoA/Cdc42 signaling in MKs significantly affects the expression of cytoskeletal proteins, resulting in severely altered F-actin and MT dynamics. The absence of β1-tubulin in native *DKO* MKs furthermore emphasizes the maturation defect of the cells.

### 4.2.7 Loss of RhoA/Cdc42 affects the transcription of genes associated with the MRTF(MKL)/SRF signaling pathway

We next investigated selected signaling pathways associated with MK maturation by immunoblotting and qPCR using cultured, BM-derived MKs, with a focus on genes that are part of established transcriptional signaling pathways in MKs or have been previously associated with platelet disorders. We first analyzed the TPO/TPO receptor (MPL)-induced JAK2/STAT signaling, which controls gene expression throughout megakaryopoiesis.[8,75] We observed slightly decreased levels of MPL (*Mpl)* mRNA (Figure 35A), however, stimulation of cultured, starved MKs with TPO resulted in a comparable increase in p-JAK2, -STAT3 and -STAT5 levels in *WT* and *DKO* (Figure 35B,C). Besides, mRNA and protein levels of the transcription factors GATA1 and RUNX1, known targets of TPO/MPL signaling, were similar in *WT* and *DKO* MKs (Figure 35A, D, E). Together, these findings did not indicate direct defects in the TPO/MPL signaling pathway in the absence of RhoA/Cdc42. However, further investigations of GATA1 and RUNX1 signaling might be required, as well as the investigation of other TFs such as FLI1 or NF-E2.

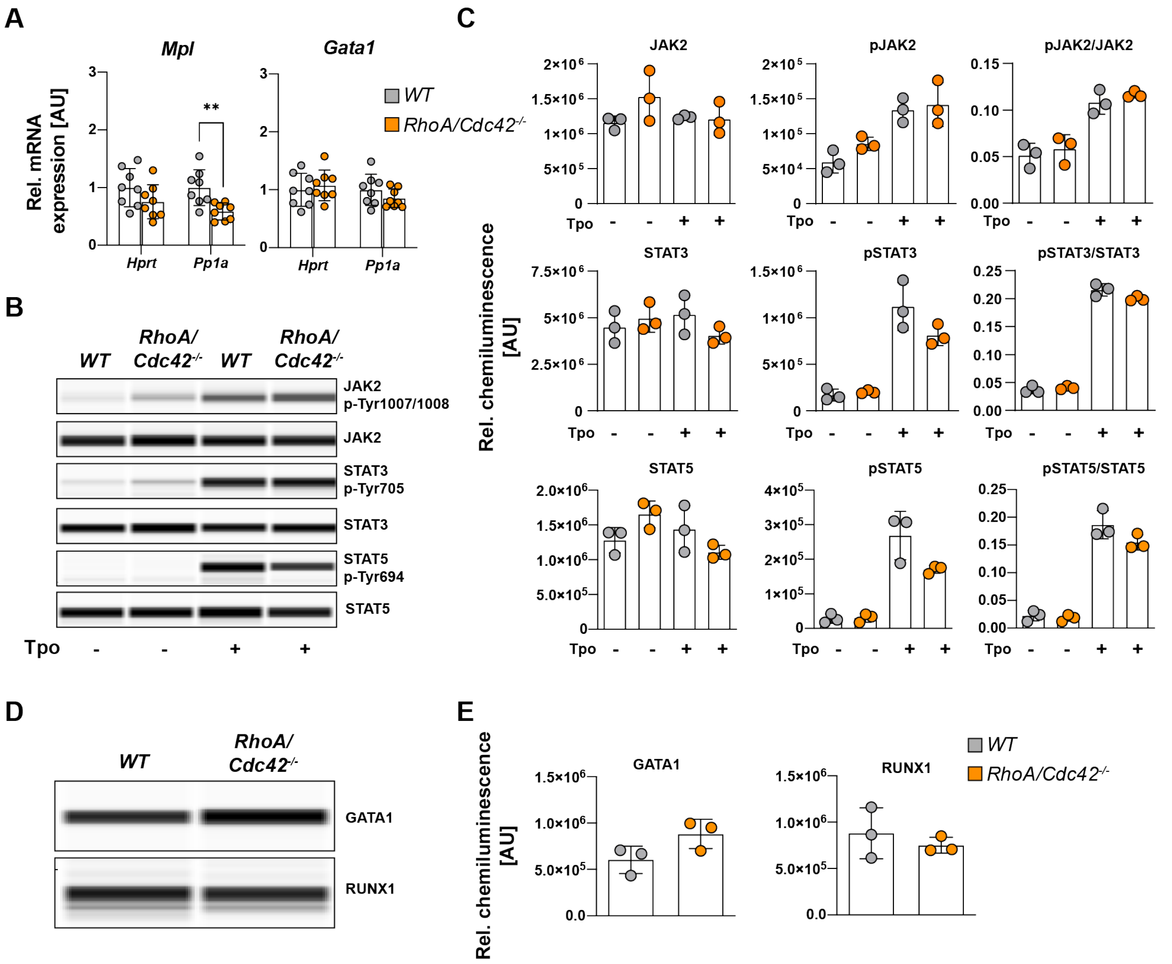

**Figure 35: Analysis of MPL/JAK/STAT signaling in *RhoA/Cdc42*$^{-/-}$ MKs. A** Analysis of mRNA expression of MPL (*Mpl*) and GATA1 (*Gata-1*) in cultured BM-derived *WT* and *DKO* MKs. Genes were normalized to *Pp1a* or *Hprt* (n = 4-8 mice per genotype. **C,D** Analysis of the TPO induced JAK2/STAT signaling in cultured BM-derived MKs of *WT* and *DKO* mice. After enrichment on a BSA gradient, MKs were starved for 4 h in DMEM media containing 0% FCS. Samples were stimulated with 0.5% TPO for 10 min, centrifuged and directly lysed. **(B)** (p)JAK2, (p)STAT3, (p)STAT5 protein expression was determined using JESS SimpleProtein analyzer **(C)** and quantified (n = 3 mice per genotype). **D,E** Analysis of the transcription factors GATA1 and RUNX1 in cultured BM-derived MKs of *WT* and *DKO* mice. **(D)** GATA1 and RUNX1 protein expression was determined using JESS SimpleProtein analyzer and **(E)** quantified (n = 3 mice per genotype). One dot represents one animal. All data are indicated as mean ± SD. Multiple unpaired two-tailed Student's t-test was used. $^{**}$P<0.01. AU = *arbitrary unit*. Data depicted in **(A)** was generated with the help of Heike Hermanns and Daniel Jahn (Hepatology Research Laboratory, Würzburg), **(B-E)** was generated by Zoltan Nagy (Experimental Biomedicine, Nieswandt Group). Heib *et al.,* **submitted.**

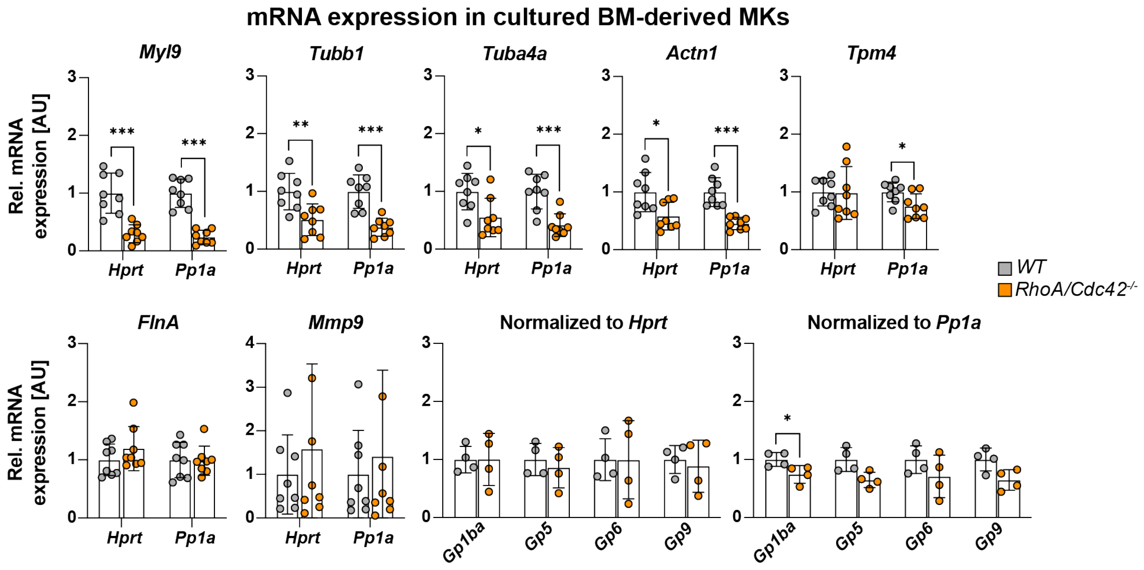

**Figure 36: Loss of RhoA/Cdc42 affects the expression of cytoskeletal regulators on mRNA level.** mRNA expression of depicted genes in cultured BM-derived *WT* and *DKO* MKs after enrichment by BSA gradient. Gene expression was normalized to *Pp1a* or *Hprt* as two independent house keeper genes (n = 4-8 mice per genotype). One dot represents one animal. All data are indicated as mean ± SD. Multiple unpaired two-tailed Student's t-test was used as well as the Mann-Whitney U test (for samples n < 6). $^{*}P \leq 0.05$, $^{**}P < 0.01$, $^{***}P < 0.001$. AU = *arbitrary unit*. Data depicted was generated with the help of Heike Hermanns and Daniel Jahn (Hepatology Research Laboratory, Würzburg). Heib *et al.,* **submitted.**

Previous studies point to a critical role of Rho GTPases, particularly RhoA-, mediated actin dynamics in the regulation of the SRF co-activators MRTF-A (MKL1) and MRTF-B (MKL2), which together form part of the MKL/SRF pathway of transcriptional regulation.[133,292] Notably, loss of *Srf* or double-deficiency of *Mkl1* and *Mkl2* in either HSCs or the MK-lineage in mice was reported to result in macrothrombocytopenia and the presence of immature MKs in the BM.[138,140] This was associated with decreased MK mRNA levels of *Myl9* (MLC2), *Tubb1* (β1-tubulin), as well as further genes of known importance for thrombopoiesis in mice and humans, such as *Tuba4a, Actn1,* and *Tpm4.*[157,217,293] Strikingly, mRNA levels of all these genes were also markedly reduced in cultured *DKO* MKs, while *Tpm4* was only significantly altered when normalized to *Pp1a* (Figure 36A). Furthermore, consistent with the published reports[138,140], levels of MK- and platelet-specific membrane GPs, namely the von Willebrand (vWF) receptor complex GPIb-IX-V (*Gp1ba*, *Gp5*, *Gp9*) and the collagen receptor GPVI (*Gp6*), were not significantly reduced in cultured *DKO* MKs compared to the *WT* control (Figure 36). However, it has to be noted that some genes associated with MKL/SRF signaling (*FlnA, Mmp9, Myh9*) (Figure 36A) were not affected in *DKO* MKs on either transcriptional or protein level.

To mechanistically investigate the functionality of the MKL/SRF pathway, we assessed levels of cytosolic and nuclear MKL1 in unstimulated, as well as serum-starved, TPO-stimulated cultured MKs.

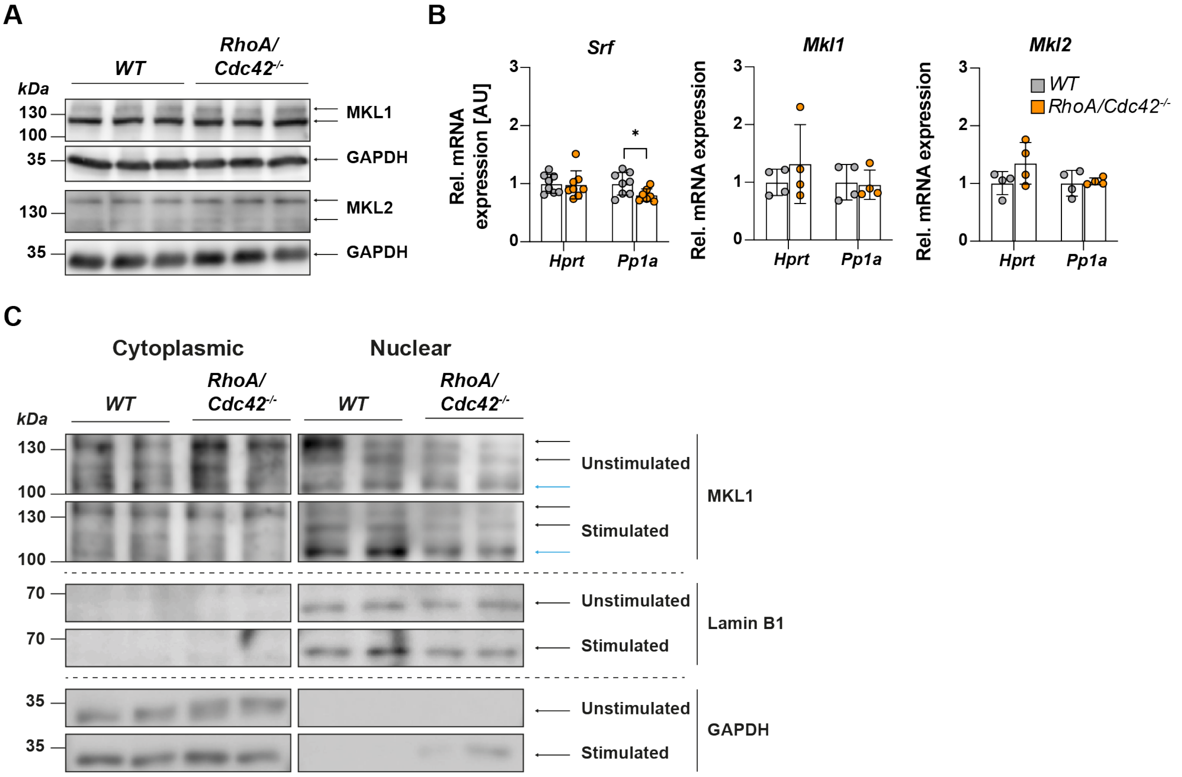

**Figure 37: Impaired MKL1/SRF signaling in RhoA/Cdc42$^{-/-}$ MKs. A** Analysis of the MKL(MRTF)/SRF signaling co-activators MKL1, MKL2 and GAPDH as a loading control by immunoblotting using lysates of cultured *WT* and *DKO* BM-derived MKs (n = 3 mice per genotype). Arrowheads indicate the different band sizes detected for MKL1 and MKL2. **B** Analysis of mRNA expression of SRF (*Srf*), MKL1 (*Mkl1*) and MKL2 (*Mkl2*) in cultured BM-derived *WT* and *DKO*. Genes were normalized to *Pp1a* or *Hprt* (n = 4-8 mice per genotype). **C** Analysis of the MKL/SRF signaling co-activator MKL1 by immunoblotting in nuclear and cytoplasmic fractions of cultured BM-derived MKs of *WT* and *DKO* mice. After enrichment, MKs were starved for 4 h in DMEM media containing 0% FCS and stimulated with 0.5% TPO for 15 min. GAPDH and Lamin B1 were used as loading controls for the cytoplasmic and nuclear fraction respectively. Black arrowheads indicate the different band sizes detected for MKL1. Blue arrowhead indicates an additional smaller band size which was highly abundant in the nuclear fraction after stimulation compared to the unstimulated control. (n = 2, for *WT* and *DKO*, MKs of two mice were pooled after enrichment, representative of two independent experiments. One dot represents one animal. All data are indicated as mean ± SD. Multiple unpaired two-tailed Student’s t-test was used as well as the Mann-Whitney U test (for samples n < 6). $^{*}$P≤0.05, $^{**}$P < 0.01, $^{***}$P < 0.001. AU = *arbitrary unit*. Data depicted was generated with the help of Heike Hermanns and Daniel Jahn (Hepatology Research Laboratory, Würzburg). Heib *et al.,* **submitted.**

Only a small or no reduction was detectable for *Srf* or *Mkl1/2,* and protein levels of MKL1/2 were unaltered in *DKO* MKs (Figure 37, Figure 36A,B), indicating that the expression of these proteins was per se largely unaffected. Strikingly, we observed decreased MKL1 accumulation within the nucleus of *DKO* MKs compared to the *WT*, indicating that the nuclear shuttling of this factor was impaired in the absence of RhoA/Cdc42 (Figure 37C).

Together, these results revealed that RhoA/Cdc42 signaling is essential for the transcriptional regulation of cytoplasmic MK maturation and indicate impaired MKL/SRF signaling in this process.

## 4.3 Investigation of candidate receptors involved in the process of transendothelial MK migration in RhoA-deficient mice

The study by Dütting *et al.*[251] proposed a regulatory circuit with RhoA and Cdc42 being key players downstream of the GPIb-axis. However, recent data from our laboratory raised the questions whether GPIb is the sole receptor involved in the regulation of PPF and the transendothelial migration of whole MKs into the BM sinusoids upon RhoA-deficiency. Besides GPIbα, several other regulators of PPF have been proposed, such as soluble factors or MK receptors that can interact with the ECM, especially with collagen type I and IV.[106] In addition, the role of the ITIM-containing receptor G6b-B and its interaction with the highly abundant sinusoidal ECM protein, the HS perlecan, in the regulation of transendothelial PPF is not known.[118] To investigate a potential role of different prominent receptors involved in the process of MK transmigration upon RhoA-deficiency, as well as physiological transendothelial PPF, mice double-deficient in RhoA and other receptors were generated and subsequently analyzed for eventual MK transmigration. Of note, we have observed significant differences in the MK transmigration phenotype between individual mouse lines, as well as the sex of the analyzed mice. Throughout, male mice lacking RhoA showed a more pronounced phenotype in terms of transendothelial MK migration compared to female RhoA-deficient mice (Figure 38). Besides, also the genetic background of the different analyzed mouse lines appeared to have an impact, not only in regard to intrasinusoidal MK localization, but also concerning the morphology of RhoA-deficient MKs in the BM. Therefore, we conducted our studies with sex-matched animals and, whenever possible, used *RhoA*$^{-/-}$ control mice bred out of the respective analyzed mouse line to counteract the strain differences, which in turn allows for a better interpretation of the results.

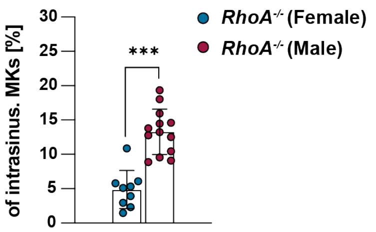

**Figure 38: Transendothelial MK migration is more evident in male RhoA-deficient mice.** Independent datasets obtained from *RhoA*$^{-/-}$ control mice of different projects were pooled and analyzed for sex differences of female vs. male *RhoA*$^{-/-}$ mice in terms of intrasinusoidal MK localization (n = 9 vs 13). One dot represents one animal. All data are indicated as mean ± SD. Unpaired two-tailed Student's t-test. *P<0.001.

### 4.3.1 Analysis of RhoA and β1 integrin double-deficiency on MK function

Integrins are obvious candidates to be involved in the regulation of transendothelial PPF, since their role in cell adhesion and cell motility is well established.[89] Interestingly, deficiency in the prominent platelet receptors αIIbβ3 (also known as Glanzmann thrombasthenia), α2β1 and GPVI does not affect circulating platelet counts in humans[294] or mice.[85,295] Also the role of α2β1 and its interactions with collagen in the regulation of PPF at the endothelial niche is cotroversely discussed.[85,296,297] While α2 forms heterodimers exclusively with β1-integrins, β1 itself can also form heterodimers with other integrins expressed in MKs and platelets (α5β1, and α6β1), thus allowing interactions with other ECM proteins in addition to collagen (e.g. fibronectin and laminin respectively).

The data and conclusions of the following project have been largely generated during the master thesis of Lou M. Wackerbarth at our department (June 2019 – February 2020). I have supervised her throughout her thesis, generated the mice, designed the experiments and supported her to analyze and interpret the data represented in this work.

#### 4.3.1.1 *RhoA/Itgb1$^{-/-}$* mice display severe macrothrombocytopenia

To study the effect of combined loss of the small GTPase RhoA and integrin β1 in MK function and localization in the BM as well as platelet production and function, we generated conditional KO mice lacking both RhoA and integrin β1 (*RhoA/Itgb1$^{-/-}$*), using the *Pf4-Cre/loxP* system. To enable the discrimination between redundant and non-redundant functions of both gene products, single-deficient *RhoA$^{-/-}$* mice were used as controls in all experiments. Conditional MK- and platelet-specific *RhoA/Itgb1$^{-/-}$* double-deficient mice were viable and born in the expected Mendelian ratios. An immunoblot (Figure 39A) confirmed the absence of both proteins in platelets. The loss of integrin β1 on the surface of platelets was additionally confirmed by flow cytometry (Lou M. Wackerbarth, Master thesis, 2020).

In accordance with the results described in the previous section of this thesis, loss of RhoA resulted in pronounced macrothrombocytopenia (Figure 39B,C). Heterozygous loss of either RhoA or β1 in combination with homozygous loss of either RhoA or β1 did not lead to significant alterations in platelet count or size compared to *WT* or *RhoA$^{-/-}$* mice and in line with the literature[295,298], also β1 single-deficient mice displayed normal platelet count and size (Figure 39B,C). Interestingly, mice deficient in both RhoA and integrin β1 exhibited a more severe reduction in platelet counts and a dramatic increase in platelet volume with two distinct platelet populations: One displayed characteristics similar to single-deficient *RhoA$^{-/-}$* mice while in the other one showed an even aggravated reduction of platelet counts and increase in platelet size.

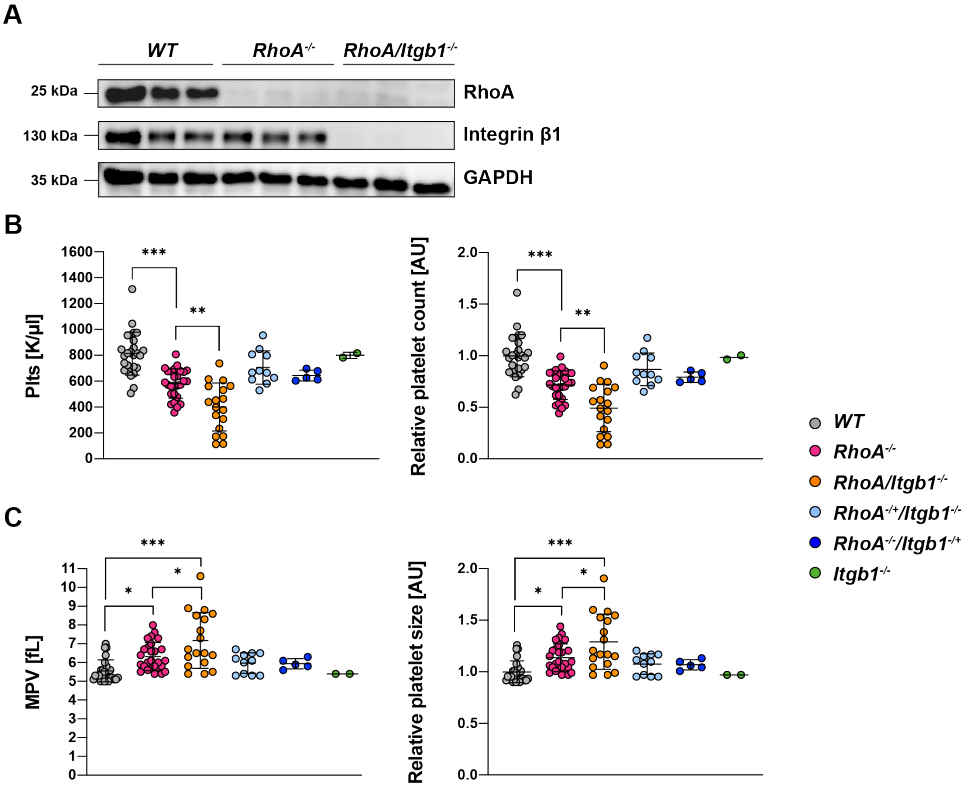

**Figure 39: Severe macrothrombocytopenia in *RhoA/Itgb1*$^{-/-}$ mice. A** Absence of RhoA and integrin β1 was verified in platelets derived from *RhoA*$^{-/-}$ and *RhoA/Itgb1*$^{-/-}$ mice by immunoblotting (n = 3). **B,C** Determination of **(B)** platelet count and **(C)** size using an automated hematology analyzer (scilVet). Right panels show normalized data to the *WT* (n = 16, 17, 18, 11, 5, 2). One dot represents one animal. All data are indicated as mean ± SD. One-way ANOVA test with Bonferroni's correction for multiple comparisons. *$P \leq 0.05$, **$P < 0.01$; ***$P < 0.001$. AU = *arbitrary unit*.

#### 4.3.1.2 Concomitant loss of integrin β1 does not affect the localization defect of RhoA-deficient BM MKs

To investigate the effect of the additional loss of integrin β1 on MK localization in the BM of RhoA-deficient mice, native cryosections of whole femora were analyzed. The overall distribution of MKs within the BM compartment was similar in *WT*, *RhoA*$^{-/-}$ and *RhoA/Itgb1*$^{-/-}$ mice (Figure 40A,B). However, in the present genetic background, the *RhoA*$^{-/-}$ MKs displayed a rather irregular morphology, while the morphology of *RhoA/Itgb1*$^{-/-}$-derived MKs was comparable to the *WT*. In addition, *RhoA*$^{-/-}$ mice showed a mild increase in total MK numbers in the BM compared to the *WT,* which is in accordance with our previous findings. Interestingly, this effect was not present in *RhoA/Itgb1*$^{-/-}$ mice (Figure 40B).

In the *WT*, the majority of *WT* MKs localized to or was in close proximity of BM sinusoids and no MKs were found inside the vessel lumen (Figure 40C). As described in the previous section, MKs in the BM of *RhoA*$^{-/-}$ mice showed elevated intrasinusoidal MK localization, albeit at much lower rates than observed before (3-4%). This change might be explained by the different background of the mice as well as the analysis of whole femura cryo sections instead of only several FOVs. Strikingly, the MK localization was similar in *RhoA/Itgb1*$^{-/-}$ and *RhoA*$^{-/-}$ mice, thus excluding a role of β1 integrins in the process of transmigration (Figure 40C).

Splitting the analysis of Figure 40C into males and females showed that MKs from female single- and double-deficient mice transmigrated only up to ~ 2%, whereas male mice showed a more pronounced phenotype with ~ 4% of intrasinusoidal MK localization (Figure 40D,E). The increased presence of intrasinusoidal MKs was only statistically significant when analyzing MKs from male *RhoA/Itgb1*$^{-/-}$ mice. This clearly demonstrates, that the genetic background of the mice can influence the transmigration of RhoA-deficient MKs.

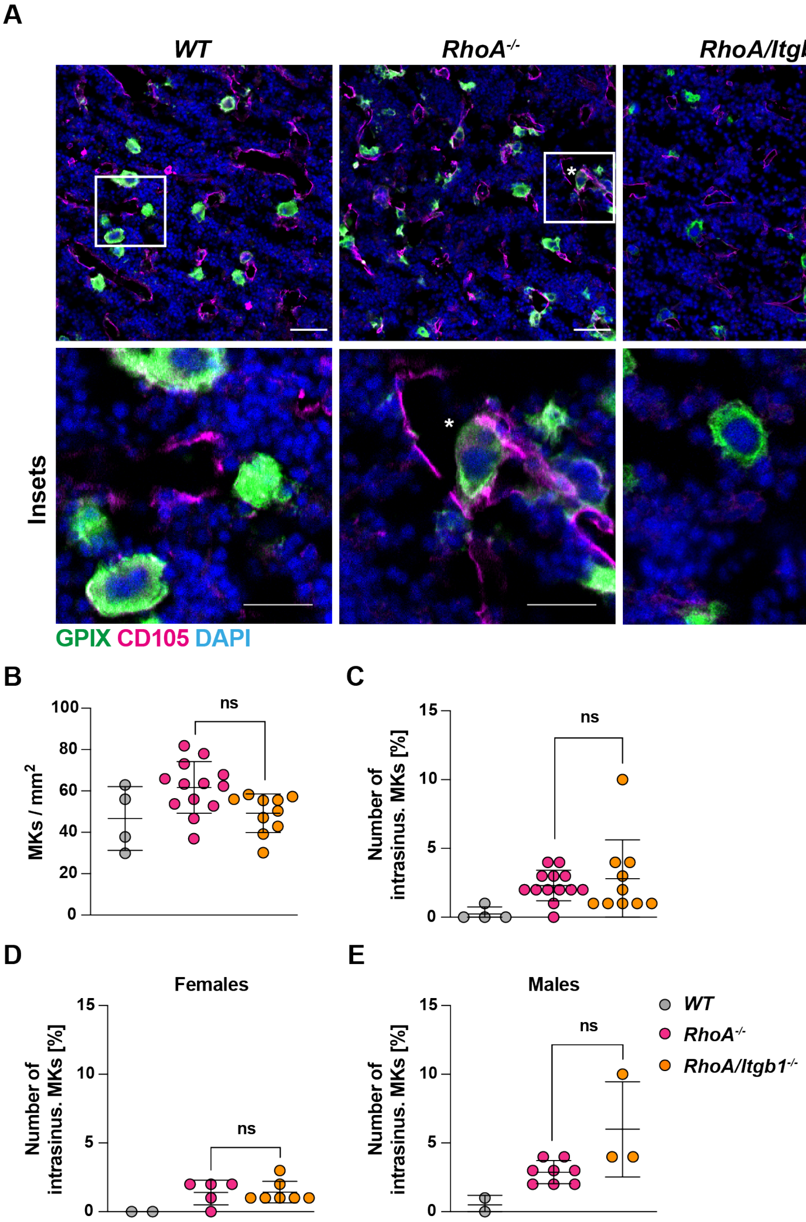

**Figure 40: BM MKs of *RhoA/Itgb1*$^{-/-}$ mice show transendothelial migration into BM sinusoids.** **A** Representative confocal microscopy images of femora cryosections of depicted mice (25x water objective, Leica TCS SP8). MKs, platelets and proplatelets are visualized by GPIX staining in green. CD105 staining (magenta) labels vessels. Nuclei were counterstained using DAPI (blue). White asterisks indicate intrasinusoidal (intrasinus.) MKs. Scale bars = 50 µm and 25 µm (Insets). **B**,**C** Quantification of **(B)** total MK numbers as well as **(C)** the number of intrasinusoidal MKs of the whole immunostained femora cryosections (n = 4, 13, 10). **D,E** Data-set from **(C)** was further differentiated between **(D)** female and **(E)** male mice. Quantification was done using Fiji software. One dot represents one animal. All data are indicated as mean ± SD. One-way ANOVA test with Bonferroni's correction for multiple comparisons was used. ns = *non-significant*.

#### 4.3.1.3 Unaltered proplatelet formation of BM-derived *RhoA/Itgb1*$^{-/-}$ MKs

Since *RhoA/Itgb1*$^{-/-}$ mice displayed a more severe macrothrombocytopenia than *RhoA*$^{-/-}$ mice we wondered whether the additional loss of β1 affects PPF *in vitro*. We therefore cultured BM-derived MKs for several days in the presence of TPO and rHirudin as described before and analyzed PPF using time-lapse microscopy over 24 h (Figure 41A).

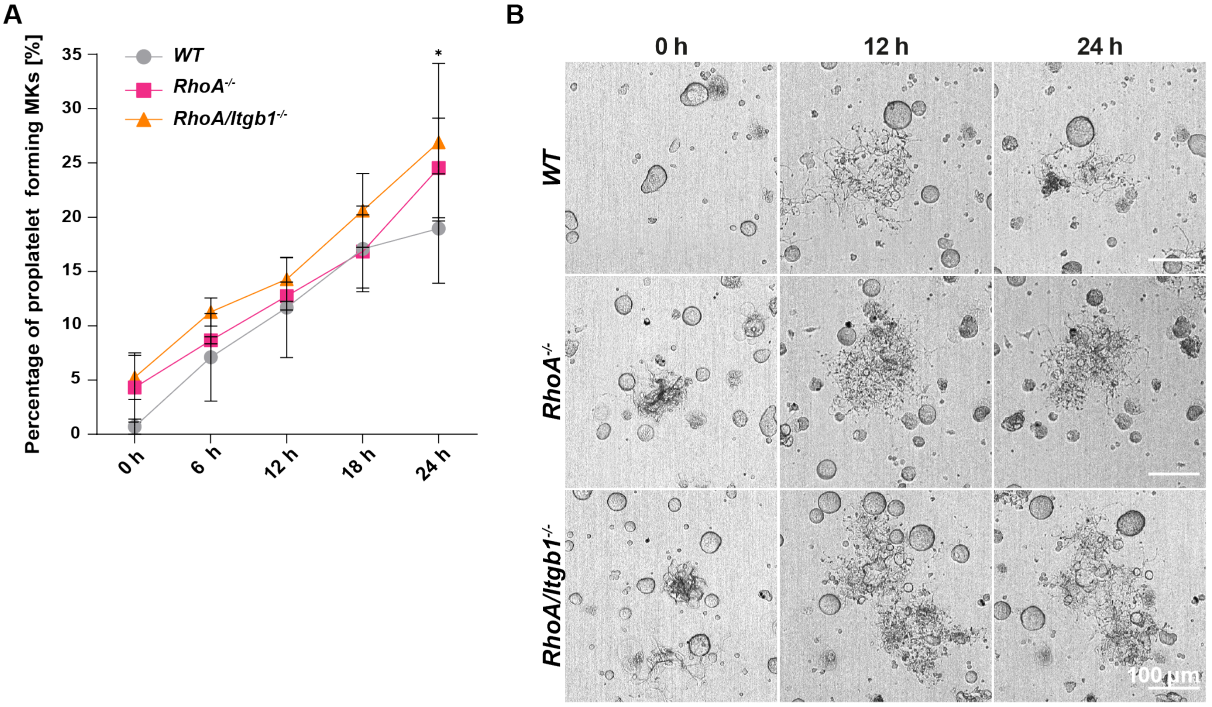

**Figure 41**: **Unaltered proplatelet formation of *RhoA/Itgb1*$^{-/-}$ MKs *in vitro*. A** PPF of cultured *WT*, *RhoA*$^{-/-}$ and *RhoA/Itgb1*$^{-/-}$ BM-derived MKs. On day 4, MKs were enriched on a BSA gradient and analyzed by time-lapse microscopy over 24h using $CO_2$-independent media. Imaging started approximately 2 h after the enrichment by BSA gradient. For each mouse, visual fields with at least >100 MKs were counted throughout different time points (n = 3 mice per genotype). **B** Representative images of proplatelet forming BM-derived MKs at different time points (0 h, 12 h and 24 h) (10x air objective, Leica TCS SP8). One dot represents one animal. All data are indicated as mean ± SD. Quantification was done using Fiji software. Two-way ANOVA test with Tukey's correction for multiple comparisons. $^{*}P \leq 0.05$ for *RhoA/Itgb1*$^{-/-}$ vs *WT*.

After 24 h, approximately 20% of the *WT* MKs displayed signs of PPF, whereas the percentage of proplatelet-forming MKs derived from *RhoA*$^{-/-}$ and *RhoA/Itgb1*$^{-/-}$ mice was elevated up to 25%, being statistically significant only for the *RhoA/Itgb1*$^{-/-}$-derived MKs, compared to *WT* MKs (Figure 41A). Further, a slightly faster onset of PPF of *RhoA*$^{-/-}$ and *RhoA/Itgb1*$^{-/-}$ MKs at the earliest timepoint was detected, comparable to our previous observations (Figure 41A,B). In summary, the loss of β1 integrins do not interfere with the localization defect observed in RhoA-deficient mice. The overall decrease in MK transmigration is due to strain-specific differences and shows the limitation of the transmigration capacity as a read-out. The mechanisms underlying the more severe macrothrombocytopenia upon the additional loss of β1 integrins in *RhoA/Itgb1*$^{-/-}$ mice require further investigations.

### 4.3.2 Analysis of RhoA and Talin-1 double-deficiency on MK function

The loss of β1 integrins did not interfere with the MK localization defect observed in RhoA-deficient mice. In addition, β1-deficient mice displayed normal platelet counts. Hence, we next aimed to focus on the general role of integrins in the process of transendothelial PPF and the migration of RhoA-deficient MKs. To address this question, we investigated the β-integrin binding protein talin, which together with kindlin plays critical roles in regulating integrin inside-out signaling.[299] The absence of Talin-1 in platelets is associated with blocked agonist-induced integrin activation[264,300], thus allowing us to examine the role of integrin inside-out signaling / activation in RhoA-deficient mice on MK function and localization in the BM.

#### 4.3.2.1 *RhoA/Talin-1*$^{-/-}$ mice display macrothrombocytopenia comparable to RhoA single-deficient mice

Since global genetic deletion of Talin-1 in mice results in lethality at embryonic days 8.5 to 9.5 because of gastrulation defects[301], we generated conditional KO mice lacking both RhoA and Talin-1 (*RhoA/Talin-1*$^{-/-}$) using the *Pf4-Cre/loxP* system. To enable the discrimination between redundant and non-redundant functions of both gene products, obtained single-deficient *RhoA*$^{-/-}$ mice were used as controls in all experiments. Conditional MK- and platelet-specific *RhoA/Talin1*$^{-/-}$ double-deficient mice were viable and born in the expected Mendelian ratios.

The absence of Talin-1 in double-deficient mice was confirmed by immunoblotting of platelet lysates (Figure 42A). As an additional confirmation, we could also reproduce the abrogated agonist-induced integrin activation by flow cytometry upon ablation of Talin-1 (Figure 42B). *RhoA/Talin-1*$^{-/-}$ mice displayed a significant macrothrombocytopenia which was comparable to RhoA single-deficient mice (Figure 42C,D). In line with previous studies, Talin-1 single-deficient mice showed normal platelet count and size compared to *WT* mice as shown by flow cytometry (Figure 42E,F).

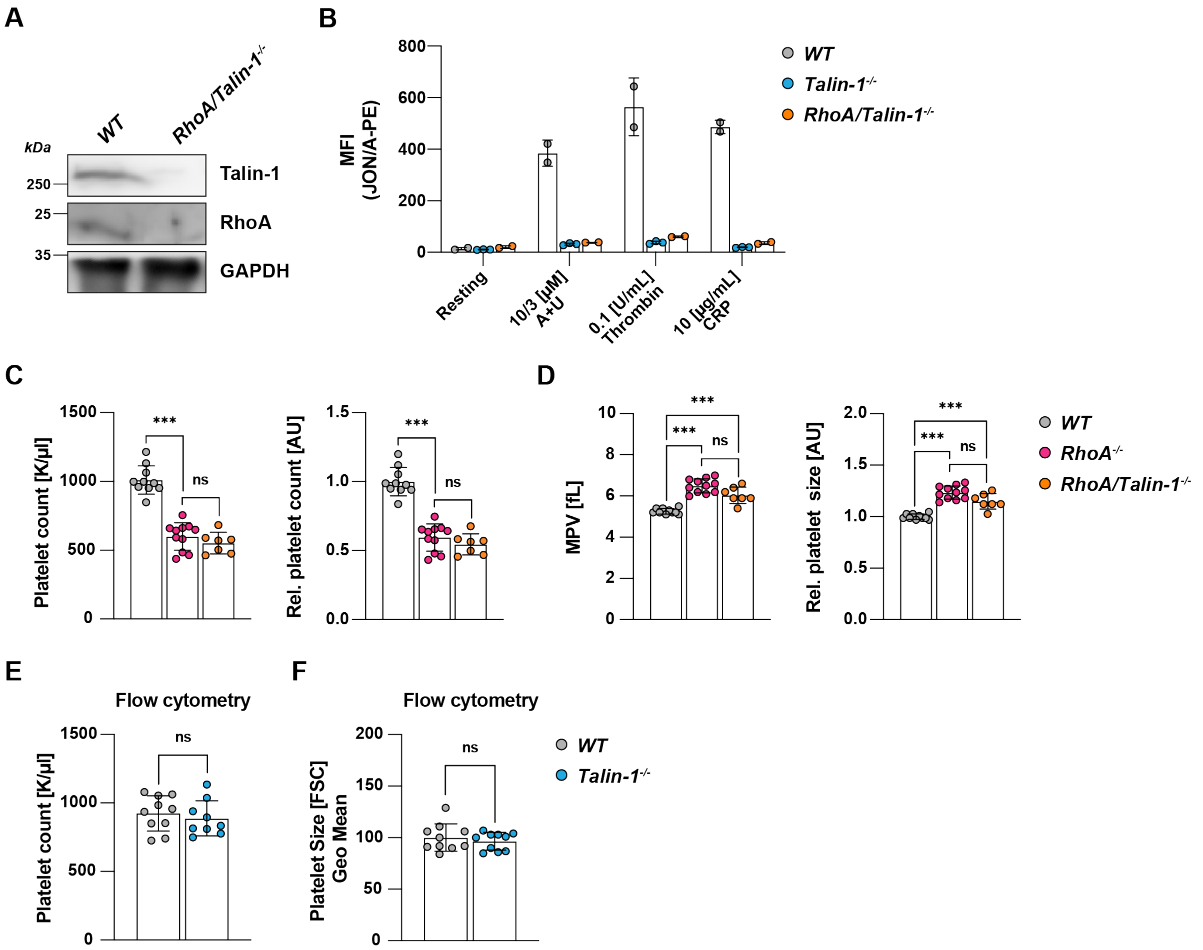

**Figure 42: Comparable macrothrombocytopenia in *RhoA/Talin-1$^{-/-}$* mice. A** Absence of RhoA and Talin-1 was verified in platelets derived from *RhoA/Talin-1$^{-/-}$* mice by immunoblotting (n = 3). **B** The integrin activation defect in *RhoA/Talin-1$^{-/-}$* platelets was verified by flow cytometry analysis (FACSCalibur, BD Biosciences) of platelets (n = 2, 3, 2). **C,D** Determination of **(C)** platelet count and **(D)** size using an automated hematology analyzer (scilVet). Right panels show normalized data to the *WT* (n = 10, 11, 8). **E, F** Platelets labeled for αIIbβ3 and GPV were analyzed by flow cytometry (FACSCelesta, BD Biosciences) and count **(E)** and size (FSC-A) **(F)** were obtained (n = 10 mice per genotype). One dot represents one animal. All data are indicated as mean ± SD. For **(C,D)** One-way ANOVA test with Tukey's correction for multiple comparisons and **(B,E,F)** unpaired two-tailed Student's t-test was used. *P≤0.05, **P<0.01; ***P<0.001. AU = *arbitrary unit*; ns = *non-significant*; A = *ADP*; U = *U46619*; CRP = *collagen-related peptide*. **(E,F)** Experiments were performed by Daniela Semeniak (Experimental Biomedicine, Nieswandt Group).

In conclusion, these results confirm the important role of Talin-1 in integrin inside-out signaling, whereas integrin activation per se seems to be dispensable for platelet production.

#### 4.3.2.2 Concomitant loss of Talin-1 does not affect the localization defect of RhoA-deficient BM MKs

To investigate the outcome of abolished β-integrin activation on MK localization in the BM of RhoA-deficient mice, native cryosections of whole mouse femora were analyzed as described before.

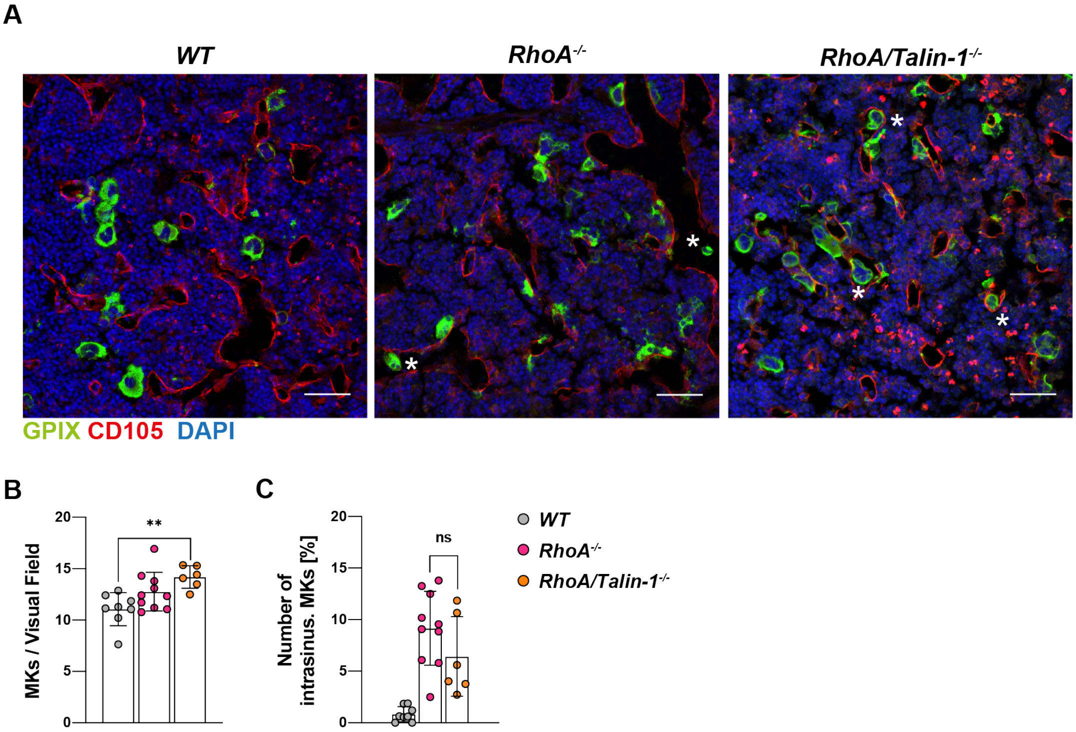

**Figure 43: *RhoA/Talin-1*$^{-/-}$ BM MKs show transendothelial migration into BM sinusoids. A** Confocal microscopy images of femora cryosections of *WT*, *RhoA*$^{-/-}$ and *RhoA/Talin-1*$^{-/-}$ mice (40x oil objective, Leica TCS SP8). MKs, platelets and proplatelets are visualized by GPIX staining in green. CD105 staining (red) labels vessels. Nuclei were counterstained using DAPI (blue). White asterisks indicate intrasinusoidal (intrasinus.) MKs. Scale bars = 50 µm. **B,C** Quantification of **(B)** total MK numbers and **(C)** the number of intrasinusoidal MKs in at least 15 visual fields (n = 8, 10, 6). Quantification was done using Fiji software. One dot represents one animal. All data are indicated as mean ± SD. One-way ANOVA test with Tukey's correction for multiple comparisons. *P≤0.05; **P< 0.01; **P<0.001. ns = *non-significant*.

In line with the previous findings, *RhoA*$^{-/-}$ mice showed a mild increase in total MK numbers in the BM compared to the *WT,* which was even more visible in *RhoA/Talin-1*$^{-/-}$ mice (Figure 43B). In the *WT*, the majority of MKs localized to or were in close proximity of BM sinusoids, while no MKs were found inside the vessel lumen (Figure 43C). MKs in the BM of *RhoA*$^{-/-}$ mice showed elevated intrasinusoidal MK localization (~ 9%), while in comparison, MK numbers were not significantly altered in *RhoA/Talin-1*$^{-/-}$ mice (~ 6.5%) (Figure 43C). In line with the results of the previous section, *RhoA*$^{-/-}$ BM MKs had an irregular morphology. Interestingly*,* the morphology of *RhoA/Talin-1*$^{-/-}$ derived MKs was comparable to *WT* MKs (Figure 43A), recapitulating the findings observed in *RhoA/Itgb1*$^{-/-}$MKs*.* Thus, in accordance with the results described in the previous sections, background-specific differences may influence the severity of transendothelial MK migration in RhoA-deficient mice (Figure 11 + Figure 40).

In summary these results exclude a role of integrin inside-out signaling in MK transmigration upon RhoA-deficiency. Moreover, the additional loss of Talin-1 did rescue the morphological appearance of *RhoA*$^{-/-}$ MKs to the same extend as the additional loss of β1 integrin, which may indicate aberrant β1 integrin signaling in *RhoA*$^{-/-}$ MKs.

### 4.3.3 Analysis of RhoA and G6b-B double-deficiency in MK function

Mice deficient in the ITIM-containing receptor G6b-B have been shown to develop severe macrothrombocytopenia and myelofibrosis along with impaired PPF, but largely unaltered endomitosis *in vitro*[112]. Similar observations of significantly lowered platelet counts and concomitant focal BM fibrosis were made in patients with variants in *MPIG6B.*[115] Recent work from our group has identified a *Mpig6b* mutant mouse line (referred to as *G6b*$^{mut}$ mice*)*, largely recapitulating the phenotypes observed in constitutive G6b-B KO mice, and further proposing G6b-B as a major regulator of MK maturation and BM homeostasis (Becker & Manukjan *et al.*, unpublished). The mechanisms underlying the impaired PPF and altered BM homeostasis, however, remain elusive. Recent studies have identified the HS perlecan, which is highly abundant in the ECM at the vascular sinusoids, to regulate G6b-B signaling and function, providing a novel mechanism, by which MK and platelet function may be regulated.[118] We were thus interested, whether the additional absence of G6b-B in *RhoA*$^{-/-}$ mice would influence the process of transendothelial MK migration.

#### 4.3.3.1 ***RhoA/G6b***$^{-/-}$ **mice display severe macrothrombocytopenia comparable to G6b-B single-deficient mice**

We generated mice lacking both RhoA and G6b-B in the MK- and platelet-lineage (referred to as *RhoA/G6b*$^{-/-}$) by intercrossing mice constitutively lacking G6b-B with mice conditionally lacking RhoA using the *Pf4-Cre/loxP* system. To enable the discrimination between redundant and non-redundant functions of both gene products obtained single-deficient *RhoA*$^{-/-}$ and *G6b*$^{-/-}$ mice were used as controls. *RhoA/G6b*$^{-/-}$ mice were viable and born in the expected Mendelian ratios.

Due to lack of specific antibodies at the time, the additional lack of G6b-B in double-deficient mice still needs to be verified by either immunoblotting or flow cytometry. However, mice lacking G6b-B were shown to suffer from a severe macrothrombocytopenia, with platelet counts lower than <20% of the *WT* mice.[112] Accordingly, we observed that loss of G6b-B resulted in pronounced macrothrombocytopenia, with a significant reduction in platelet count (<20% of *WT*) and an increase in platelet volume (Figure 44A,B). *RhoA/G6b*$^{-/-}$ mice displayed a comparable reduction in platelet counts, although a tendency towards even lower platelet counts (~ 20% vs ~ 13%) was evident (Figure 44A,B).

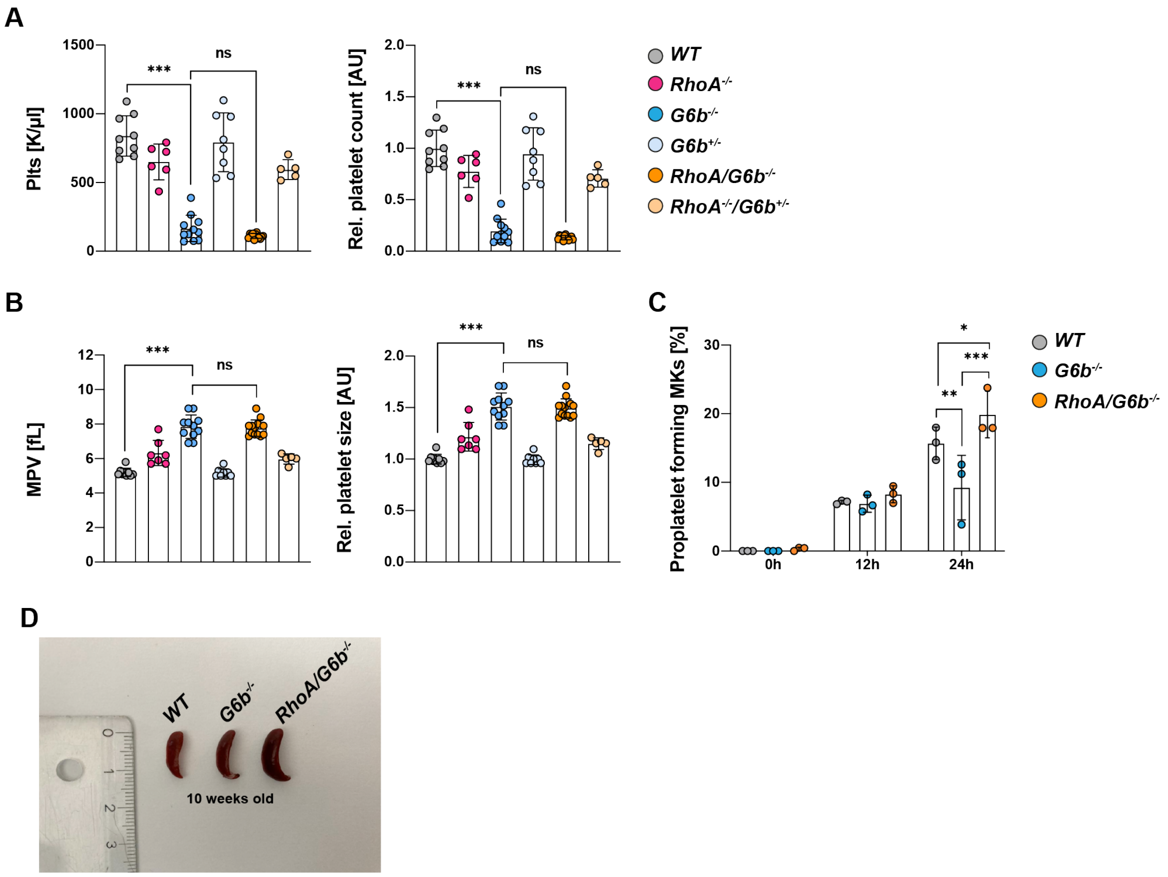

**Figure 44: *RhoA/G6b$^{-/-}$* mice display severe macrothrombocytopenia. A,B** Determination of **(A)** platelet count and **(B)** size using an automated hematology analyzer (scilVet). Right panels show normalized data to the *WT* (n = 9, 6, 11, 13, 5). **C** PPF of cultured BM-derived MKs. On day 4, MKs were enriched on a BSA gradient and analyzed by time-lapse microscopy over 24h using $CO_2$-independent media. Imaging started approximately 2 h after the enrichment on the BSA gradient. For each mouse, visual fields with at least >100 MKs were counted throughout different time points (n = 3 mice per genotype). **D** Representative spleen pictures of depicted mice. Ruler displays centimeter (cm) (n = 4 mice per genotype). One dot represents one animal. All data are indicated as mean ± SD. Quantification was done using Fiji software. One-way ANOVA test with Tukey's correction for multiple comparisons. $^{*}P \leq 0.05$, $^{**}P < 0.01$; $^{***}P < 0.001$. AU = *arbitrary unit*; ns = *non-significant*.

We next asked whether the lower platelet counts resulted from impaired PPF of BM-derived MKs as previously described.[112] Indeed, PPF of *in vitro*-matured*,* BM-derived MKs was significantly impaired upon ablation of G6b-B after 24 h compared to the *WT.* Interestingly, *RhoA/G6b$^{-/-}$* mice exhibited enhanced PPF after 24 h, thus positively influencing the defective PPF observed upon lack of G6b-B alone (Figure 44C). Note that the same observations of rather enhanced PPF have been made when analyzing *RhoA/Itgb1$^{-/-}$* mice (Figure 41), thus confirming the potential role of RhoA as a negative regulator of PPF. How the additional loss of RhoA promotes PPF under the here present conditions requires further investigation.

Interestingly, *RhoA/G6b*$^{-/-}$ mice presented with an even more severe splenomegaly compared to *G6b*$^{-/-}$ mice, suggesting extramedullary hematopoiesis in these animals (Figure 44D). Further detailed analyses of the spleen in double-deficient mice are currently in progress.

In summary our results revealed, that G6b-B single-deficiency is sufficient to impair PPF *in vivo* and to some extend *in vitro*. Interestingly, concomitant loss of RhoA could rescue the PPF defect *in vitro* but not *in vivo*, thus arguing for a differential regulation of PPF in both settings as previously discussed (1.5.3).[60,83]

#### 4.3.3.2 The effect of RhoA/G6b-B double-deficiency on myelofibrosis

G6b-B-deficiency has been associated with the development of myelofibrosis in mice and humans.[112,115] The same effect has also been extensively studied in *G6b*$^{mut}$ mice (Becker & Manukjan *et al.*, unpublished). The indication of elevated number of MKs in the spleen of *RhoA/G6b*$^{-/-}$ mice prompted us to further investigate the morphology of the BM as the main site of hematopoiesis. In *G6b*$^{mut}$ mice, a more pronounced myelofibrosis and an increased vessel density in 8-week old female mice compared to male mice was evident. Associated with the myeolofibrosis, female *G6b*$^{mut}$ mice additionally exhibited a progressive osteosclerosisa. Marked by a thickening and irregularity of the bony in the BM cavity,[302] leading to loss of BM cell mass, as well as an accumulation of adipocytes (Becker & Manukjan *et al.*, unpublished). While adipocytes have not been investigated, we were also able to clearly detect the osteosclerosis in 10-week old female and to a lesser extent in male *G6b*$^{-/-}$ mice (Figure 45A). These oberservations were further associated with increased vessel density and a dilated appearance of the vessels (Figure 47A). The reduction in BM cellularity was reflected by a reduced recovered BM mass after centrifugation of long bones (Figure 45B), especially in female *G6b*$^{-/-}$ mice. In contrast, the BM architecture of *RhoA*$^{-/-}$ mice was unaltered (Figure 45A). Strikingly, although still suffering from a severe macrothrombocytopenia, *RhoA/G6b*$^{-/-}$ mice displayed a strong reduction of the osteosclerotic phenotype in female and also the male mice (Figure 45A). This finding was also reflected by in an increase of recovered BM mass after centrifugation on the long bones (Figure 45B).

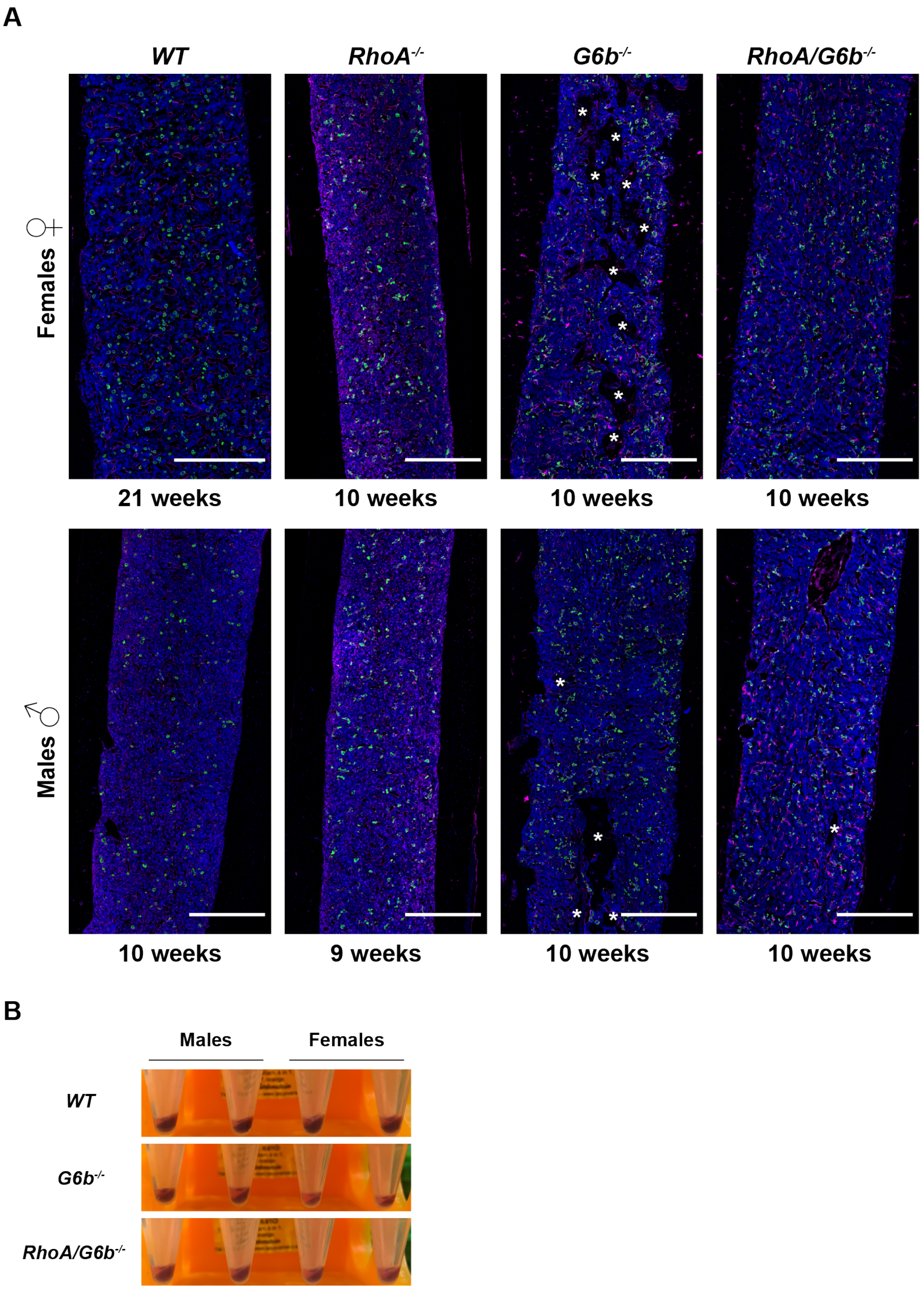

**Figure 45: Reduced osteosclerosis in *RhoA/G6b*$^{-/-}$ mice. A** Representative confocal microscopy images of female and male femora cryosections of depicted mice (20x water objective, Leica TCS SP8). MKs are shown by GPIX staining in green. CD105 staining (magenta) labels vessels. Nuclei were counterstained using DAPI (blue). Scale bars = 200 µm. White asterisks indicate spots of osteosclerosis. **B** Representative pictures of BM cell pellets obtained after spin isolation of the depicted mice (n = 4 mice per genotype).

We were thus interested in further investigating the connection of osteosclerosis and myelofibrosis to RhoA in the double-deficient mice (Figure 46). It is well established that an elevated release of TGFβ1 promotes collagen and reticulin deposition due to increased collagen synthesis and inhibited metalloproteinase activity[303,304], and in combination with other factors, e.g. the proinflammatory cytokine IL-6, accelerates myelofibrosis progression. A progressive myelofibrotic phenotype has been described in *G6b*$^{-/-}$ mice[112] with enhanced deposition of collagen and reticulin, which was also found in *G6b*$^{mut}$ mice. Moreover, immunosorbent assays revealed that the myelofibrotic phenotype in the BM of *G6b*$^{mut}$ mice was accompanied by elevated TGFβ1 concentrations in the harvested BM plasma (Becker & Manukjan *et al.*, unpublished).

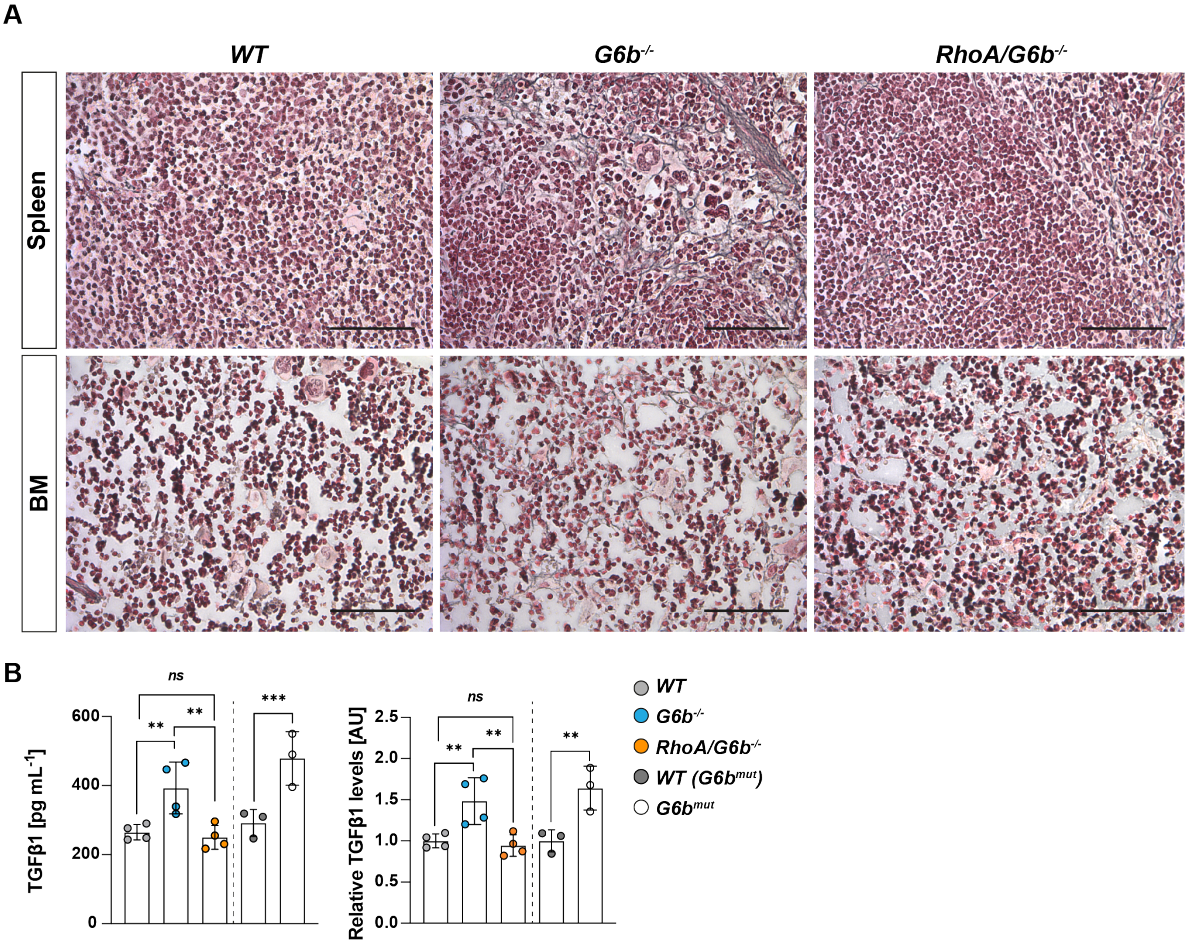

**Figure 46: Reduced osteosclerosis is associated with ameliorated myolefibrosis in *RhoA/G6b*$^{-/-}$ mice.** **A** Representative paraffin sections of the mouse spleen and femur stained for reticulin fibers (grey/black appearance) and nuclei (pink/red appearance) (n = 4 mice per genotype). Scale bars = 75 µm. **B** Levels of TGFβ1 in BM plasma of depicted mice using purchased enzyme-linked immunosorbent assays (n = 4, 4, 4, 3, 3). One dot represents one animal. All data are indicated as mean ± SD. One-way ANOVA test with Tukey's correction for multiple comparisons. *P≤0.05, **P<0.01; ***P<0.001. AU = *arbitrary unit*; ns = *non-significant*. The data of this figure was kindly provided by Isabelle C. Becker (Experimental Biomedicine, Nieswandt Group).

Comparable to the *G6b*$^{mut}$ mice, *G6b*$^{-/-}$ mice indeed presented with a myelofibrotic phenotype both in the spleen and the BM, associated with increased TGFβ1 concentrations in the BM plasma (Figure 46A,B). Strikingly, TGFβ1 levels in the BM plasma of *RhoA/G6b*$^{-/-}$ mice were normalized to *WT* levels (Figure 46B), which was reflected by a visible reduction of the myelofibrotic phenotype (Figure 46A), thus in turn explaining the reduction in osteosclerosis. In summary, our results indicate that, albeit a severe macrothrombocytopenia and splenomegaly in *RhoA/G6b*$^{-/-}$ mice, the additional loss of RhoA presumably interferes with TGFβ1 secretion and thereby ameliorates the myelofibrosis and osteosclerosis caused upon G6b-B ablation.

#### 4.3.3.3 RhoA/G6b-B MKs display increased intrasinusoidal localization

To investigate the effect of additional G6b-B depletion on MK localization in the BM of RhoA-deficient mice, native cryosections of whole femora were analyzed by immunohistochemistry (Figure 45A + Figure 47A). Besides the myelofibrosis in *G6b*$^{-/-}$ mice, we detected a high level of MK fragmentation and MKs with an irregular morphology, which clustered around the sinusoids within the BM of *RhoA/G6b*$^{-/-}$ and *G6b*$^{-/-}$ mice. These alterations made it difficult to determine an exact MK number in the BM of these mice, although an increase compared to the *WT* was clearly visible (Figure 45A + Figure 47C). In line with the previous results described in this thesis, MKs localized at BM sinusoids in *WT* mice. Notably, the MK morphology in *RhoA*$^{-/-}$ mice was similar to our observations described in sections 4.3.1.2 and 4.3.2.2, reflected by a rather irregular appearance (Figure 47B), while at the same time smaller proportions of intact MKs were situated in the sinusoidal lumen of *RhoA*$^{-/-}$ mice (Figure 47B). Unexpectedly, intrasinusoidal localization was also partially visible in *G6b*$^{-/-}$ mice (Figure 47B), which, however, may at least in part be caused by the aberrant and dilated vessel structures in the BM of these mice (Figure 47A). Interestingly, *RhoA/G6b*$^{-/-}$ mice showed strongly enhanced transmigration of BM MKs compared to either of the single-deficient mice (Figure 47A,B). In summary, the loss of G6b-B did not prevent the transmigration of RhoA-deficient MKs but rather facilitated the process to some extent. Whether this is particularly due to alterations in the vessel architecture of these mice or other regulatory mechanisms remains to be investigated.

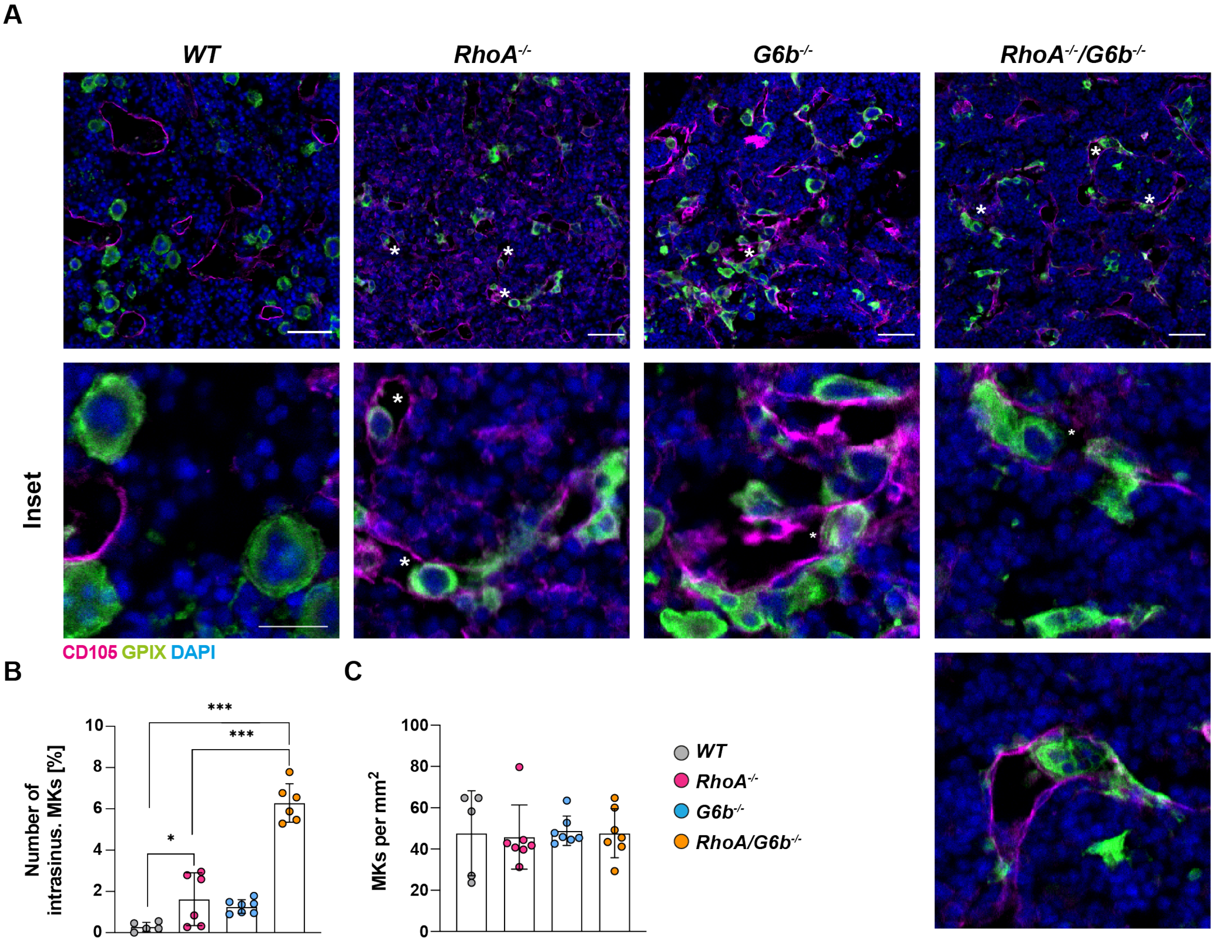

**Figure 47: Analysis of BM MK localization in *RhoA/G6b*$^{-/-}$ mice. A** Representative confocal microscopy images femora cryosections of depicted mice (20x water objective, Leica TCS SP8). MKs are shown by GPIX staining in green. CD105 staining (magenta) labels vessels. Nuclei were counterstained using DAPI (blue). Scale bars = 50 µm and 25 µm for insets. White asterisks intrasinusoidal (intrasinusoid.) MKs. **B,C** Quantification of **(B)** intrasinusoidal MKs and **(C)** total MKs of whole immunostained femora cryosections (n = 5, 6, 7, 6). Quantification was done using Fiji software. One dot represents one animal. All data are indicated as mean ± SD. One-way ANOVA test with Tukey's correction for multiple comparisons. *P≤0.05, **P<0.01, ***P<0.001.

### 4.3.3.4 Functional endomitosis in RhoA/G6b double-deficient mice

The abnormal appearance and clustering of the *RhoA/G6b*$^{-/-}$ and *G6b*$^{-/-}$ BM MKs was similar to what was observed in RhoA/Cdc42 double-deficient mice. To decipher maturation defects in these mice, an ultrastructural analysis of the BM *in situ* by TEM is ongoing. However, we already aimed to address whether these mice also suffer from endomitosis defects.

Therefore, we used a modified version of our current ploidy assay (see Figure 9), by double-staining for MKs with anti-GPIIba (CD41) and anti-GPIX antibodies (CD42a), instead of an anti-CD41 antibody only, in order to allow for a better discrimination of MK populations. For labelling the nuclear content, we furthermore substituted the PI staining with SYTOX™ Orange, allowing for better resolution and for a compensation of the flow cytometry signals (Gating: Figure 49A).

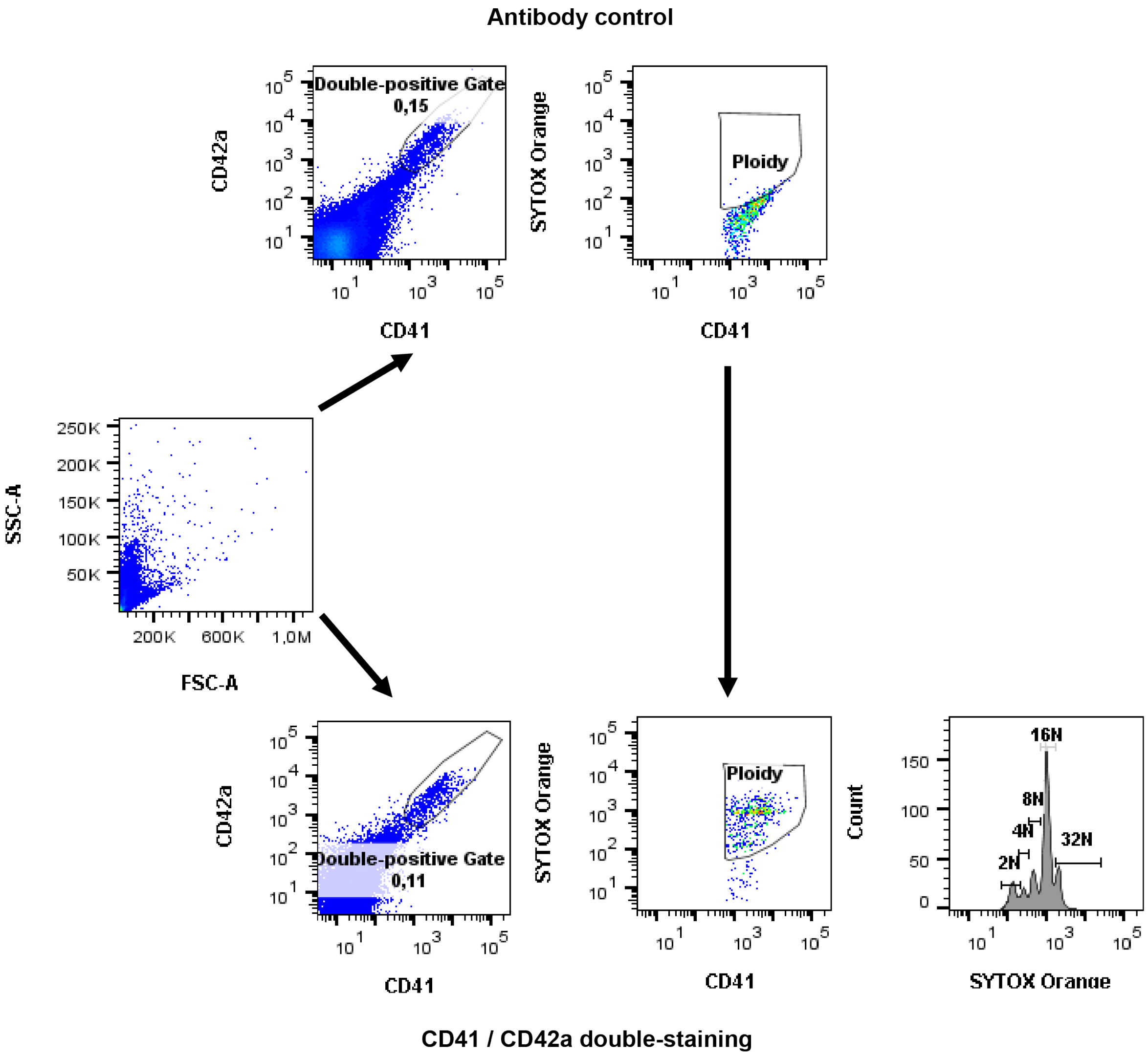

**Figure 48: Gating strategy for the analysis of ploidy in primary BM MKs by double-staining.** Gating strategy for ploidy measurements of isolated native BM MKs by flow cytometry (FACSCelesta, BD Biosciences). Cells were identified by FSC and SSC properties. CD41$^+$Cd42a$^+$-cells were considered MKs and plotted against the SYTOX Orange signal to determine the ploidy distribution, which was quantified by histogram analysis.

Using primary BM MKs, *WT* mice displayed comparable distributions to what we observed in previous measurements, displaying a major 16N MK population and a mean ploidy of about 16N (15.2N) (Figure 49A,B). Interestingly, *RhoA/G6b*$^{-/-}$ and *G6b*$^{-/-}$ MKs dsiplayed an increase in both 2N and 4N MK populations along with a significant reduction in the 16N population, but largely unaltered >32N MKs, with even slightly higher abundance in *RhoA/G6b$^{-/-}$* mice. Overall, these alterations resulted in a significant lower mean ploidy in *G6b$^{-/-}$* mice (12.4N). We thus asked whether the increase in the 2N and 4N population might be explained by higher proportions of CD41$^{+}$CD42a$^{+}$ cells. Indeed, we detected higher amount of CD41$^{+}$CD42a$^{+}$ cells in *RhoA/G6b$^{-/-}$* and *G6b$^{-/-}$* mice (5x10$^{6}$ total cells measured) (Figure 49C), thus confirming our visual observations from cryosections.

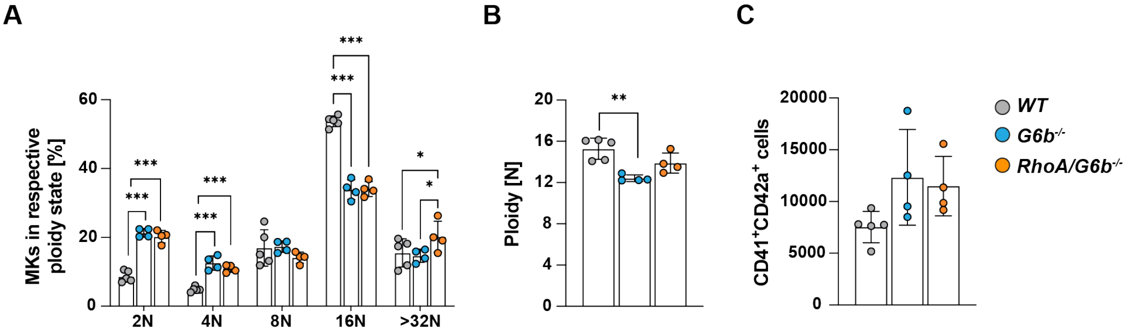

**Figure 49: Functional endomitosis in *RhoA/G6b$^{-/-}$* mice. A** Ploidy distribution of isolated primary BM MKs. **B** Mean MK ploidy. **C** Proportion of CD41$^{+}$Cd42a$^{+}$-cells out of 5x10$^{6}$ total cells measured. One dot represents one animal. All data are indicated as mean ± SD. For **(A)** Two-way ANOVA and **(B,C)** one-way ANOVA test with Tukey's correction for multiple comparisons was used. *P≤0.05, **P<0.01, ***P<0.001.

In summary, G6b-B deficiency was not able to revert the transmigration of RhoA-deficient MKs. In contrast, we detected a significantly increased transmigration of *RhoA/G6b$^{-/-}$* MKs in comparison to *RhoA$^{-/-}$* MKs in line with an elevated amount of *G6b$^{-/-}$* MKs within the sinusoids, most likely due to aberrant and dilated vessel structures in the BM of these mice. These findings again confirm that *RhoA$^{-/-}$* deficiency increases MK mobility, while the degree of transmigration is influenced by several factors, including the genetic background and the BM architecture. Furthermore, we could show that endomitosis, although an enrichment of 2N and 4N populations was detected, seems to be largely unaffected in the absence of G6b-B, which was also true for *in vitro* cultured BM-derived MKs.[112]

### 4.3.4 Higher intrasinusoidal abundance of *RhoA*$^{-/-}$ MKs does not significantly correlate with a more severe macrothrombocytopenia

Throughout all the here described projects, highly varying levels of intrasinusoidal MK localization were observed for the different *RhoA*$^{-/-}$ control mice. We noted not only a sex-dependent, but also strain-specific differences in the degree of MK transmigration. This emphasizes the need to always use matching *RhoA*$^{-/-}$ controls, as used in this thesis for analysis of *RhoA/Cdc42*$^{-/-}$, *RhoA/Itgb1*$^{-/-}$, *RhoA/Talin-1*$^{-/-}$, and *RhoA/G6b*$^{-/-}$ mice.

In addition, technical improvements play a role: During the course of this thesis it became possible to easily image and quantify whole BM sections. This allowed us to quantify and count more MKs of each section and to draw more accurate conclusions by eliminating the error of choosing several FOVs for quantification manually. Importantly, the MK transmigration was present in every RhoA-deficient mouse line analyzed, albeit at a varying abundance.

It seemed plausible to us that a higher intrasinusoidal abundance of *RhoA*$^{-/-}$ MKs might correlate with a more pronounced thrombocytopenia in *RhoA*$^{-/-}$ mice. To investigate this hypothesis, the platelet counts of *RhoA*$^{-/-}$ mice displaying a high abundance of intrasinusoidal MKs (~ 8% and higher; *RhoA*$^{High}$) were compared to those of *RhoA*$^{-/-}$ mice displaying a low abundance of IS MKs (<8%). Respective *WT* mice were used as controls (*WT*$^{Low}$; *WT*$^{High}$). *RhoA*$^{High}$ mice showed in average a 10% lower platelet count than *RhoA*$^{Low}$ mice, which was, however, not statistically significantly (*RhoA*$^{High}$: 58%; *RhoA*$^{Low}$: 68% of *WT* controls) (Figure 50A). No difference was observed when comparing the platelet size (Figure 50B). In conclusion, no direct evidence of a correlation between intrasinusoidal MK localization and the degree of macrothrombocytopenia in *RhoA*$^{-/-}$ mice exists, indicating that enhanced transmigration is likely not the sole cause for the impaired PPF *in vivo* and thus requires further investigations.

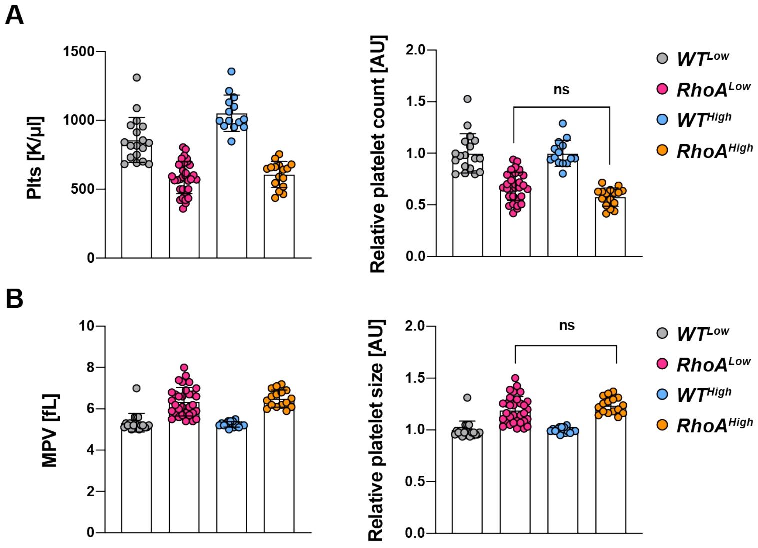

**Figure 50: Higher intrasinusoidal abundance of *RhoA*$^{-/-}$ MKs does not significantly correlate with a more severe macrothrombocytopenia. A,B** Determination of **(A)** platelet count and **(B)** size of *RhoA*$^{Low}$ (<8% of intrasinusoidal MKs) and *RhoA*$^{High}$ (>8% of intrasinusoidal MKs) mice using an automated hematology analyzer (scilVet). Different experimental sets were pooled and normalized to their respective *WT*$^{\text{Low}}$ or *WT*$^{\text{High}}$ controls (right panel) (n = 18, 32, 14, 16). One dot represents one animal. All data are indicated as mean ± SD. One-way ANOVA test with Tukey's correction for multiple comparisons was. AU = *arbitrary unit*; ns = *non-siginficant*.

### 4.3.5 Macrothrombocytopenia and transmigration in *RhoA*$^{-/-}$ mice is not due to *Pf4-Cre*-mediated off-target effects

Recent studies have reported that the *Pf4-Cre* does recombine not only in MKs but also in a small subset of stem and progenitor cells and all their developing progenies, especially immune cells.[236,237] Transplantation studies were carried out to address whether the mislocalization defects observed in RhoA-deficient mice using the *Pf4-Cre* system are potentially due to off-target effects, thus explaining the highly varying differences in the number of intrasinusoidal MKs in these mice throughout the different projects. Therefore, male and female *WT* as well as *RhoA*$^{-/-}$ mice were lethally irradiated and transplanted with BM derived from either *WT* or *RhoA*$^{-/-}$ mice*.* Only male mice were used as donors due to the sex specific differences in terms of intrasinusoidal localization in *RhoA*$^{-/-}$ mice (Figure 38). Platelet count and size as well as well localization of the MKs in the BM were analyzed. Both WT and *RhoA*$^{-/-}$ mice which received BM cells of *RhoA*$^{-/-}$ mice, developed a significant macrothrombocytopenia with ~ 40% decreased platelet counts) and an increase in platelet size (Figure 51A,B).

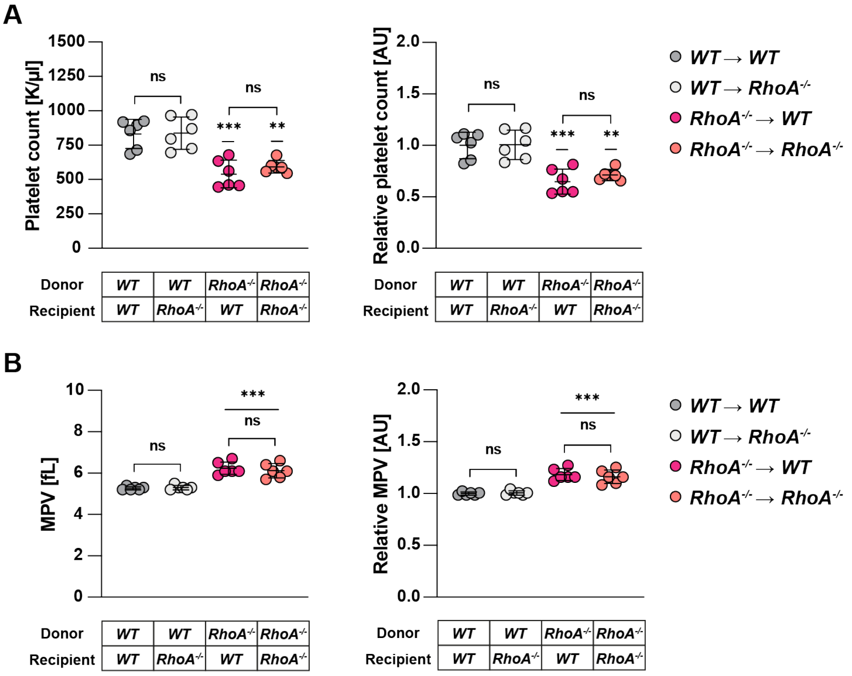

**Figure 51: Macrothrombocytopenia in BM-chimeric *RhoA*$^{-/-}$ mice is not due to *Pf4-Cre*-mediated off target effects. A,B** Determination of **(A)** platelet count and **(B)** size of different *Donor → Recipient* mice using an automated hematology analyzer (scilVet). Right panels show normalized data to the *WT → WT* control group (n = 6 mice per condition). One dot represents one animal. All data are indicated as mean ± SD. One-way ANOVA test with Tukey's correction for multiple comparisons was. AU = *arbitrary unit*; ns = *non-significant*. $^{**}p<0.01$; $^{***}p<0.001$ compared to *WT → WT* control.

In contrast, *WT* and *RhoA*$^{-/-}$ mice which received WT BM cells displayed normal platelet count and size. Thus, these results confirmed that the macrothrombocytopenia caused by *Pf4-Cre*-mediated deletion of *RhoA* has a hematopoietic cell intrinsic origin and is not due to potential off-target effects on e.g. endothelial cells. Next, native cryosections of whole femora were analyzed by immunohistochemistry (Figure 52A). While we usually observed a mild increase in MK numbers in the BM in *RhoA*$^{-/-}$ mice (see sections 4.2.1, 4.3.1.2, 4.3.2.2, 4.3.3.3), the MK count was overall lower, but comparable between the transplanted groups of this experiment (Figure 52B). Although only a low proportion of transmigration was observed in *WT* or *RhoA*$^{-/-}$ mice that received *RhoA*$^{-/-}$ BM cells (<2%), the difference was still significant compared to *WT* or *RhoA*$^{-/-}$ mice which had received *WT* BM cells (Figure 52C). However, the lower MK count as well as additionally influenced MK transmigration phenotype is most likely due to the irradiation effect. Note that mice which received *RhoA*$^{-/-}$ BM cells, also displayed abnormal irregular MK morphology.

In summary, the BM transplantation experiments revealed, that not only the macrothrombocytopenia, but also the aberrant transmigration of *RhoA*$^{-/-}$ MKs is due to cell intrinsic defects and not related to *Pf4-Cre* off target effects in non-hematopoietic cells. Together with the sections before, it proved again, that the aberrant intrasinusoidal transmigration itself is a weak marker and the underlying alterations in RhoA-deficient MKs needs to be further investigated and understood.

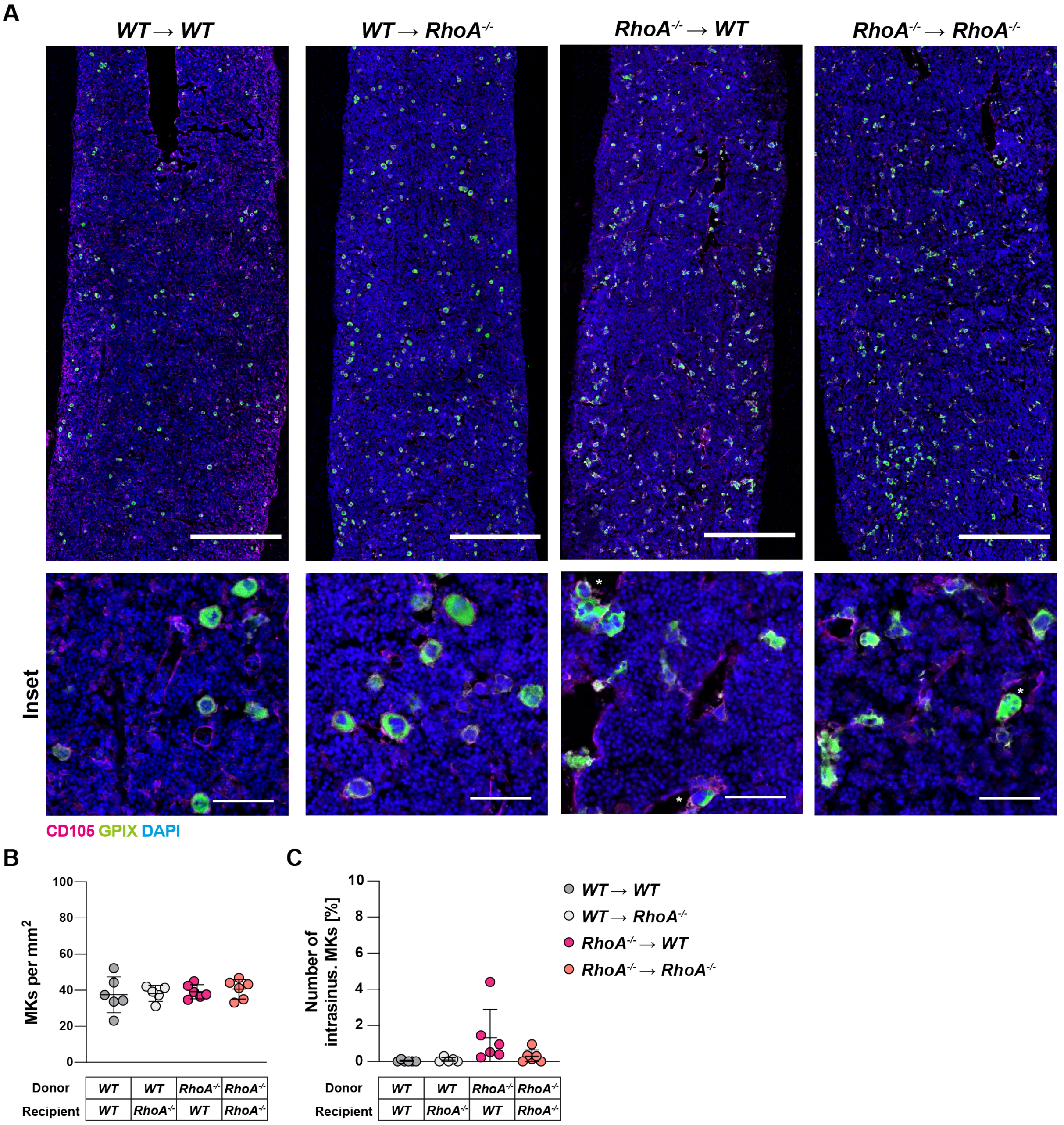

**Figure 52: Intrasinusoidal MK localization in BM-chimeric *RhoA*$^{-/-}$ mice is not due to *Pf4-Cre*-mediated off target effects. A** Representative confocal microscopy images of femora cryosections of different *Donor → Recipient* mice (20x water objective, Leica TCS SP8). MKs are shown by GPIX staining in green. CD105 staining (magenta) labels vessels. Nuclei were counterstained using DAPI (blue). Scale bars = 200 µm (Overview) and 50 µm (Inset). **B,C** Quantification of **(B)** total MK numbers of the whole immunostained femora cryosections as well as **(C)** the number of intrasinusoidal (intrasinus.) MKs (n = 6, 5, 6, 6, one independent experiment). One dot represents one animal. All data are indicated as mean ± SD. One-way ANOVA test with Tukey's correction for multiple comparisons was used. *p≤0.05; **p<0.01; ***p<0.001.

## 4.4 Analysis of MK- and platelet-specific RhoA deficiency using the *Gp1ba-Cre* mouse model

So far, MK- and platelet-specific RhoA deficiency and its implication on MK biology as well as on platelet production and function was only studied using the *Pf4-Cre* transgenic mouse model.[246] However, recent studies addressed the fact that MK lineage-specific expression of the *Pf4-Cre* transgene is not as specific as it was thought to be, leading to an expression in a variety of leukocyte populations, including monocytes, macrophages, granulocytes, and dendritic and B and T cells.[237,305] In the previous section we could already exclude, that the transmigration in RhoA-deficient mice using the *Pf4-Cre* system is due to off-target effects in non-hematopoietic cells. To follow up on this, we used in parallel the novel transgenic MK- and platelet-specific *Gp1ba-Cre* deleter mouse line to achieve a potentially more specific ablation of proteins in the MK lineage as described in the literature.[238]

The data and conclusions of the following project have been largely generated during the master thesis of Lou Martha Wackerbarth at our department (June 2019 – February 2020). I have supervised her throughout her thesis, generated the mice, designed the experiments and supported her to analyze and interpret the data represented in this work.

### 4.4.1 *RhoA*$^{Gp1ba\text{-}Cre}$ mice exhibit only partially reduced RhoA expression

Conditional MK- and platelet-specific RhoA-deficient mice, *RhoA*$^{fl/fl}$*; Gp1ba-Cre*$^{KI/+}$ (*RhoA*$^{Gp1ba\text{-}Cre}$) were viable and born in the expected Mendelian ratios. Due to intrinsic alterations observed in *Gp1ba-Cre*$^{KI/+}$ mice[238], *RhoA*$^{+/+}$*; Gp1ba-Cre*$^{KI/+}$ (*WT*$^{Gp1ba\text{-}Cre}$) control mice were used in addition to normal *WT* controls. Immunoblot analysis of platelet lysates demonstrated a pronounced downregulation of RhoA expression (~ 80%) in platelets of *RhoA*$^{Gp1ba\text{-}Cre}$ mice compared to both control groups (Figure 53A,C). In comparison, using the *Pf4-Cre* system, RhoA expression was virtually absent in *RhoA*$^{fl/fl}$*; PF4-Cre*$^{tg/+}$ (*RhoA*$^{Pf4\text{-}Cre}$) platelet lysates (Figure 53B,D).

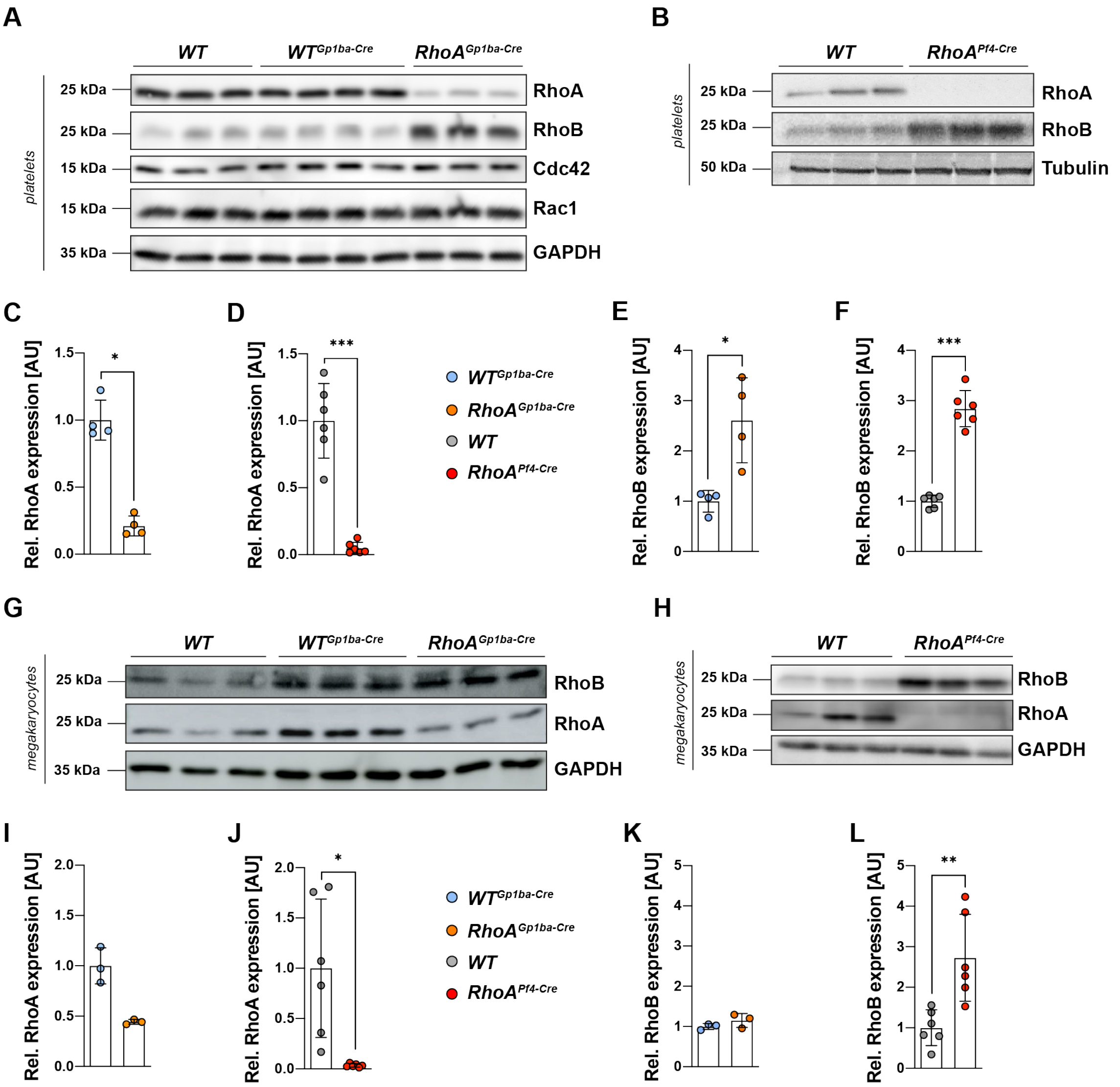

**Figure 53: *RhoA*$^{Gp1ba\text{-}Cre}$ mice exhibit reduced RhoA but increased RhoB expression. A,B** Washed platelets from **(A)** *WT*, *WT*$^{Gp1ba\text{-}Cre}$ and *RhoA*$^{Gp1ba\text{-}Cre}$ (n = 3, 4, 3) and **(B)** from *WT* and *RhoA*$^{Pf4\text{-}Cre}$ mice (n = 3 mice per genotype) were immunoblotted. **C-F** Expression of **(C,D)** RhoA and **(E,F)** RhoB in both mouse lines was compared by densitometric analysis. Data was normalized to GAPDH or tubulin and subsequently to the respective control group *WT* or *WT*$^{Gp1ba\text{-}Cre}$. **G,H** Enriched *in vitro* cultured BM MKs of **(G)** *WT*, *WT*$^{Gp1ba\text{-}Cre}$ and *RhoA*$^{Gp1ba\text{-}Cre}$ (n = 3 mice per genotype) as well as from **(H)** *WT* and *RhoA*$^{Pf4\text{-}Cre}$ (n = 6 mice per genotype) mice were immunoblotted. **I-L** Expression of **(I,J)** RhoA and **(K,L)** RhoB in MKs of both mouse lines was compared by densitometric analysis. Data was normalized to GAPDH and subsequently to the respective control group *WT* or *WT*$^{Gp1ba\text{-}Cre}$. Quantification was done using Fiji software. One dot represents one animal. All data are indicated as mean ± SD. Unpaired Student's t-test, *P≤0.05, **P<0.01; ***P<0.001. AU = *arbitrary unit*.

Immunoblotting of *in vitro* cultured *RhoA*$^{Gp1ba\text{-}Cre}$ BM MKs revealed a reduction on RhoA levels by only 60%, compared to obsolete expression using the *Pf4-Cre* system (Figure 53G-J).

An intense regulatory crosstalk between the major Rho GTPases Rac1, Cdc42, RhoB and RhoA has been described.[235] Furthermore, prior studies in our laboratory using the *Pf4-Cre* system revealed a pronounced upregulation of the GTPase RhoB in MKs and platelets lacking RhoA. We could further demonstrate that double deficiency of RhoA and RhoB was sufficient to revert the transmigration of BM MKs and studies on the role of RhoB in MK biology and transendothelial MK migration in RhoA-deficient mice using the *Pf4-Cre* system are still ongoing (Aurbach *et al.*, unpublished data). While expression of Rac1 and Cdc42 was unaltered in *RhoA*$^{Gp1ba\text{-}Cre}$ platelets, expression of RhoB was markedly increased in both *RhoA*$^{Gp1ba\text{-}Cre}$ and *RhoA*$^{Pf4\text{-}Cre}$ platelets. Quantification revealed approximately three times higher RhoB protein expression in the absence of RhoA, giving comparable results independently of the used mouse model (Figure 53E,F). Similarly, RhoB expression was comparably increased in both *RhoA*$^{Gp1ba\text{-}Cre}$ and *RhoA*$^{Pf4\text{-}Cre}$ MK lysates, albeit less pronounced as observed in the respective platelet lysates (Figure 53K,L). In summary these results revealed an insufficient depletion of RhoA using the *Gp1ba-Cre* system which therefore harbors the problem that reminiscent expression could influence the phenotype of these mice compared to the complete depletion using the *Pf4-Cre* mouse model.

### 4.4.2 *RhoA*$^{Gp1ba\text{-}Cre}$ mice display thrombocytopenia

MK- and platelet-specific RhoA ablation using the *Pf4-Cre* system results in a significant macrothrombocytopenia. To elucidate the effect of the *Gp1ba-Cre* mouse model, basic blood parameters were analyzed (Figure 54). We found platelet counts between both control groups *WT* and *WT*$^{Gp1ba\text{-}Cre}$ to be nearly the same. Moreover, in line with the literature[238], we found an increase in platelet volume in *WT*$^{Gp1ba\text{-}Cre}$ mice (Figure 54A,B). Since deficiency in GPIbα causes macrothrombocytopenia (BSS in humans), the increased platelet size in *Gp1ba-Cre* mice could be explained by reduced GPIbα expression (reduction by 33%) due to the constitutive KI of a T2A-improved-Cre inserted in the endogenous *Gp1ba* gene locus. *RhoA*$^{Gp1ba\text{-}Cre}$ mice exhibited a thrombocytopenia with significantly decreased platelet counts compared to both control groups (~ 70% of *WT*$^{Gp1ba\text{-}Cre}$ control). The increase in platelet size, however, was only significantly increased when compared to *WT* control mice (Figure 54A,B). Analysis of heterozygous *RhoA*$^{fl/+}$*; Gp1ba-Cre*$^{KI/+}$ mice did not reveal any alterations in platelet count. Unexpectedly, compared to *WT*$^{Gp1ba\text{-}Cre}$ control mice, platelet size was significantly decreased to levels of *WT* control mice (Figure 54A,B).

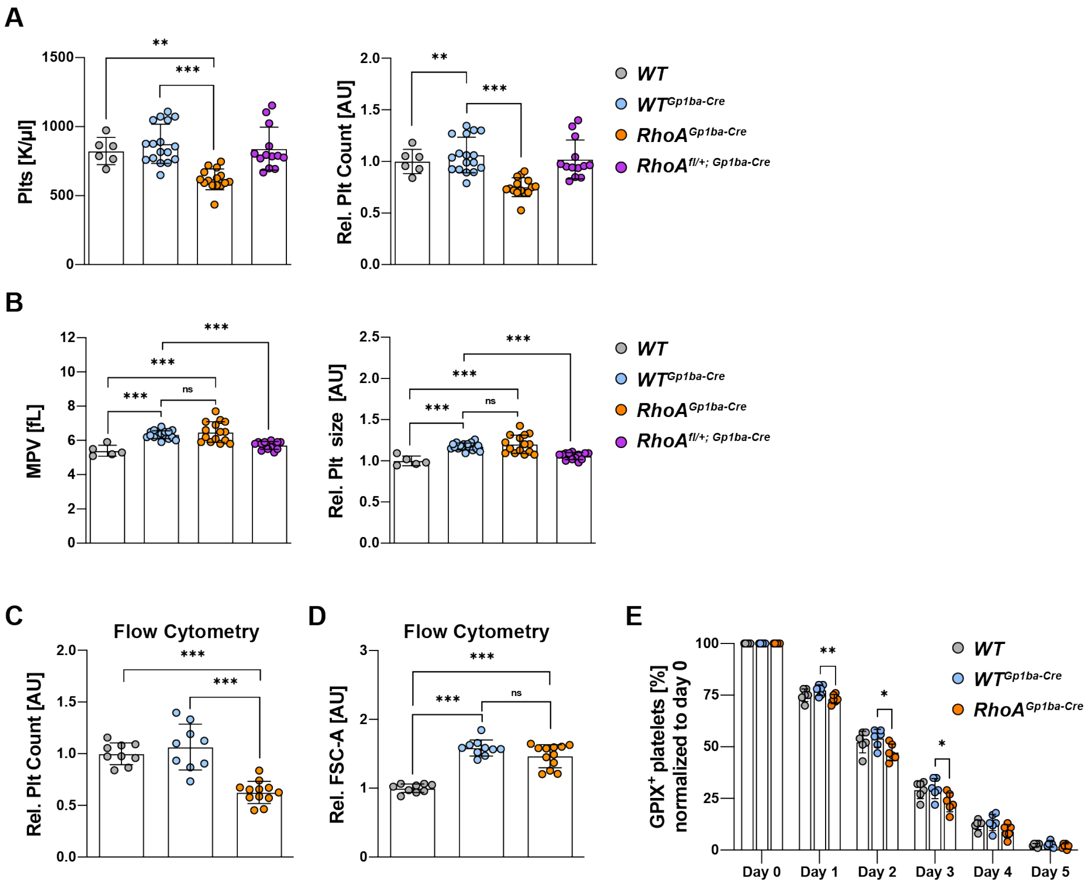

**Figure 54: *RhoA*$^{Gp1ba\text{-}Cre}$ mice exhibit thrombocytopenia. A,B** Determination of **(A)** platelet count and **(B)** size using an automated hematology analyzer (scilVet). Right panels show normalized data to the *WT* control group (n = 6, 17, 15, 13). **C,D** Further, platelets labeled for αIIbβ3 and GPV were analyzed by flow cytometry (FACSCelesta, BD Biosciences) and **(C)** count (30 sec) and **(D)** size (FSC-A) were obtained (n = 9, 10, 12). Data was normalized to the *WT* control group. **E** Platelet lifespan of *WT*, *WT*$^{Gp1ba\text{-}Cre}$ and *RhoA*$^{Gp1ba\text{-}Cre}$ platelets in the circulation was determined by flow cytometry (FACSCelesta, BD Biosciences) by quantifying the percentage of fluorescently labeled GPIX$^+$ platelets at the indicated time points after injection of an AF488-conjugated anti-GPIX-antibody (n = 5 mice per genotype, one independent experiment). One dot represents one animal. All data are indicated as mean ± SD. For **(A, B)** One-way ANOVA test with Bonferroni's or **(C-D)** Tukey's correction for multiple comparisons and **(E)** Two-way ANOVA test with Tukey's correction for multiple comparisons was used. *P≤0.05, **P<0.01; ***P<0.001; AU = *arbitrary unit*; ns = *non-significant*;

The use of a hematology analyzer such as the scilVet allows rapid screening of blood parameters, while a flow cytometric approach has been proposed to be more precise and useful to measure platelet count and size in murine whole blood.[265] However, platelet counts obtained by flow cytometric analysis matched the scilVet data (Figure 54C). Slightly different results were obtained for platelet size using the FSC characteristics (Figure 54D), showing an even more pronounced increase in platelet size of *WT*$^{Gp1ba\text{-}Cre}$ compared to *WT* mice (~ 50%).

Nevertheless, platelet size in *RhoA*$^{Gp1ba\text{-}Cre}$ mice was still indistinguishable compared to *WT*$^{Gp1ba\text{-}Cre}$ mice. The scilVet data indicated that the platelet size of *RhoA*$^{Gp1ba\text{-}Cre}$ mice was more heterogeneously distributed compared to the *WT*$^{Gp1ba\text{-}Cre}$ control. Keeping in mind that the heterozygous *RhoA*$^{fl/+}$*; Gp1ba-Cre*$^{KI/+}$ mice displayed normal platelet size, the flow cytometry analysis also allowed to distinguish between two populations of *RhoA*$^{Gp1ba\text{-}Cre}$ mice, one with slightly smaller platelets, and one with slightly bigger platelets compared to the *WT*$^{Gp1ba\text{-}Cre}$. These results emphasize that the flow cytometry approach indeed allows a more detailed interpretation of platelet size.

Analysis of their ultrastructure by TEM revealed no striking differences between *WT*$^{Gp1ba\text{-}Cre}$ and *RhoA*$^{Gp1ba\text{-}Cre}$ compared to *WT* platelets, except a heterogenous and overall increased size (Figure 55). Interestingly, the *RhoA*$^{Gp1ba\text{-}Cre}$ platelets did not display the roundish appearance observed in *RhoA*$^{Pf4\text{-}Cre}$ mice as described in the literature.

Thrombocytopenia may be caused by enhanced platelet clearance by the reticuloendothelial systems in the liver and spleen. In addition, the role of GPIb in platelet clearance is extensively discussed in the literature.[306] Hence, platelet lifespan was assessed using *WT*$^{Gp1ba\text{-}Cre}$, *RhoA*$^{Gp1ba\text{-}Cre}$ as well as *WT* control mice (Figure 54E). The platelet lifespan for *WT* and *WT*$^{Gp1ba\text{-}Cre}$ mice was comparable (5 days), whereas only a mild but significant reduction throughout day 1-3 was observed for *RhoA*$^{Gp1ba\text{-}Cre}$ mice, thus showing that the low platelet counts most likely is not correlated to the slightly enhanced platelet clearance. Note, for *RhoA*$^{Pf4\text{-}Cre}$ mice the platelet life span was significantly reduced to four days, compared to five days in *WT* (Figure 11).[246]

In summary, the differences in platelet morphology as well as the only slightly reduced lifespan in *RhoA*$^{Gp1ba\text{-}Cre}$ mice, may on the one hand be explained by altered Gp1bα expression in these mice, as well as the likely impact of reminiscent RhoA expression.

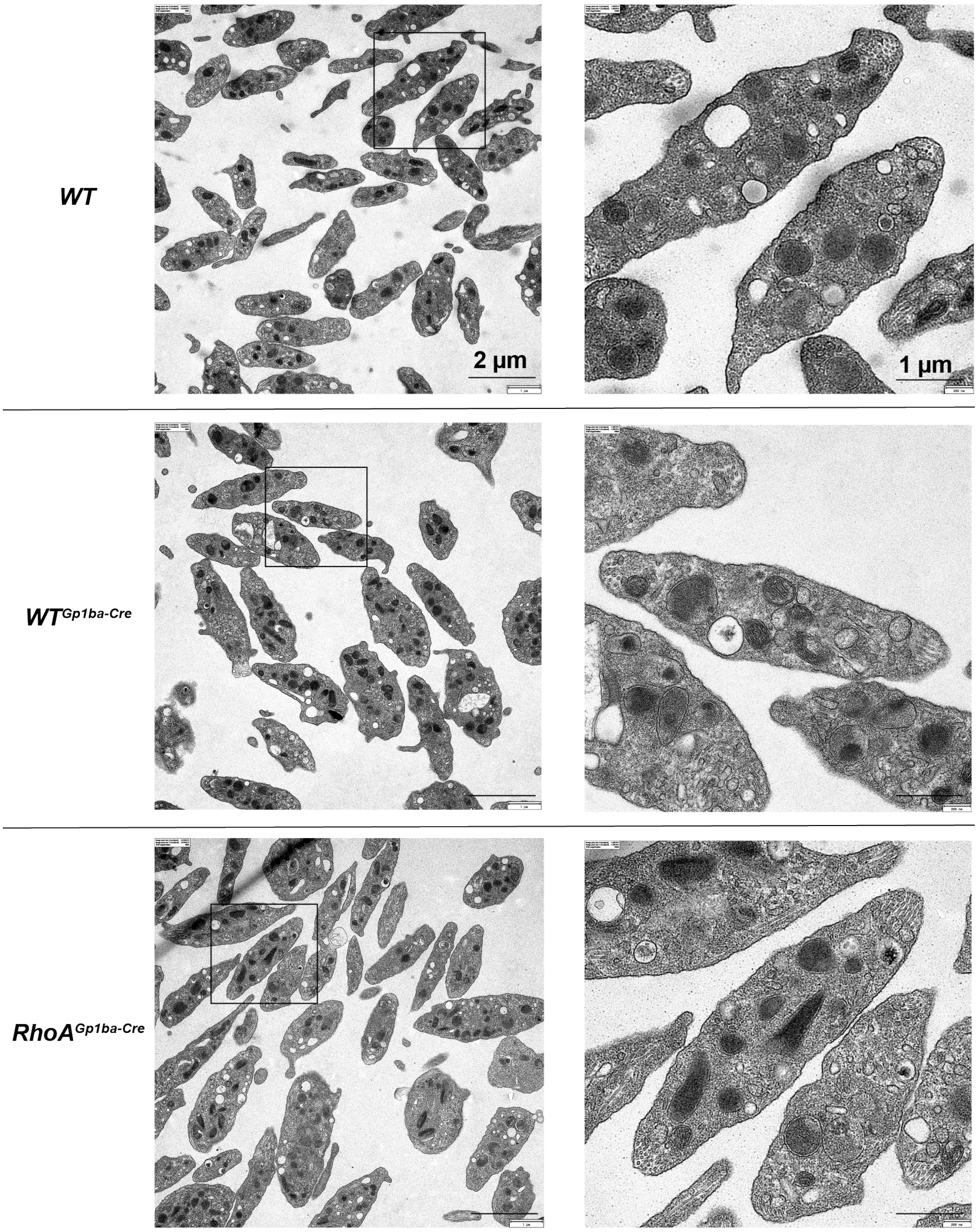

**Figure 55: Analysis of platelet ultrastructure by TEM.** Representative TEM images illustrating the heterogenous and overall increased size in platelets from *WT*$^{Gp1ba\text{-}Cre}$ and *RhoA*$^{Gp1ba\text{-}Cre}$ mice (n = 4).

### 4.4.3 No localization defect of *RhoA*$^{Gp1ba\text{-}Cre}$ BM MKs *in situ*

To investigate MK localization in the BM of *RhoA*$^{Gp1ba\text{-}Cre}$ mice in respect to the transendothelial MK migration observed in *RhoA*$^{Pf4\text{-}Cre}$ mice, native cryosections of whole femora were analyzed by immunohistochemistry. As shown in Figure 56A, MK morphology appeared roundish and MK distribution and number was largely similar in all mice (Figure 56B). However, *RhoA*$^{Gp1ba\text{-}Cre}$

MKs also displayed irregular shapes, comparable to the observations in *RhoA*$^{\mathit{Pf4\text{-}Cre}}$ mice described in the previous sections. The localization of *WT* and *WT*$^{\mathit{Gp1ba\text{-}Cre}}$ MKs in the BM was the same. Strikingly, there was no transendothelial MK migration detectable in *RhoA*$^{\mathit{Gp1ba\text{-}Cre}}$ mice (Figure 56C).

This stands in contrast to our previous findings using *Pf4-Cre* system. Thus, although RhoA$^{\text{Gp1ba-Cre}}$ mice still display a macrothrombocytopenia, comparable to *RhoA*$^{\mathit{PF4\text{-}Cre}}$ mice, the differences in transendothelial MK migration can most likely be explained by the insufficient deletion of RhoA using the *Gp1ba-Cre* mouse model.

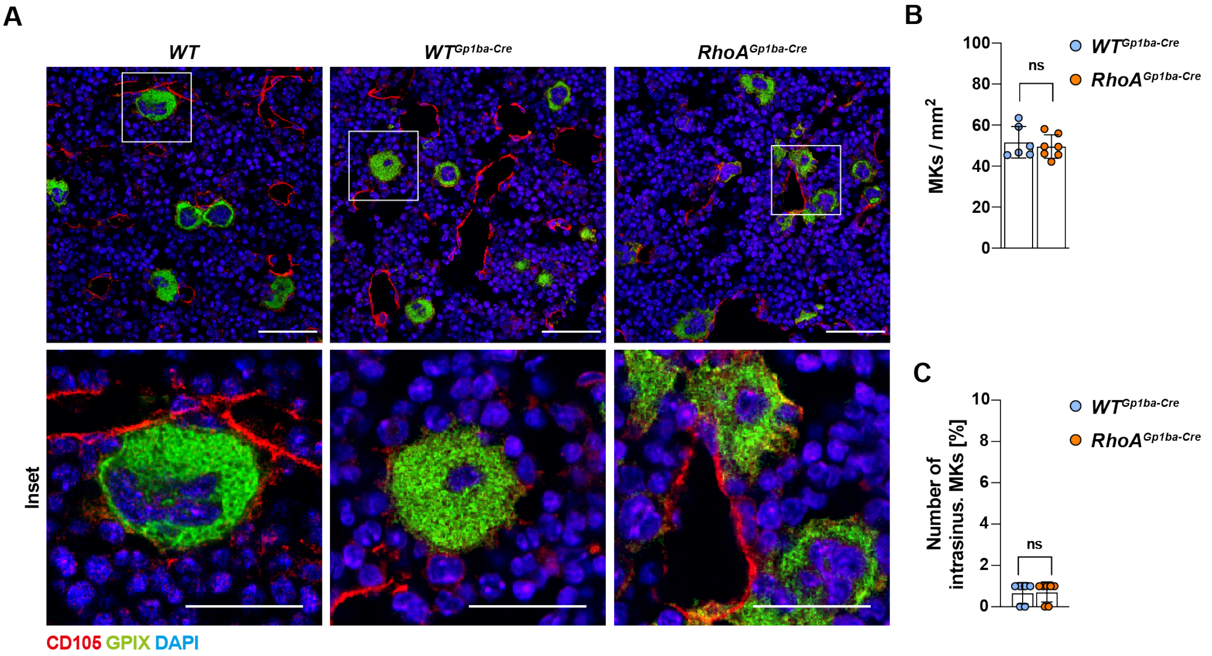

**Figure 56**: **BM MKs from *RhoA*$^{\mathit{Gp1ba\text{-}Cre}}$ mice show no transendothelial migration into BM sinusoids.** **A** Representative confocal microscopy images of femora cryosections (40x oil objective, Leica TCS SP8). MKs are shown by GPIX staining in green. CD105 staining (red) labels vessels. Nuclei were counterstained using DAPI (blue). Scale bars = 50 µm and 25 µm (Inset). **B,C** Quantification of **(B)** total MK numbers as well as **(C)** the number of intrasinusoidal (intrasinus.) of the whole immunostained femora cryosections (n = 6, 7). Quantification was done using Fiji software. One dot represents one animal. All data are indicated as mean ± SD. ns = *non-significant*.

### 4.4.4 Impaired PPF of *WT*$^{\mathit{Gp1ba\text{-}Cre}}$ but not *RhoA*$^{\mathit{Gp1ba\text{-}Cre}}$ MKs

Our results using the *Pf4-Cre* system indicated that defects in platelet biogenesis *in vivo* are the main reason for the thrombocytopenia observed in mice lacking RhoA. Therefore, PPF of *in vitro* cultured BM-derived MKs of *RhoA*$^{\mathit{Gp1ba\text{-}Cre}}$ mice and both control groups were further investigated by time-lapse video microscopy as described before. At 24h, about 15% of the

*WT* MKs formed proplatelets, evident by multiple branched protrusions with characteristic swellings ('beads-on-a-string') and nascent proplatelet-tips containing peripheral tubulin coils.[278] Notably, at 24h, less than 10% of the MKs derived from *WT*$^{Gp1ba\text{-}Cre}$ mice showed signs of PPF. In contrast, PPF of *RhoA*$^{Gp1ba\text{-}Cre}$ MKs was increased compared to *WT*$^{Gp1ba\text{-}Cre}$ mice, whereas there was no difference compared to the *WT* control group (Figure 57A).

In the first 6 h of imaging, PPF capacities of all three analyzed groups were comparable, whereas at the following time points, PPF of *WT*$^{Gp1ba\text{-}Cre}$ MKs was significantly than of *WT* and *RhoA*$^{Gp1ba\text{-}Cre}$ MKs. To verify these observations, further *WT*$^{Gp1ba\text{-}Cre}$ and matching *WT* MKs were analyzed using the 24h time-point. In these experiments, experimental sets were normalized to the respective *WT* control, to minimize the effect between individual experiments. Although an overall heterogenous response of the *WT*$^{Gp1ba\text{-}Cre}$ mice in the *in vitro* PPF assay was observed, a significant reduction of approximately 35% compared to the *WT* was evident (Figure 57B). This reduction was also confirmed by the static PPF assay to rule out technical errors due to the usage of the $CO_2$ independent medium during time-lapse microscopy (Figure 57C).

Furthermore, PPF was visualized using confocal microscopy by staining the proplatelet-forming MKs for F-actin and α-tubulin (Figure 57D). In line with *RhoA*$^{Pf4\text{-}Cre}$ MKs, the appearance of *RhoA*$^{Gp1ba\text{-}Cre}$ proplatelet-forming MKs was not obviously altered compared to the *WT* (Figure 23). However, in line with the time-lapse microscopy experiments, *WT*$^{Gp1ba\text{-}Cre}$ MKs displayed impaired PPF. This was illustrated by the presence of thickened and shortened proplatelet shafts with larger swellings and the absence of the characteristic tubular tree-like structures with shafts of uniform diameters, as well as less pronounced tubulin coils in the proplatelet tips (Figure 57D). In summary, this indicated a so far unknown effect of the *Gp1ba-Cre*$^{KI/+}$ transgene on platelet biogenesis which raise doubts regarding the suitability of the *Gp1ba-Cre* system to investigate MK biology. Of note, *WT*$^{Gp1ba\text{-}Cre}$ mice have normal platelet counts, thus arguing for the relevance of the observed platelet biogenesis defects *in vivo*. Interestingly, even the only partial reduction of RhoA protein levels in *RhoA*$^{Gp1ba\text{-}Cre}$ mice seems to confirm its role as a negative regulator of PPF under certain conditions.

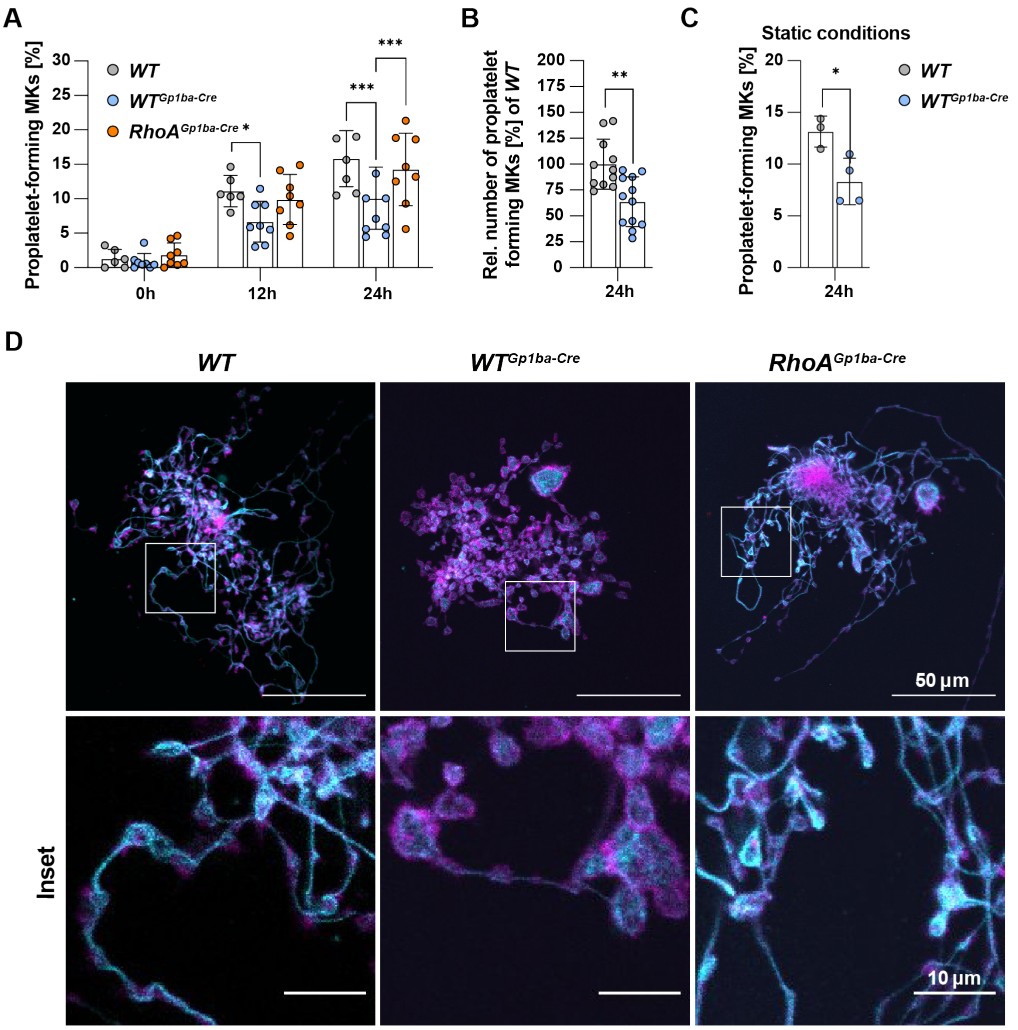

**Figure 57: Impaired PPF of *WT*$^{Gp1ba\text{-}Cre}$ but not *RhoA*$^{Gp1ba\text{-}Cre}$ mice *in vitro*. A** PPF of depicted *in vitro* BM-derived MKs were analyzed using time-lapse video microscopy over 24 h. Note, imaging started approximately 2 h after the enrichment on a BSA gradient. For each mouse, visual fields with at least >100 MKs were counted throughout indicated time points (n = 8 mice per genotype, data of two independent experiments was pooled). **B** For further comparison, different experimental sets using time-lapse video microscopy to analyze the PPF of *WT* and *WT*$^{Gp1ba\text{-}Cre}$ were pooled and normalized to their respective *WT* control (n = 11 vs 12 mice, three independent experiments). **C** PPF of *in vitro* cultured MKs was counted after 24 h under static conditions to exclude technical errors due to the CO$_2$-independent medium used for time-lapse video microscopy (n = 3 vs 4, one independent experiment)**. D** Representative images of proplatelet forming MKs on day 4 of culture. (40x objective, Leica TCS SP8). Visualization of proplatelets by F-actin staining using phalloidin Atto647N (magenta), MT are shown by α-tubulin staining in cyan. Nuclei were counterstained using DAPI (grey). Quantification of PPF was done using Fiji software. One dot represents one animal. All data are indicated as mean ± SD. For **(A)** Two-way ANOVA test with Tukey's correction for multiple comparisons and **(B, C)** an unpaired Student’s t-test was used. *P≤0.05, **P<0.01; ***P<0.001.

### 4.4.5 Altered ultrastructure of *$WT^{Gp1ba\text{-}Cre}$* and *$RhoA^{Gp1ba\text{-}Cre}$* MKs *in situ*

Functional GPIb is key for DMS formation and subsequently for MK maturation and PPF.[39] We were thus wondering, whether the approximately 33% reduction in GPIbα expression in *$WT^{Gp1ba\text{-}Cre}$* mice may also perturb MK maturation. Therefore, BM MK ultrastructure was analyzed by TEM *in situ* (Figure 58).

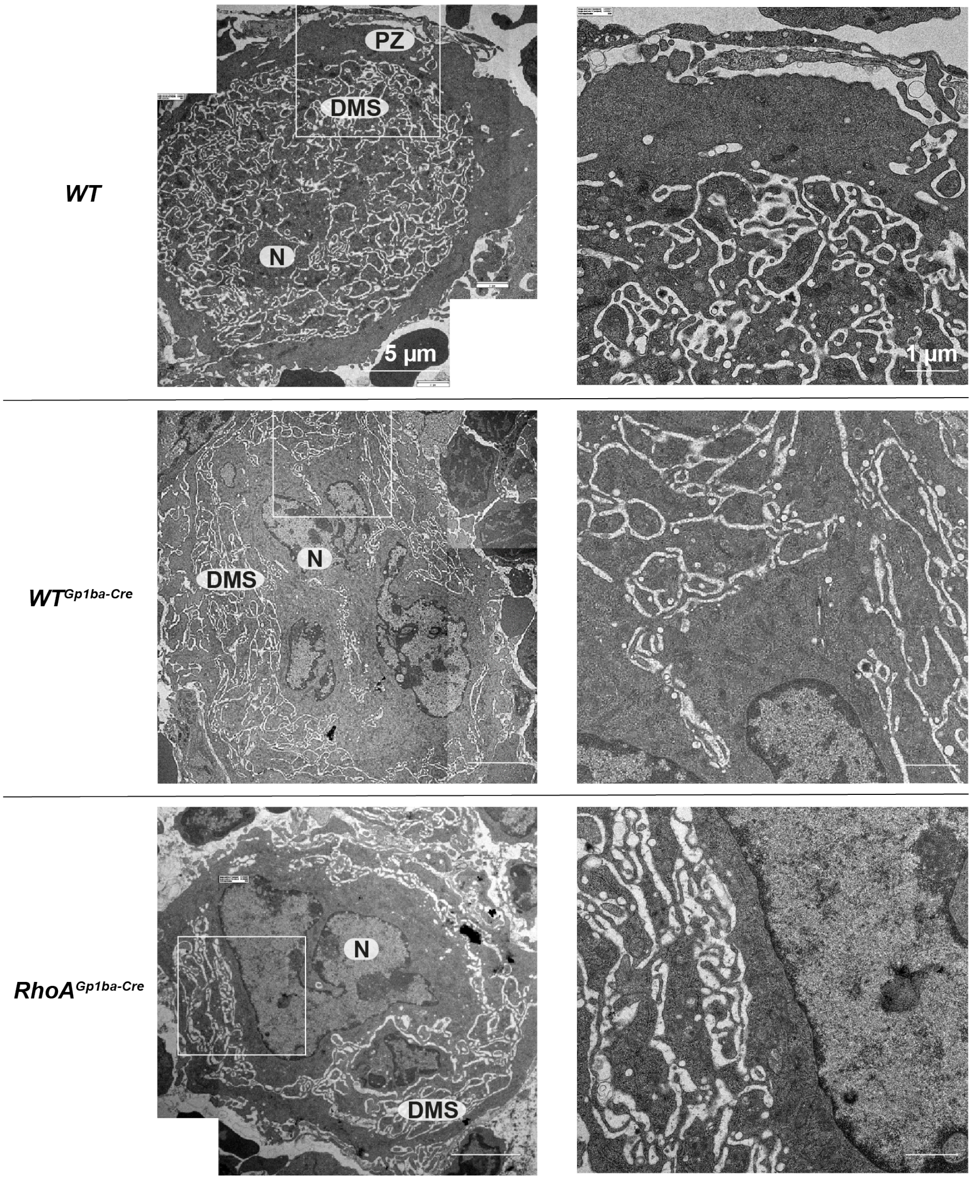

**Figure 58: Ultrastructural analysis of BM MKs *in situ*.** TEM analysis of BM MKs (femur) revealed impaired DMS formation in *$WT^{Gp1ba\text{-}Cre}$* mice and additional morphological alterations in *$RhoA^{Gp1ba\text{-}Cre}$* mice (n = 4). N = *nucleus*; DMS = *demarcation membrane system*; PZ = *peripheral zone*. Pictures were acquired by Dr. Irina Pleines-Meinhold (Experimental Biomedicine).

As described in section 4.2.2, *WT* MKs displayed a well-defined DMS and a PZ largely devoid of granules[7,35], clearly separating the MKs from surrounding cells. In contrast, *WT*$^{Gp1ba\text{-}Cre}$ were still able to develop the DMS but had decreased and less structured DMS invaginations. In addition, the PZ was not clearly detectable. The same was also true for *RhoA*$^{Gp1ba\text{-}Cre}$ MKs. In addition, the overall morphology of *RhoA*$^{Gp1ba\text{-}Cre}$ MKs was irregular, not clearly separating the MKs from surrounding cells. Interestingly, we also found some intrasinusoidal MKs and larger MK fragments devoid of the nucleus in *RhoA*$^{Gp1ba\text{-}Cre}$ mice by TEM.

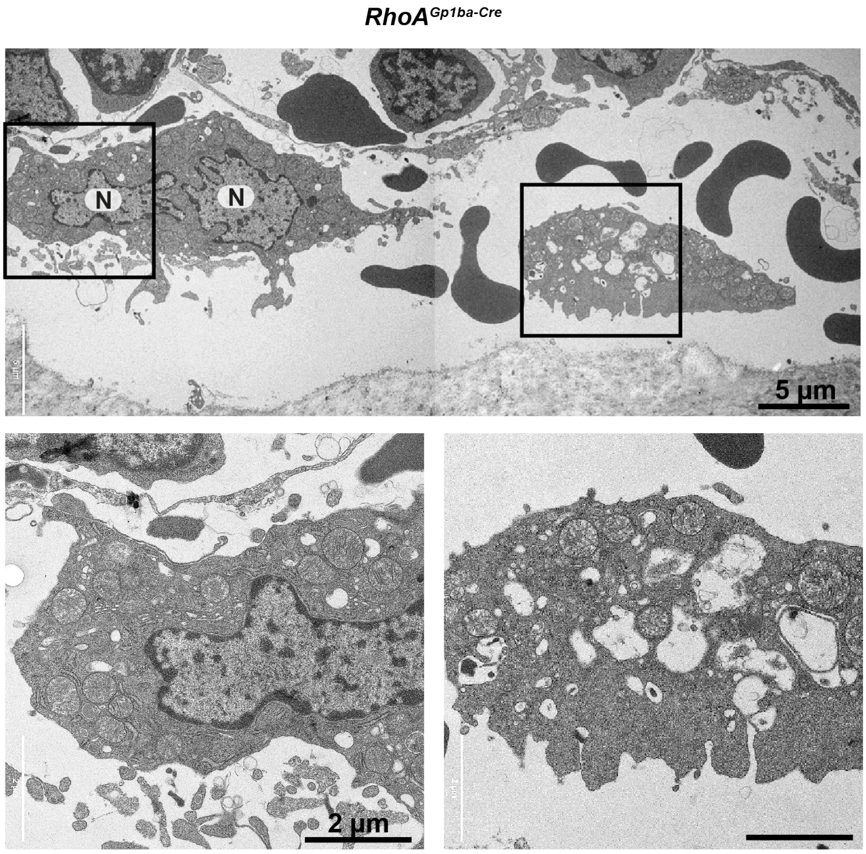

***RhoA*$^{Gp1ba\text{-}Cre}$**

**Figure 59: Intrasinusoidal MK fragments in *RhoA*$^{Gp1ba\text{-}Cre}$ mice revealed by TEM.** TEM analysis of BM MKs (femur) surprisingly revealed large MK fragments and fragments devoid of the nucleus in the sinusoids of *RhoA*$^{Gp1ba\text{-}Cre}$ mice (n = 4). N = *nucleus*. Pictures were acquired by Dr. Irina Pleines-Meinhold (Experimental Biomedicine).

Interestingly, the impaired MK morphology in the BM compartment of *Rho*$^{Gp1ba\text{-}Cre}$ mice was comparable to IF images of *RhoA*$^{Pf4\text{-}Cre}$ femora in the previous sections (4.3.1.2, 4.3.2.2, 4.3.3.3). In both cases, the mice displayed lower numbers of intrasinusoidal MKs as compared to *RhoA*$^{-/-}$ mice with rather roundish morphology comparable to the *WT* and higher number of intrasinusoidal MKs (Figure 11). Nevertheless, the finding of intrasinusoidal MKs by TEM stands in contrast to our observations using IF on native cryosections (Figure 59). The *Gp1ba-Cre* seems to impair DMS formation as well as overall cellular integrity of *WT*$^{Gp1ba\text{-}Cre}$ MKs, which was even more pronounced in *RhoA*$^{Gp1ba\text{-}Cre}$ MKs. Moreover, the intrasinusoidal MKs were marked by a disrupted and irregular morphology, which may explain why they were omitted in the analysis of IF femur cryosections.

In summary, these findings strengthened the importance of GPIb during DMS formation and at the same time questioned the suitability of the *Gp1ba-Cre* to investigate platelet biogenesis.

# 5 DISCUSSION

## 5.1 Isolation of murine BM by centrifugation or flushing for the analysis of hematopoietic cells – a comparative study

Investigation of the BM as the main compartment for hematopoiesis is critical in many research fields, including hematology, stem cell biology, cancer metastasis, and transplantation studies. Mice are commonly used to investigate the function of hematopoietic cells originating from the BM compartment.[272,273] Due to the focus of our work in the department, we are required to use transgenic mouse models to investigate the biology of MKs and their progeny, the platelets, in health and disease.[196,251,293,307,308] One general limitation when studying BM-derived hematopoietic cells in mice is that only a limited number of cells can be recovered from a single animal. The isolation of BM cells from murine long bones is traditionally achieved by the flush isolation, which however is rather time consuming and prone to variability regarding cell yield and quality.[83] Alternatively, a more rapid BM isolation method using centrifugation of hind leg mouse bones has been described.[268,274] In this study, we developed a modified, more gentle version of the centrifugation-based method (spin isolation) described by Amend *et al.*[268], suitable for downstream transcriptional, biochemical or functional studies of the BM cells, and compared it to the traditional flush isolation. We not only analyzed primary BM HSC and immune cell populations (Carina Gross, Thesis, 2020)[275], but also primary MKs in regard to their ploidy distribution, which are highly fragile and therefore prone to fragmentation during the isolation procedure. Furthermore, we assessed the suitability of the recovered cells for *in vitro* culture by studying thrombopoietin/hirudin-induced maturation of MKs and their subsequent fragmentation into proplatelets.[281] With the comparative study, we show overall comparable results between both methods. Strikingly, our spin isolation is three times faster than the flush isolation while at the same time increasing the cell yield by approximately 30%. In the course of this thesis we have also exploited the new spin isolation and have not only used them for culturing MKs, but also to perform ELISA assays with the recovered BM supernatant after centrifugation (Figure 45) or to minimize the number of donor mice needed for BM transplantation (Figure 52). We therefore conclude that the spin isolation method reduces experimental time, costs and animals and is highly suitable for studies on primary and *in vitro* cultured BM-derived cells for multiple experiments, particularly those requiring high cell numbers.[275]

## 5.2 RhoA/Cdc42 signaling drives cytoplasmic maturation but not endomitosis in MKs

We have recently shown that Cdc42 and RhoA orchestrate a regulatory circuit that controls MK localization and transendothelial platelet biogenesis *in vivo.*[251] Here, we uncover that, in addition to these separate rather opposing functions, synergistic RhoA/Cdc42 signaling is a prerequisite for cytoplasmic MK maturation, but not endomitosis. Combined deficiency of RhoA/Cdc42 in MKs resulted in reduced mRNA and protein levels of MK-specific GPs, as well as cytoskeletal regulators of known importance in MK maturation and PPF, thereby virtually abolishing functional platelet biogenesis *in vitro* and to a large extend *in vivo*, as described before.[251]

We show that multiple genes (and proteins) that are normally upregulated in the course of MK maturation, such as MK- and platelet-specific membrane GPs, MLC2 (Myl9), β1-tubulin (Tubb1), Tuba4a, Actn1, and Tpm4 were markedly reduced in *DKO* MKs. Loss of function mutations in *TUBB1*[151], *TUBA4A*[157], *TPM4*[293], or *ACTN1*[217] are directly associated with platelet disorders in humans. Strikingly, our findings indicate that RhoA/Cdc42 signaling directly modulates gene transcription and/or mRNA stability in the course of MK maturation. The TPO/MPL signaling pathway is an obvious candidate in this context as it regulates gene transcription throughout megakaryopoiesis.[309] However, although mRNA levels of Mpl, the gene encoding MPL, were slightly reduced, our results indicate that TPO-induced JAK/STAT signaling is largely functional in the absence of RhoA/Cdc42. Notably, an absence of MYL9 and the reduction of TUBB1 in MKs are characteristic of patients with macrothrombocytopenia due to mutations in the *RUNX1* gene.[130] However, RUNX1 protein levels were unaltered in RhoA/Cdc42-deficient MKs. The same was true for the transcription factor GATA1, specific mutations in which have been reported to cause isolated thrombocytopenia associated with immature platelets.[310] This emphasizes that reduced Tubb1 or Myl9 expression may be a general characteristic of immature MKs. However, further investigations of GATA1 and RUNX1 signaling might be required, since only the steady-state protein levels have been addressed. Besides, further functional investigations of other TFs such as NFE2 or FLI1 are required. Transcriptional targets of NFE2 for example include TUBB1 and also the loss of FLI1 is associated with Paris-Trousseau syndrome, an inherited thrombocytopenia. FLI1 is also of further interest due to its regulation of MK-related genes such *as GPIBA, GP9, ITGA2B and MPL,* although all of them seemed to be only mildly affected on mRNA levels in *DKO* mice.[122,142-144]

In contrast, we provide direct evidence that the MRTF (MKL)/SRF pathway is impaired in the absence of RhoA/Cdc42. MKL-mediated activation of the transcription factor SRF predominantly modulates the expression of cytoskeletal genes and has mainly been studied in the context of cell motility, which is dependent on rapid cytoskeletal remodeling.[132,133] MKL shuttling to the nucleus requires its dissociation from monomeric G-actin and Rho GTPases, particularly RhoA, have been shown to regulate MKL1-dependent SRF activation via their ability to modulate actin polymerization.[133,134] The importance of the MKL/SRF pathway in megakaryopoiesis and platelet production was revealed by knockdown studies in human MKs[139], as well as in conditional KO mice lacking Srf and Mkl1/2 in MKs. Strikingly, a number of findings from these reports were recapitulated in our analysis of RhoA/Cdc42 *DKO* mice. First, ablation of Srf or Mkl1/2 likewise resulted in thrombocytopenia, immature MKs, decreased PPF, and aberrant actin stress fiber formation in the case of Srf deficiency.[136-140] Moreover, as observed in Srf/Mkl KO MKs, mRNA levels of *Tubb1*, *Myl9*, *Tpm4*, *Tuba4a* as well as *Mpl* and *Srf* itself, were downregulated in RhoA/Cdc42 *DKO* MKs. Strikingly, stimulation of serum-starved *DKO* MKs with TPO resulted in decreased shuttling of MKL1 into the nucleus, thus pointing to defects of the MKL/SRF signaling pathway in the absence of RhoA/Cdc42. It has to be noted that some genes associated with MKL/SRF signaling (*FlnA*, *Mmp9*, *Myh9*) were not affected in *DKO* MKs. This may on the one hand be explained by the fact that, in contrast to the Srf/Mkl KO studies, protein levels of MKL1/2 were not altered in cultured *DKO* MKs. Furthermore, an alternative, mitogen-activated protein kinase (MAPK)-dependent pathway of SRF activation exists, which may still be at least in part functional in the absence of RhoA/Cdc42.[133-135]

The association of MKL to G-actin in the cytoplasm prevents its shuttling into the nucleus and binding to SRF, while assembly of G-actin into filaments (F-actin), or competition with other actin-binding proteins releases this inhibitory effect. The LIMK/Cof1 pathway - an effector pathway of both RhoA and Cdc42 - is a major regulator of F-actin assembly and turnover. Cof1 is one of the most abundant proteins in human and mouse platelets[311,312] and its deficiency in MKs results in macrothrombocytopenia and aberrant F-actin accumulations in MKs.[191,196] Our results reveal markedly deregulated LIMK/Cof1 signaling in the absence of RhoA/Cdc42 and point to the accumulation of inactive Cof1 as a major reason for aberrantly increased actin stress fiber formation in *DKO* MKs observed after MK spreading on different ECM matrices. Note that the spreading defects were a combination of the respective single-deficient MKs. Moreover, a combination of functional defects observed in the respective single-deficient platelets, was also observed in RhoA/Cdc42 *DKO* platelets. As a result, integrin activation was pronouncedly reduced while granule secretion was largely preserved. This phenotype may explain the contrasting findings of defective *in vivo* hemostasis but largely preserved experimentally induced thrombus formation in the absence of RhoA and Cdc42 as described before (Deya Cherpokova, Thesis, 2015).[279]

Of note, our observation of impaired rather than enhanced MKL/SRF signaling in *DKO* MKs may seem somewhat perplexing in the light of this finding. On the other hand, active Cof1 has been linked to the nuclear import of MKL1 *in vitro*[313], suggesting that this process may be impaired in the absence of RhoA/Cdc42. In addition, Cof1 was reported to be involved in the import of actin into the nucleus to support actin-dependent gene transcription and *in vitro* studies indicate that non-phosphorylated, active Cof1 accumulates in the nucleus.[314] Thus, the strongly increased levels of inactive Cof1 in *DKO* MKs may directly or indirectly contribute to the transcriptional changes upon loss of RhoA/Cdc42.

RhoA/Cdc42 deficiency in BM(-derived) MKs nearly abrogated PPF *in vitro* and *in vivo*. The fundamental requirement for MT for proplatelet elongation/PPF and platelet release[221,222] suggests that the marked imbalance of tubulin isoforms, most notably the reduction in β1-tubulin and α4a-Tubulin, contributed to the PPF defect in the absence of RhoA/Cdc42. Besides the established roles of these tubulin isoforms for platelet production in humans, downregulation of Tuba4a has been associated with the upregulation of tyrosinated and downregulation of detyrosinated MTs[157], which was likewise evident in *DKO* MKs. Of note, deficiency of Cdc42 alone resulted in a significant decrease in PPF compared to the *WT*, in line with observations from fetal liver cell-derived and human MKs.[39,240] However, Cdc42 single-deficiency only very moderately affected the ultrastructure of native BM MKs or the produced platelets. Thus, while our results are in line with other reports indicating that Cdc42 is a positive regulator of DMS formation and PPF in mice and humans[232,242], its function in the transcriptional regulation during MK maturation can be largely taken over by RhoA. Single deficiency of RhoA, on the other hand, neither affected cytoplasmic MK maturation nor PPF, but instead rather increased PPF, in line with other studies.[243,244] Thus, our results emphasize that the defective cytoplasmic maturation of *DKO* MKs accounted for the completely abrogated PPF *in vitro* and *in vivo*. Interestingly, *DKO* MKs not only showed aberrantly increased actin stress fiber formation, but also largely impaired podosome formation. Given the importance of podosome formation for initial MK protrusion formation[224], our results thus propose an additional explanation for the impaired PPF in these double-deficient mice *in vivo*. Moreover, previous studies carried out in our department have also shown, that PPF *in vitro* of double-deficient FLC-derived MKs was unaffected (Deya Cherpokova, Thesis, 2015).[279] The differences between the DKO FLC-derived and BM-derived MKs has yet not been addressed and requires further investigations. While HSCs stem cells successively populate the embryonic yolk sac at around day 7.5 in mice and around the third week in humans, this process is followed by a subsequent population of the fetal liver and spleen as well as later on the fetal BM. After birth, there is a switch from thrombopoiesis in the FL to the BM of the mice, which also comes along with different characteristics of the HSCs and subsequent MKs and platelets.[315,316] Therefore, it would be of interest, to check whether neonatal mice are already suffering from a macrothrombocytopenia in the first days of life, or whether the defects are specific and limited to the adult BM MKs.

In contrast to the defective cytoplasmic MK maturation, endomitosis, another major hallmark of MK maturation, was not affected in RhoA/Cdc42 *DKO* MKs, confirming that these two processes can be affected independently.[141] Since Pf4-Cre-mediated deletion resulted in a virtually complete absence of RhoA and Cdc42 protein in cultured MKs, as well as in circulating platelets of *DKO* mice, our data strongly suggest that RhoA and Cdc42 are fully dispensable for DNA endoreplication in MKs. Given the general importance of particularly RhoA during cell division[248], this finding was not readily expected. On the other hand, it is established from *in vitro* studies that downregulation of the RhoA/Rock pathway is required during the process MK endomitosis[27,249,286] and MKs from mice conditionally lacking RhoA or Cdc42 likewise do not show impaired MK polyploidization. Our findings thus point to MK endomitosis and cytoplasmic maturation as two independent, mechanistically uncoupled processes and that the latter is essentially driven by RhoA/Cdc42 signaling. The novel findings of this study are summarized in Figure 60.

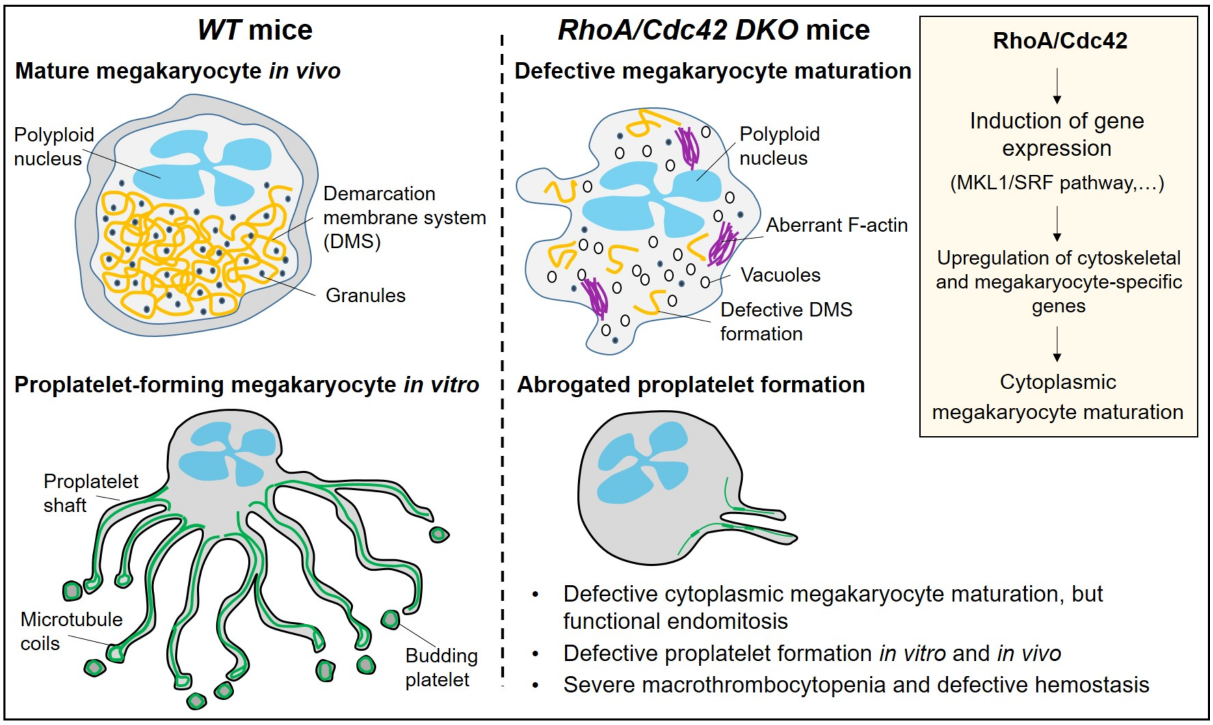

- Defective cytoplasmic megakaryocyte maturation, but functional endomitosis
- Defective proplatelet formation *in vitro* and *in vivo*
- Severe macrothrombocytopenia and defective hemostasis

**Figure 60: RhoA/Ccd42 signaling drives cytoplasmic maturation but not endomitosis in MKs.** Heib *et al.*, **submitted.**

## 5.3 Investigation of candidate receptors involved in the process of transendothelial MK migration in RhoA-deficient mice

In the first part of this study we identified molecular pathways explaining the severe macrothrombocytopenia upon loss of functional RhoA/Cdc42 signaling. Possible receptors involved in the transendothelial migration of whole MKs into the BM sinusoids upon RhoA-deficiency, however, remained unidentified so far. Besides the mechanoreceptor GPIbα,[251] several other regulators of transendothelial PPF have been proposed, such as soluble factors or the interaction of MKs with the ECM. Previous studies have indicated a role of collagen type I and IV in regulating thrombopoiesis via integrin β1 and GPVI.[106] Moreover, the role of the ITIM-containing receptor G6b-B and its interaction with the highly abundant sinusoidal HS perlecan in the regulation of transendothelial PPF is yet not carified.[118] Strikingly, concomitant loss of β1 integrins (*RhoA/Itgb1*$^{-/-}$*)*, integrin function (*RhoA/Talin-1*$^{-/-}$*)* or G6b-B (*RhoA/G6b*$^{-/-}$) did not interfere with the aberrant transendothelial MK migration, but at the same time revealed exciting results in regard to MK biology, especially for the process of PPF or during disease conditions, as demonstrated with the *RhoA/Itgb1*$^{-/-}$ and *RhoA/G6b*$^{-/-}$ mice, respectively.

As mentioned above, recent studies indicated that integrin α2β1 is involved in regulating PPF from MKs at the vascular niche and acts in concert with GPVI. However, its exact role in the regulation of PPF *in vitro* remains elusive. Mice lacking integrin α2 and/or GPVI as well as mice with *Mx1-Cre*-mediated β1 integrin deficiency showed no alterations in circulating platelet counts.[85,298] This is in line with the here presented mice lacking β1 integrins by using the *Pf4-Cre* system (Figure 39), thus questioning the requirement of β1 integrins in PPF. However, aberrant activation of β1 integrin was shown to impair thrombopoiesis and HSC homeostasis.[297] While α2 forms heterodimers exclusively with β1, MKs and platelets also express the α5β1 and α6β1 heterodimers, which bind to fibronectin and laminin, respectively. β1 integrins have further been associated with the transendothelial migration of immune cells, such as leucocytes[98], as well as cancer cells.[99]

BM MKs of *RhoA*$^{-/-}$ controls bred out of the *RhoA/Itgb1*$^{-/-}$ mouse line, displayed an irregular MK morphology as well as markedly low numbers of intrasinusoidal MKs. These observations are in contrast to the *RhoA*$^{-/-}$ controls analyzed e.g. for the RhoA/Cdc42 *DKO* project or in the study of Dütting *et al*. from our department.[251] Here, MKs were rather indistinguishable from *WT* MKs and also their intrasinusoidal appearance was roundish and intact. Varying numbers of intrasinusoidal MKs, but a persistent irregular MK morphology accompanied by rather roundish intrasinusoidal MKs (~ 2-10%) has also been observed upon analysis of *RhoA/Talin-1*$^{-/-}$ and *RhoA/G6b*$^{-/-}$ mice. This contrasts with the studies of Dütting *et al.*[251], showing approximately 30% of intrasinusoidal BM MKs in *RhoA*$^{-/-}$ mice. Of note, *RhoA*$^{-/-}$ mice used in earlier studies had a more SV129-BL/6J-driven mixed background, while they slowly shifted towards a C57BL/6J background, thus highlighting the impact of the genetic backgrounds on the phenotype of these mice. This was, however, unavoidable for breeding out *RhoA*$^{-/-}$ controls during the *DKO* generation, since most of the single-deficient mice were kept on a C57BL/6J background (*Talin-1*$^{-/-}$ and *G6b-B*$^{-/-}$) or not well defined SV129-BL/6J background (*Itgb1*$^{-/-}$).

In regard to MK morphology, however, concomitant loss of integrin β1 using the *Pf4-Cre* system revealed an additional deterioration of the macrothrombocytopenia described in RhoA single-deficient mice (Figure 39).[246] Due to the normal platelet counts in *Itgb1*$^{-/-}$ mice, our data indicate additional alterations upon the concomitant loss of β1 in the process of PPF. Interestingly, double-deficient mice displayed largely unaltered PPF *in vitro* compared to *WT* and *RhoA*$^{-/-}$ mice (Figure 41), with a minor increase in the proportion of proplatelet-forming MKs after 24 h. This demonstrates that the double-deficient MKs are principally still able to form proplatelet protrusions *in vitro*, while the *in vivo* situation might differ and remains to be addressed by 2P-IVM and TEM.

Recent work from Lou M. Wackerbarth during her master thesis at our department also showed the surprising ability of *RhoA/Itgb1*$^{-/-}$ MKs to spread on Horm collagen, which consists to 95% of collagen type I and 5% collagen type III.[317] Furthermore, it is proposed that integrin engagement and clustering through matrix molecules might affect podosome formation, especially integrin β1 in the core region of podosomes.[318] Again, double-deficient MKs were unexpectedly able to form podosomes comparable to the *WT.*

Interestingly, MKs from Itga2-deficient mice were previously shown not to adhere to collagen type I (Harald Schulze, unpublished data) and a first pilot run by us also showed impaired binding of *RhoA/Itgb1*$^{-/-}$ MKs to purified collagen type I, but not Horm collagen or fibrinogen, thus confirming the importance of β1 integrins for the binding to collagen type I. Thus, the results upon spreading on Horm collagen show a potential involvement of collagen type III in MKs. Binding to collagen III is likely mediated by the *G protein-coupled receptor 56* (GPR56), potentially upstream of RhoA.[319] Aberrant upregulation of GPR56 expression has been associated with AML.[320] Together, these results raise questions regarding the suitability of Horm collagen for spreading and adhesion assays compared to pure collagen subtypes and results obtained with Horm collagen need to be treated with caution. We further suggest the use of a blocking antibody for integrin β1, namely mAb 9EG7[321], which would allow to mimic the double-deficiency of RhoA and β1 upon Horm collagen-mediated spreading/adhesion and at the same time dissect whether the functional blockage of β1 integrin recapitulates a loss of the protein in MKs and platelets. Furthermore, *RhoA/Itgb1*$^{-/-}$ MKs displayed an increased proportion PPF on fibrinogen, thus supporting the finding of a slightly hyperactive state of the double-deficient MKs observed during live acquisition of PPF (Lou M. Wackerbarth, Master Thesis, 2020). Whether there is a functional upregulation of other receptors upon concomitant loss of β1 integrin in RhoA-deficient mice needs to be addressed.

In summary, mice lacking the small GTPase RhoA as well as integrin β1 displayed a severe macrothrombocytopenia, while MK as well as platelet functions seemed to be largely unaffected (as shown by Lou M. Wackerbarth, Master Thesis, 2020). More interestingly, concomitant lack of β1 was not able to revert the transmigration of RhoA-deficient MKs into BM sinusoids. This led us to the hypothesis, to further investigate the involvement of integrins per se and analyze mice double-deficient in RhoA and Talin-1 (*RhoA/Talin-1*$^{-/-}$), the cytoplasmatic protein required for integrin activation and integrin inside-out signaling.

As mentioned above, matching *RhoA*$^{-/-}$ controls exhibited irregular BM MK morphology, while the additional loss of Talin-1 did rescue the morphological appearance to the same extend observed as in *RhoA/Itgb1*$^{-/-}$ mice. Our results thus suggest that aberrant integrin signaling in *RhoA*$^{-/-}$ MKs might be the reason for the altered morphology of the cells. On the other hand, our results exclude a role of integrin inside-out signaling in MK transendothelial migration upon RhoA-deficiency and propose an integrin-independent process. In contrast to *RhoA/Itgb1*$^{-/-}$ mice, *RhoA/Talin-1*$^{-/-}$ mice exhibited a platelet count and size comparable to RhoA-single deficient mice, which however was more more pronouncedly affected upon the concomitant loss of β1 integrins, thus leaving open questions comparing both the MK and blood parameter phenotypes of the double-deficient mice.

In line with potential aberrant integrin function, abnormal spreading behavior of RhoA-deficient MKs has been observed on both Horm collagen and fibrinogen, displayed by abnormal long protrusions (Figure 25 + Figure 27). While the involvement of other potential collagen receptors such as GPR56 has been discussed above, the role of the prominent MK- and platelet-specific receptor αIIbβ3 has not been further addressed. Comparable to α2β1 and GPVI, deficiency in the prominent MK-specific receptor αIIbβ3 (also known as Glanzmann thrombasthenia), does not affect circulating platelet counts in humans[294] or mice[85,295], while aberrant β1-signaling[107] or gain-of-function mutations in the genes encoding for αIIb and β3 have both been associated with defective thrombopoiesis and thrombocytopenia.[322-325] Together, the increased spreading of *RhoA*$^{-/-}$ MKs on fibrinogen (Figure 27) and the increased proportion of proplatelet-forming *RhoA/Itgb1*$^{-/-}$ BM-derived MKs on fibrinogen, associated with increased αIIbβ3 levels on the platelet surface of these mice (Lou M. Wackerbarth, Master thesis, 2020), indicate aberrant αIIbβ3 signaling in the absence of RhoA. Thus, these data suggest that integrin activity needs to be well-controlled in MKs during the process of (pro)platelet formation in the BM. Therefore, it would be interesting not only to verify the hypothesis of aberrant integrin signaling in *RhoA*$^{-/-}$ and *RhoA/Itgb1*$^{-/-}$ mice, but also analyze mice double-deficient in β1 and β3 integrins. Besides Talin-1, also the intracellular adapter protein Kindlin-3 in platelets and MKs is required for integrin inside-out activation, but comparable to Talin-1, Kindlin-3-deficient mice show normal platelet count and size.[92] While the mode of action of Kindlin-3 during activation remains to be solved, a direct interaction of Kindlin-3 with αIIbβ3 has been shown to be critical for supporting arterial thrombosis.[326] Although the integrin activation defect in our mice upon the loss of Talin-1 was clear and apparently had no impact on platelet count and size, it would be interesting to analyze mice double-deficient in Talin-1 and Kindlin-3 in regard to MK biology.

G6b-B-deficiency in mice results in severe macrothrombocytopenia due to impaired PPF from MKs.[112] Similar findings were made in signaling-incompetent mice with mutated ITIM.[114] The *Mpig6b* mutant mouse line (*G6b*$^{mut}$), largely reacpitulates the phenotypes observed in constitutive G6b-B KO mice, proposing that G6b-B is a major regulator of MK maturation and BM homeostasis (Becker & Manukjan *et al.*, unpublished). In line with the literature, *G6b*$^{-/-}$ mice suffered from a severe macrothrombocytopenia and displayed impaired PPF *in vitro*. Mice deficient in RhoA and G6b-B were indistinguishable from *G6b*$^{-/-}$ mice, thus showing that the sole loss of G6b-B is sufficient to impair PPF. Furthermore, both the single and double-deficient mice display unaltered ploidy distribution in primary MKs, except a drop in 16N MKs and an increase in 2N MKs, which might be explained by the vast increase in immature MKs in the BM of these mice. Together with the analysis performed on *G6b*$^{mut}$ mice (Becker & Manukjan *et al.*, unpublished), these results confirm that G6b-B is dispensable for endomitosis, but similar to RhoA/Cdc42, important for MK maturation. The HS perlecan has been recently identified as a new ligand of G6b-B[118] and enhanced megakaryopoiesis in mice overexpressing heparanase, an endoglucoronidase responsible for the cleavage of heparan sulfate proteoglycans such as perlecan has been shown.[327] These findings thus highlight the potential importance of G6b-B and perlecan during the regulation of PPF. However, concomitant loss of G6b-B did not interfere with the transmigration in RhoA-deficient MKs. In contrast, we even observed enhanced transmigration in the double-deficient mice. However, we also observed slightly enhanced numbers of intrasinusoidal MKs in the BM of G6b-B single deficient mice associated with dilated and partly disrupted vessel structures. G6b-B-deficiency has been linked to the development of myelofibrosis in mice and humans.[112,114,115] The same effect has also been extensively studied in *G6b*$^{mut}$ mice along with a pronounced osteosclerosis and altered cytokine levels in the BM, especially increased TGFβ1 levels and enhanced collagen and reticulin deposition (Becker & Manukjan *et al.*, unpublished). The secondary effects caused by the inflamed BM microenvironment, such as the dilated vessel structures may thus promote the transendothelial migration of RhoA-deficient MKs.

Comparable to *G6b*$^{mut}$ mice, we identified a pronounced osteosclerosis, loss of BM cell mass and an increased vessel density in *G6b*$^{-/-}$ female mice, and also to a much lesser extend in male mice. Elevated estrogen concentrations in female mice have been reported to promote TGFβ1-secretion from osteoblasts, thus stimulating the osteoclast apoptosis, which in turn might explain the elevated osteosclerosis in female mice.[328] Of note, the slight changes observed in male mice could also be only due to the myelofibrosis.

Strikingly, although still suffering from a severe macrothrombocytopenia, we show that both female and male *RhoA/G6b*$^{-/-}$ mice displayed a strong reduction of the myelofibrotic and osteosclerotic phenotype associated with increased cellularity and TGFβ1 levels normalized to the *WT* levels (Figure 45 + Figure 46). In summary, our results indicate that, albeit a severe macrothrombocytopenia and splenomegaly in *RhoA/G6b*$^{-/-}$ mice, the additional loss of RhoA interfered with TGFβ1 release and thereby positively influenced the myelofibrosis and osteosclerosis caused upon G6b-B ablation. These finding thus might be of further interest for patients suffering from MPNssince the involvement of the RhoA/ROCK pathway in such disease conditions is known and whether the treatment of G6b-B-deficient mice with the clinical ROCK1/2 inhibitor fasudil recapitulates our results, needs to be further investigated.[329,330]

### Macrothrombocytopenia and transendothelial MK migration in *RhoA*$^{-/-}$ mice is due to cell intrinsic defects

Throughout all the projects in this thesis, highly varying levels of intrasinusoidal MK localization were observed for the different *RhoA*$^{-/-}$ control mice. We noted not only a sex-dependent, but also strain-specific differences in the degree of MK transmigration (*RhoA*$^{Low}$: 2-10%; *RhoA*$^{High}$: >10%). We therefore clearly show during the course of this thesis that it is mandatory to always use both sex and background matched *RhoA*$^{-/-}$ controls, but also that the transendothelial migration of MKs proposes an overall a rather weak read-out. To also overcome the issue of 2D sections, high volume 3D imaging should be performed using light sheet microscopy.[69] By comparing the large amount of data created throughout the thesis, we show no direct evidence of a correlation between intrasinusoidal MK localization and the degree of macrothrombocytopenia in *RhoA*$^{-/-}$ mice.

It has been shown that ´ectopic´ expression of Cre in the *Pf4-Cre* mice leads to the ablation of target genes not only in leukocytes and macrophages but also outside the hematopoietic lineage, e.g. in epithelial cells of the colon, potentially leading to a phenotype unrelated to MKs and platelets.[305] This raised the question as to whether this reported broader PF4-Cre activity might also be present in endothelial cells in the BM compartment. Normally, endothelial cells of BM sinusoids enable proplatelet protrusions from mature MKs to penetrate the basement membrane, which eventually enables the release of proplatelets into the blood stream.[318] A possible ectopic PF4-Cre expression in endothelial cells resulting in an unintended loss of RhoA in endothelial cells might negatively affect endothelial barrier capacities in *RhoA*$^{-/-}$ mice and thus promote transednothelial migration of the RhoA-deficient MKs. Importantly, with the BM transplantation experiments, we could rule out that not only the macrothrombocytopenia, but also the aberrant transmigration of *RhoA*$^{-/-}$ MKs is due *Pf4-Cre*-mediated side effects on non-hematopoietic cells.

To find out more about the underyling mechanisms, we initiated a systemic proteomics approach for the more detailed analysis and comparison of BM-derived RhoA/Cdc42 single and double-deficient MKs, which is currently being analyzed. Initial results showed that many results obtained by qPCR correlate with the proteomics data set. Recent studies this year have shown, that NMMIIA actomyosin contractility is important to ensure podosome formation as well as proper PPF at the vascular sinusoids.[225] Thus highlighting one of our findings from the proteomics data-set, we not only found a strong downregulation of Myl9 (MLC2) in the *DKO* mice as reported in Figure 33, but also a pronounced downregulation RhoA and Cdc42 single-deficient mice, while Myh9 levels were unaltered (Figure 61).

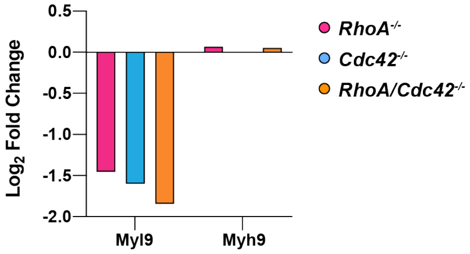

**Figure 61: Proteomics on *in vitro* cultured BM-derived MKs.** Preliminary analysis of proteomics data revealed a significant downregulation of MLC2 (Myl9) but not Myh9 in the depicted genotypes compared to the respective *WT* (n = 5 vs 5, 4 vs 2 and 5 vs 5). Analysis performed by Johannes Balkenhol (Rudolf-Virchow-Center, Heinze Group).

In summary the enhanced transmigration is likely not the reason for the impaired PPF and macrothrombocytopenia in *RhoA*$^{-/-}$ mice and thus requires further investigations, such as currently performed with a more systemic proteomics approach of *in vitro* cultured BM-derived MKs. Furthermore, a comparison with a more in-depth systemic transcriptomics and approach of both *in vitro* cultured and primary *in vivo* BM MKs would be of interest.

## 5.4 Analysis of MK- and platelet-specific RhoA deficiency using the *Gp1ba-Cre* deleter strain

In the last part of this study we aimed to analyze RhoA depletion in MKplatelets and platelets using the novel *Gp1ba-Cre* deleter mouse line and compare the findings to the *Pf4-Cre* system.[238]

Incomplete depletion of highly abundant proteins has been previously described using the *Gp1ba-Cre* transgenic mice in order to generate a MK- and platelet-specific KO.[238] The importance of RhoA during embryonic development has been shown in mice constitutively lacking RhoA, while its absence resulted in early embryonic lethality.[235] *Gp1ba-Cre* mediated depletion, however, resulted in residual RhoA expression in both MKs and platelets, with remaining protein levels of ~ 20% and ~ 45% respectively. These findings stand in contrast to the *Pf4-Cre* system, showing complete ablation using traditional immunoblotting. The residual protein expression is likely to be explained due to the later onset of the GPIbα-Cre expression[238] compared to the *Cxcl4* promoter driven PF4-Cre.[237] The later onset of the GPIbα-Cre expression during megakaryopoiesis thus likely results in later gene deletion in the MKs and therefore shortens the timeframe for the present mRNA and protein to be degraded. [238,331] In the future, not only comparative mRNA studies but also the more quantitative immunoassay platform the SimpleProtein Jess should be used to compare both mRNA and proteins levels in *RhoA*$^{Gp1ba\text{-}Cre}$ and *RhoA*$^{Pf4\text{-}Cre}$ MKs and platelets.

Analysis of basic platelet parameters revealed a slightly less pronounced thrombocytopenia in *RhoA*$^{Gp1ba\text{-}Cre}$ compared to *RhoA*$^{Pf4\text{-}Cre}$ mice used during this thesis and the literature.[246] *WT*$^{Gp1ba\text{-}Cre}$ platelets showed an increase in platelet size which could be explained by reduced GPIbα expression on the platelet surface (~ 33%) due to the constitutive KI of a T2A-improved-Cre inserted in the endogenous *Gp1ba* gene locus.[238] Unlike *RhoA*$^{Pf4\text{-}Cre}$ mice, we also observed only marginally affected platelet clearance in *RhoA*$^{Gp1ba\text{-}Cre}$ mice. In summary, the residual expression of RhoA as well as altered GPIbα expression thus seems to interfere with the platelet phenotypes observed for *RhoA*$^{Pf4\text{-}Cre}$ mice, which we also confirmed by ultrastructural analysis *RhoA*$^{Gp1ba\text{-}Cre}$ platelets by TEM.

Surprisingly, MKs from *RhoA*$^{Gp1ba\text{-}Cre}$ mice seemed to be normally localized in the BM hematopoietic compartment and showed no signs of increased transendothelial MK migration. Interestingly, we found that *RhoA*$^{Gp1ba\text{-}Cre}$ MKs also displayed irregular shapes, comparable to the observations in *RhoA*$^{Pf4\text{-}Cre}$ mice described in the previous sections. Strikingly however, we demonstrated a so far unknown effect of the *Gp1ba-Cre* transgene on PPF *in vitro*. These findings in summary raise doubts regarding the suitability of the *Gp1ba-Cre* system to investigate MK biology. This hypothesis was also strengthened by the TEM observation, that both *WT*$^{Gp1ba\text{-}Cre}$ controls and *Rho*$^{Gp1ba\text{-}Cre}$ mice displayed impaired DMS formation. Strikingly, we found a few intrasinusoidal MKs in *Rho*$^{Gp1ba\text{-}Cre}$ mich, which displayed disrupted and irregular morphology. However, the *Gp1ba-Cre* transgene does not only seems to impair DMS formation but also the overall cellular integrity of *WT*$^{Gp1ba\text{-}Cre}$ MKs, which was even more pronounced in *RhoA*$^{Gp1ba\text{-}Cre}$ MKs and may explain why the intrasinusoidal MKs were omitted in the analysis of IF femur cryosections. Showing the importance of proper GPIbα expression and function, the FlnA-GPIbα linkage has been described to regulates platelet size but also to maintain the mechanical stability of the platelet plasma membrane and is also critical for MKs.

Loss of FlnA in mice leads to a severe macrothrombocytopenia, with large and fragile premature platelet release and increased bleeding times[211,212], similar to BSS like phenotype in GPIbα/β-null mice.[213,214] Therefore, it should also be considered to compare the results to mice with a heterozygous loss off GPIbα or FlnA.

Our findings thus strengthen the importance of GPIb during DMS formation also in light of recent publications showing, that DMS formation starts with GPIb-positive clusters at the cell membrane.[35] These results at the same time question the suitability of the *Gp1ba-Cre* to investigate platelet biogenesis. Whether the differences in intrasinusoidal MK localization of *RhoA*$^{Gp1ba\text{-}Cre}$ compared to *RhoA*$^{Pf4\text{-}Cre}$ mice is due to perturbed DMS formation, persisting expression of RhoA or the additional defects in overall integrity of the cells due to perturbed GPIbα expression remains to be clarified. Systemic comparison of *RhoA*$^{Pf4\text{-}Cre}$ and *RhoA*$^{Gp1ba\text{-}Cre}$ MKs/platelets by proteomics or transcriptomics could also further help to better understand which changes are causative for either the transmigration or thrombocytopenia.

In summary, we demonstrated that *Gp1ba-Cre*-mediated deletion of RhoA in MKs and platelets is not suitable for the study of this Rho GTPase in MK biology, due to intrinsic MK defects in *Gp1ba-Cre* mice and insufficient depletion of RhoA. Therefore, *Pf4-Cre* remains the preferable model for studying megakaryopiesis/platelet biogenesis for genes, which are ubiquitously expressed and/or early throughout MK development. The cell type specificity of *Gp1ba-Cre*, together with the profound but incomplete depletion of RhoA, and possibly other widely expressed genes, may, however, provide an elegant tool to study gene dosage effects in MKs/platelets and also help to better understand the macrothrombocytopenia observed in *RhoA*$^{Pf4\text{-}Cre}$ mice.

## 5.5 Concluding remarks and future plans

We showed that double-deficiency of RhoA/Cdc42 in MKs resulted in reduced mRNA and protein levels of MK-specific GPs, as well as cytoskeletal regulators of known importance in MK maturation and PPF, thereby virtually abolishing functional platelet biogenesis *in vitro* and to a large extend *in vivo*. We thus uncovered that synergistic RhoA/Cdc42 signaling is a prerequisite for cytoplasmic MK maturation, but not endomitosis. However, the molecular mechanisms underlying the macrothrombocytopenia in RhoA- and Cdc42-deficient mice are still not fully resolved. Recent studies have highlighted the important differences between the undirected PPF *in vitro* and the directed PPF at the vascular sinusoids *in vivo*, associated with different characteristica. *In vivo*, MKs seem to predominantely enter the vascular sinusoids in larger fragments, while smaller fragments are subsequently shed off and matured to platelets in the circulation. In order to penetrate the endothelium, the formation of podosomes as well as controlled NMMIIA activity in the MK are required. Whether the latter mechanisms are required or similar to the process of membrane budding, just recently claimed to be a major mechanism of *in vivo* platelet biogenesis[332], remains to be identified. Due to the strong involvement of the MK cytoskeleton in these processes, the usage of our mouse lines deficient in the Rho GTPases RhoA or Cdc42 could be useful to further unravel fundamental mechanisms important for the process of MK PPF *in vivo.* Therefore, a combination of more detailed and high quality 2P-IVM microscopy, together with systemic approaches such as transcriptomics and proteomics of primary and *in vitro* cultured MKs are unavoidable for the future. In addition, it would also be of interest to establish *in vitro* assays which could mimic the penetration of MKs through the endothelial layer in a 2D/3D environment and combine these assays with flow conditions, to mimic the *in vivo* situation.

In the third part of this thesis we analyzed mice double-deficient in RhoA and prominent MK receptors and thereby showed that integrins as well as the ITIM-containing receptor G6b-B are dispensable for the transendothelial transmigration in RhoA-deficient MKs. Interstingly, our data indicated potential abberant signaling of αIIbβ3 upon the loss of β1 integrins in RhoA-deficient mice. Therefore, it would be of interest to to generate and analyze mice deficient in β1 and β3 integrins, as well as mice double-deficient in Talin-1 and Kindlin-3, due to direct interactions of Kindlin-3 and αIIbβ3. Furthermore, the importance of β1 intergrins for podosome formation should be clarified. Besides the integrins, also potential redundant functions of the GPR56 in RhoA-deficient mice should be considered. Moreover, RhoA seems to be critically involved in the process of myelofibrosis and osteosclerosis associated with the loss of G6b-B in mice. The clinical ROCK1/2 inhibitor, namely Fasudil could be used in future studies to further dissect the potential impact of the Rho/ROCK signaling in G6b-B deficient, but also *G6b*$^{mut}$ mice.

In the last part of this study we demonstrated that the new MK- and platelet-specific *Gp1ba-Cre* deleter mouse comes along with intrinsic MK defects and results in incomplete depletion of RhoA compared to *Pf4-Cre*, positioning *Pf4-Cre* as the new-old golden standard, indispensable for studying MK biology. However, the mouse could still be used to study gene dosage effects due to insufficient depletion as well as the temporal effect of depletion, due to the later onset of the *Gp1ba-Cre*. Furthermore, the implication of the *Gp1ba-Cre* alterations in GPIbα expression levels in thrombosis and ischemic stroke should still be assessed. Whether the generation of a novel *G6b-B-Cre* mouse may be an alternative to the *Pf4-Cre* could be considered.

# 6 REFERENCES

1. Mehta A, Mahtta D, Gulati M, Sperling LS, Blumenthal RS, Virani SS. Cardiovascular Disease Prevention in Focus: Highlights from the 2019 American Heart Association Scientific Sessions. *Curr Atheroscler Rep*. 2020;22(1):3.
2. Nieswandt B, Pleines I, Bender M. Platelet adhesion and activation mechanisms in arterial thrombosis and ischaemic stroke. *J Thromb Haemost*. 2011;9 Suppl 1:92-104.
3. Wright J. The histogenesis of the blood platelets. *J Morphol*. 1910;21(2):263–278.
4. Noetzli Leila J, French Shauna L, Machlus Kellie R. New Insights Into the Differentiation of Megakaryocytes From Hematopoietic Progenitors. *Arteriosclerosis, Thrombosis, and Vascular Biology*. 2019;39(7):1288-1300.
5. Mazzi S, Lordier L, Debili N, Raslova H, Vainchenker W. Megakaryocyte and polyploidization. *Exp Hematol*. 2018;57:1-13.
6. Machlus KR, Italiano JE, Jr. The incredible journey: From megakaryocyte development to platelet formation. *J Cell Biol*. 2013;201(6):785-796.
7. Schulze H, Korpal M, Hurov J, et al. Characterization of the megakaryocyte demarcation membrane system and its role in thrombopoiesis. *Blood*. 2006;107(10):3868-3875.
8. Tijssen MR, Ghevaert C. Transcription factors in late megakaryopoiesis and related platelet disorders. *J Thromb Haemost*. 2013;11(4):593-604.
9. Long MW. Megakaryocyte differentiation events. *Seminars in Hematology*. 1998;35(3):192-199.
10. Italiano JE, Jr., Lecine P, Shivdasani RA, Hartwig JH. Blood platelets are assembled principally at the ends of proplatelet processes produced by differentiated megakaryocytes. *J Cell Biol*. 1999;147(6):1299-1312.
11. Ogawa M. Differentiation and proliferation of hematopoietic stem cells. *Blood*. 1993;81(11):2844-2853.
12. Akashi K, Traver D, Miyamoto T, Weissman IL. A clonogenic common myeloid progenitor that gives rise to all myeloid lineages. *Nature*. 2000;404(6774):193-197.
13. Debili N, Coulombel L, Croisille L, et al. Characterization of a bipotent erythro-megakaryocytic progenitor in human bone marrow. *Blood*. 1996;88(4):1284-1296.
14. Noetzli LJ, French SL, Machlus KR. New Insights Into the Differentiation of Megakaryocytes From Hematopoietic Progenitors. *Arterioscler Thromb Vasc Biol*. 2019;39(7):1288-1300.
15. Xavier-Ferrucio J, Krause DS. Concise Review: Bipotent Megakaryocytic-Erythroid Progenitors: Concepts and Controversies. *Stem Cells*. 2018;36(8):1138-1145.
16. Ebbe S, Stohlman F, Jr. Megakaryocytopoiesis in the Rat. *Blood*. 1965;26:20-35.
17. Ebbe S. Biology of megakaryocytes. *Prog Hemost Thromb*. 1976;3:211-229.
18. Therman E, Sarto GE, Stubblefield PA. Endomitosis: a reappraisal. *Hum Genet*. 1983;63(1):13-18.
19. Odell TT, Jr., Jackson CW, Friday TJ. Megakaryocytopoiesis in rats with special reference to polyploidy. *Blood*. 1970;35(6):775-782.
20. Vitrat N, Cohen-Solal K, Pique C, et al. Endomitosis of human megakaryocytes are due to abortive mitosis. *Blood*. 1998;91(10):3711-3723.
21. Mattia G, Vulcano F, Milazzo L, et al. Different ploidy levels of megakaryocytes generated from peripheral or cord blood CD34+ cells are correlated with different levels of platelet release. *Blood*. 2002;99(3):888-897.
22. Hegyi E, Navarro S, Debili N, et al. Regulation of human megakaryocytopoiesis: analysis of proliferation, ploidy and maturation in liquid cultures. *Int J Cell Cloning*. 1990;8(4):236-244.
23. Liu ZJ, Italiano J, Jr., Ferrer-Marin F, et al. Developmental differences in megakaryocytopoiesis are associated with up-regulated TPO signaling through mTOR and elevated GATA-1 levels in neonatal megakaryocytes. *Blood*. 2011;117(15):4106-4117.
24. Vainchenker W, Guichard J, Breton-Gorius J. [Differentiation of human megakaryocytes in culture starting from the primordial circulating cells in the newborn]. *C R Acad Hebd Seances Acad Sci D*. 1978;287(3):177-179.
25. Ravid K, Lu J, Zimmet JM, Jones MR. Roads to polyploidy: the megakaryocyte example. *J Cell Physiol*. 2002;190(1):7-20.
26. Geddis AE, Fox NE, Tkachenko E, Kaushansky K. Endomitotic megakaryocytes that form a bipolar spindle exhibit cleavage furrow ingression followed by furrow regression. *Cell Cycle (Georgetown, Tex)*. 2007;6(4):455-460.
27. Lordier L, Jalil A, Aurade F, et al. Megakaryocyte endomitosis is a failure of late cytokinesis related to defects in the contractile ring and Rho/Rock signaling. *Blood*. 2008;112(8):3164-3174.
28. Lordier L, Chang Y, Jalil A, et al. Aurora B is dispensable for megakaryocyte polyploidization, but contributes to the endomitotic process. *Blood*. 2010;116(13):2345-2355.
29. Odell TT, Jr., Jackson CW. Polyploidy and maturation of rat megakaryocytes. *Blood*. 1968;32(1):102-110.
30. Lepage A, Leboeuf M, Cazenave JP, de la Salle C, Lanza F, Uzan G. The alpha(IIb)beta(3) integrin and GPIb-V-IX complex identify distinct stages in the maturation of CD34(+) cord blood cells to megakaryocytes. *Blood*. 2000;96(13):4169-4177.
31. Margraf A, Zarbock A. Platelets in Inflammation and Resolution. *J Immunol*. 2019;203(9):2357-2367.
32. Kahr WH, Hinckley J, Li L, et al. Mutations in NBEAL2, encoding a BEACH protein, cause gray platelet syndrome. *Nat Genet*. 2011;43(8):738-740.

33. Albers CA, Cvejic A, Favier R, et al. Exome sequencing identifies NBEAL2 as the causative gene for gray platelet syndrome. *Nat Genet*. 2011;43(8):735-737.

34. Deppermann C, Cherpokova D, Nurden P, et al. Gray platelet syndrome and defective thrombo-inflammation in Nbeal2-deficient mice. *J Clin Invest*. 2013.

35. Eckly A, Heijnen H, Pertuy F, et al. Biogenesis of the demarcation membrane system (DMS) in megakaryocytes. *Blood*. 2014;123(6):921-930.

36. Machlus KR, Italiano JE. Megakaryocyte Development and Platelet Formation. In: Michelson A, Cattaneo M, Frelinger A, Newman P, eds. Platelets, 4th edition: Elsevier; 2019.

37. Chen Y, Aardema J, Kale S, et al. Loss of the F-BAR protein CIP4 reduces platelet production by impairing membrane-cytoskeleton remodeling. *Blood*. 2013;122(10):1695-1706.

38. Begonja AJ, Pluthero FG, Suphamungmee W, et al. FlnA binding to PACSIN2 F-BAR domain regulates membrane tubulation in megakaryocytes and platelets. *Blood*. 2015;126(1):80-88.

39. Antkowiak A, Viaud J, Severin S, et al. Cdc42-dependent F-actin dynamics drive structuration of the demarcation membrane system in megakaryocytes. *J Thromb Haemost*. 2016;14(6):1268-1284.

40. Leon C, Dupuis A, Gachet C, Lanza F. The contribution of mouse models to the understanding of constitutional thrombocytopenia. *Haematologica*. 2016;101(8):896-908.

41. Pleines I, Cherpokova D, Bender M. Rho GTPases and their downstream effectors in megakaryocyte biology. *Platelets*. 2019;30(1):9-16.

42. Daimon T, Gotoh Y. Cytochemical evidence of the origin of the dense tubular system in the mouse platelet. *Histochemistry*. 1982;76(2):189-196.

43. Gerrard JM, White JG, Rao GH, Townsend D. Localization of platelet prostaglandin production in the platelet dense tubular system. *Am J Pathol*. 1976;83(2):283-298.

44. Yamada E. The fine structure of the megakaryocyte in the mouse spleen. *Acta Anat (Basel)*. 1957;29(3):267-290.

45. Kosaki G. In vivo platelet production from mature megakaryocytes: does platelet release occur via proplatelets? *Int J Hematol*. 2005;81(3):208-219.

46. Shaklai M, Loskutoff D, Tavassoli M. Membrane characteristics of cultured endothelial cells: identification of gap junction. *Isr J Med Sci*. 1978;14(3):306-313.

47. Radley JM, Hartshorn MA. Megakaryocyte fragments and the microtubule coil. *Blood Cells*. 1987;12(3):603-614.

48. Radley JM, Haller CJ. The demarcation membrane system of the megakaryocyte: a misnomer? *Blood*. 1982;60(1):213-219.

49. Becker RP, De Bruyn PP. The transmural passage of blood cells into myeloid sinusoids and the entry of platelets into the sinusoidal circulation; a scanning electron microscopic investigation. *Am J Anat*. 1976;145(2):183-205.

50. Bartley TD, Bogenberger J, Hunt P, et al. Identification and cloning of a megakaryocyte growth and development factor that is a ligand for the cytokine receptor Mpl. *Cell*. 1994;77(7):1117-1124.

51. de Sauvage FJ, Hass PE, Spencer SD, et al. Stimulation of megakaryocytopoiesis and thrombopoiesis by the c-Mpl ligand. *Nature*. 1994;369(6481):533-538.

52. Kaushansky K, Lok S, Holly RD, et al. Promotion of megakaryocyte progenitor expansion and differentiation by the c-Mpl ligand thrombopoietin. *Nature*. 1994;369(6481):568-571.

53. Lok S, Kaushansky K, Holly RD, et al. Cloning and expression of murine thrombopoietin cDNA and stimulation of platelet production in vivo. *Nature*. 1994;369(6481):565-568.

54. Kaushansky K. The mpl ligand: molecular and cellular biology of the critical regulator of megakaryocyte development. *Stem Cells*. 1994;12 Suppl 1:91-96; discussion 96-97.

55. Kuter DJ, Beeler DL, Rosenberg RD. The purification of megapoietin: a physiological regulator of megakaryocyte growth and platelet production. *Proc Natl Acad Sci U S A*. 1994;91(23):11104-11108.

56. Sohma Y, Akahori H, Seki N, et al. Molecular cloning and chromosomal localization of the human thrombopoietin gene. *FEBS Lett*. 1994;353(1):57-61.

57. Wendling F, Maraskovsky E, Debili N, et al. cMpl ligand is a humoral regulator of megakaryocytopoiesis. *Nature*. 1994;369(6481):571-574.

58. Italiano JE. Megakaryopoiesis and Platelet Biogenesis: Springer, Cham; 2016.

59. Junt T, Schulze H, Chen Z, et al. Dynamic visualization of thrombopoiesis within bone marrow. *Science*. 2007;317(5845):1767-1770.

60. Bornert A, Boscher J, Pertuy F, et al. Cytoskeletal-based mechanisms differently regulate in vivo and in vitro proplatelet formation. *Haematologica*. 2020.

61. Brown E, Carlin LM, Nerlov C, Lo Celso C, Poole AW. Multiple membrane extrusion sites drive megakaryocyte migration into bone marrow blood vessels. *Life Sci Alliance*. 2018;1(2).

62. Nishimura S, Nagasaki M, Kunishima S, et al. IL-1alpha induces thrombopoiesis through megakaryocyte rupture in response to acute platelet needs. *J Cell Biol*. 2015;209(3):453-466.

63. Patel SR, Hartwig JH, Italiano JE, Jr. The biogenesis of platelets from megakaryocyte proplatelets. *J Clin Invest*. 2005;115(12):3348-3354.

64. Behnke O, Forer A. From megakaryocytes to platelets: platelet morphogenesis takes place in the bloodstream. *Eur J Haematol Suppl*. 1998;61:3-23.

65. Howell WH, Donahue DD. The Production of Blood Platelets in the Lungs. *J Exp Med*. 1937;65(2):177-203.

66. Martin JF, Trowbridge EA, Salmon GL, Slater DN. The relationship between platelet and megakaryocyte volumes. *Thromb Res*. 1982;28(4):447-459.

67. Zucker-Franklin D, Philipp CS. Platelet production in the pulmonary capillary bed: new ultrastructural evidence for an old concept. *Am J Pathol*. 2000;157(1):69-74.

68. Lefrancais E, Ortiz-Munoz G, Caudrillier A, et al. The lung is a site of platelet biogenesis and a reservoir for haematopoietic progenitors. *Nature*. 2017;544(7648):105-109.

69. Stegner D, vanEeuwijk JMM, Angay O, et al. Thrombopoiesis is spatially regulated by the bone marrow vasculature. *Nat Commun*. 2017;8(1):127.

70. Thon JN, Dykstra BJ, Beaulieu LM. Platelet bioreactor: accelerated evolution of design and manufacture. *Platelets*. 2017;28(5):472-477.

71. Ito Y, Nakamura S, Sugimoto N, et al. Turbulence Activates Platelet Biogenesis to Enable Clinical Scale Ex Vivo Production. *Cell*. 2018;174(3):636-648 e618.

72. Fielder PJ, Hass P, Nagel M, et al. Human platelets as a model for the binding and degradation of thrombopoietin. *Blood*. 1997;89(8):2782-2788.

73. Kuter DJ, Rosenberg RD. The reciprocal relationship of thrombopoietin (c-Mpl ligand) to changes in the platelet mass during busulfan-induced thrombocytopenia in the rabbit. *Blood*. 1995;85(10):2720-2730.

74. McCarty JM, Sprugel KH, Fox NE, Sabath DE, Kaushansky K. Murine thrombopoietin mRNA levels are modulated by platelet count. *Blood*. 1995;86(10):3668-3675.

75. Geddis AE. Megakaryopoiesis. *Semin Hematol*. 2010;47(3):212-219.

76. Behrens K, Alexander WS. Cytokine control of megakaryopoiesis. *Growth Factors*. 2018;36(3-4):89-103.

77. Hitchcock IS, Kaushansky K. Thrombopoietin from beginning to end. *Br J Haematol*. 2014;165(2):259-268.

78. van den Oudenrijn S, Bruin M, Folman CC, et al. Mutations in the thrombopoietin receptor, Mpl, in children with congenital amegakaryocytic thrombocytopenia. *Br J Haematol*. 2000;110(2):441-448.

79. Machlus KR, Johnson KE, Kulenthirarajan R, et al. CCL5 derived from platelets increases megakaryocyte proplatelet formation. *Blood*. 2016;127(7):921-926.

80. Nieswandt B, Stritt S. Megakaryocyte rupture for acute platelet needs. *The Journal of Cell Biology*. 2015;209(3):327-328.

81. Avecilla ST, Hattori K, Heissig B, et al. Chemokine-mediated interaction of hematopoietic progenitors with the bone marrow vascular niche is required for thrombopoiesis. *Nat Med*. 2004;10(1):64-71.

82. Zhang L, Orban M, Lorenz M, et al. A novel role of sphingosine 1-phosphate receptor S1pr1 in mouse thrombopoiesis. *J Exp Med*. 2012;209(12):2165-2181.

83. Aguilar A, Boscher J, Pertuy F, Gachet C, Léon C. Three-Dimensional Culture in a Methylcellulose-Based Hydrogel to Study the Impact of Stiffness on Megakaryocyte Differentiation. In: Gibbins JM, Mahaut-Smith M, eds. Platelets and Megakaryocytes : Volume 4, Advanced Protocols and Perspectives. New York, NY: Springer New York; 2018:139-153.

84. Malara A, Currao M, Gruppi C, et al. Megakaryocytes Contribute to the Bone Marrow-Matrix Environment by Expressing Fibronectin, Type IV Collagen, and Laminin. *Stem Cells*. 2014;32(4):926-937.

85. Semeniak D, Faber K, Öftering P, Manukjan G, Schulze H. Impact of Itga2-Gp6-double collagen receptor deficient mice for bone marrow megakaryocytes and platelets. *PLoS ONE*. 2019;14(8).

86. Smith CW, Thomas SG, Raslan Z, et al. Mice Lacking the Inhibitory Collagen Receptor LAIR-1 Exhibit a Mild Thrombocytosis and Hyperactive Platelets. *Arterioscler Thromb Vasc Biol*. 2017;37(5):823-835.

87. Abbonante V, Gruppi C, Rubel D, Gross O, Moratti R, Balduini A. Discoidin domain receptor 1 protein is a novel modulator of megakaryocyte-collagen interactions. *J Biol Chem*. 2013;288(23):16738-16746.

88. Dutting S, Bender M, Nieswandt B. Platelet GPVI: a target for antithrombotic therapy?! *Trends Pharmacol Sci*. 2012;33(11):583-590.

89. Adorno-Cruz V, Liu H. Regulation and functions of integrin alpha2 in cell adhesion and disease. *Genes Dis*. 2019;6(1):16-24.

90. Emsley J, Knight CG, Farndale RW, Barnes MJ, Liddington RC. Structural basis of collagen recognition by integrin alpha2beta1. *Cell*. 2000;101(1):47-56.

91. Etoh T, Thomas L, Pastel-Levy C, Colvin RB, Mihm MC, Jr., Byers HR. Role of integrin alpha 2 beta 1 (VLA-2) in the migration of human melanoma cells on laminin and type IV collagen. *J Invest Dermatol*. 1993;100(5):640-647.

92. Moser M, Nieswandt B, Ussar S, Pozgajova M, Fassler R. Kindlin-3 is essential for integrin activation and platelet aggregation. *Nat Med*. 2008;14(3):325-330.

93. Moser M, Legate KR, Zent R, Fassler R. The tail of integrins, talin, and kindlins. *Science*. 2009;324(5929):895-899.

94. Gruner S, Prostredna M, Schulte V, et al. Multiple integrin-ligand interactions synergize in shear-resistant platelet adhesion at sites of arterial injury in vivo. *Blood*. 2003;102(12):4021-4027.

95. Sarratt KL, Chen H, Zutter MM, Santoro SA, Hammer DA, Kahn ML. GPVI and alpha2beta1 play independent critical roles during platelet adhesion and aggregate formation to collagen under flow. *Blood*. 2005;106(4):1268-1277.

96. He L, Pappan LK, Grenache DG, et al. The contributions of the alpha 2 beta 1 integrin to vascular thrombosis in vivo. *Blood*. 2003;102(10):3652-3657.

97. Marjoram RJ, Li Z, He L, et al. alpha2beta1 integrin, GPVI receptor, and common FcRgamma chain on mouse platelets mediate distinct responses to collagen in models of thrombosis. *PLoS One*. 2014;9(11):e114035.

98. Nourshargh S, Alon R. Leukocyte migration into inflamed tissues. *Immunity*. 2014;41(5):694-707.

99. Reymond N, Im JH, Garg R, et al. Cdc42 promotes transendothelial migration of cancer cells through beta1 integrin. *J Cell Biol*. 2012;199(4):653-668.

100. Mohle R, Bautz F, Denzlinger C, Kanz L. Transendothelial migration of hematopoietic progenitor cells. Role of chemotactic factors. *Ann N Y Acad Sci*. 2001;938:26-34; discussion 34-25.

101. Larson MK, Watson SP. A product of their environment: do megakaryocytes rely on extracellular cues for proplatelet formation? *Platelets*. 2006;17(7):435-440.

102. Balduini A, Pallotta I, Malara A, et al. Adhesive receptors, extracellular proteins and myosin IIA orchestrate proplatelet formation by human megakaryocytes. *J Thromb Haemost*. 2008;6(11):1900-1907.

103. Malara A, Gruppi C, Rebuzzini P, et al. Megakaryocyte-matrix interaction within bone marrow: new roles for fibronectin and factor XIII-A. *Blood*. 2011;117(8):2476-2483.

104. Sabri S, Jandrot-Perrus M, Bertoglio J, et al. Differential regulation of actin stress fiber assembly and proplatelet formation by alpha2beta1 integrin and GPVI in human megakaryocytes. *Blood*. 2004;104(10):3117-3125.

105. Malara A, Currao M, Gruppi C, et al. Megakaryocytes contribute to the bone marrow-matrix environment by expressing fibronectin, type IV collagen, and laminin. *Stem Cells*. 2014;32(4):926-937.

106. Semeniak D, Kulawig R, Stegner D, et al. Proplatelet formation is selectively inhibited by collagen type I through Syk-independent GPVI signaling. *J Cell Sci*. 2016;129(18):3473-3484.

107. Giannini S, Lee-Sundlov MM, Rivadeneyra L, et al. beta4GALT1 controls beta1 integrin function to govern thrombopoiesis and hematopoietic stem cell homeostasis. *Nat Commun*. 2020;11(1):356.

108. Qasba PK, Ramakrishnan B, Boeggeman E. Structure and function of beta -1,4-galactosyltransferase. *Curr Drug Targets*. 2008;9(4):292-309.

109. Coxon CH, Geer MJ, Senis YA. ITIM receptors: more than just inhibitors of platelet activation. *Blood*. 2017;129(26):3407-3418.

110. Nagy Z, Smolenski A. Cyclic nucleotide-dependent inhibitory signaling interweaves with activating pathways to determine platelet responses. *Res Pract Thromb Haemost*. 2018;2(3):558-571.

111. Senis YA, Tomlinson MG, Garcia A, et al. A comprehensive proteomics and genomics analysis reveals novel transmembrane proteins in human platelets and mouse megakaryocytes including G6b-B, a novel immunoreceptor tyrosine-based inhibitory motif protein. *Mol Cell Proteomics*. 2007;6(3):548-564.

112. Mazharian A, Wang YJ, Mori J, et al. Mice lacking the ITIM-containing receptor G6b-B exhibit macrothrombocytopenia and aberrant platelet function. *Sci Signal*. 2012;5(248):ra78.

113. Mazharian A, Mori J, Wang YJ, et al. Megakaryocyte-specific deletion of the protein-tyrosine phosphatases Shp1 and Shp2 causes abnormal megakaryocyte development, platelet production, and function. *Blood*. 2013;121(20):4205-4220.

114. Geer MJ, van Geffen JP, Gopalasingam P, et al. Uncoupling ITIM receptor G6b-B from tyrosine phosphatases Shp1 and Shp2 disrupts murine platelet homeostasis. *Blood*. 2018;132(13):1413-1425.

115. Hofmann I, Geer MJ, Vogtle T, et al. Congenital macrothrombocytopenia with focal myelofibrosis due to mutations in human G6b-B is rescued in humanized mice. *Blood*. 2018;132(13):1399-1412.

116. Melhem M, Abu-Farha M, Antony D, et al. Novel G6B gene variant causes familial autosomal recessive thrombocytopenia and anemia. *Eur J Haematol*. 2017;98(3):218-227.

117. de Vet EC, Newland SA, Lyons PA, Aguado B, Campbell RD. The cell surface receptor G6b, a member of the immunoglobulin superfamily, binds heparin. *FEBS Lett*. 2005;579(11):2355-2358.

118. Vogtle T, Sharma S, Mori J, et al. Heparan sulfates are critical regulators of the inhibitory megakaryocyte-platelet receptor G6b-B. *Elife*. 2019;8.

119. Nugent MA, Nugent HM, Iozzo RV, Sanchack K, Edelman ER. Perlecan is required to inhibit thrombosis after deep vascular injury and contributes to endothelial cell-mediated inhibition of intimal hyperplasia. *Proc Natl Acad Sci U S A*. 2000;97(12):6722-6727.

120. Whitelock JM, Melrose J, Iozzo RV. Diverse cell signaling events modulated by perlecan. *Biochemistry*. 2008;47(43):11174-11183.

121. Blood Platelets Are Assembled Principally at the Ends of Proplatelet Processes Produced by Differentiated Megakaryocytes.

122. Tijssen MR, Moreau T, Ghevaert C. Transcriptional Regulation of Platelet Formation: Harnessing the Complexity for Efficient Platelet Production In Vitro. In: Schulze H., Italiano J. (eds) Molecular and Cellular Biology of Platelet Formation. *Springer, Cham*. 2016.

123. Chang AN, Cantor AB, Fujiwara Y, et al. GATA-factor dependence of the multitype zinc-finger protein FOG-1 for its essential role in megakaryopoiesis. *Proc Natl Acad Sci U S A*. 2002;99(14):9237-9242.

124. Shivdasani RA, Fujiwara Y, McDevitt MA, Orkin SH. A lineage-selective knockout establishes the critical role of transcription factor GATA-1 in megakaryocyte growth and platelet development. *EMBO J*. 1997;16(13):3965-3973.
125. Vyas P, McDevitt MA, Cantor AB, Katz SG, Fujiwara Y, Orkin SH. Different sequence requirements for expression in erythroid and megakaryocytic cells within a regulatory element upstream of the GATA-1 gene. *Development*. 1999;126(12):2799-2811.
126. Muntean AG, Pang L, Poncz M, Dowdy SF, Blobel GA, Crispino JD. Cyclin D-Cdk4 is regulated by GATA-1 and required for megakaryocyte growth and polyploidization. *Blood*. 2007;109(12):5199-5207.
127. Ciovacco WA, Raskind WH, Kacena MA. Human phenotypes associated with GATA-1 mutations. *Gene*. 2008;427(1-2):1-6.
128. Pencovich N, Jaschek R, Dicken J, et al. Cell-autonomous function of Runx1 transcriptionally regulates mouse megakaryocytic maturation. *PLoS One*. 2013;8(5):e64248.
129. Heller PG, Glembotsky AC, Gandhi MJ, et al. Low Mpl receptor expression in a pedigree with familial platelet disorder with predisposition to acute myelogenous leukemia and a novel AML1 mutation. *Blood*. 2005;105(12):4664-4670.
130. Sun L, Gorospe JR, Hoffman EP, Rao AK. Decreased platelet expression of myosin regulatory light chain polypeptide (MYL9) and other genes with platelet dysfunction and CBFA2/RUNX1 mutation: insights from platelet expression profiling. *J Thromb Haemost*. 2007;5(1):146-154.
131. Jalagadugula G, Mao G, Kaur G, Goldfinger LE, Dhanasekaran DN, Rao AK. Regulation of platelet myosin light chain (MYL9) by RUNX1: implications for thrombocytopenia and platelet dysfunction in RUNX1 haplodeficiency. *Blood*. 2010;116(26):6037-6045.
132. Miralles F, Posern G, Zaromytidou AI, Treisman R. Actin dynamics control SRF activity by regulation of its coactivator MAL. *Cell*. 2003;113(3):329-342.
133. Olson EN, Nordheim A. Linking actin dynamics and gene transcription to drive cellular motile functions. *Nat Rev Mol Cell Biol*. 2010;11(5):353-365.
134. Hill CS, Wynne J, Treisman R. The Rho family GTPases RhoA, Rac1, and CDC42Hs regulate transcriptional activation by SRF. *Cell*. 1995;81(7):1159-1170.
135. Buchwalter G, Gross C, Wasylyk B. Ets ternary complex transcription factors. *Gene*. 2004;324:1-14.
136. Ragu C, Boukour S, Elain G, et al. The serum response factor (SRF)/megakaryocytic acute leukemia (MAL) network participates in megakaryocyte development. *Leukemia*. 2010;24(6):1227-1230.
137. Cheng EC, Luo Q, Bruscia EM, et al. Role for MKL1 in megakaryocytic maturation. *Blood*. 2009;113(12):2826-2834.
138. Halene S, Gao Y, Hahn K, et al. Serum response factor is an essential transcription factor in megakaryocytic maturation. *Blood*. 2010;116(11):1942-1950.
139. Gilles L, Bluteau D, Boukour S, et al. MAL/SRF complex is involved in platelet formation and megakaryocyte migration by regulating MYL9 (MLC2) and MMP9. *Blood*. 2009;114(19):4221-4232.
140. Smith EC, Thon JN, Devine MT, et al. MKL1 and MKL2 play redundant and crucial roles in megakaryocyte maturation and platelet formation. *Blood*. 2012;120(11):2317-2329.
141. Lecine P, Villeval JL, Vyas P, Swencki B, Xu Y, Shivdasani RA. Mice lacking transcription factor NF-E2 provide in vivo validation of the proplatelet model of thrombocytopoiesis and show a platelet production defect that is intrinsic to megakaryocytes. *Blood*. 1998;92(5):1608-1616.
142. Lecine P, Italiano JE, Kim S-W, Villeval J-L, Shivdasani RA. Hematopoietic-specific β1 tubulin participates in a pathway of platelet biogenesis dependent on the transcription factor NF-E2. *Blood*. 2000;96(4):1366-1373.
143. Schwer HD, Lecine P, Tiwari S, Italiano JE, Jr., Hartwig JH, Shivdasani RA. A lineage-restricted and divergent beta-tubulin isoform is essential for the biogenesis, structure and function of blood platelets. *Curr Biol*. 2001;11(8):579-586.
144. Kunishima S, Kobayashi R, Itoh TJ, Hamaguchi M, Saito H. Mutation of the β1-tubulin gene associated with congenital macrothrombocytopenia affecting microtubule assembly. *Blood*. 2009;113(2):458-461.
145. Goerttler PS, Kreutz C, Donauer J, et al. Gene expression profiling in polycythaemia vera: overexpression of transcription factor NF-E2. *Br J Haematol*. 2005;129(1):138-150.
146. Wang W, Schwemmers S, Hexner EO, Pahl HL. AML1 is overexpressed in patients with myeloproliferative neoplasms and mediates JAK2V617F-independent overexpression of NF-E2. *Blood*. 2010;116(2):254-266.
147. Patel-Hett S, Wang H, Begonja AJ, et al. The spectrin-based membrane skeleton stabilizes mouse megakaryocyte membrane systems and is essential for proplatelet and platelet formation. *Blood*. 2011;118(6):1641-1652.
148. Weisenberg RC. Microtubule formation in vitro in solutions containing low calcium concentrations. *Science (New York, NY)*. 1972;177(4054):1104-1105.
149. Chrétien D, Metoz F, Verde F, Karsenti E, Wade RH. Lattice defects in microtubules: protofilament numbers vary within individual microtubules. *The Journal of Cell Biology*. 1992;117(5):1031-1040.
150. White JG, Krivit W. An ultrastructural basis for the shape changes induced in platelets by chilling. *Blood*. 1967;30(5):625-635.
151. Kunishima S, Kobayashi R, Itoh TJ, Hamaguchi M, Saito H. Mutation of the beta1-tubulin gene associated with congenital macrothrombocytopenia affecting microtubule assembly. *Blood*. 2009;113(2):458-461.

152. Walker RA, O'Brien ET, Pryer NK, et al. Dynamic instability of individual microtubules analyzed by video light microscopy: rate constants and transition frequencies. *J Cell Biol*. 1988;107(4):1437-1448.

153. Mitchison T, Kirschner M. Dynamic instability of microtubule growth. *Nature*. 1984;312(5991):237-242.

154. Akhmanova A, Steinmetz MO. Microtubule +TIPs at a glance. *J Cell Sci*. 2010;123(Pt 20):3415-3419.

155. Rubin CI, Atweh GF. The role of stathmin in the regulation of the cell cycle. *J Cell Biochem*. 2004;93(2):242-250.

156. Song Y, Brady ST. Post-translational modifications of tubulin: pathways to functional diversity of microtubules. *Trends Cell Biol*. 2015;25(3):125-136.

157. Strassel C, Magiera MM, Dupuis A, et al. An essential role for alpha4A-tubulin in platelet biogenesis. *Life Sci Alliance*. 2019;2(1).

158. Grosse R, Vartiainen MK. To be or not to be assembled: progressing into nuclear actin filaments. *Nat Rev Mol Cell Biol*. 2013;14(11):693-697.

159. Plessner M, Grosse R. Extracellular signaling cues for nuclear actin polymerization. *Eur J Cell Biol*. 2015;94(7-9):359-362.

160. Baarlink C, Wang H, Grosse R. Nuclear actin network assembly by formins regulates the SRF coactivator MAL. *Science*. 2013;340(6134):864-867.

161. Belin BJ, Lee T, Mullins RD. DNA damage induces nuclear actin filament assembly by Formin -2 and Spire-(1/2) that promotes efficient DNA repair. [corrected]. *Elife*. 2015;4:e07735.

162. Plessner M, Melak M, Chinchilla P, Baarlink C, Grosse R. Nuclear F-actin formation and reorganization upon cell spreading. *J Biol Chem*. 2015;290(18):11209-11216.

163. Baarlink C, Plessner M, Sherrard A, et al. A transient pool of nuclear F-actin at mitotic exit controls chromatin organization. *Nat Cell Biol*. 2017;19(12):1389-1399.

164. Pollard TD, Mooseker MS. Direct measurement of actin polymerization rate constants by electron microscopy of actin filaments nucleated by isolated microvillus cores. *J Cell Biol*. 1981;88(3):654-659.

165. Pollard TD. Actin and Actin-Binding Proteins. *Cold Spring Harb Perspect Biol*. 2016;8(8).

166. Oda T, Iwasa M, Aihara T, Maeda Y, Narita A. The nature of the globular- to fibrous-actin transition. *Nature*. 2009;457(7228):441-445.

167. Tondeleir D, Vandamme D, Vandekerckhove J, Ampe C, Lambrechts A. Actin isoform expression patterns during mammalian development and in pathology: Insights from mouse models. *Cell Motility*. 2009;66(10):798-815.

168. Ghalloussi D, Dhenge A, Bergmeier W. New insights into cytoskeletal remodeling during platelet production. *J Thromb Haemost*. 2019;17(9):1430-1439.

169. Courtemanche N, Pollard TD. Interaction of profilin with the barbed end of actin filaments. *Biochemistry*. 2013;52(37):6456-6466.

170. Xue B, Leyrat C, Grimes JM, Robinson RC. Structural basis of thymosin-beta4/profilin exchange leading to actin filament polymerization. *Proc Natl Acad Sci U S A*. 2014;111(43):E4596-4605.

171. Bender M, Stritt S, Nurden P, et al. Megakaryocyte-specific Profilin1-deficiency alters microtubule stability and causes a Wiskott-Aldrich syndrome-like platelet defect. *Nat Commun*. 2014;5:4746.

172. Faix J, Grosse R. Staying in shape with formins. *Dev Cell*. 2006;10(6):693-706.

173. Symons M, Derry JM, Karlak B, et al. Wiskott-Aldrich syndrome protein, a novel effector for the GTPase CDC42Hs, is implicated in actin polymerization. *Cell*. 1996;84(5):723-734.

174. de la Fuente MA, Sasahara Y, Calamito M, et al. WIP is a chaperone for Wiskott-Aldrich syndrome protein (WASP). *Proc Natl Acad Sci U S A*. 2007;104(3):926-931.

175. Falet H, Marchetti MP, Hoffmeister KM, Massaad MJ, Geha RS, Hartwig JH. Platelet-associated IgAs and impaired GPVI responses in platelets lacking WIP. *Blood*. 2009;114(21):4729-4737.

176. Paul DS, Casari C, Wu C, et al. Deletion of the Arp2/3 complex in megakaryocytes leads to microthrombocytopenia in mice. *Blood Adv*. 2017;1(18):1398-1408.

177. Sabri S, Foudi A, Boukour S, et al. Deficiency in the Wiskott-Aldrich protein induces premature proplatelet formation and platelet production in the bone marrow compartment. *Blood*. 2006;108(1):134-140.

178. Kahr WH, Pluthero FG, Elkadri A, et al. Loss of the Arp2/3 complex component ARPC1B causes platelet abnormalities and predisposes to inflammatory disease. *Nat Commun*. 2017;8:14816.

179. Villa A, Notarangelo L, Macchi P, et al. X-linked thrombocytopenia and Wiskott-Aldrich syndrome are allelic diseases with mutations in the WASP gene. *Nat Genet*. 1995;9(4):414-417.

180. Zhu Q, Zhang M, Blaese RM, et al. The Wiskott-Aldrich syndrome and X-linked congenital thrombocytopenia are caused by mutations of the same gene. *Blood*. 1995;86(10):3797-3804.

181. Thrasher AJ, Burns SO. WASP: a key immunological multitasker. *Nat Rev Immunol*. 2010;10(3):182-192.

182. Lanzi G, Moratto D, Vairo D, et al. A novel primary human immunodeficiency due to deficiency in the WASP-interacting protein WIP. *J Exp Med*. 2012;209(1):29-34.

183. Curcio C, Pannellini T, Lanzardo S, Forni G, Musiani P, Anton IM. WIP null mice display a progressive immunological disorder that resembles Wiskott-Aldrich syndrome. *J Pathol*. 2007;211(1):67-75.

184. Paul AS, Pollard TD. Review of the mechanism of processive actin filament elongation by formins. *Cell Motil Cytoskeleton*. 2009;66(8):606-617.

185. Harris ES, Higgs HN. Actin cytoskeleton: formins lead the way. *Curr Biol*. 2004;14(13):R520-522.

186. Zigmond SH, Evangelista M, Boone C, et al. Formin leaky cap allows elongation in the presence of tight capping proteins. *Curr Biol*. 2003;13(20):1820-1823.
187. Pan J, Lordier L, Meyran D, et al. The formin DIAPH1 (mDia1) regulates megakaryocyte proplatelet formation by remodeling the actin and microtubule cytoskeletons. *Blood*. 2014;124(26):3967-3977.
188. Stritt S, Nurden P, Turro E, et al. A gain-of-function variant in DIAPH1 causes dominant macrothrombocytopenia and hearing loss. *Blood*. 2016;127(23):2903-2914.
189. Carlier MF, Laurent V, Santolini J, et al. Actin depolymerizing factor (ADF/cofilin) enhances the rate of filament turnover: implication in actin-based motility. *J Cell Biol*. 1997;136(6):1307-1322.
190. McCullough BR, Grintsevich EE, Chen CK, et al. Cofilin-linked changes in actin filament flexibility promote severing. *Biophys J*. 2011;101(1):151-159.
191. Bender M, Eckly A, Hartwig JH, et al. ADF/n-cofilin-dependent actin turnover determines platelet formation and sizing. *Blood*. 2010;116(10):1767-1775.
192. Estevez B, Stojanovic-Terpo A, Delaney MK, et al. LIM kinase-1 selectively promotes glycoprotein Ib-IX-mediated TXA2 synthesis, platelet activation, and thrombosis. *Blood*. 2013;121(22):4586-4594.
193. Johnston AB, Collins A, Goode BL. High-speed depolymerization at actin filament ends jointly catalysed by Twinfilin and Srv2/CAP. *Nat Cell Biol*. 2015;17(11):1504-1511.
194. Paavilainen VO, Oksanen E, Goldman A, Lappalainen P. Structure of the actin-depolymerizing factor homology domain in complex with actin. *J Cell Biol*. 2008;182(1):51-59.
195. Stritt S, Beck S, Becker IC, et al. Twinfilin 2a regulates platelet reactivity and turnover in mice. *Blood*. 2017;130(15):1746-1756.
196. Becker IC, Scheller I, Wackerbarth LM, et al. Actin/microtubule crosstalk during platelet biogenesis in mice is critically regulated by Twinfilin1 and Cofilin1. *Blood Adv*. 2020;4(10):2124-2134.
197. Scheller I, Stritt S, Beck S, et al. Coactosin-like 1 integrates signaling critical for shear-dependent thrombus formation in mouse platelets. *Haematologica*. 2020;105(6):1667-1676.
198. Balduini CL, Pecci A, Savoia A. Recent advances in the understanding and management of MYH9-related inherited thrombocytopenias. *Br J Haematol*. 2011;154(2):161-174.
199. Vicente-Manzanares M, Ma X, Adelstein RS, Horwitz AR. Non-muscle myosin II takes centre stage in cell adhesion and migration. *Nat Rev Mol Cell Biol*. 2009;10(11):778-790.
200. Roy A, Lordier L, Mazzi S, et al. Activity of nonmuscle myosin II isoforms determines localization at the cleavage furrow of megakaryocytes. *Blood*. 2016;128(26):3137-3145.
201. Zhang Y, Conti MA, Malide D, et al. Mouse models of MYH9-related disease: mutations in nonmuscle myosin II-A. *Blood*. 2012;119(1):238-250.
202. Chen Y, Boukour S, Milloud R, et al. The abnormal proplatelet formation in MYH9-related macrothrombocytopenia results from an increased actomyosin contractility and is rescued by myosin IIA inhibition. *J Thromb Haemost*. 2013;11(12):2163-2175.
203. Eckly A, Strassel C, Freund M, et al. Abnormal megakaryocyte morphology and proplatelet formation in mice with megakaryocyte-restricted MYH9 inactivation. *Blood*. 2009;113(14):3182-3189.
204. Rosenberg S, Stracher A. Effect of actin-binding protein on the sedimentation properties of actin. *J Cell Biol*. 1982;94(1):51-55.
205. Rosenberg S, Stracher A, Burridge K. Isolation and characterization of a calcium-sensitive alpha-actinin-like protein from human platelet cytoskeletons. *J Biol Chem*. 1981;256(24):12986-12991.
206. Flanagan LA, Chou J, Falet H, Neujahr R, Hartwig JH, Stossel TP. Filamin A, the Arp2/3 complex, and the morphology and function of cortical actin filaments in human melanoma cells. *J Cell Biol*. 2001;155(4):511-517.
207. Stossel TP, Condeelis J, Cooley L, et al. Filamins as integrators of cell mechanics and signalling. *Nat Rev Mol Cell Biol*. 2001;2(2):138-145.
208. Ohta Y, Suzuki N, Nakamura S, Hartwig JH, Stossel TP. The small GTPase RalA targets filamin to induce filopodia. *Proc Natl Acad Sci U S A*. 1999;96(5):2122-2128.
209. Kovacsovics TJ, Bachelot C, Toker A, et al. Phosphoinositide 3-kinase inhibition spares actin assembly in activating platelets but reverses platelet aggregation. *J Biol Chem*. 1995;270(19):11358-11366.
210. Gorlin JB, Henske E, Warren ST, et al. Actin-binding protein (ABP-280) filamin gene (FLN) maps telomeric to the color vision locus (R/GCP) and centromeric to G6PD in Xq28. *Genomics*. 1993;17(2):496-498.
211. Falet H, Pollitt AY, Begonja AJ, et al. A novel interaction between FlnA and Syk regulates platelet ITAM-mediated receptor signaling and function. *J Exp Med*. 2010;207(9):1967-1979.
212. Jurak Begonja A, Hoffmeister KM, Hartwig JH, Falet H. FlnA-null megakaryocytes prematurely release large and fragile platelets that circulate poorly. *Blood*. 2011;118(8):2285-2295.
213. Ware J, Russell S, Ruggeri ZM. Generation and rescue of a murine model of platelet dysfunction: the Bernard-Soulier syndrome. *Proc Natl Acad Sci U S A*. 2000;97(6):2803-2808.
214. Kato K, Martinez C, Russell S, et al. Genetic deletion of mouse platelet glycoprotein Ibbeta produces a Bernard-Soulier phenotype with increased alpha-granule size. *Blood*. 2004;104(8):2339-2344.
215. Falet H, Pollitt AY, Begonja AJ, et al. A novel interaction between FlnA and Syk regulates platelet ITAM-mediated receptor signaling and function. *The Journal of Experimental Medicine*. 2010;207(9):1967-1979.
216. Kanaji T, Ware J, Okamura T, Newman PJ. GPIbα regulates platelet size by controlling the subcellular localization of filamin. *Blood*. 2012;119(12):2906-2913.

217. Kunishima S, Okuno Y, Yoshida K, et al. ACTN1 mutations cause congenital macrothrombocytopenia. *Am J Hum Genet*. 2013;92(3):431-438.
218. Gueguen P, Rouault K, Chen JM, et al. A missense mutation in the alpha-actinin 1 gene (ACTN1) is the cause of autosomal dominant macrothrombocytopenia in a large French family. *PLoS One*. 2013;8(9):e74728.
219. Bottega R, Marconi C, Faleschini M, et al. ACTN1-related thrombocytopenia: identification of novel families for phenotypic characterization. *Blood*. 2015;125(5):869-872.
220. Patel SR, Richardson JL, Schulze H, et al. Differential roles of microtubule assembly and sliding in proplatelet formation by megakaryocytes. *Blood*. 2005;106(13):4076-4085.
221. Machlus KR, Thon JN, Italiano JE, Jr. Interpreting the developmental dance of the megakaryocyte: a review of the cellular and molecular processes mediating platelet formation. *Br J Haematol*. 2014;165(2):227-236.
222. Bender M, Thon JN, Ehrlicher AJ, et al. Microtubule sliding drives proplatelet elongation and is dependent on cytoplasmic dynein. *Blood*. 2015;125(5):860-868.
223. Richardson JL, Shivdasani RA, Boers C, Hartwig JH, Italiano JE, Jr. Mechanisms of organelle transport and capture along proplatelets during platelet production. *Blood*. 2005;106(13):4066-4075.
224. Schachtner H, Calaminus SD, Sinclair A, et al. Megakaryocytes assemble podosomes that degrade matrix and protrude through basement membrane. *Blood*. 2013;121(13):2542-2552.
225. Eckly A, Scandola C, Oprescu A, et al. Megakaryocytes use in vivo podosome-like structures working collectively to penetrate the endothelial barrier of bone marrow sinusoids. *J Thromb Haemost*. 2020.
226. Spindler M, van Eeuwijk JMM, Schurr Y, et al. ADAP deficiency impairs megakaryocyte polarization with ectopic proplatelet release and causes microthrombocytopenia. *Blood*. 2018;132(6):635-646.
227. Brown E, Carlin LM, Nerlov C, Lo Celso C, Poole AW. Multiple membrane extrusion sites drive megakaryocyte migration into bone marrow blood vessels. *Life Science Alliance*. 2018;1(2).
228. Italiano JE, Patel‐Hett S, Hartwig JH. Mechanics of proplatelet elaboration. *Journal of Thrombosis and Haemostasis*. 2007;5(s1):18-23.
229. Heasman SJ, Ridley AJ. Mammalian Rho GTPases: new insights into their functions from in vivo studies. *Nat Rev Mol Cell Biol*. 2008;9(9):690-701.
230. Haga RB, Ridley AJ. Rho GTPases: Regulation and roles in cancer cell biology. *Small GTPases*. 2016;7(4):207-221.
231. Jaffe AB, Hall A. Rho GTPases: biochemistry and biology. *Annu Rev Cell Dev Biol*. 2005;21:247-269.
232. Pleines I, Eckly A, Elvers M, et al. Multiple alterations of platelet functions dominated by increased secretion in mice lacking Cdc42 in platelets. *Blood*. 2010;115(16):3364-3373.
233. Clayton NS, Ridley AJ. Targeting Rho GTPase Signaling Networks in Cancer. *Front Cell Dev Biol*. 2020;8:222.
234. Tiedt R, Schomber T, Hao-Shen H, Skoda RC. Pf4-Cre transgenic mice allow the generation of lineage-restricted gene knockouts for studying megakaryocyte and platelet function in vivo. *Blood*. 2007;109(4):1503-1506.
235. Pedersen E, Brakebusch C. Rho GTPase function in development: how in vivo models change our view. *Experimental Cell Research*. 2012;318(14):1779-1787.
236. Velasco-Hernandez T, Säwén P, Bryder D, Cammenga J. Potential Pitfalls of the Mx1-Cre System: Implications for Experimental Modeling of Normal and Malignant Hematopoiesis. *Stem Cell Reports*. 2016;7(1):11-18.
237. Pertuy F, Aguilar A, Strassel C, et al. Broader expression of the mouse platelet factor 4-cre transgene beyond the megakaryocyte lineage. *J Thromb Haemost*. 2015;13(1):115-125.
238. Nagy Z, Vogtle T, Geer MJ, et al. The Gp1ba-Cre transgenic mouse: a new model to delineate platelet and leukocyte functions. *Blood*. 2019;133(4):331-343.
239. Aslan JE, McCarty OJ. Rho GTPases in platelet function. *J Thromb Haemost*. 2013;11(1):35-46.
240. Pleines I, Dutting S, Cherpokova D, et al. Defective tubulin organization and proplatelet formation in murine megakaryocytes lacking Rac1 and Cdc42. *Blood*. 2013;122(18):3178-3187.
241. Wen Y, Eng CH, Schmoranzer J, et al. EB1 and APC bind to mDia to stabilize microtubules downstream of Rho and promote cell migration. *Nat Cell Biol*. 2004;6(9):820-830.
242. Palazzo A, Bluteau O, Messaoudi K, et al. The cell division control protein 42-Src family kinase-neural Wiskott-Aldrich syndrome protein pathway regulates human proplatelet formation. *J Thromb Haemost*. 2016;14(12):2524-2535.
243. Chen Z, Naveiras O, Balduini A, et al. The May-Hegglin anomaly gene MYH9 is a negative regulator of platelet biogenesis modulated by the Rho-ROCK pathway. *Blood*. 2007;110(1):171-179.
244. Chang Y, Aurade F, Larbret F, et al. Proplatelet formation is regulated by the Rho/ROCK pathway. *Blood*. 2007;109(10):4229-4236.
245. Suzuki A, Shin JW, Wang Y, et al. RhoA is essential for maintaining normal megakaryocyte ploidy and platelet generation. *PLoS One*. 2013;8(7):e69315.
246. Pleines I, Hagedorn I, Gupta S, et al. Megakaryocyte-specific RhoA deficiency causes macrothrombocytopenia and defective platelet activation in hemostasis and thrombosis. *Blood*. 2012;119(4):1054-1063.
247. Pecci A, Malara A, Badalucco S, et al. Megakaryocytes of patients with MYH9-related thrombocytopenia present an altered proplatelet formation. *Thromb Haemost*. 2009;102(1):90-96.

248. Basant A, Glotzer M. Spatiotemporal Regulation of RhoA during Cytokinesis. *Curr Biol*. 2018;28(9):R570-R580.

249. Gao Y, Smith E, Ker E, et al. Role of RhoA-specific guanine exchange factors in regulation of endomitosis in megakaryocytes. *Dev Cell*. 2012;22(3):573-584.

250. Lordier L, Bluteau D, Jalil A, et al. RUNX1-induced silencing of non-muscle myosin heavy chain IIB contributes to megakaryocyte polyploidization. *Nat Commun*. 2012;3:717.

251. Dutting S, Gaits-Iacovoni F, Stegner D, et al. A Cdc42/RhoA regulatory circuit downstream of glycoprotein Ib guides transendothelial platelet biogenesis. *Nat Commun*. 2017;8:15838.

252. Villeval JL, Cohen-Solal K, Tulliez M, et al. High thrombopoietin production by hematopoietic cells induces a fatal myeloproliferative syndrome in mice. *Blood*. 1997;90(11):4369-4383.

253. Nieswandt B, Bergmeier W, Rackebrandt K, Gessner JE, Zirngibl H. Identification of critical antigen-specific mechanisms in the development of immune thrombocytopenic purpura in mice. *Blood*. 2000;96(7):2520-2527.

254. Massberg S, Gawaz M, Gruner S, et al. A crucial role of glycoprotein VI for platelet recruitment to the injured arterial wall in vivo. *J Exp Med*. 2003;197(1):41-49.

255. Nieswandt B, Schulte V, Bergmeier W, et al. Long-term antithrombotic protection by in vivo depletion of platelet glycoprotein VI in mice. *J Exp Med*. 2001;193(4):459-469.

256. May F, Hagedorn I, Pleines I, et al. CLEC-2 is an essential platelet-activating receptor in hemostasis and thrombosis. *Blood*. 2009;114(16):3464-3472.

257. Nieswandt B, Bergmeier W, Schulte V, Rackebrandt K, Gessner JE, Zirngibl H. Expression and function of the mouse collagen receptor glycoprotein VI is strictly dependent on its association with the FcRgamma chain. *J Biol Chem*. 2000;275(31):23998-24002.

258. Bergmeier W, Rackebrandt K, Schroder W, Zirngibl H, Nieswandt B. Structural and functional characterization of the mouse von Willebrand factor receptor GPIb-IX with novel monoclonal antibodies. *Blood*. 2000;95(3):886-893.

259. Bergmeier W, Schulte V, Brockhoff G, Bier U, Zirngibl H, Nieswandt B. Flow cytometric detection of activated mouse integrin alphaIIbbeta3 with a novel monoclonal antibody. *Cytometry*. 2002;48(2):80-86.

260. Schulte V, Rabie T, Prostredna M, Aktas B, Gruner S, Nieswandt B. Targeting of the collagen-binding site on glycoprotein VI is not essential for in vivo depletion of the receptor. *Blood*. 2003;101(10):3948-3952.

261. Unkeless JC. Characterization of a monoclonal antibody directed against mouse macrophage and lymphocyte Fc receptors. *J Exp Med*. 1979;150(3):580-596.

262. Nieswandt B, Echtenacher B, Wachs FP, et al. Acute systemic reaction and lung alterations induced by an antiplatelet integrin gpIIb/IIIa antibody in mice. *Blood*. 1999;94(2):684-693.

263. Raghavan S, Bauer C, Mundschau G, Li Q, Fuchs E. Conditional ablation of beta1 integrin in skin. Severe defects in epidermal proliferation, basement membrane formation, and hair follicle invagination. *J Cell Biol*. 2000;150(5):1149-1160.

264. Petrich BG, Marchese P, Ruggeri ZM, et al. Talin is required for integrin-mediated platelet function in hemostasis and thrombosis. *J Exp Med*. 2007;204(13):3103-3111.

265. Aurbach K, Spindler M, Haining EJ, Bender M, Pleines I. Blood collection, platelet isolation and measurement of platelet count and size in mice-a practical guide. *Platelets*. 2019;30(6):698-707.

266. van de Linde S, Loschberger A, Klein T, et al. Direct stochastic optical reconstruction microscopy with standard fluorescent probes. *Nat Protoc*. 2011;6(7):991-1009.

267. Wolter S, Loschberger A, Holm T, et al. rapidSTORM: accurate, fast open-source software for localization microscopy. *Nat Methods*. 2012;9(11):1040-1041.

268. Amend SR, Valkenburg KC, Pienta KJ. Murine Hind Limb Long Bone Dissection and Bone Marrow Isolation. *J Vis Exp*. 2016(110).

269. Morodomi Y, Kanaji S, Won E, Kawamoto T, Kanaji T. Modified application of Kawamoto's film method for super-resolution imaging of megakaryocytes in undecalcified bone marrow. *Res Pract Thromb Haemost*. 2020;4(1):86-91.

270. Kawamoto T, Shimizu M. A method for preparing 2- to 50-micron-thick fresh-frozen sections of large samples and undecalcified hard tissues. *Histochem Cell Biol*. 2000;113(5):331-339.

271. Cervero P, Panzer L, Linder S. Podosome reformation in macrophages: assays and analysis. *Methods Mol Biol*. 2013;1046:97-121.

272. Reddy P, Negrin R, Hill GR. Mouse models of bone marrow transplantation. *Biol Blood Marrow Transplant*. 2008;14(1 Suppl 1):129-135.

273. Abarrategi A, Mian SA, Passaro D, Rouault-Pierre K, Grey W, Bonnet D. Modeling the human bone marrow niche in mice: From host bone marrow engraftment to bioengineering approaches. *The Journal of Experimental Medicine*. 2018;215(3):729-743.

274. Dobson KR, Reading L, Haberey M, Marine X, Scutt A. Centrifugal isolation of bone marrow from bone: an improved method for the recovery and quantitation of bone marrow osteoprogenitor cells from rat tibiae and femurae. *Calcif Tissue Int*. 1999;65(5):411-413.

275. Heib T, Gross C, Muller ML, Stegner D, Pleines I. Isolation of murine bone marrow by centrifugation or flushing for the analysis of hematopoietic cells - a comparative study. *Platelets*. 2020:1-7.

276. Pleines I, Dütting S, Cherpokova D, et al. Defective tubulin organization and proplatelet formation in murine megakaryocytes lacking Rac1 and Cdc42. *Blood*. 2013;122(18):3178-3187.
277. Strassel C, Eckly A, Léon C, et al. Hirudin and heparin enable efficient megakaryocyte differentiation of mouse bone marrow progenitors. *Experimental cell research*. 2012;318(1):25-32.
278. Hartwig JH, Italiano JE, Jr. Cytoskeletal mechanisms for platelet production. *Blood Cells Mol Dis*. 2006;36(2):99-103.
279. Cherpokova D. Studies on modulators of platelet (hem)ITAM signaling and platelet production in genetically modified mice
Untersuchungen an Modulatoren des thrombozytären (hem)ITAM-Signalwegs und der Thrombozytenbildung in genetisch veränderten Mäusen; 2017.
280. Kaushansky K. Determinants of platelet number and regulation of thrombopoiesis. *Hematology Am Soc Hematol Educ Program*. 2009:147-152.
281. Strassel C, Eckly A, Leon C, et al. Hirudin and heparin enable efficient megakaryocyte differentiation of mouse bone marrow progenitors. *Exp Cell Res*. 2012;318(1):25-32.
282. Eckly A, Strassel C, Cazenave JP, Lanza F, Leon C, Gachet C. Characterization of megakaryocyte development in the native bone marrow environment. *Methods Mol Biol*. 2012;788:175-192.
283. Josefsson EC, Burnett DL, Lebois M, et al. Platelet production proceeds independently of the intrinsic and extrinsic apoptosis pathways. *Nat Commun*. 2014;5:3455.
284. Zhang J, Shehabeldin A, da Cruz LA, et al. Antigen receptor-induced activation and cytoskeletal rearrangement are impaired in Wiskott-Aldrich syndrome protein-deficient lymphocytes. *J Exp Med*. 1999;190(9):1329-1342.
285. Snapper SB, Rosen FS, Mizoguchi E, et al. Wiskott-Aldrich syndrome protein-deficient mice reveal a role for WASP in T but not B cell activation. *Immunity*. 1998;9(1):81-91.
286. Avanzi MP, Goldberg F, Davila J, Langhi D, Chiattone C, Mitchell WB. Rho kinase inhibition drives megakaryocyte polyploidization and proplatelet formation through MYC and NFE2 downregulation. *Br J Haematol*. 2014;164(6):867-876.
287. Rottner K, Faix J, Bogdan S, Linder S, Kerkhoff E. Actin assembly mechanisms at a glance. *J Cell Sci*. 2017;130(20):3427-3435.
288. Kauskot A, Poirault-Chassac S, Adam F, et al. LIM kinase/cofilin dysregulation promotes macrothrombocytopenia in severe von Willebrand disease-type 2B. *JCI Insight*. 2016;1(16):e88643.
289. Mori J, Nagy Z, Di Nunzio G, et al. Maintenance of murine platelet homeostasis by the kinase Csk and phosphatase CD148. *Blood*. 2018;131(10):1122-1144.
290. Webster DR, Borisy GG. Microtubules are acetylated in domains that turn over slowly. *J Cell Sci*. 1989;92 ( Pt 1):57-65.
291. Webster DR, Wehland J, Weber K, Borisy GG. Detyrosination of alpha tubulin does not stabilize microtubules in vivo. *J Cell Biol*. 1990;111(1):113-122.
292. Smith EC, Teixeira AM, Chen RC, et al. Induction of megakaryocyte differentiation drives nuclear accumulation and transcriptional function of MKL1 via actin polymerization and RhoA activation. *Blood*. 2013;121(7):1094-1101.
293. Pleines I, Woods J, Chappaz S, et al. Mutations in tropomyosin 4 underlie a rare form of human macrothrombocytopenia. *J Clin Invest*. 2017;127(3):814-829.
294. Nurden AT. Glanzmann thrombasthenia. *Orphanet Journal of Rare Diseases*. 2006;1:10.
295. Nieswandt B, Brakebusch C, Bergmeier W, et al. Glycoprotein VI but not α2β1 integrin is essential for platelet interaction with collagen. *The EMBO Journal*. 2001;20(9):2120-2130.
296. Semeniak D, Kulawig R, Stegner D, et al. Proplatelet formation is selectively inhibited by collagen type I through Syk-independent GPVI signaling. *Journal of Cell Science*. 2016;129(18):3473-3484.
297. Giannini S, Lee-Sundlov MM, Rivadeneyra L, et al. β4GALT1 controls β1 integrin function to govern thrombopoiesis and hematopoietic stem cell homeostasis. *Nature Communications*. 2020;11(1):1-15.
298. Petzold T, Ruppert R, Pandey D, et al. β1 integrin−mediated signals are required for platelet granule secretion and hemostasis in mouse. *Blood*. 2013;122(15):2723-2731.
299. Calderwood DA, Campbell ID, Critchley DR. Talins and kindlins: partners in integrin-mediated adhesion. *Nat Rev Mol Cell Biol*. 2013;14(8):503-517.
300. Nieswandt B, Moser M, Pleines I, et al. Loss of talin1 in platelets abrogates integrin activation, platelet aggregation, and thrombus formation in vitro and in vivo. *J Exp Med*. 2007;204(13):3113-3118.
301. Monkley SJ, Zhou XH, Kinston SJ, et al. Disruption of the talin gene arrests mouse development at the gastrulation stage. *Dev Dyn*. 2000;219(4):560-574.
302. Tefferi A. Myelofibrosis with myeloid metaplasia. *N Engl J Med*. 2000;342(17):1255-1265.
303. Badalucco S, Di Buduo CA, Campanelli R, et al. Involvement of TGFbeta1 in autocrine regulation of proplatelet formation in healthy subjects and patients with primary myelofibrosis. *Haematologica*. 2013;98(4):514-517.
304. Ciurea SO, Merchant D, Mahmud N, et al. Pivotal contributions of megakaryocytes to the biology of idiopathic myelofibrosis. *Blood*. 2007;110(3):986-993.

305. Calaminus SD, Guitart AV, Sinclair A, et al. Lineage tracing of Pf4-Cre marks hematopoietic stem cells and their progeny. *PLoS One*. 2012;7(12):e51361.
306. Quach ME, Chen W, Li R. Mechanisms of platelet clearance and translation to improve platelet storage. *Blood*. 2018;131(14):1512-1521.
307. Geue S, Aurbach K, Manke M-C, et al. Pivotal role of PDK1 in megakaryocyte cytoskeletal dynamics and polarization during platelet biogenesis. *Blood*. 2019;134(21):1847-1858.
308. Stegner D, Hofmann S, Schuhmann MK, et al. Loss of Orai2-Mediated Capacitative Ca(2+) Entry Is Neuroprotective in Acute Ischemic Stroke. *Stroke*. 2019;50(11):3238-3245.
309. Pang L, Weiss MJ, Poncz M. Megakaryocyte biology and related disorders. *J Clin Invest*. 2005;115(12):3332-3338.
310. Freson K, Devriendt K, Matthijs G, et al. Platelet characteristics in patients with X-linked macrothrombocytopenia because of a novel GATA1 mutation. *Blood*. 2001;98(1):85-92.
311. Zeiler M, Moser M, Mann M. Copy number analysis of the murine platelet proteome spanning the complete abundance range. *Mol Cell Proteomics*. 2014;13(12):3435-3445.
312. Burkhart JM, Vaudel M, Gambaryan S, et al. The first comprehensive and quantitative analysis of human platelet protein composition allows the comparative analysis of structural and functional pathways. *Blood*. 2012;120(15):e73-82.
313. McGee KM, Vartiainen MK, Khaw PT, Treisman R, Bailly M. Nuclear transport of the serum response factor coactivator MRTF-A is downregulated at tensional homeostasis. *EMBO Rep*. 2011;12(9):963-970.
314. Rajakyla EK, Vartiainen MK. Rho, nuclear actin, and actin-binding proteins in the regulation of transcription and gene expression. *Small GTPases*. 2014;5:e27539.
315. Davenport P, Liu ZJ, Sola-Visner M. Changes in megakaryopoiesis over ontogeny and their implications in health and disease. *Platelets*. 2020:1-8.
316. Margraf A, Nussbaum C, Sperandio M. Ontogeny of platelet function. *Blood Adv*. 2019;3(4):692-703.
317. Favaloro EJ. Collagen binding assay for von Willebrand factor (VWF:CBA): detection of von Willebrands Disease (VWD), and discrimination of VWD subtypes, depends on collagen source. *Thrombosis and Haemostasis*. 2000;83(1):127-135.
318. Schachtner H, Calaminus SD, Thomas SG, Machesky LM. Podosomes in adhesion, migration, mechanosensing and matrix remodeling. *Cytoskeleton (Hoboken)*. 2013;70(10):572-589.
319. Luo R, Jeong SJ, Jin Z, Strokes N, Li S, Piao X. G protein-coupled receptor 56 and collagen III, a receptor-ligand pair, regulates cortical development and lamination. *Proc Natl Acad Sci U S A*. 2011;108(31):12925-12930.
320. Saha HR, Kaneda-Nakashima K, Shimosaki S, et al. Suppression of GPR56 expression by pyrrole-imidazole polyamide represents a novel therapeutic drug for AML with high EVI1 expression. *Sci Rep*. 2018;8(1):13741.
321. Bazzoni G, Shih D-T, Buck CA, Hemler ME. Monoclonal Antibody 9EG7 Defines a Novel β1 Integrin Epitope Induced by Soluble Ligand and Manganese, but Inhibited by Calcium. *Journal of Biological Chemistry*. 1995;270(43):25570-25577.
322. Bury L, Falcinelli E, Chiasserini D, Springer TA, Italiano JE, Jr., Gresele P. Cytoskeletal perturbation leads to platelet dysfunction and thrombocytopenia in variant forms of Glanzmann thrombasthenia. *Haematologica*. 2016;101(1):46-56.
323. Kashiwagi H, Kunishima S, Kiyomizu K, et al. Demonstration of novel gain-of-function mutations of alphaIIbbeta3: association with macrothrombocytopenia and glanzmann thrombasthenia-like phenotype. *Mol Genet Genomic Med*. 2013;1(2):77-86.
324. Bury L, Malara A, Gresele P, Balduini A. Outside-in signalling generated by a constitutively activated integrin alphaIIbbeta3 impairs proplatelet formation in human megakaryocytes. *PLoS One*. 2012;7(4):e34449.
325. Favier M, Bordet JC, Favier R, et al. Mutations of the integrin alphaIIb/beta3 intracytoplasmic salt bridge cause macrothrombocytopenia and enlarged platelet alpha-granules. *Am J Hematol*. 2018;93(2):195-204.
326. Xu Z, Chen X, Zhi H, et al. Direct interaction of kindlin-3 with integrin alphaIIbbeta3 in platelets is required for supporting arterial thrombosis in mice. *Arterioscler Thromb Vasc Biol*. 2014;34(9):1961-1967.
327. Tan YX, Cui H, Wan LM, et al. Overexpression of heparanase in mice promoted megakaryopoiesis. *Glycobiology*. 2018;28(5):269-275.
328. Hughes DE, Dai A, Tiffee JC, Li HH, Mundy GR, Boyce BF. Estrogen promotes apoptosis of murine osteoclasts mediated by TGF-beta. *Nat Med*. 1996;2(10):1132-1136.
329. Yang Q, Crispino JD, Wen QJ. Kinase signaling and targeted therapy for primary myelofibrosis. *Exp Hematol*. 2017;48:32-38.
330. William BM, An W, Feng D, et al. Fasudil, a clinically safe ROCK inhibitor, decreases disease burden in a Cbl/Cbl-b deficiency-driven murine model of myeloproliferative disorders. *Hematology*. 2016;21(4):218-224.
331. Gollomp K, Poncz M. Gp1ba-Cre or Pf4-Cre: pick your poison. *Blood*. 2019;133(4):287-288.
332. Potts KS, Farley A, Dawson CA, et al. Membrane budding is a major mechanism of in vivo platelet biogenesis. *J Exp Med*. 2020;217(9).

# 7 APPENDIX

## 7.1 Abbreviations

| | |
|---|---|
| 3D | 3-dimensional |
| ABP | Actin-binding proteins |
| ADAP | Adapter protein |
| ADF | Actin-depolymerizing factor |
| ADP | Adenosine di-phosphate |
| AF | Alexa Fluor |
| AMKL | Acute megakaryoblastic leukemia |
| AML | Acute myeloid leukemia |
| AML1 | Acute myeloid leukemia 1 |
| APC | Adenomatous polyposis coli |
| APS | Ammonium peroxodisulfate |
| Arp | Actin-related protein |
| ATP | Adenosine tri-phosphate |
| AU | Arbitrary units |
| BM | Bone marrow |
| BSA | Bovine serum albumin |
| BSS | Bernard-Soulier syndrome |
| BW | Bodyweight |
| CBFB | Core-binding factor, beta subunit |
| CCL5 | Chemokine (C-C motif) ligand 5 |
| CD | Cluster of differentiation |
| Cdc42 | Cell division control protein 42 |
| CMP | Common myeloid progenitor |
| Cof1 | Cofilin 1 |
| Cotl1 | Coactosin-like 1 |
| CP | Capping proteins |
| CRP | Collagen-related peptide |
| CVX | Convulxin |
| CXCL12 | (C-X-C motif) ligand 12 |
| Cy | Cyanine |
| DAPI | 4',6-diamidino-2-phenylindole |
| DDR-1 | Discoid domain receptor 1 |
| DKO | Double-knockout |
| DMS | Demarcation membrane system |
| DMSO | Dimethyl sulfoxide |
| dNTP | Deoxynucleotide triphosphates |
| *d*STORM | Direct stochastical optical reconstruction microscopy |
| DTT | Dithiothreito |
| EB | End-binding proteins |
| ECL | Enhanced chemiluminescence |
| ECM | Extracellular matrix |
| EDTA | Ethylenediaminetetraacetic acid |
| ELC | Essential light chain |
| EPI | Epifluorescence |
| ER | Endoplasmic reticulum |
| ETV6 | ETS variant 6 |
| F-actin | Filamentous actin |
| FcRγ | Fc receptor γ-chain |
| FCS | Fetal calf serum |
| FGF4 | Fibroblast growth factor 4 |
| FITC | Fluorescein isothiocyanate |
| FLC | Fetal liver cell |
| FLI1 | Friend leukaemia virus integration |
| Fln | Filamin |
| FOG1 | Friend of GATA1 |
| FPD | Familial platelet disorder |
| FSC | Forward scatter |
| G-actin | Globular actin |
| GABPA | GA-binding protein TF alpha subunit |
| GAG | Glycosaminoglycan |
| GAP | GTPase-activating protein |
| GDI | Guanine nucleotide-dissociation inhibitor |
| GDP | Guanosine diphosphate |
| GEF | Guanine nucleotide-exchange factor |
| GFI1B | Growth Factor Independent 1B |
| GP | Glycoprotein |
| GPCR | G protein-coupled receptor |
| GTP | Guanosine-5'-triphosphate |
| HBSS | Hank's Balanced Salt Solution |
| HDR | High dynamic range |
| HRP | Horseradish peroxidase |
| HS | Heparan sulfate |
| HSC | Hematopoietic stem cells |
| HSPCs | Hematopoietic stem and progenitor cells |
| IF | Immunofluoresence |
| IL1α | Interleukin 1 alpha |
| IMS | Invaginated membrane system |
| ITAM | Immunoreceptor tyrosine-based activation motif |
| ITIM | Immunoreceptor tyrosine-based inhibiton motif |
| JAK2 | Janus Kinase-2 |
| KCl | Potassium chloride |

| | |
|---|---|
| KI | Knock-in |
| KO | Knockout |
| KO | Knockout |
| LAIR-1 | Leukocyte-associated immunoglobulin-like receptor-1 |
| LAT | Linker of activated T cells |
| LIMK | LIM kinase |
| LIMKi | LIMK inhibitor |
| Lin$^-$ | Lineage negative |
| LT-HSC | Long-term hematopoietic stem cells |
| Mac-1 | Macrophage antigen 1 |
| MAL | Megakaryoblastic leukemia 1 |
| MAPK | Mitogen-activated protein kinase |
| mDia | Mammalian diaphanous |
| MEM | Modified Eagle´s Medium |
| MEP | Megakaryocyte-erythroid progenitor |
| MFI | Mean fluorescence intensity |
| MK | Megakaryocyte |
| MKP | Megakaryocyte progenitor |
| MPL | Myeloproliferative leukemia protein |
| MPP | Multipotent progenitor |
| MRCK | Myotonic dystrophy kinase-related Cdc42-binding kinases |
| MT | Microtubule |
| MYH9-RD | MYH9-related |
| MYL9 | Myosin light chain 9 |
| MYPT1 | Myosin phosphatase 1 |
| $NaH_2PO_4$ | Sodium-Di-HydrogenPhosphate Monohydrate |
| NFE2 | Nuclear Factor, Erythroid 2 |
| NMMII | Non-muscle myosin II |
| O/N | Over night |
| $OsO_4$ | Osmium tetroxide |
| p | Phospho |
| P/S | Penicillin/Streptomycin |
| PAGE | Polyacrylamide Gel Electrophoresis |
| PAK1 | P21 (Rac1) Activated Kinase 1 |
| PBS | Phosphate buffered saline |
| PBS | Phosphate-buffered saline |
| PCR | Polymerase chain reaction |
| PE | R-phycoerythrin |
| Pf4 | Platelet factor 4 |
| PFA | Paraformaldehyde |
| $PGI_2$ | Prostaglandine 2 |
| PMSF | Phenylmethylsulfonyl fluoride |
| PI | Propidium iodide |
| PI3K | Phosphatidylinositol 3-kinase |
| PIPES | Piperazine-N,N′-bis(2-ethanesulfonic acid) |
| PLCγ2 | Phospholipase C gamma 2 |
| PLL | Poly-L-lysine |
| PPF | Proplatelet formation |
| PRP | Platelet-rich-plasma |
| PVDF | Polyvinylidene fluoride |
| PZ | Peripheral zone |
| Rac1 | Ras-related C3 botulinum toxin substrate 1 |
| RalA | Ras-related protein A |
| RANTES | Regulated on activation, normal T cell expressed and secreted |
| RBC | Red blood cell |
| RC | Rhodocytin |
| rHirudin | Recombinant hirudin |
| Rho | Ras homolog family member |
| RLC | Regulatory light chain |
| ROCK | Rho-associated coiled-coil containing protein kinase |
| RUNX1 | Runt-related transcription factor 1 |
| S1P | Sphingosine-1-phosphate |
| SCEM | Super cryo embedding medium |
| SCF | Stem cell factor |
| SD | Standard deviation |
| SDF1α | Stromal cell-derived factor-1 alpha |
| SDS | Sodium dodecyl sulfate |
| SFK | Src family kinases |
| Shp1 | Src homology 2 domain-containing protein-tyrosine phosphatases |
| SRF | Serum response factor |
| SSC | Side scatter |
| STAT | Signal transducer and activator of transcription |
| Syk | Spleen tyrosine kinase |
| TAL1 | T-cell acute lymphocytic leukaemia 1 |
| TBS | Tris-buffered saline |
| TEM | Transmission electron microscopy |
| TEMED | Tetramethylethylenediamine |
| TF | Transcription factors |
| TIRF | Total internal reflection fluorescence |
| TMD | Transient myeoloproliferative disorder |
| TMS | Tubular membrane structures |
| TO | Thiazole orange |
| TPO | Thrombopoietin |
| MPL | Thrombopoietin receptor |
| TRIS | Tris(hydroxymethyl)aminomethane |
| Twf | Twinfilins |

| | |
|---|---|
| UV | Ultra violet |
| V | Volts |
| vWF | Von Willebrand factor |
| WAS | Wiskott-Aldrich-Syndrome |
| WASp | Wiskott-Aldrich syndrome family protein |
| WAVE | WASP-family verprolin-homologous protein |
| WIP | WASp-interacting protein |
| WT | Wild type |

## 7.2 Acknowledgements

The here presented work was performed in the Institute of Experimental Biomedicine I at the University Hospital and Rudolf-Virchow-Center, University of Würzburg, in the group of Prof. Dr. Bernhard Nieswandt between October 2016 and August 2020.

I would like to thank many people, without whom I would not have been able to finish this thesis:

My supervisor Dr. Irina Pleines-Meinhold for her immeasurable support from the start until the very last day, countless ideas, fruitful discussions and her endless encouragement and dedication for our work. I wish you all the best for your future life and career.

Prof. Dr. Bernhard Nieswandt for giving me the opportunity to pursue my PhD in his group, for allowing me to develop own ideas, to present my data at national and international conferences and for introducing me to the scientific community.

My thesis committee members PD Dr. Heike Hermanns and Prof. Dr. Katrin Heinze for scientific discussions and reviewing my thesis.

Dr. Zoltan Nagy for his support, ideas, assistance in many projects as well as proofreading my thesis.

Carina Gross and Dr. David Stegner for their great collaboration and enthusiasm resulting in a joint publication.

Our remaining collaboration partners for contributing to our projects, fruitful scientific discussions and providing vital reagents.

All the members of the ‘MK’ seminar for their support and ideas, which helped to overcome many obstacles, especially Prof. Dr. Harald Schulze, Dr. Georgi Manukjan, Dr. Markus Bender and Dr. Markus Spindler.

A special thanks to Dr. Christine Mais, but also our technicians Juliana, Birgit, Sylvie, Ewa, Daniela and Steffi for their support and their willingness to keep the lab running (even if we sometimes make their life very difficult).

Dr. Katharina Remer and Dr. Heike Wagner, as well as the animal caretakers, without whom our work would not be possible. Thank you for taking such good care of our animals.

The Bioimaging Centre for providing access to the microscopy facility and technical support.

The Graduate School of Life Sciences for allowing us to participate in numerous transferable skill courses and for the coordination of the PhD program.

Isabelle Becker: Thank you so much for everything you did. We became not only great colleagues, but also good friends over the past years. I am amazed by the dedication for the work you do and thankful for your endless support as well as for proofreading my thesis. I wish you all the best for your future life and career.

Lou Wackerbarth: Thank you for deciding to do your master thesis in our lab. I am thankful for your unlimited support not only at but also outside of work, for proofreading my thesis and having you around as a friend. I hope you will be happy in Munich and wish you all the best.

Katja Aurbach: Thank you for introducing me to the work when I started and also the group itself. We had a great time as colleagues with a lot of good (non-)scientific discussions. I wish you all the best for your future in Würzburg.

All other members of Office 3: Stefano (my favorite Italian friend), Bodo, Andreas, Charly, Maxi, Timothy. Also, a big thanks to my colleague and friend Philipp Burkard (Phipsi). Lab life wouldn’t have been the same without all of you.

Dr. Timo Vögtle for proofreading my thesis.

All other members of the Nieswandt lab, who made my time in the group unforgettable and with whom I happily spent countless hours laughing (in the lab and outside). Thank you for providing me with a new bicycle helmet, by the time I really needed a new one.

A big thanks also to all the great people I have met during my one year stay in the USA when I was only 17-years old, especially Sherrol Ledbetter who still helps me out wherever she can in terms of proofreading.

My friends which by now are scattered all around Germany, but also the ones I have met over the past years in Würzburg and especially my good old friends back in Püttlingen, Saarland. Thank you for your support.

Theresa Moos, for keeping my back throughout the past two years and showing me her immeasurable support.

And last my parents Ursula and Eugen, my brother Kevin, as well as the rest of my family and the ones who already passed away: I cannot imagine life without your unlimited love and strength. I can always count on you and your endless support and I am sure, that I would have not finished all of that without you. I am eternally grateful for having you.

## 7.3 Publications

### 7.3.1 Articles

Heib T*, Gross C*, Muller ML, Stegner D, Pleines I. **Isolation of murine bone marrow by centrifugation or flushing for the analysis of hematopoietic cells - a comparative study**. Platelets. 2020:1-7. doi:10.1080/09537104.2020.1797323

Heib T, Hermanns HM, Manukjan G, Nagy Z, Kusch C, Becker IC, Wackerbarth LM, Englert M, Burkard P, Jahn D, Beck S, Meub M, Dütting S, Stigloher C, Sauer M, Cherpokova D, Schulze H, Brakebusch C, Nieswandt B, Pleines I. **RhoA/Cdc42 signaling drives cytoplasmic maturation but not endomitosis in megakaryocytes.** Submitted, 2020

Becker IC*, Scheller I*, Wackerbarth LM, Beck S, Heib T, Aurbach K, Manukjan G, Gross C, Spindler M, Nagy Z, Witke W, Lappalainen P, Bender M, Schulze H, Pleines I, Nieswandt B. **Actin/microtubule crosstalk during platelet biogenesis in mice is critically regulated by twinfilin1 and cofilin1**. Blood Adv. 2020;4:2124-2134. doi: 10.1182/bloodadvances.2019001303

Dütting S, Gaits-Iacovoni F, Stegner D, Popp M, Antkowiak A, van Eeuwijk JMM, Nurden P, Stritt S, Heib T, Aurbach K, Angay O, Cherpokova D, Heinz N, Baig AA, Gorelashvili MG, Gerner F, Heinze KG, Ware J, Krohne G, Ruggeri ZM, Nurden AT, Schulze H, Modlich U, Pleines I, Brakebusch C, Nieswandt B. **A Cdc42/RhoA regulatory circuit downstream of glycoprotein Ib guides transendothelial platelet biogenesis.** Nat Commun. 2017;8:15838. doi.org/10.1038/ncomms15838

### 7.3.2 Oral presentations

Gordon Research Seminar: Cell Biology of Megakaryocytes and Platelets, Galvestone, TX, USA, February 2019. **‘Redundant and non-redundant roles of RhoA and Cdc42 in platelet biogenesis and function’.**

### 7.3.3 Poster presentations

Gordon Research Seminar / Gordon Research Conference: Cell Biology of Megakaryocytes and Platelets, Galvestone, TX, USA, February 2019. **‘Redundant and non-redundant roles of RhoA and Cdc42 in platelet biogenesis and function’.**

International Symposium of the Graduate School of Life Science: EUREKA!, Würzburg, Germany, October 2019. **‘Redundant and non-redundant roles of RhoA and Cdc42 in platelet biogenesis and function’.**

International Symposium of the Graduate School of Life Science: EUREKA!, Würzburg, Germany, October 2018. **‘Regulation of thrombopoiesis by the Rho GTPases RhoA and Cdc42’.**

International Symposium of the Graduate School of Life Science: EUREKA!, Würzburg, Germany, October 2017. **‘Regulation of platelet biogenesis by Glycoprotein Ib and Rho GTPases’.**

Joint Symposium of the Collaborative Research Center 688 and the Comprehensive Heart Failure Center Würzburg, Germany, October 2017. **‘Regulation of platelet biogenesis by Glycoprotein Ib and Rho GTPases’.**

## 7.4 Curriculum vitae

## 7.5 Affidavit

I hereby confirm that my thesis entitled 'The role of Rho GTPases in megakaryopoiesis and thrombopoieses' is the result of my own work. I did not receive any help or support from commercial consultants. All sources and/or materials applied are listed and specified in the thesis.

Furthermore, I confirm that this thesis has not yet been submitted as part of another examination process neither in identical nor in similar form.

Würzburg, August 2020 ________________________

Tobias Heib

## 7.6 Eidesstattliche Erklärung

Hiermit erkläre ich an Eides statt, die Dissertation „Die Rolle von Rho GTPasen in der Megakaryopoese und Thrombopoese" eigenständig, d.h. insbesondere selbstständig und ohne Hilfe eines kommerziellen Promotionsberaters, angefertigt und keine anderen als die von mir angegebenen Quellen und Hilfsmittel verwendet zu haben.

Ich erkläre außerdem, dass die Dissertation weder in gleicher noch in ähnlicher Form bereits in einem anderen Prüfungsverfahren vorgelegen hat.

Würzburg, August 2020 ________________________

Tobias Heib